

## **Precious metal loaded organically modified silica for organic transformations**

Qazi, Asma R.

The copyright of this thesis rests with the author and no quotation from it or information derived from it may be published without the prior written consent of the author

For additional information about this publication click this link.

<https://qmro.qmul.ac.uk/jspui/handle/123456789/674>

Information about this research object was correct at the time of download; we occasionally make corrections to records, please therefore check the published record when citing. For more information contact [scholarlycommunications@qmul.ac.uk](mailto:scholarlycommunications@qmul.ac.uk)



**School of Biological & Chemical Sciences**

**Precious Metal Loaded  
Organically Modified Silica for  
Organic Transformations**

**A Thesis Submitted for the Degree of Doctor of Philosophy**

**By**

***Asma R. Qazi MSci. (Hons)***

## **Declaration**

The work and results presented in this thesis is predominantly by that of the author. Some of the work mentioned was carried out by, or with the assistance of other workers and this is fully acknowledged in the text.

Asma Qazi

For my Family, Teachers, Friends and all the nice  
people in life

## Acknowledgements

I would like to begin by expressing my gratitude for my supervisor, Prof. Alice Sullivan. Throughout the PhD her enthusiasm, inspirational attitude and eloquent manner has really made the subject highly interesting and fun for me. Prof. Sullivan has always been a great pillar of support to me and given excellent teaching and fantastic company. I truly am thankful for her encouragement, motivation and support and can only hope to aspire to be as a wonderful scientist as she is.

I would also like to thank my second supervisor, Dr John Wilson for his brilliant teaching and the great ideas and sound advice he gave; working with him has been such an honor and I will honestly miss our meetings. I would also like to thank the researchers at PhosponicS Ltd who I have had the privilege to work with, in particular Dr Siud P. Man, Dr Michael Suggate, Dr Meritxell Guino, Dr Andy Zhang and Dr. Nico Gallufo.

I would like to thank the following people for their help and services; Dr Harold Toms for solid state NMR, Dr Zophia Luklinska and Mick Willis for TEM studies and Dr Karen Wilson for XPS studies. I would also like to thank the technical support given by John Hayes, Alan Bradshaw, Jalal Hamdan and Alan Scott. I would like to thank Dr Isaac Abrahams and Dr Peter Wyatt for their advice and stimulating discussions.

I have always had a passion for chemistry and my love for the subject grew in sixth form from having such an inspirational chemistry teacher Dr Ijaz Qureshi. During the PhD, I have had the privilege to have worked with some truly incredible researchers and undergraduate students who have provided an enjoyable and stimulating environment to learn. I am indebted to many of my colleagues in the Sullivan research group who I have had the privilege to work with especially Dr Majda Sebah, Dr Ester Buchaca, Dr Mohammed Al Hashimi, Amammanet Bugrayev, Cecilia, Rukeme, Krystelle, Pat, Jahangir, Binal, Mithila, Yovann, Sai and Sebastian.

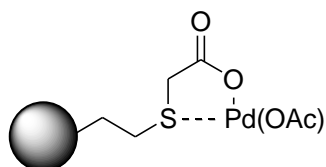
Completing a PhD is certainly no piece of cake ( even though I ate a lot of cake during it ☺) but to have some great friends accompany you along the journey has made it a more enjoyable trip. I have met some wonderful people during the PhD and have made some great friends Alhamdulillah; I would like to thank Alia Hussain for her amazing friendship and encouragement especially at the beginning of the PhD, Sultana Khanom for all the continual love and support especially during writing up and my dear friends Bema Khanam, Ana Khan, Bushra Ansari, Zahrah Ansari, Omma Ahmed and Rizwana Hussain for being there for me always.

Lastly I am thankful to my family; my wonderful parents have taught me so much and supported me in a number of ways that I will always be indebted to them. My brothers, sisters, nephew and nieces have encouraged, inspired and supported me throughout my life for which I am very grateful. It is difficult to describe the gratitude I have for my younger sister, Fozia, she has been a great friend and I anticipate that she realises how grateful I am to her. I hope this thesis can make my family proud of me.

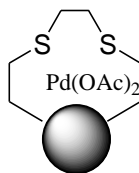
## Abstract of Thesis

### Precious Metal Loaded Organically Modified Silica for Organic Transformations

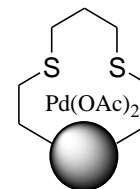
Highly active heterogeneous silica supported palladium ethylthioglycolate, **silica-60-G<sub>1</sub>-Pd(OAc)** and silica supported 1,2-bis(ethylthio)ethane palladium, **silica-60-C<sub>2</sub>-Pd(OAc)<sub>2</sub>** and 1,2-bis(ethylthio)propane palladium, **silica-60-C<sub>3</sub>-Pd(OAc)<sub>2</sub>** catalysts were prepared and characterised (using elemental analysis, solid state NMR, electron microscopy and nitrogen sorption porosimetry). The catalysts have been shown to be very active, recyclable and resistant to leaching in a representative selection of Suzuki-Miyaura cross-couplings. Two sets of conditions were employed; those regularly reported in the literature, high temperature with xylene, and much milder reaction conditions, room temperature with isopropanol. In both reaction conditions, catalysts **silica-60-G<sub>1</sub>-Pd(OAc)**, **silica-60-C<sub>2</sub>-Pd(OAc)<sub>2</sub>** and **silica-60-C<sub>3</sub>-Pd(OAc)<sub>2</sub>** gave cross coupled products in high yields. Microwave-assisted cross coupling reactions of more difficult aryl bromides with substituted phenylboronic acid employing catalyst **silica-60-C<sub>3</sub>-Pd(OAc)<sub>2</sub>** were also investigated. These reactions proceeded smoothly with excellent yields.



silica-60-G<sub>1</sub>-Pd(OAc)<sub>2</sub>



silica-60-C<sub>2</sub>-Pd(OAc)<sub>2</sub>



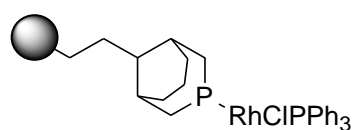
silica-60-C<sub>3</sub>-Pd(OAc)<sub>2</sub>

Catalyst **silica-60-C<sub>3</sub>-Pd(OAc)<sub>2</sub>** was also assessed for the more difficult Mizoroki-Heck cross coupling and displayed slow conversions. Modification of this catalyst with replacement of Pd(OAc)<sub>2</sub> with PdCl<sub>2</sub> to give **silica-60-C<sub>3</sub>-PdCl<sub>2</sub>**, gave excellent conversions in which aryl halides were combined with styrene. Reactions were carried out in NMP with K<sub>2</sub>CO<sub>3</sub> as a base. Activity was retained in recycles and the catalyst was again found to be resistant to leaching. Microwave assisted reactions of more difficult substrates were also found to give good conversions.

Further application of catalyst **silica-60-C<sub>3</sub>-Pd(OAc)<sub>2</sub>** was explored in the hydrogenation reaction of alkenes, nitriles and imines. High conversions were found as well as effective re-

use of the catalyst several times without loss in activity. Further studies of the pore size effects in the hydrogenation of nitrobenzene revealed catalysts prepared with smaller pores to be more active possibly as a result of the more confined environment. Interesting examples of one-pot tandem hydrogenation and Suzuki-Miyaura cross-coupling reactions catalysed by **silica-60-C<sub>3</sub>-Pd(OAc)<sub>2</sub>** were also elaborated. Asymmetric hydrogenations were also explored with palladium chiral cysteine derivatised ligands immobilised on silica, **silica-60-N-derivatised-L-cysteine-Pd(OAc)**. Although high conversions were achieved, the selectivity of these catalysts in the hydrogenation of highly substituted imines was very low.

Novel active heterogeneous ethylphosphatrioxadamantane (PAD) ruthenium catalysts, **silica-110-PAD-Ru-DPEN** with chiral amine ligands were also prepared for the asymmetric hydrogenation of ketones. These results gave quantitative conversions to the alcohol but low selectivity (18% *e.e*) was found. So attention was turned to using these immobilised phosphorus ligands, **silica-110-PAD**, to complex Rhodium compounds and utilising these materials as catalysts in hydroformylation reactions.




silica-110-PAD-RhCl(PPh<sub>3</sub>)<sub>2</sub>

Hydroformylation reactions of styrene were carried out using CO:H<sub>2</sub> in a 1:1 ratio with toluene as a solvent and with **silica-110-PAD-RhCl(PPh<sub>3</sub>)<sub>2</sub>** as catalyst. Reactions carried out at room temperature were found to favour the formation of branched aldehydes (73:27). At high temperatures, although activity was improved this was coupled with a decrease in the regioselectivity and in some cases some hydrogenated product was also formed. Interestingly, change of the rhodium salt to Rh(CO)<sub>2</sub>(acac) was found to give better chemoselectivity with no hydrogenated product.

Structure activity behaviour of the catalysts was rationalised against their materials characteristics including immobilised ligand, surface area, pore diameters and volumes, metal loading and oxidation state. The work included a study of the relative metal uptake efficiency of the different materials using ICP-OES and a further study of the relative mobility of the immobilised ligands using <sup>13</sup>C CP MAS T<sub>1</sub> measurements and effects of dipolar dephasing.



## List of Abbreviations

IUPAC	International Union of Pure and Applied Chemistry
MCM	Mobil Composition of matter
SDA	Structure directing agents
SBA	Santa Barbara amorphous
TMOS	Tetramethyl orthosilicate
TEOS	Tetraethyl orthosilicate
NMR	Nuclear magnetic resonance
IR	Infrared
MAS	Magic angle spin
CP	Cross polarisation
TEM	Transmission electron microscopy
EDS	Energy dispersion spectroscopy
FSM	Folded sheet mesoporous silica
API	Active pharmaceutical ingredient
	Silica support
TGA	Thermogravimetric analysis
ICP-OES	Inductively coupled plasma-optical emission spectroscopy
BJH	Barrett Joyner Halenda
MPTMS	3-Mercaptopropyltrimethoxysilane
DMF	Dimethylformamide
THF	Tetrahydrofuran
GC	Gas chromatography
XPS	X-ray photoelectron spectroscopy
GC-MS	Gas chromatography-mass spectrometry
AAPTS	N-(2-aminoethyl)-3-aminopropyltrimethoxysilane
APTS	(3-aminopropyl)trimethoxysilane
KHMDS	Potassium hexamethyldisilazane
NHC	N-heterocyclic carbene
NMP	N-methyl pyrrolidinone
MW	Microwave
TOF	Turnover frequency

XRD	X-ray diffraction
HRTEM	High resolution transmission electron microscopy
PAMAM	Poly(amido amine)
HPLC	High performance liquid chromatography
DTA	Differential thermal analysis
DRIFT	Diffuse reflectance infrared Fourier transform
DPEN	Diphenylethylamine

# Chapter 1

## Introduction to Organically Modified Mesoporous Silicas

### List of Figures

Figure	Table	Page
1.1	Types of pores found in solid materials.	1
1.2	W.R. Grace micronized silica gel production process	3
1.3	Structure of mesoporous M41S materials: (a) MCM-41, (b) MCM-48 (c) MCM-51	4
1.4	Types of sorption isotherms	13
1.5	Types of hysteresis loops	14

### List of Schemes

Scheme	Table	Page
1.1	Formation of mesoporous materials by structure directing agents (SDAs)	4
1.2	Grafting for organic modification of mesoporous pure silica with terminal organosilanes of the type $(RO)_3SiR'$ , R= organic functional group	7
1.3	Co-condensation method for the organic modification of mesoporous silica phases (R=organic functionality)	7
1.4	Co condensation method with use of structure directing agents for organic modification of mesoporous pure silica phases (R= organic functional group)	8
1.5	General synthetic route to periodic mesoporous organosilicas constructed from bissilylated organic bridging groups and silica.	9

## Chapter 2

### Organically Modified Mesoporous Silica; Synthesis, Characterisation and Pd uptake

#### List of Figures

Figure	Title	Page
2.1	Silica supported phosphonic acid, silica-60-PO(OH) <sub>2</sub> and silica supported sulfonic acid, silica-60-PhSO <sub>3</sub> H	22
2.2	Sorption isotherm for silica-60	24
2.3	Pore size distribution chart for silica-60	25
2.4	TGA graph for silica-60Å after pyridine adsorption total 10% loss	26
2.5	<sup>1</sup> H NMR (NaOD/ D <sub>2</sub> O) of silica-60-G <sub>1</sub>	28
2.6	<sup>13</sup> C CP MAS NMR of silica-60-G <sub>1</sub>	29
2.7	<sup>29</sup> Si MAS NMR of silica-60-G <sub>1</sub> with Gaussian fitting	30
2.8	Solid state IR spectroscopy of silica-60-G <sub>1</sub>	31
2.9	T <sub>1</sub> measurements for silica-60-G <sub>1</sub> with a dephasing time delay of 120 seconds	32
2.10	T <sub>1</sub> values of decanoic acid	33
2.11	T <sub>1</sub> values of silica-60-G <sub>1</sub>	33
2.12	Dipolar dephasing experiment for silica-60-G <sub>1</sub> (a) normal spectrum (b) dipolar dephasing experiment	34
2.13	TEM image of silica-60-G <sub>1</sub> at 100k	35
2.14	TEM image of silica-60-G <sub>1</sub> at 200k	36
2.15	Image of silica-60-G <sub>1</sub> particles	36

---

<b>2.16</b>	$^1\text{H}$ NMR spectrum of silica-60-C <sub>2</sub>	39
<b>2.17</b>	$^1\text{H}$ NMR of silica-60-C <sub>3</sub>	40
<b>2.18</b>	$^{13}\text{C}$ CP MAS NMR of silica-60-C <sub>3</sub>	41
<b>2.19</b>	$^{29}\text{Si}$ MAS NMR of silica-60-C <sub>2</sub> with Gaussian fitting.	42
<b>2.20</b>	$^{29}\text{Si}$ MAS NMR of silica-60-C <sub>3</sub> with Gaussian fitting.	43
<b>2.21</b>	Dipolar dephasing for silica-60-C <sub>3</sub> (a) normal spectrum (b) spectrum run with time delay of 180 seconds	44
<b>2.22</b>	Dipolar dephasing for silica-60-C <sub>2</sub> (a) normal spectrum (b) spectrum run with time delay of 180 seconds	45
<b>2.23</b>	T <sub>1</sub> measurements for silica-60-C <sub>3</sub>	46
<b>2.24</b>	TEM analysis of silica-60-C <sub>3</sub> reveals particles with spherical like shape	48
<b>2.25</b>	$^{13}\text{C}$ CP MAS NMR of silica-90-C <sub>3</sub>	49
<b>2.26</b>	$^{29}\text{Si}$ MAS NMR of silica-90-C <sub>3</sub>	50
<b>2.27</b>	$^{13}\text{C}$ CP NMR of silica-60-N-acetyl- <i>L</i> -cysteine	53
<b>2.28</b>	$^{29}\text{Si}$ MAS NMR of silica-60-N-acetyl- <i>L</i> -cysteine with Gaussian fitting	54
<b>2.29</b>	Dipolar dephasing experiment for silica-60-N-acetyl- <i>L</i> -cysteine (a) is the normal experiment. (b) run with time delay of 180s.	55
<b>2.30</b>	T <sub>1</sub> measurements for silica-60-N-acetyl- <i>L</i> -cysteine with a Dephasing time delay of 120 seconds	56
<b>2.31</b>	IR spectrum of silica-60-N-4-methoxybenzyl- <i>L</i> -cysteine	60
<b>2.32</b>	$^{13}\text{C}$ CP MAS NMR of silica-60-G <sub>1</sub> -Pd(OAc)	62
<b>2.33</b>	Solid state IR spectroscopy of silica-60-G <sub>1</sub> -Pd(OAc)	63

---

---

<b>2.34</b>	Isotherm graph for silica-60-G <sub>1</sub> and silica-60-G <sub>1</sub> -Pd(OAc)	64
<b>2.35</b>	Pore Size distribution chart for silica-60-G <sub>1</sub> & silica-60-G <sub>1</sub> -Pd(OAc)	65
<b>2.36</b>	<sup>13</sup> C CP MAS NMR for silica-60-C <sub>3</sub> -Pd(OAc) <sub>2</sub>	67
<b>2.37</b>	Solid state IR spectrum for silica-60-C <sub>3</sub> -Pd(OAc) <sub>2</sub>	68
<b>2.38</b>	Isotherm graph for silica-60-C <sub>2</sub> and silica-60-C <sub>2</sub> -Pd(OAc) <sub>2</sub>	69
<b>2.39</b>	Pore size distribution chart silica-60-C <sub>2</sub> and silica-60-C <sub>2</sub> -Pd(OAc) <sub>2</sub>	70
<b>2.40</b>	Isotherm graph for silica-60-C <sub>3</sub> and silica-60-C <sub>3</sub> -Pd(OAc) <sub>2</sub>	71
<b>2.41</b>	Pore size distribution chart for silica-60-C <sub>3</sub> and silica-60-C <sub>3</sub> -Pd(OAc) <sub>2</sub>	72
<b>2.42</b>	TEM image of silica-60-C <sub>3</sub> -Pd(OAc) <sub>2</sub>	73
<b>2.43</b>	Sorption isotherms for silica-90-C <sub>3</sub> and silica-150-C <sub>3</sub>	74
<b>2.44</b>	Pore size distribution graph for silica-150-C <sub>3</sub> and silica-150-C <sub>3</sub> -Pd(OAc) <sub>2</sub>	76
<b>2.45</b>	Isotherm graph for silica-60-C <sub>3</sub> -PdCl <sub>2</sub>	78
<b>2.46</b>	Pore Size distribution graph for silica-60-C <sub>3</sub> -PdCl <sub>2</sub>	78
<b>2.47</b>	<sup>13</sup> C CP MAS NMR of silica-60-N-acetyl-L-cysteine-Pd(OAc)	80
<b>2.48</b>	IR spectroscopy for silica-60-N-acetyl-L-cysteine-Pd(OAc)	81
<b>2.49</b>	Isotherm graph for silica-60-N-acetyl-L-cysteine and silica-60-N-acetyl-L-cysteine-Pd(OAc)	82
<b>2.50</b>	Pore Size distribution chart for silica-60-N-acetyl-L-cysteine and silica-60-N-acetyl-L-cysteine-Pd(OAc)	83
<b>2.51</b>	Isotherm graph for silica-60-N-4-methoxybenzyl-L-cysteine-Pd(OAc)	84
<b>2.52</b>	Pore size distribution chart for silica-60-N-4-methoxybenzyl-L-cysteine-Pd(OAc)	85

---

<b>2.53</b>	Comparative uptake of Pd(OAc) <sub>2</sub> at different Pd/Ligand ratios for materials silica-60-G <sub>1</sub> , silica-60-C <sub>2</sub> , silica-60-C <sub>3</sub> and silica-60-C <sub>3</sub> SSH	86
-------------	--	----

### List of Schemes

<b>Scheme</b>	<b>Title</b>	<b>Page</b>
<b>2.1</b>	Free radical transfer addition of a mercaptan to an olefin	23
<b>2.2</b>	Co-condensation reaction of surface silanol groups and organoalkoxysilane compounds. R' = trialkoxysilyl	23
<b>2.3</b>	Free radical reaction of vinyl trimethoxysilane and methyl thioglycolate	27
<b>2.4</b>	Synthesis of methylthioglycolate silica.	27
<b>2.5</b>	Synthesis of silica-60-G <sub>1</sub>	27
<b>2.6</b>	Synthesis of compounds 1,2-bis(trimethoxysilylethylthio)ethane and 1,3-bis(trimethoxysilylethylthio)propane	38
<b>2.7</b>	Synthesis of silica-60-C <sub>2</sub> and silica-60-C <sub>3</sub>	38
<b>2.8</b>	Synthesis of S-trimethoxysilylethyl-N-acetyl-L-cysteine	52
<b>2.9</b>	Synthesis of silica-60-N-acetyl-L-cysteine	52
<b>2.10</b>	Synthesis of N-4-methoxybenzyl-L-cysteine	57
<b>2.11</b>	Synthesis of S-trimethoxysilyl-ethyl-L-cysteine hydrochloride	58
<b>2.12</b>	Synthesis of silica-60-L-cysteine-ethyl ester	58
<b>2.13</b>	Synthesis of silica-60-N-4-methoxybenzyl-L-cysteine	58
<b>2.14</b>	Synthesis of silica-60-G <sub>1</sub> -Pd(OAc)	62

<b>2.15</b>	Synthesis of silica-60-C <sub>2</sub> -Pd(OAc) <sub>2</sub>	66
<b>2.16</b>	Synthesis of silica-60-C <sub>3</sub> -Pd(OAc) <sub>2</sub>	66
<b>2.17</b>	Preparation of silica-60- N-acetyl- <i>L</i> -cysteine-Pd(OAc)	79

### List of Tables

<b>Table</b>	<b>Title</b>	<b>Page</b>
<b>2.1</b>	Calculated spin relaxation times T <sub>1</sub> and correlation times τ <sub>c</sub> for material silica-60-G <sub>1</sub>	32
<b>2.2</b>	Calculated correlation times for material silica-60-C <sub>3</sub>	46
<b>2.3</b>	T <sub>1</sub> measurement, R <sub>1</sub> and τ <sub>c</sub> measurements calculated for silica-60-C <sub>2</sub>	47
<b>2.4</b>	Calculated correlation times for material silica-60-N-acetyl- <i>L</i> -cysteine	56
<b>2.5</b>	Porosimetry data for silica-60-G <sub>1</sub> and silica-60-G <sub>1</sub> - Pd(OAc)	64
<b>2.6</b>	Porosimetry values for silica-60-C <sub>2</sub> using BJH method	69
<b>2.7</b>	Porosimetry Data for chart silica-60-C <sub>3</sub> and silica-60-C <sub>3</sub> -Pd(OAc) <sub>2</sub>	71
<b>2.8</b>	The calculated porosimetry data from the BJH method for materials silica-90-C <sub>3</sub> and silica-150-C <sub>3</sub> before and after metal introduction.	75
<b>2.9</b>	Porosity values for silica-60-C <sub>3</sub> -PdCl <sub>2</sub> as calculated from the BJH method.	77
<b>2.10</b>	Porosimetry Data for silica-60-N-acetyl- <i>L</i> -cysteine and silica-60-N-acetyl- <i>L</i> -cysteine-Pd(OAc) as calculated from BJH method.	82
<b>2.11</b>	Porosimetry data for silica-60-N-4-methoxybenzyl- <i>L</i> -cysteine-Pd(OAc) as calculated from the BJH method	84



## Chapter 3

### Organosilica supported palladium catalyzed cross coupling reactions

#### List of Figures

Figure	Title	Page
3.1	Examples of macromolecules where the bond formed by the Suzuki-Miyaura reaction is shown in red	91
3.2	silica-60-G <sub>1</sub> -Pd(OAc)	105
3.3	Catalysts silica-60-C <sub>2</sub> -Pd(OAc) <sub>2</sub> (S loading 0.56 mmol/g , Pd loading 0.26 mmol/g) and silica-60-C <sub>3</sub> -Pd(OAc) <sub>2</sub> (S loading 0.50 mmol/g , Pd loading 0.42 mmol/g)	108
3.4	Kinetic profile for the Suzuki-Miyaura reaction of 4-chlorobromobenzene and bromobenzene with phenylboronic acid at room temperature catalysed by silica-60-C <sub>2</sub> Pd(OAc) <sub>2</sub> .	115
3.5	Kinetic profile for the Suzuki-Miyaura reaction of 4-chlorobromobenzene and bromobenzene with phenylboronic acid at room temperature catalysed by silica-60-C <sub>3</sub> -Pd(OAc) <sub>2</sub> .	115
3.6	TEM image of silica-60-C <sub>3</sub> -Pd(OAc) <sub>2</sub> after catalysis at room temperature	119
3.7	TEM image of silica-60-G <sub>1</sub> -Pd(OAc) after catalysis at high temperature	119
3.8	XPS of catalysts silica-60-C <sub>2</sub> -Pd(OAc) <sub>2</sub> , silica-60-C <sub>3</sub> -Pd(OAc) <sub>2</sub> , silica-60-G <sub>1</sub> -Pd(OAc) before and after catalysis	121
3.9	Clark <i>et al.</i> amino modified silica Pd catalyst	130

## List of Schemes

Scheme	Title	Page
3.1	Textbook catalytic cycle for Suzuki-Miyaura reaction	92
3.2	Standard textbook mechanism for the Mizoroki-Heck reaction	94
3.3	Mechanism for Pd catalysed Heck reactions involving anionic intermediates	95
3.4	Synthesis of Corma and Garcia's carbapalladacycle	97
3.5	Synthesis of Corma and Garcia's catalyst PdL@SiO <sub>2</sub> via grafting route	98
3.6	Preparation methods of silica modified mercaptopropyl Pd catalysts: (a) grafting (b) Pd complex adsorption (c) single step. PdL <sub>n</sub> = Pd(0) or Pd(II)	100
3.7	Preparation of Bedford <i>et al.</i> catalyst SiO <sub>2</sub> -Imine-palladacycle	101
3.8	Preparation of Bedford <i>et al.</i> catalyst SiO <sub>2</sub> -Imine-PdPPh <sub>3</sub>	101
3.9	Synthesis of covalently modified silica by Bedford <i>et al.</i>	102
3.10	Synthetic pathway of Clark <i>et al.</i> catalysts	103
3.11	Mechanistic proposal of reduction with isopropanol	118
3.12	Nickel catalysed Suzuki-Miyaura coupling of aryl carbamates with phenyl boroxines	124
3.13	Preparation of silica-AAPTS-Pd	127
3.14	Preparation of silica-APTS-Pd	127
3.15	Synthesis of trialkoxysilane intermediate	128
3.16	Preparation of Karimi and Enders silica supported NHC-Pd catalyst	129
3.17	Preparation Imidazolone based Pd catalyst I-Pd (Polshettiwar <i>et al.</i> ).	131

<b>3.18</b>	Intramolecular Mizoroki-Heck reaction in the total synthesis of (±)-dehydrotubifoline (Rawal <i>et al.</i> )	132
-------------	---	-----

### List of Tables

Table	Title	Page
<b>3.1</b>	Suzuki-Miyaura reaction of aryl bromides with phenyl boronic acid catalysed by silica-60-G <sub>1</sub> -Pd(OAc)	107
<b>3.2</b>	Suzuki-Miyaura cross coupling of phenyl boronic acid and aryl halides catalysed by silica-60-C <sub>2</sub> -Pd(OAc) <sub>2</sub> and silica-60-C <sub>3</sub> -Pd(OAc) <sub>2</sub>	109
<b>3.3</b>	The Suzuki-Miyaura reaction catalyzed by silica-60-G <sub>1</sub> -Pd(OAc), silica-60-C <sub>2</sub> -Pd(OAc) <sub>2</sub> and silica-60-C <sub>3</sub> -Pd(OAc) <sub>2</sub> at room temperature	113
<b>3.4</b>	Suzuki-Miyaura reaction with the use of different bases	117
<b>3.5</b>	Binding energies (eV) of Pd in catalysts silica-60-C <sub>2</sub> -Pd(OAc) <sub>2</sub> , silica-60-C <sub>3</sub> -Pd(OAc) <sub>2</sub> , silica-60-G <sub>1</sub> -Pd(OAc) before and after use in the Suzuki-Miyaura reaction	122
<b>3.6</b>	Microwave assisted Suzuki-Miyaura reaction with 1.5 mol % silica-60-C <sub>3</sub> -Pd(OAc) <sub>2</sub>	125
<b>3.7</b>	The Mizoroki-Heck reaction of Bromoanisole and Styrene	135
<b>3.8</b>	Mizoroki-Heck reactions with silica-60-C <sub>3</sub> -PdCl <sub>2</sub>	136
<b>3.9</b>	Microwave assisted Mizoroki-Heck reactions with 2.5 mol % silica-60-C <sub>3</sub> -PdCl <sub>2</sub>	138

## Chapter 4

### Hydrogenation reactions with organosilica supported palladium catalysts

#### List of Figures

Figure	Title	Page
4.1	Diosady <i>et al.</i> silica supported Ru catalyst	145
4.2	Catalyst silica-60-C <sub>3</sub> -Pd(OAc) <sub>2</sub>	149
4.3	Kinetic profile for the hydrogenation of nitrobenzene with catalysts silica-60-C <sub>3</sub> - Pd(OAc) <sub>2</sub> , silica-90-C <sub>3</sub> -Pd(OAc) <sub>2</sub> and silica-150-C <sub>3</sub> -Pd(OAc) <sub>2</sub>	157
4.4	Sorption isotherm graph for silica-60-C <sub>3</sub> -Pd(OAc) <sub>2</sub> , silica-90-C <sub>3</sub> -Pd(OAc) <sub>2</sub> and silica-150-C <sub>3</sub> -Pd(OAc) <sub>2</sub>	159
4.5	Pore size distribution chart as calculated from desorption point by the BJH method for catalysts silica-60-C <sub>3</sub> -Pd(OAc) <sub>2</sub> , silica-90-C <sub>3</sub> -Pd(OAc) <sub>2</sub> and silica-150-C <sub>3</sub> -Pd(OAc) <sub>2</sub> .	160
4.6	silica-60- <i>N</i> -4-methoxybenzyl- <i>L</i> -cysteine-Pd(OAc)	168
4.7	Catalyst silica-60- <i>N</i> -isopropyl- <i>L</i> -cysteine-Pd(OAc)	170
4.8	Possible co ordination of Pd metal to the ligand sites of silica-60- <i>N</i> -derivatised- <i>L</i> -cysteine	171

#### List of Schemes

Scheme	Title	Page
4.1	Synthesis of alkoxy-silyl substituted phosphines	144
4.2	Synthesis of phosphine modified silica	145
4.3	Synthesis of Rh-pol	145
4.4	Hydrogenation of nitrobenzene by silica supported Co nanoparticles	147

---

<b>4.5</b>	Hydrogenation of protected imines using asymmetric Rh catalysts with tangphos ligands	148
<b>4.6</b>	Hydrogenation of 1-octene	150
<b>4.7</b>	Hydrogenation of nitrobenzene	151
<b>4.8</b>	Synthesis of highly substituted $\alpha$ -imino ester, (4-methoxy-phenylimino)-phenyl-acetic acid methyl ester	153
<b>4.9</b>	Hydrogenation of (4-methoxy-phenylimino)-phenyl-acetic acid methyl ester	154
<b>4.10</b>	Hydrogenation of nitrobenzene	155
<b>4.11</b>	Room temperature Suzuki-Miyaura hydrogenation reaction catalysed by silica-60-C <sub>3</sub> -Pd(OAc) <sub>2</sub>	163
<b>4.12</b>	Possible one-pot Suzuki- Miyaura hydrogenation pathways (a) and (b) Suzuki-Miyaura cross coupling occurs first and then hydrogenation; pathways (c) and (d) hydrogenation occurs first then cross coupling.	166
<b>4.13</b>	Hydrogenation of (4-methoxy-phenylimino)-phenyl-acetic acid methyl ester with silica-60-N-acetyl- <i>L</i> -cysteine-Pd(OAc)	167
<b>4.14</b>	Hydrogenation of 2-phenyl-2propylimino ethanol with silica-60-N-4-methoxybenzyl- <i>L</i> -cysteine-Pd(OAc)	169
<b>4.15</b>	Hydrogenation of 2-(4-mthoxy-phenylimino)-nonanoic acid methyl ester with silica-60-N-4-methoxybenzyl- <i>L</i> -cysteine-Pd(OAc)	169
<b>4.16</b>	Asymmetric addition of diethyl zinc to benzaldehyde using silica ethyl-(1R, 2S)-ephidrine phosphiniamide chloride as a chiral auxiliary	172
<b>4.17</b>	Asymmetric addition of diethyl zinc to benzaldehyde using silica-60-N-4-methoxybenzyl- <i>L</i> -cysteine as a chiral auxiliary catalyst	172

---

## List of Tables

Table	Title	Page
4.1	Hydrogenations with 0.4 mol % Pd, with catalyst silica-60-C <sub>3</sub> -Pd(OAc) <sub>2</sub>	150
4.2	Hydrogenations of nitrobenzene with 0.1 mol % Pd, with catalyst silica-60-C <sub>3</sub> -Pd(OAc) <sub>2</sub>	151
4.3	Hydrogenations of benzonitrile with 0.5 mol % Pd, with catalyst silica-60-C <sub>3</sub> -Pd(OAc) <sub>2</sub>	152
4.4	Hydrogenation of (4-methoxy-phenylimino)-phenyl-acetic acid methyl ester	154
4.5	Hydrogenation of nitrobenzene with catalyst silica-C <sub>3</sub> -Pd(OAc) <sub>2</sub> of different pore sizes	156
4.6	The calculated pore size measurements from the BJH method for catalysts silica-60-C <sub>3</sub> -Pd(OAc) <sub>2</sub> , silica-90-C <sub>3</sub> -Pd(OAc) <sub>2</sub> and silica-150-C <sub>3</sub> -Pd(OAc) <sub>2</sub>	158
4.7	Pd and ligand loading for catalysts silica-60-C <sub>3</sub> -Pd(OAc) <sub>2</sub> , silica-90-C <sub>3</sub> -Pd(OAc) <sub>2</sub> and silica-150-C <sub>3</sub> -Pd(OAc) <sub>2</sub>	161
4.8	Room temperature Suzuki-Miyaura Hydrogenation reactions with catalyst silica-60-C <sub>3</sub> -Pd(OAc) <sub>2</sub>	163
4.9	Microwave-assisted Suzuki-Miyaura and hydrogenation with catalyst silica-60-C <sub>3</sub> -Pd(OAc) <sub>2</sub>	165

## Chapter 5

### Hydroformylations with Precious Metal Silica-Phosphadamantane Catalysts

#### List of Figures

Figure	Title	Page
5.1	Sandee <i>et al.</i> Hydroformylation catalyst $[\text{Rh}(\text{siloxPNP})\text{CO}]^+$	180
5.2	Some of the phosphorus modifiers used in the study by Li <i>et al.</i>	181
5.3	$^{13}\text{C}$ CP MAS NMR of silica-110-PAD	188
5.4	$^{29}\text{Si}$ MAS NMR of silica-110-PAD with Gaussian fitting	189
5.5	$^{31}\text{P}$ CP MAS NMR of silica-110-PAD	189
5.6	Sorption isotherm for silica-110-PAD	190
5.7	Pore Size distribution chart for silica-110-PAD	191
5.8	Isotherm for silica-110-PAD-Rh complexes	192
5.9	Pore size distribution chart for silica-110-Rh complexes	193

#### List of Schemes

Scheme	Title	Page
5.1	Hydroformylation reaction	175
5.2	Preparation of MCM- <i>Pr</i> PPhRhCl(CO)(PPh <sub>3</sub> ) catalyst	177
5.3	Possible structure for Rh-P1/2N-MCM-41 or Rh-P2/2N-MCM-41 as proposed by Peng <i>et al.</i>	178
5.4	Schematic illustration of the preparation of sol gel immobilized $[\text{HRh}(\text{siloxantphos})(\text{CO})_2]$	179

<b>5.5</b>	Functionalisation of SBA-15 by aminotriethoxysilane	182
<b>5.6</b>	Michael addition of Methyl acrylate to the amino groups of the surface of SBA-15	182
<b>5.7</b>	Amidation of terminal groups on the surface of SBA-15 with ethyldiamine to give 1 <sup>st</sup> generation PAMAM modified SBA-15.	182
<b>5.8</b>	Phosphine cages PAD are racemic mixtures (labelled $\alpha$ and $\beta$ ) and are associated with the $C_1$ symmetry of the cages.	183
<b>5.9</b>	Preparation of 1,3,5,7-tetramethyl-2,4,8-trioxa-6-phosphaadamantane	184
<b>5.10</b>	Synthesis of trimethoxysilyl-PAD	186
<b>5.11</b>	Synthesis of silica-110-PAD	187
<b>5.12</b>	Synthesis of silica-110-PAD-Rh complex	191
<b>5.13</b>	Hydroformylation of 1-octene with silica-110-PAD-RhCl(PPh <sub>3</sub> ) <sub>2</sub>	195
<b>5.14</b>	Hydroformylation of styrene with silica-110-PAD-RhCl(PPh <sub>3</sub> ) <sub>2</sub>	197
<b>5.15</b>	Hydroformylation of styrene with silica-60-C <sub>3</sub> -RhCl(PPh <sub>3</sub> ) <sub>2</sub> /Pd(OAc) <sub>2</sub>	198
<b>5.16</b>	Hydroformylation of styrene with silica-110-PAD-RhCO(acac)	199

---

### List of Tables

Table	Title	Page
<b>5.1</b>	Porosimetry data for silica-110-PAD as calculated by the BJH method	190
<b>5.2</b>	Porosimetry data for silica-110-PAD-Rh complexes as calculated by BJH method	193
<b>5.3</b>	Hydroformylation of 1-octene with silica-110-PAD-RhClPPh <sub>3</sub>	195

---



---

<b>5.4</b>	Hydroformylation of 1-octene with silica-110-PAD-RhClPPh <sub>3</sub>	197
<b>5.5</b>	Hydroformylation of styrene at 60 °C with silica-60-C <sub>3</sub> -Pd(OAc) <sub>2</sub> and silica-60-C <sub>3</sub> -RhClPPh <sub>3</sub>	198
<b>5.6</b>	Hydroformylation of styrene with silica-110-PAD-RhCO(acac)	199

---

# Precious Metal Loaded Organically Modified Silica for Organic Transformations

<b>Contents</b>	<b>Page</b>
<b>Declaration</b>	II
<b>Acknowledgements</b>	III
<b>Abstract</b>	VI
<b>List of Abbreviations, Figures, Schemes and Tables</b>	VIII
<hr/>	
<b>Chapter 1</b>	
<b>Introduction to Organically Modified Mesoporous Silicas</b>	
<b>1.1 Porous materials</b>	1
<b>1.2 Amorphous Mesoporous silica</b>	2
<b>1.3 Ordered Mesoporous Silica</b>	3
1.3.1 Templating methods	5
1.3.1.1 Soft templating methods	5
1.3.1.2 Hard templating methods	5
<b>1.4 Synthesis of organically modified mesoporous silica</b>	6
1.4.1 Grafting methods	6
1.4.2 Co-condensation method	7
1.4.3 Periodic Mesoporous Organosilanes PMOs.	9
<b>1.5 Techniques for Characterisation of organically modified mesoporous silica</b>	10
1.5.1 Introduction	10
1.5.2 Solid state NMR	10
1.5.3 $^{13}\text{C}$ and $^{29}\text{Si}$ NMR	11
1.5.4 Pulse sequence experiments (Dipolar dephasing and $T_1$ measurements)	11
1.5.5 Porosimetry	13
1.5.6 Electron Microscopy	15
<b>1.6 Catalytic Applications of organically modified mesoporous silica</b>	15
1.6.1 Heterogeneous Catalysis	16
1.6.2 Acid catalysis	16
1.6.3 Enantioselective dihydroxylation	17

1.6.4 Organic transformations with metal loaded organically modified silica phases	17
<b>1.7 Conclusions</b>	18
<b>1.8 References</b>	20

## Chapter 2

### Organically Modified Mesoporous Silica: Synthesis, Characterisation and Palladium Uptake

<b>2.1 Introduction</b>	22
<b>2.2. Characterisation of Silica-60Å</b>	24
2.2.1. Porosimetry Studies	24
2.2.2. Determination of silanol groups in silica-60	25
<b>2.3. Synthesis of silica immobilised sulfur based ligands</b>	26
2.3.1. Synthesis of Silica ethyl thioglycolic acid, silica-60-G <sub>1</sub>	26
2.3.2 Characterisation of silica-60-G <sub>1</sub>	28
2.3.3 Solution state <sup>1</sup> H NMR	28
2.3.4 <sup>13</sup> C CP MAS NMR	29
2.3.5 <sup>29</sup> Si MAS NMR and Elemental Analysis	29
2.3.6 IR Spectroscopy	30
2.3.7 T <sub>1</sub> measurements	31
2.3.8 Dipolar dephasing	34
2.3.9 Transmission Electron Microscopy (TEM) and Energy Dispersive X-ray Spectroscopy (EDS)	35
<b>2.4 Synthesis of silica bis(alkyldithio)alkanes</b>	37
2.4.1 Characterisation of silica-60-C <sub>2</sub> and silica-60-C <sub>3</sub>	39
2.4.2 Solution state <sup>1</sup> H NMR	39
2.4.3 <sup>13</sup> C CP MAS NMR	40
2.4.4 <sup>29</sup> Si MAS NMR	41
2.4.5Elemental Analysis	43
2.4.6 IR Spectroscopy	43
2.4.7 Dipolar Dephasing Experiment	44
2.4.8 T <sub>1</sub> measurements	45
2.4.9 Microscopy Studies	48
2.4.10 Synthesis and Characterisation of silica-90-C <sub>3</sub> and silica-150-C <sub>3</sub>	48

2.4.11 Summary	50
<b>2.5 Synthesis of Chiral Sulfur based ligands immobilised on silica</b>	51
2.5.1 Synthesis of silica-60-N-Acetyl-L-Cysteine	52
2.5.2 Solid state NMR	53
2.5.3 Dipolar Dephasing	54
2.5.4 T <sub>1</sub> measurements	55
2.5.5 Synthesis of Silica-N-4-methoxybenzyl-L-cysteine	57
2.5.6 Solution state NMR	59
2.5.7 IR spectroscopy	59
2.5.8 Ligand Loading	60
2.5.9 Summary	60
<b>2.6 Pd derivatised G<sub>1</sub>, C<sub>2</sub> and C<sub>3</sub> organosilica materials: synthesis and characterisation</b>	
2.6.1 Synthesis of silica-60-G <sub>1</sub> -Pd(OAc)	61
2.6.2 <sup>13</sup> C CP MAS NMR of silica-60-G <sub>1</sub> -Pd(OAc)	62
2.6.3 Solid state IR spectroscopy for silica-60-G <sub>1</sub> - Pd(OAc)	63
2.6.4 Porosimetry Studies of silica-60-G <sub>1</sub> -Pd(OAc)	63
2.6.5 Palladium analysis in silica-60-G <sub>1</sub> -Pd(OAc)	65
2.6.6 Synthesis of silica-60-C <sub>2</sub> -Pd(OAc) <sub>2</sub> and silica-60-C <sub>3</sub> -Pd(OAc) <sub>2</sub>	66
2.6.7 Solid state NMR silica-60-C <sub>2</sub> -Pd(OAc) <sub>2</sub> and silica-60-C <sub>3</sub> -Pd(OAc) <sub>2</sub>	67
2.6.8 Solid state IR spectroscopy	68
2.6.9 Porosimetry	68
2.6.10 Palladium analysis	72
2.6.11 TEM analysis	73
2.6.12 Synthesis of silica-90-C <sub>3</sub> -Pd(OAc) <sub>2</sub> and silica-150-C <sub>3</sub> -Pd(OAc) <sub>2</sub>	73
2.6.13 Porosimetry silica-90-C <sub>3</sub> -Pd(OAc) <sub>2</sub> and silica-150-C <sub>3</sub> -Pd(OAc) <sub>2</sub>	75
2.6.14 Palladium analysis	76
2.6.15 Synthesis and characterisation of silica-60-C <sub>3</sub> -PdCl <sub>2</sub>	77
2.6.16 Porosimetry	77
2.6.17 Pd analysis	79
<b>2.7 Pd derivatised cysteine silica materials: synthesis and characterisation</b>	79
2.7.1 Synthesis of silica-60- N-derivatised-cysteine-Pd(OAc)	79
2.7.2 <sup>13</sup> C CP MAS NMR Spectroscopy	80
2.7.3 IR spectroscopy	80

2.7.4 Porosimetry	81
2.7.5 Palladium loading	85
<b>2.8 Comparative Palladium Binding Study</b>	85
<b>2.9 Conclusions</b>	87
<b>2.10 References</b>	89

## Chapter 3

### Organosilica supported palladium catalyzed cross coupling reactions

<b>3.1 Cross coupling reactions</b>	91
<b>3.2 The Suzuki-Miyaura reaction catalyzed by silica-60-G<sub>1</sub>-Pd(OAc), silica-60-C<sub>2</sub>-Pd(OAc)<sub>2</sub> and silica-60-C<sub>3</sub>-Pd(OAc)<sub>2</sub></b>	97
3.2.1 Background literature	97
<b>3.3 Results and Discussion</b>	105
3.3.1 Suzuki-Miyaura reaction at high temperature with silica-60-G <sub>1</sub> -Pd(OAc), silica-60-C <sub>2</sub> -Pd(OAc) <sub>2</sub> and silica-60-C <sub>3</sub> -Pd(OAc) <sub>2</sub>	105
3.3.2 Palladium leaching tests	110
3.3.3 Suzuki Miyaura reactions catalysed by silica-60-G <sub>1</sub> -Pd(OAc), silica-60-C <sub>2</sub> -Pd(OAc) <sub>2</sub> and silica-60-C <sub>3</sub> -Pd(OAc) <sub>2</sub> at room temperature	111
3.3.4 Kinetic Studies	114
3.3.5 Suzuki-Miyaura reaction with low Pd loading silica-60-C <sub>3</sub> -Pd(OAc) <sub>2</sub>	116
3.3.6 Suzuki-Miyaura reaction with silica-60-C <sub>3</sub> -Pd(OAc) <sub>2</sub> and different bases.	116
3.3.7 Palladium Leaching tests	117
3.3.8 TEM of silica-60-G <sub>1</sub> -Pd(OAc), silica-60-C <sub>2</sub> -Pd(OAc) <sub>2</sub> and silica-60-C <sub>3</sub> -Pd(OAc) <sub>2</sub>	118
3.3.9 X-ray photoelectron spectroscopy silica-60-G <sub>1</sub> -Pd(OAc), silica-60-C <sub>2</sub> -Pd(OAc) <sub>2</sub> and silica-60-C <sub>3</sub> -Pd(OAc) <sub>2</sub>	120
3.3.10 Suzuki-Miyaura reaction at room temperature with silica-60-C <sub>3</sub> -Ni(OAc) <sub>2</sub>	123
3.3.11 Microwave assisted Suzuki-Miyaura silica-60-C <sub>3</sub> -Pd(OAc) <sub>2</sub>	124
3.3.12 Suzuki-Miyaura reaction with silica-60-C <sub>3</sub> -Pd( $\eta^3$ -allyl)chloride	126
<b>3.4 Mizoroki-Heck reactions catalysed by Silica supported Pd catalyst</b>	126
3.4.1 Background literature	126

3.4.2 Results and discussion	133
3.4.2.1 Mizoroki-Heck reaction with silica-60-C <sub>3</sub> -PdCl <sub>2</sub>	136
3.4.2.2 Microwave assisted Mizoroki-Heck reactions with silica-60-C <sub>3</sub> -PdCl <sub>2</sub>	137
<b>3.5 Conclusions</b>	139
<b>3.6 References</b>	141

## Chapter 4

### Hydrogenation reactions with organosilica supported palladium catalysts

<b>4.1. Background literature</b>	143
<b>4.2 Results and Discussion</b>	148
4.2.1 Hydrogenations with catalyst silica-60-C <sub>3</sub> -Pd(OAc) <sub>2</sub>	149
4.2.2. Pore size effects on the hydrogenation of nitrobenzene	155
4.2.3 Summary	161
4.2.4 Room temperature cross-coupling and hydrogenation catalysed by silica-60-C <sub>3</sub> -Pd(OAc) <sub>2</sub>	162
4.2.5 Microwave-assisted cross-coupling and hydrogenation catalysed by silica-60-C <sub>3</sub> .Pd(OAc) <sub>2</sub>	164
4.2.6 Conclusion	166
<b>4.3. Asymmetric hydrogenation of imines with silica-60-N-derivatised-L-cysteine Pd catalysts</b>	167
4.3.1 Results and Discussion	167
4.3.2 Pd co-ordination to N-derivatised cysteine ligands	170
4.3.3 Conclusions	171
<b>4.4 Enantioselective addition of Diethylzinc to benzaldehyde</b>	171
<b>4.5 References</b>	173

<b>Chapter 5</b>	
<b>Hydroformylations with Precious Metal Silica-Phosphadamantane Catalysts</b>	
<b>5.1 Background literature</b>	175
<b>5.2 Results and Discussion</b>	186
5.2.1 Synthesis of silica-110-PAD	186
5.2.2 Solid state NMR	187
5.2.3 Porosimetry	190
5.2.4 Synthesis of silica-110-PAD-Rh	191
5.2.5 Porosimetry of silica-110-PAD-Rh	192
5.2.6 Catalytic activity in Hydroformylation reactions	194
<b>5.3 Conclusion</b>	200
<b>5.4 References</b>	201
<hr/>	
<b>Chapter 6</b>	
<b>Experimental Section</b>	
<b>6.1 General Background information</b>	203
<b>6.2 Chapter 2 experimental</b>	206
<b>6.3 Chapter 3 experimental</b>	218
<b>6.4 Chapter 4 experimental</b>	227
<b>6.5 Chapter 6 experimental</b>	237
<b>6.6 References</b>	242
<hr/>	
<b>Appendices</b>	
<b>Appendix 1</b> B. J. H. equation	243
<b>Appendix 2</b> Quantification of silanol groups	245
<b>Appendix 3</b> T <sub>1</sub> measurement experiment	247
<b>Appendix 4</b> Synthesis of silica-60-N-isopropyl-L-cysteine-Pd(OAc)	249
<b>Appendix 5</b> Asymmetric hydrogenation of acetophenone with silica supported PAD chiral amine Ru catalysts	252

## Chapter 1

### Introduction to Organically Modified Mesoporous Silicas

#### 1.1 Porous materials

Porous materials can be defined as “any solid material which contains cavities, channels or interstices”.<sup>1</sup> The IUPAC definition of a pore can be further defined using the diagram shown in **Figure 1.1**. Pores are classified according to their availability to an external fluid. Pores such as (a) which are totally excluded from their neighbours are described as closed pores. These pores are said to influence properties such as bulk density, mechanical strength and thermal conductivity but are said to be inactive in processes such as adsorption of gases. In the other case, pores which are said to have a constant channel of communication with the external surface of the body, as (b), (c), (d), (e) and (f) are described as open pores. These can further be categorised as blind pores, such as (b) and (f) as they are only open at one end, and pores open from both ends as is the case for (e) are called through pores.

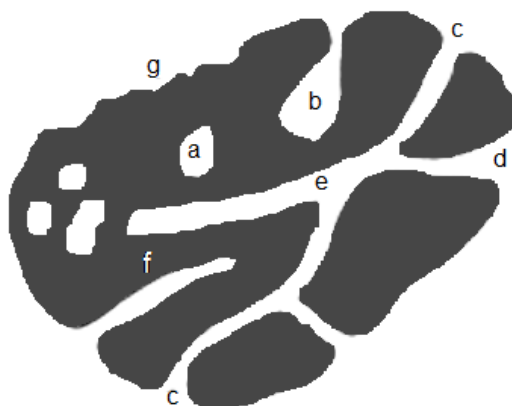


**Figure 1.1** Types of pores found in solid materials.<sup>1</sup>

Pores can further be classified by their shapes; they can be cylindrical pores (open like (c) or blind like (f)), ink-bottle shaped (b), funnel shaped (d) or slit shaped (e). Porous materials have generated much interest from different technology sectors of the science community, including electronics, biotechnology, environment and medicine. According to IUPAC porous materials can be classified as three types depending on pore size; microporous materials have pore diameters  $< 20 \text{ \AA}$ , mesoporous materials have pore sizes in the range of  $20\text{-}500 \text{ \AA}$  and macroporous materials which have pore sizes  $> 500 \text{ \AA}$ .<sup>2</sup> Porous materials may



also exhibit high surface areas, uniform pore sizes and tuneable properties which make them highly attractive to various research fields.<sup>3,4</sup>

Microporous materials such as zeolites have long been utilized as industrial catalysts, however owing to their small sized pores; these materials are limited in their applications to reactions with relatively small molecules. Conversely, macroporous materials have been applied as adsorbents (for gas or liquid). However, as macroporous materials have low surface areas and large pores, they make relatively poor hosts. In comparison to microporous materials, mesoporous materials have been shown to have reduced mass transport limitations and easily allow the entrance and exit of large molecules.<sup>4</sup>

### 1.2 Amorphous Mesoporous Silica

Porous materials such as silica are macromolecular arrangements of silicon and oxygen atoms with surface hydroxyl groups.<sup>5</sup> Silica gel is made up of randomly linked spherical polymerized silicate particles, also known as primary particles. The properties of silica gel arise from the size and aggregation of the primary particles and their surface chemistry. W. R. Grace offer silica gel composed of nearly 100% of SiO<sub>2</sub> with tailor made pore systems and surface areas.

Industrial preparation of silica gel employs sulfuric acid hydrolysis of aqueous sodium silicate (**Figure 1.2**).<sup>6</sup> The primary particles formed under controlled conditions polycondense to give the raw gel from which all types of silica gel are made. The glass-like gel formed is then broken down into granules and then washed, aged and dried to give the highly porous materials. Physical parameters such as porosity, pore size and surface area can be adjusted in this way by controlling the washing, aging and drying conditions. Structurally silica gel is a highly porous material exhibiting thick pore walls.

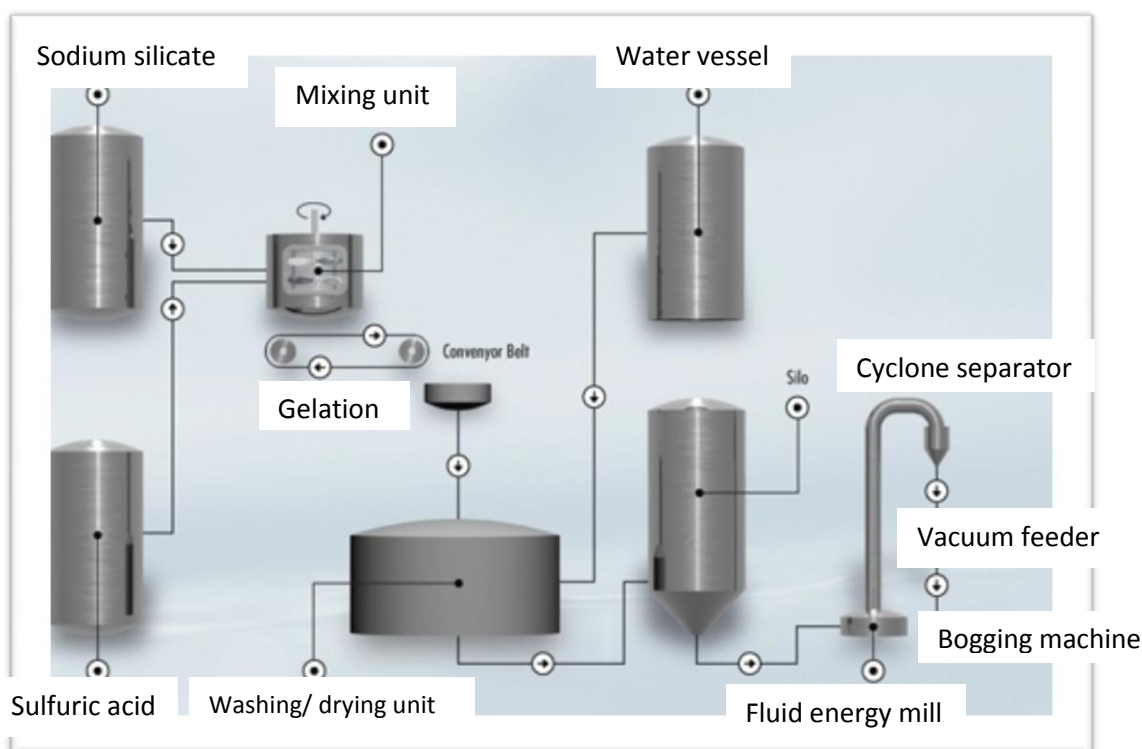


**Figure 1.2** W.R. Grace micronized silica gel production process <sup>6</sup>

### 1.3 Ordered Mesoporous Silica

Although amorphous mesoporous silica is widely used, the emergence of ordered mesoporous silica has become a very attractive class of materials with uniform mesopores in the range 20-500 Å as well as large surface areas ( $> 500 \text{ m}^2/\text{g}$ ). In 1992, the Mobil Oil Company developed this new class of periodic mesoporous silicas known as the M41S phase. These materials were characterized with large specific surface areas, ordered pore system and well defined pore radius, just like the microporous crystalline zeolites. However, unlike the zeolites, these M41S materials had pore diameters from 20-150 Å and exhibited amorphous pore walls. The most well known examples of this class of silica solids are the MCM-41, MCM-48 and MCM-50. As shown in the figure below, MCM-41 has a hexagonal arrangement of the mesopores, MCM-48 exhibits a cubic arrangement of the mesopores and MCM-50 shows a lamellar structure.

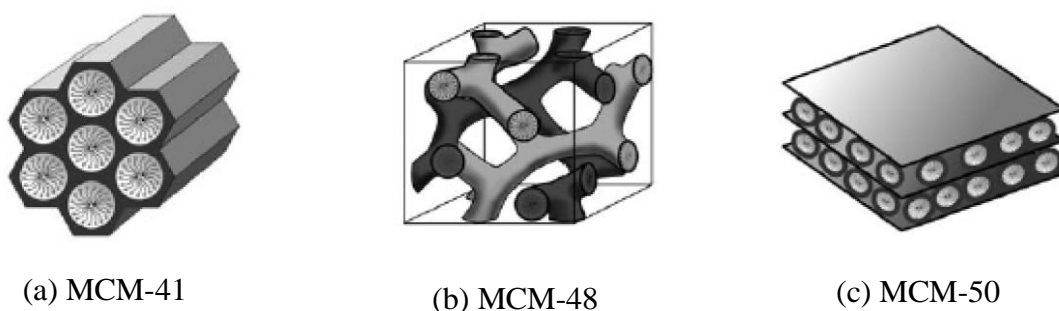
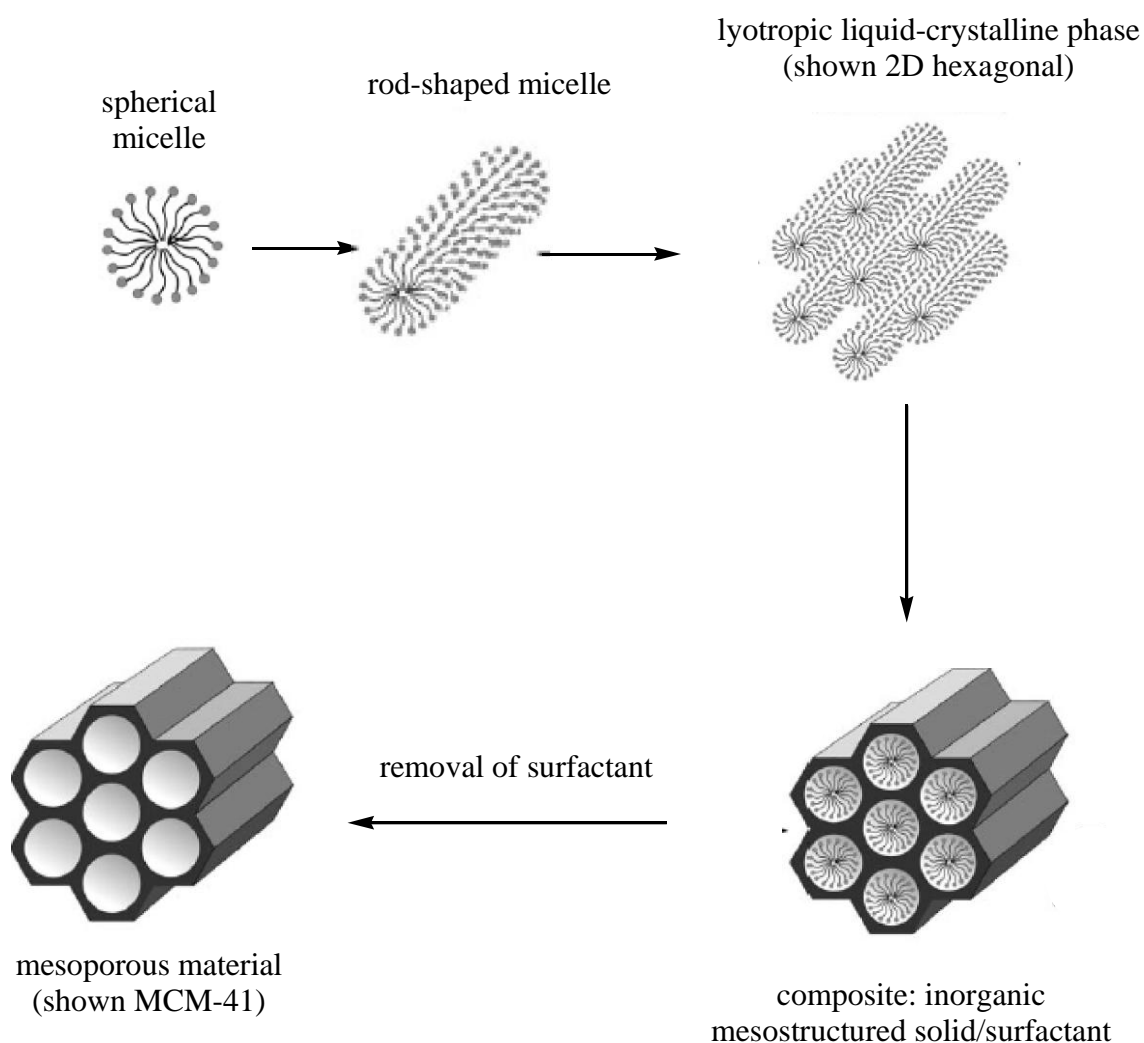


**Figure 1.3** Structure of mesoporous M41S materials: (a) MCM-41, (b) MCM-48 (c) MCM-50 <sup>8</sup>

These M41S materials were prepared by the use of supramolecular aggregates of ionic surfactants, such as long chain trimethylammonium chlorides, as structure directing agents (SDA). Under basic conditions, these SDAs in the form of a lyotropic liquid crystalline phase lead to the formation of an ordered mesostructure composite during the condensation of the silica precursors.



**Scheme 1.1** Formation of mesoporous materials by structure directing agents (SDAs) <sup>8</sup>

Removal of the surfactant by calcinations or extraction gives the mesoporous materials. A strong interaction between the template and the silica precursor is fundamentally important in order to ensure inclusion of the structure director without phase separation taking place in this method. Templating synthetic routes such as described here and shown in the figure above are classified as endotemplate methods or ‘soft templating methods’.

### 1.3.1 Templating methods

The preparation of mesoporous materials often involves the use of templates with geometry opposite to that of the derived product. There are two main classes of templates; ‘soft’ templates such as surfactants and block copolymers in solution and ‘hard’ templates such as porous silica and carbons. The void space areas are filled with a precursor chemical which is then fused together to form the product. Removal of the template is either by combustion or dissolution.

#### 1.3.1.1 *Soft templating methods*

A wide variety of ionic and non-ionic surfactants have been used to prepare materials with different porous and morphological characteristics. As described earlier, the M41S family of solids have been prepared using alkyl ammonium surfactants and TEOS or sodium silicate in a basic medium. The use of cationic surfactants in an acidic medium yielded the first type of SBA type materials with different mesostructures. The SBA family of solids have porous characteristics similar to M41-S type materials, however they exhibit larger pores of 50-300 Å. SBA-15 and SBA-16 were prepared using non ionic surfactants known as Pluronics derived of polypropylene oxide -polyethylene oxide triblock co-polymers in acidic medium.<sup>7</sup>

#### 1.3.1.2 *Hard templating methods*

In exotemplate or ‘hard’ matter templating methods, a porous solid is used as a template in place of the surfactant. An inorganic precursor is used to fill the hollow spaces of the exotemplate framework, which is then transformed under suitable conditions. A key issue in the processing of mesoporous materials with templates is that of the replication of the nanostructured template employed. ‘Hard’ templates such as silicas may only have partial filling of their pores before the material being templated condenses externally to the mesoporous scaffold. During nanocasting, the amount of pore filling varies in accordance with the deposition method employed and the infiltrate material.

The use of SDAs is clearly laborious and costly and particularly on an industrial scale. However ordered pore systems, especially those with narrow pore radius distributions have advantages in terms of transport properties. For example, these ordered mesoporous silica materials may be more suited to active compound release and transport (of insecticides and pharmaceuticals) than their amorphous counterparts.

#### 1.4 Synthesis of organically modified mesoporous silica

The combination of the properties of inorganic and organic building blocks present within a single material is a very attractive concept, in particular from the viewpoint of materials scientists. This would coalesce the huge array of organic functionality with the advantages of a thermally stable and robust inorganic component. Such a combination is of particular interest to the area of heterogeneous catalysis. The symbiosis of organic and inorganic components can produce materials whose properties differ greatly from those of the individual, isolated components. A real interest is the modification of the inorganic materials with organic functionalities, such as alcohols, thiols, amines, carboxylic and sulfonic acids which would allow, for example, reactions to be carried out on a stable, solid inorganic matrix.<sup>8</sup>

Organically modified silica can be prepared by three methods;

- (1) Grafting which is the subsequent modification of the pore surface of a purely inorganic silica material,
- (2) Co-condensation which is the simultaneous hydrolysis and condensation of silica and organosilica precursors
- (3) Production of Periodic Mesoporous Organosilicas (PMOs), the incorporation of organic groups as bridging components directly and specifically into the pore walls by the use of bis-silylated single-source organosilica precursors.

These methods have been discussed further below.

##### 1.4.1 Grafting method

This is the standard preparation technique for organic hybrid materials. The process is carried out by reaction of organosilanes  $(R'O)_3SiR$  with silanol groups of the pore surface of silica (**Scheme 1.2**). By this method, a variety of functional groups can be immobilized onto the silica surface by variation of the organic residue R. The main advantage of the grafting method is that, under the synthetic conditions used, the mesoporous character of the starting

silica phase is usually retained, with the lining of the pore walls experiencing a relatively small reduction in the porosity in the hybrid material, the extent of which is dependent on the size of the organic residue and the loading. The main disadvantage of the grafting method can be poor loading control; this can be variable and is affected by numerous factors.

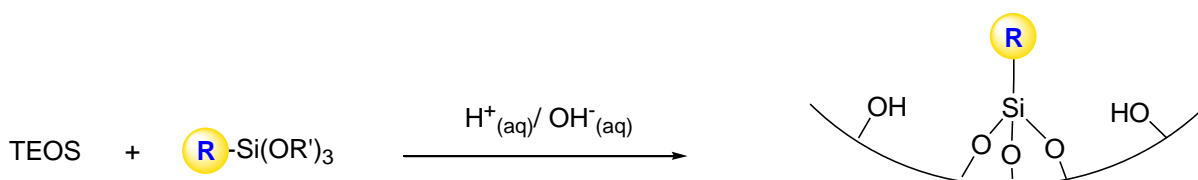


**Scheme 1.2** Grafting for organic modification of mesoporous pure silica with terminal organosilanes of the type  $(RO)_3SiR'$ , R= organic functional group

The density of surface silanol groups is of key importance and the choice of solvent and temperature can influence the extent of silane aggregate formation. Condensation of organosilanes at the pore openings during the initial stages of the synthetic process can limit diffusion of further silane into pores leading to a non homogeneous distribution of organic groups within the pores and possibly a lower degree of surface modification. In extreme cases, for example with bulky organic components, this can lead to pore blockage.

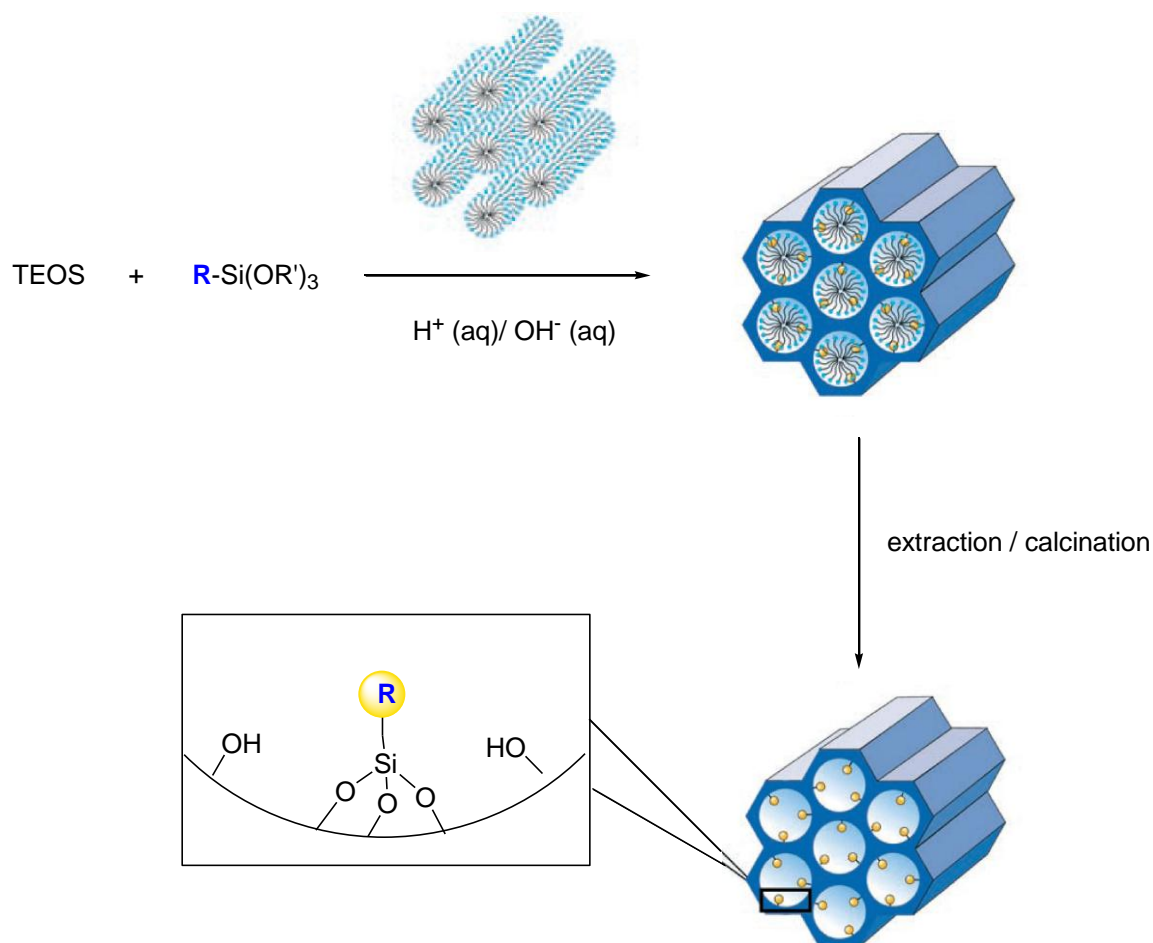
#### 1.4.2 Co-condensation method

The co-condensation method, or be it one pot synthesis or sol gel processing, involves the synthesis of a mesostructured silica phase, by the co-condensation of tetraalkoxysilanes  $(RO)_4Si$ , for example TMOS and TEOS, along with terminal trialkoxy organosilanes of the type  $(R'O)_3SiR$ , often in the presence of structure directing agents to give a material with organic residues anchored covalently to the pore walls (**Scheme 1.3**).



**Scheme 1.3** Co-condensation method for the organic modification of mesoporous silica phases (R=organic functionality)

The use of structure directing agents has been shown to afford organically modified silicas in such a way that the organic functionalities are projected into the pores (**Scheme 1.4**). As the organic functionalities are direct components of the silica framework, pore blocking is not a problem in the co-condensation method. Further, in this method, the distribution of the organic functionality is more homogeneous in comparison to the grafting method. However, a huge drawback in using this method is that with the increasing concentration of  $(R'O)_3SiR$  in the reaction mixture, the degree of ordered mesoporous character of the product decreases, resulting in disordered product. In addition, the proportion of terminal organic groups incorporated into the pore wall network is generally lower than would correspond to the starting concentration of the reaction mixture. This can be explained by the favoured homocondensation reaction with increasing  $(R'O)_3SiR$  in the reaction mixture in place of the cross linking co-condensation reaction with the silica precursor.

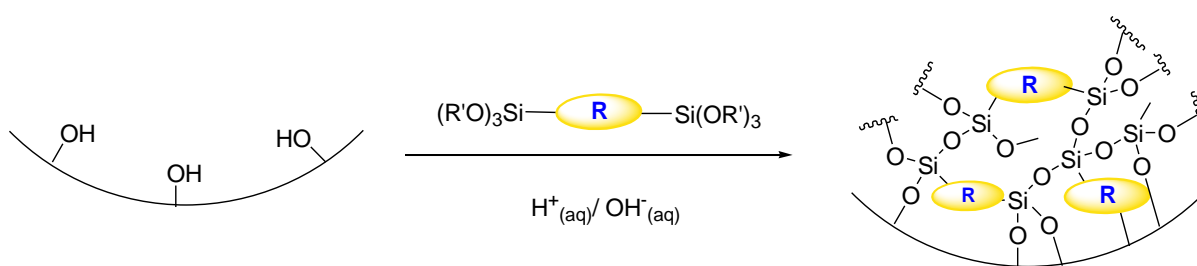


**Scheme 1.4** Co-condensation method with use of structure directing agents for organic modification of mesoporous pure silica phases (R= organic functional group).<sup>10</sup>

In addition, an increase in the loading of incorporated organic groups can lead to a significant reduction in pore diameter, pore volume and specific surface area. In the case of co-condensation reactions with the use of surfactants, care needs to be taken in the removal of the surfactant, in order to not destroy the organic functionality. For this reason only extractive methods can be used, and calcination is found to be an unsuitable method in most cases.

### 1.4.3 Synthesis Periodic Mesoporous Organosilanes

The synthesis of organic-inorganic hybrid materials by hydrolysis and condensation reactions of bridged organosilica precursors of the type  $(R'O)_3Si-R-Si(OR')_3$  has been known from sol gel chemistry for a long time.<sup>9</sup> The organic functionality in this case is embedded into the three dimensional network structure of the silica matrix via two covalent bonds and so distributed homogeneously into the pore walls. These materials can have large inner surface areas of  $1800 \text{ m}^2/\text{g}$  and excellent thermal stability.<sup>10</sup> However, they also exhibit a completely disordered pore system with a relatively wide distribution of pore radii. This problem can be overcome by modelling the concept of structure directing synthesis of pure silica mesophases by surfactants to the bisilylated organosilica precursors as described above and in doing so allowing the construction of a new class of mesostructured organic-inorganic hybrid materials, periodic mesoporous organosilicas. In these materials, the organic bridges are a central component of the silica network. In comparison to the amorphous aero- and xerogels, periodic mesoporous organosilicas are characterised by a periodically organised organic pore system and a very narrow pore radii distribution.



**Scheme 1.5** General synthetic route to periodic mesoporous organosilicas constructed from bisilylated organic bridging groups and silica.

Periodic mesoporous organosilica materials have been considered to be highly promising candidates for a series of technical applications including catalysis and active compound release systems.



## 1.5 Techniques for characterization of organically modified mesoporous silica

### 1.5.1 Introduction

The analysis of solid state materials can be a very complex task that requires several different techniques. These modified silica materials differ quite significantly from their starting alkoxy silane reagents in both physical and chemical characteristics. For example, the precursor starting materials are usually soluble monomers and the final product insoluble extended framework systems. In addition, due to the huge variety of preparation methods, the physical and chemical properties of solid state materials can cover a broad range, for example from nano particulate to bulk mesoporous materials.

A number of techniques are commonly used to characterise these modified silicas including solid state  $^{13}\text{C}$  NMR and  $^{29}\text{Si}$  NMR, IR spectroscopy, electron microscopy, porosimetry and elemental analysis. Some of these techniques are further described below.

### 1.5.2 Solid State NMR

Solid samples produce broad bands in their NMR spectra in comparison to samples measured by solution state NMR. This is a result of dipolar interactions and chemical shift anisotropy, wherein there is an incomplete averaging of the external magnetic field owing to the shielding created by other nuclei in the sample. These interactions are reduced by molecular motion owing to their angular dependence.

Spinning the solid at a magic angle of  $55^{\circ}54'$  recreates the molecular tumbling as found in solution and gives an averaged magnetic field. This so called magic angle is the angle at which the angular,  $\theta$ , dependence of the interactions goes to zero e.g.  $3\cos^2\theta - 1 = 0$

This effectively averages the dipolar interactions and eliminates the chemical shift anisotropy provided the spinning frequency is in close proximity to the frequency spread of the signal.

For spectra wherein, the spread of the frequency is particularly broad and the spinning rate cannot match the spread of the signal, a series of spinning side bands are observed. In this case, the spectrum is collected at two speeds where the spinning side bands move with changing speed but the central resonance remains fixed. In general MAS (magic angle spinning) NMR spectra take longer to acquire due to slower spin relaxation. For example, for nuclei such as Si, relaxation times between pulses can be between 120-600s.

### 1.5.3 $^{13}\text{C}$ and $^{29}\text{Si}$ NMR

Solid state  $^{13}\text{C}$  CP NMR can be used to confirm and identify the organic functionality within organically modified mesoporous silica. Solid state  $^{29}\text{Si}$  NMR can also be used to identify the chemical environment of a silicon atom within the silica framework. Such a technique is characterised by three parameters; chemical shift, peak intensity and line width. For silica the chemical shifts are usually in the range of -70 to -120 ppm. At the low field side of the spectrum, monomeric  $\text{Q}^0$  units are expected and from here a decrease in approximately 10 ppm relates to an additional Si-O-Si connection made to the central Si atom.

In solid state NMR, line broadening tends to increase from  $\text{Q}^0$  to  $\text{Q}^4$  reflecting the increasing internuclear interactions for the different silicon environments. The intensities of the signals are generally proportional to the number of corresponding atoms and so integration of these peaks give the distribution of the different structural sites.<sup>11</sup>

$^{29}\text{Si}$  can also be used to measure the degree of condensation of organically modified silica. The extent of this can be determined by the intensity of the given T-substructures. The terminal structural units of siloxane precursors, have three functional groups responsible for condensation reactions, giving rise to signals,  $\text{T}^1$ ,  $\text{T}^2$  and  $\text{T}^3$ . The  $\text{T}^1$  units contain two residual methoxy groups, the  $\text{T}^2$  units contain one residual methoxy group and the  $\text{T}^3$  units indicate that all three methoxy groups take part in the condensation reaction.<sup>12</sup> These peaks appear in the range at -55 to -75 ppm respectively.

### 1.5.4 Pulse sequence experiments (dipolar dephasing and $\text{T}_1$ measurements)

Dipolar Dephasing experiments use the differences found in the strength of C-H dipolar coupling to provide the distinction between protonated and non-protonated carbon atoms, and molecularly rigid and mobile carbons. In dipolar dephasing experiments, the high power proton decoupler is turned off for a short period (the Dephasing delay) between polarisation and detection, during which time  $^{13}\text{C}$  signal is lost through  $\text{T}_2$  broadening. The rate of signal loss is dependent on the strength of C-H dipolar coupling, which is primarily determined by the proximity of the closest proton neighbours. Non protonated carbons dephase more slowly than carbons with directly attached protons, where little signal is observed after 40-60 $\mu\text{s}$ . Molecular motion is a complicated subject; methyl groups dephase slowly despite the presence of three attached protons, as rapid rotation largely diminishes the strength of

coupling. The extent of the  $^{13}\text{C}$  magnetization is mainly determined by the dipolar interaction between the  $^{13}\text{C}$  nuclei and the nearest surrounding proton environment system. Dipolar Dephasing experiments show that the carbon environments with sharp resonances are diminished to a greater extent than those associated with broad resonances. In this work the focus is on different methylene  $\text{CH}_2$  environments and the expectation is that those with stronger dipole coupling would diminish to a greater extent in a dipolar dephasing experiment and build up intensity faster in the contact time variation experiments.

Spin lattice relaxation times,  $T_1$ , provide information about dynamic behaviour for a given structure. Information on the mobility and molecular packing that is on the presence of rigid and mobile regions within a material can be determined. Spin lattice relaxation times are governed by three possible relaxation mechanisms,  $^{13}\text{C}$ - $^1\text{H}$  dipole-dipole interactions, chemical shift anisotropy and spin-spin rotation interactions; the first of these is expected to be the predominant for protonated carbons.

The correlation time,  $\tau_c$ , is the average time a molecule spends in a given orientation and the spin lattice relaxation rate,  $R_1$  ( $1/T_1$ ) can be related to the correlation time  $\tau_c$  through the equation below.

$$R_1 = \hbar^2 \gamma_c^2 \gamma_H^2 r^{-6} \tau_c N \quad \text{Equation (1)}$$

$\gamma_c$  and  $\gamma_H$  are the gyromagnetic ratios for the  $^{13}\text{C}$  and  $^1\text{H}$  nuclei respectively,  $r$  is C-H internuclear distance,  $N$  is the number of protons on the carbon and  $\hbar = h/2\pi$ , where  $h$  is Planck's constant.

The molecular motion influences  $R_1$  through  $\tau_c$ , and so  $R_1$  is a probe for molecular dynamics. The correlation time can be calculated by simplifying **Equation (1)** to the following.<sup>1</sup>

$$\tau_c = r^6 / K T_1 N \quad \text{Equation (2)}$$

$$\text{Whereby} \quad r = 1.09 \text{ \AA}, \quad K = 3.56 \times 10^{10} \text{ \AA}^6 \text{sec}^{-2},$$

Through analysis of the relaxation times of a given chemical environment, the rigid and flexible components of a molecule can be estimated.

### 1.5.5. Porosimetry

A key characterisation technique of porous materials derives from the use of nitrogen sorption data determined at liquid nitrogen boiling temperature. Construction of an adsorption-desorption isotherm can give a good understanding of surface area and porosity of an adsorbent. An adsorption isotherm is obtained by measuring the quantity of nitrogen on a surface over a wide range of relative pressures at constant temperature. By feeding the mesoporous material successive known volumes of nitrogen and measuring the equilibrium pressure, the adsorption isotherm is obtained point by point. Desorption isotherms can be obtained by measuring the quantities of gas removed from the sample as the relative pressure is lowered.

Adsorption isotherms are plots of the amount of gas adsorbed at equilibrium as a function of the partial pressure  $P/P_0$  at constant temperature; the gas is usually nitrogen at its boiling point (77.4K). The obtained isotherms can generally be grouped into five classes, the characteristic features of which are shown in the figure below (**Figure 1.4**). Isotherm type I is typically the result of microporous materials (pore sizes  $<20\text{\AA}$ ). Type II isotherms are typical for non-porous materials and type III and V isotherms are gained from very weak adsorption interactions of which the fundamentals are not very well understood. Type IV isotherms are generally obtained from mesoporous materials.

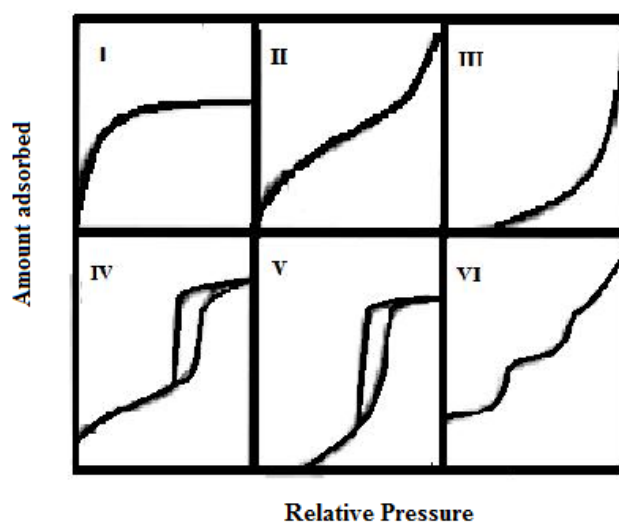


**Figure 1.4** Types of sorption isotherms

The ‘loop’ or hysteresis shown by the adsorption-desorption data can be explained by the Kelvin equation (see **Appendix 1**). The Kelvin equation relates relative pressure to pore

radius and since adsorption and desorption behaviour at curved surfaces will differ from that at planar surfaces so the extent of desorption from pore walls can differ from the extent of adsorption at fixed relative pressure of adsorbate.

Hysteresis loops may exhibit a wide range of shapes (**Figure 1.5**). Type H1 shows the two branches of the hysteresis loop almost vertical and nearly parallel over a given range of gas uptake. In the case of type H4, the two branches remain horizontal and parallel over a wide range of  $P/P_0$ . An important point to note is that closure of the hysteresis loop occurs at relative pressure of 0.42 when nitrogen is the adsorbate.

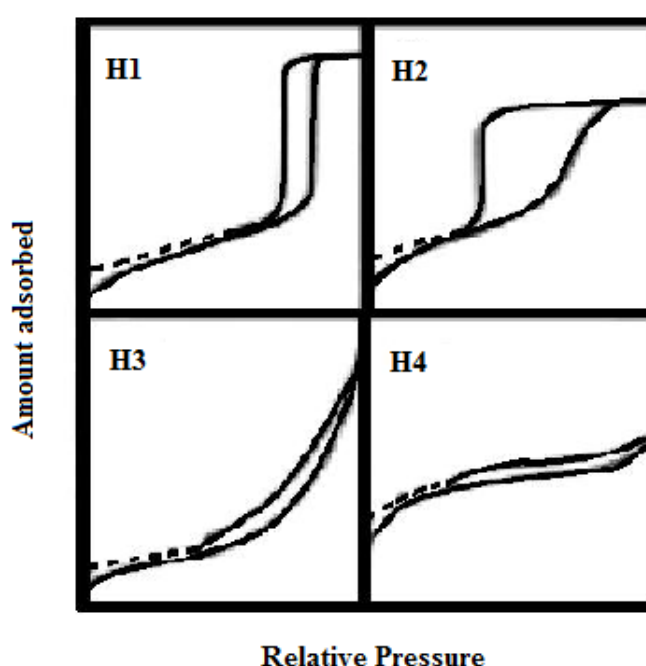


**Figure 1.5** Types of hysteresis loops

Type H1 is usually associated with porous materials, often with narrow distribution of pore sizes. This type of hysteresis loop is given by open ended cylindrical pores. Type H2 is said to be associated with ink bottle neck pores, with loop shape arising from the difference in mechanism in the condensation and evaporation. Type H3 is associated with slit shaped pores while type H4 is often associated with narrow slit like pores.

With many systems, low pressure hysteresis (as indicated by the dashed lines in **Figure 1.5**) may be observed at the lowest attainable pressure. Such a phenomenon may be linked to the swelling of non rigid porous structure or with the irreversible uptake of gas molecules in the pores or through entrances of the same width as the adsorbate molecules.

### 1.5.6 Electron Microscopy

TEM (transmission electron microscopy) analysis is a technique which provides information about the topography (surface features, textures and visual concept), morphology (shape and size of particles) and composition of a given material being analysed. The technique works by focusing a beam of electrons onto a thin specimen deposited on a transparent carbon grid and the transmitted part of the beam is subsequently captured and converted to an image. Transmission electron microscopy (TEM) can give structural information over a wide range of magnifications. Further information on the chemical composition can be obtained from Energy Dispersion Spectroscopy (EDS).

### 1.6 Catalytic applications of organically modified mesoporous silica

As described earlier, mesoporous silica materials show high surface areas, high pore volumes, and uniform pore diameters.<sup>13</sup> Thus it is these highly desirable properties that find these materials applied in many different research fields. For example, mesoporous materials are often used in the area of catalysis as heterogeneous catalysts, for enzyme immobilization, chromatography column development, polymer reinforcement and synthesis of raw materials by using them as templates.<sup>14</sup>

Organically modified silica catalysts possess properties that render them extremely effective solid phase catalysts. These materials possess excellent mechanical, chemical and thermal stability as well as showing broader solvent and operating stability. Many researchers have focused on immobilising a single functional group onto the silica surface, most often this functional group being a potential ligand for a metal or metal complex. There are three main strategies undertaken to immobilise homogeneous catalysts onto silica supports. These include adsorption, entrapment and covalent immobilisation (as described before). Adsorption relies on Van der Waals interaction between the catalyst and the support and as this is only a weak interaction this can often lead to leaching of the active catalyst into solution. Encapsulation is a rather elegant technique in which the catalyst is much larger than the size of the pores and is usually assembled within the pores of a support. In such a system there is no interaction between the active catalyst and the support, which means there is no change in the ligand electronic properties or conformation. However, the assembly of such

systems can be rather complex. Covalent tethering of functionalities is undoubtedly the preferred method of immobilisation as this method produces very stable catalysts.

### 1.5.1 Heterogeneous catalysis

In heterogeneous catalysis, phase boundaries are present between the catalysts and the reactant. In homogeneous catalysis, starting reactant material and catalysts are in the same phase, thus homogeneous catalysts have a higher degree of dispersion than heterogeneous catalytic systems. The individual active sites are all accessible in the homogeneous systems. However, in the case of heterogeneous systems, only surface functionality are generally active.

Further, a higher degree of dispersion in homogeneous catalysts means that these systems exhibit greater activity per unit mass of metal than the heterogeneous catalysts. Consequently, the greater mobility of the catalytic molecules in the reaction media means that the number of collisions with substrate molecules is increased. Approach to the catalytically active centre can be from any direction and activity at one active centre does not inhibit possible activity at neighbouring sites. Thus, lower catalyst concentrations at milder reaction conditions can be employed.

The great advantage however, of the heterogeneous catalytic systems is the easy separation of the solid catalyst from the liquid reaction media and hence the ease in catalyst re-use. This is undoubtedly a very paramount feature of heterogeneous systems. Homogeneous systems often require laborious and lengthy procedures to recover the active catalysts and as a result this makes recycling and re-use difficult. Some examples of organically modified catalysts and the activity in organic transformations are described in the text below.

### 1.5.2 Acid catalysis

Acid catalysts prepared via the grafting method have received much attention. These heterogeneous catalysts, analogous to Bronsted acidic zeolites, have larger pores that would be able to incorporate larger substrates. The immobilisation of sulfonic acid derivatives onto MCM-41 and MCM-48 materials by Das *et al.* is relevant in this context.<sup>15</sup> Propylthiol groups were initially immobilized and these were then converted to propylsulfonic acid groups under mild oxidative conditions employing hydrogen peroxide. Shimizu *et al.* also reported on the modification of FSM-16 and SBA-15 materials via this pathway as well.<sup>16</sup> These solid state acid catalysts gave high activity in the acetylation of acetophenone with

ethylene glycol and in the preparation of di-butyl ether from 1-butanol in a dehydration reaction.

### 1.6.3 Enantioselective dihydroxylation

Organically modified mesoporous silica phases have also proven to be excellent catalytic systems for enantioselective conversions as reported by Motorino and Crudden.<sup>17</sup> The authors report on using SBA-15 functionalised with a cinchona derivative, as prepared by the grafting method, for the asymmetric dihydroxylation of olefins under Sharpless conditions and successfully achieved enantioselectivities (up to 99%) that were identical to those obtained by the corresponding homogeneous systems.

### 1.6.4 Organic transformations with metal loaded organically modified silica phases

So far the examples described have been without the use of immobilised metals on the support. Organically modified silica complexed with precious metals is a key area of research interest particularly in the pharmaceutical industry wherein many of the reactions employed to synthesize APIs are catalysed by metals. The use of homogeneous systems leads to retention of precious metal in target products. Aside from the additional purification steps taken to form metal-free product, the loss of often expensive catalysts is a further issue. Thus metal loaded organically modified silicas are sustainable alternatives as catalysts for a number of organic transformations.

The Pd catalysed Sonogashira reaction has emerged recently as an important synthetic procedure for the synthesis of alkynes.<sup>18</sup> The preparation of aryl alkynes has found importance in the materials sector as well as with the synthetic chemists because of their presence in many natural bioactive products. A recent contribution by Li and Wang reports on the excellent activity of aminopropyl modified silica with palladium, prepared via the grafting method, in the Sonogashira cross coupling reaction of electron rich and electron poor aryl bromides with alkynes without the need for phosphine ligands or copper promoters, with yields obtained from 85-98 %.<sup>19</sup> The total reaction times were 8 hours and these reactions were carried out at 100 °C, employing 0.01 mol % Pd, which is very low indeed. Further, the authors report that the catalyst was simply filtered and separated from the reaction mixture and used 30 times consecutively without loss in activity.

The Mizoroki-Heck reaction is one of the most comprehensively used reactions for carbon-carbon bond formation. Mercaptopropyl-modified SBA-15 palladium catalysts were found to



be highly active catalytic systems for the cross coupling reactions of styrene and aryl bromides employing 2 mol % Pd.<sup>20</sup> Reactions were carried out at 120 °C and quantitative conversions were reported. Leaching tests revealed negligible amounts of palladium in solution, and further tests for heterogeneity demonstrated the heterogeneous nature of these systems. More recently, Jana *et al.* report on excellent activity and high TONs demonstrated by Pd(0)-MCM-41 catalysts in the Mizoroki-Heck reactions of aryl bromides and the more difficult aryl chlorides.<sup>21</sup> Further examples of organically modified silica phases incorporating palladium are described in chapter 3.

### 1.7 Conclusions

In the area of catalysis, the activity of organically modified silica catalysts prepared from amorphous silica and those prepared with SDAs generally give comparable activity (see literature review in chapters 3, 4 and 5). In addition, for silicas prepared in the absence of SDAs, the grafting method, as opposed to co-polycondensation, is the most suitable technique for organic modification as this avoids extensive homocoupling of alkoxy silanes and ensures that parent material pore size distribution is retained.

Metal loaded organically modified systems are promising catalysts for a number of organic transformations owing to their high surface areas and narrow pore size distribution. To attain good heterogeneous catalysts, a number of desired properties are required. Firstly, chemically strong immobilisation of active species to the silica supports. This restricts leaching of metal into solution and secondly allows for catalyst re-use. Further catalyst activity is usually required to be comparable to homogeneous counterparts. Although in some cases heterogeneous catalytic systems have been reported to show higher activity, often catalytic activity is found to be more sluggish with heterogeneous catalysts. Organic transformations should be accomplished with very low metal mol% as this avoids metal leaching into products, limits costs of metal recovery and hence reduces overall costs. Although heterogeneous catalysts have their fair share of drawbacks, the choice of parameters such as choice of functional group and loading, choice of metal and loading, as well as reaction conditions, such as choice of solvent or base and reaction temperatures can effectively optimise the catalytic activity so that it at least mirrors the catalytic activity demonstrated by the homogeneous counterpart.

This thesis contains a series of catalysis studies of commercially sourced mesoporous silicas subsequently organically modified with ligands having high affinity for precious metals.

Thus organic functionality with soft donor atoms sulfur or phosphorus were chosen and important organic transformations typically catalysed by precious metal complexes or impregnated materials e.g. carbon-carbon coupling, hydrogenation and hydroformylation were studied. Data was generated from a range of experimental work to give further insight about the actual and relative performance of the catalysts including; outcome of variations in reaction conditions, changes in material texture, influence of pore size, influence of metal and metal loading, metal redox changes, mobility of surface species and relative affinity of supports for metal. These studies are presented in the following chapters and the data generated rationalised in its context.

## 1.8 References

- <sup>1</sup> J. Rouquerol, D. Avnir, C. W. Fairbridge, D. H. Everett, J. H. Haynes, N. Pernicone, J. D. F. Ramsay, K. S. W. Sing and K. K. Unger, *Pure & Appl. Chem.*, 1994, **66**, 8, 1739-1758;
- <sup>2</sup> K. S. W. Sing, D. H. Everett, R. A. W. Hall, L. Moscou, R. A. Pierotti, J. Rouquerol and T. Siemieniewska, *Pure & Appl. Chem.*, 1985, **57**, 4, 603;
- <sup>3</sup> T. Yanagisawa, T. Shimizu, K. Kuroda and C. Kato, *Bull. Chem. Soc. Jpn.*, 1990, **63**, 988; J. S. Beck, J. C. Vartuli, W. J. Roth, M. E. Leonowicz, C. T. Kresge, K. D. Schmitt, C. T. W. Shu, D. H. Olson, E. W. Sheppard, S. B. McCullen, J. B. Higgins and J. L. Schlenker, *J. Am. Chem. Soc.*, 1992, **114**, 10834;
- <sup>4</sup> Y. Yamauchi, N. Suzuki, L. Radhakrishnan and L. Wang, *Chem. Rec.*, 2009, **9**, 321-339;
- <sup>5</sup> J. Clayden, N. Greeves, S. Warren and P. Wothers, *Organic Chemistry*, Oxford University press, 2001;
- <sup>6</sup> [www.grace.com/EngineeredMaterials/MaterialSciences/SilicaGel/SilicaGelProduction.aspx](http://www.grace.com/EngineeredMaterials/MaterialSciences/SilicaGel/SilicaGelProduction.aspx)
- <sup>7</sup> D. Zhao, J. Feng, Q. Huo, N. Melosh, G. H. Fredrickson, B. F. Chmelka and G. D. Stucky, *Science*, 1998, **279**, 548; D. Zhao, Q. Huo, J. Feng, B. F. Chmelka and G. D. Stucky, *J. Am. Chem. Soc.* 1998, **120**, 6024;
- <sup>8</sup> F. Hoffman, M. Cornelius, J. Morell and M. Froba, *Angew. Chem. Int. Ed.*, 2006, **45**, 3216-3251;
- <sup>9</sup> H-S. Xia, C-H. (Clayton) Zhou, D. S. Tong and C. S. Li, *J. Porous Mater.*, 2010, **17**, 225-252;
- <sup>10</sup> D. A. Loy and K. J. Shea, *Chem. Rev.*, 1995, **95**, 1431-1442; K. J. Shea and D. A. Loy, *Chem. Mater.*, 2001, **13**, 3306-3319;
- <sup>11</sup> N. Suyah, D. Hoebbel, M. Mennig and H. Schmidt, *J. Mater. Chem.*, 1999, **9**, 3061-3067;
- <sup>12</sup> Q. G. Zhang, Q. L. Liu, F. F. Shi and Y. Xiong, *J. Mater. Chem.*, 2008, **18**, 4646-4653;
- <sup>13</sup> G. J. D. A. A. Soler-Illia, E. L. Crepaldi, D. Grosso and C. Sanchez, *Curr. Opin. Colloid Interface Sci.*, 2003, **8**, 109;
- <sup>14</sup> (a) L. F. Giraldo, B. L. Lopez, L. Perez, L. Perez, S. Urrego and L. Sierra, M. Mesa, *Macromol. Symp.*, 2007, **258**, 129-141; (b) C. Mateo, J. M. Palomo, G. Fernandez-Lorente, J. M. Guisan and R. Fernandez-Lafuente, *Enzyme Microb. Technol.*, 2007, **40**, 1451-1463; (c) C. Jayasuriya and J. Premachandra, "Physical Properties of Polymers handbook", Springer, New York, 2007, 551; (d) J. Lee, J. Kim and T. Hyeon, *Adv. Mater.*, 2006, **18**, 2073;

- <sup>15</sup> D. Das, J-F. Lee and S. Cheng, *J. Catal.*, 2004, **223**, 152-160; D. Das, J-F. Lee and S. Cheng, *Chem. Commun.*, 2001, 2178-2179;
- <sup>16</sup> K. Shimizu, E. Hayashi, T. Hatamachi, T. Kodama, T. Higuchi, A. Satsuma and Y. Kitayama, *J. Catal.*, 2005, **231**, 131-138;
- <sup>17</sup> I. Motorino and C. M. Crudden, *Org. Lett.*, 2001, **3**, 2325-2328;
- <sup>18</sup> (a) F. Diederich and P.J. Stang, "Metal-Catalysed Cross-Coupling Reactions", VCH, Weinheim, 1998; (b) N. Yoneda, S. Matsuoka, N. Miyaura, T. Fukuhara and A. Suzuki, *Bull. Chem. Soc. Jpn.*, 1990, **63**, 2124;
- <sup>19</sup> P.-H. Li and L. Wang, *Adv. Synth. Catal.*, 2006, 348, 681;
- <sup>20</sup> C.M. Crudden, M. Sateesh and R. Lewis, *J. Am. Chem. Soc.*, 2005, **127**, 10045;
- <sup>21</sup> S. Jana, B. Dutta, R. Bera and, S. Koner, *Inorg. Chem.*, 2008, **47**, 5512.

## Chapter Two

# Organically Modified Mesoporous Silica; Synthesis, Characterisation and Palladium uptake

### 2.1 Introduction

Many novel functional silica materials have been developed by the Sullivan research group at Queen Mary University of London. In particular, phosphonate and phosphonic acid ligands immobilised on silica **silica-60-PO(OH)<sub>2</sub>** have been found to be useful for a number of organic transformations (**Figure 2.1**).<sup>1</sup> When used in the acid form, these systems can serve as effective acid catalysts and when derivatised with metals such as cerium and vanadium, they are found to selectively oxidise sulphides to sulfoxides.<sup>2</sup> In addition, silica immobilised mercaptophenyl sulfonic acids **silica-60-PhSO<sub>3</sub>H** have shown to be excellent solid acid catalysts for esterification and transesterification processes.<sup>3</sup>

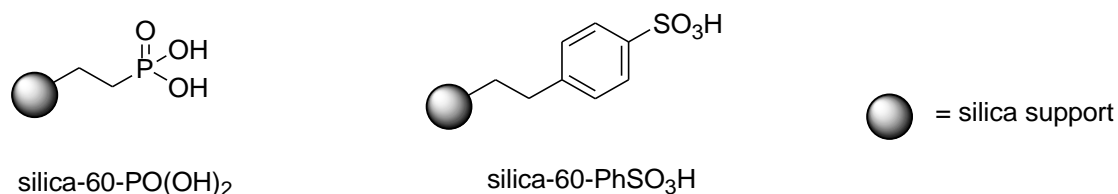
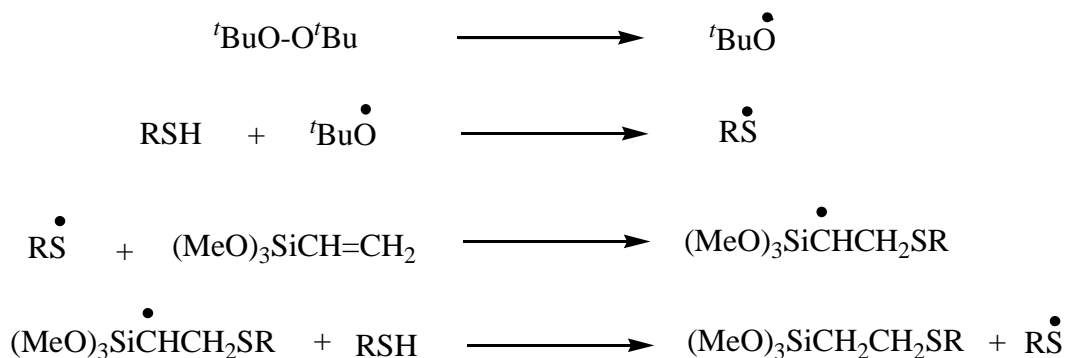


**Figure 2.1.** Silica supported phosphonic acid, **silica-60-PO(OH)<sub>2</sub>** and silica supported sulfonic acid, **silica-60-PhSO<sub>3</sub>H**

These organically modified materials were prepared by the method of grafting, following the general synthetic route as shown in **Schemes 2.1** and **2.2**. The grafting method involves the modification of the pore surfaces of an inorganic silica material with an organic group. Such a process is carried out by reaction of silica surface silanol groups with an appropriate organosilane, such as trimethoxysilane or triethoxysilane, in a suitable solvent, usually toluene at reflux. By using such a method, the structure of the silica framework remains intact.

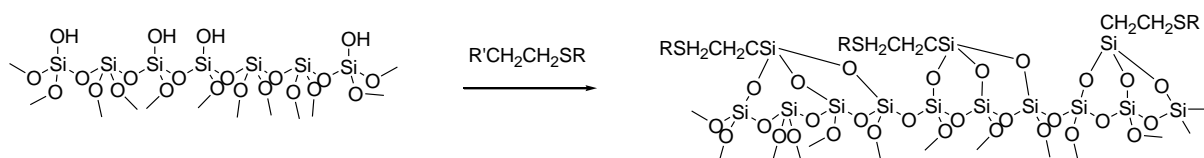
In this chapter the synthesis of novel sulfur based silica immobilised ligands is described. These systems have been designed with high affinity for precious metals such as Pd in mind

making them effective for use in important metal catalyzed reactions. A general synthetic route is shown in **Scheme 2.1** for peroxide catalysed addition reactions involving alkenyl silanes that lead to organotrialkoxysilane compounds suitable for surface modification of silica. Thus mercaptans can react with alkenylsilanes to give thioethers. A number of compounds can be developed depending on the choice of mercaptan and alkenyl silane used.



**Scheme 2. 1.** Free radical transfer addition of a mercaptan to an olefin.

The second step involves the hydrolysis and co-condensation of the organotrialkoxy silane and silica surface silanols; in this step functional groups are introduced to the pore surface (**Scheme 2.2**). This occurs via the reaction of the surface silanol groups of the silica with the alkoxy groups of the linker–ligand compounds usually at the solvent reflux temperature. The reaction between organo trialkoxysilanes and the surface silanol group is facilitated by the *in situ* reaction with water adsorbed on the silica surface. The choice of solvent is important; toluene is used as it limits the formation of oligomers from the alkyl silane reagents.<sup>4</sup>



**Scheme 2.2.** Co-condensation reaction of surface silanol groups and organoalkoxysilane compounds. R' = trialkoxysilyl

## 2.2. Characterisation of Silica-60Å

### 2.2.1. Porosimetry Studies

The silica used for these studies was commercially available from W. R. Grace & Co. With particle size 100-200  $\mu\text{m}$ , with average pore sizes of 60 Å unless otherwise stated. Porosimetry studies revealed this silica to have a surface area of  $551\text{m}^2/\text{g}$ , pore volume of  $0.791\text{cc/g}$  and an average pore diameter of 63 Å.

The sorption isotherm obtained for silica-60 clearly shows the mesoporous nature of the material (type IV isotherm). In addition, the shape of the hysteresis loop obtained reveals the pores to be of ink bottle shape according to the IUPAC classification.

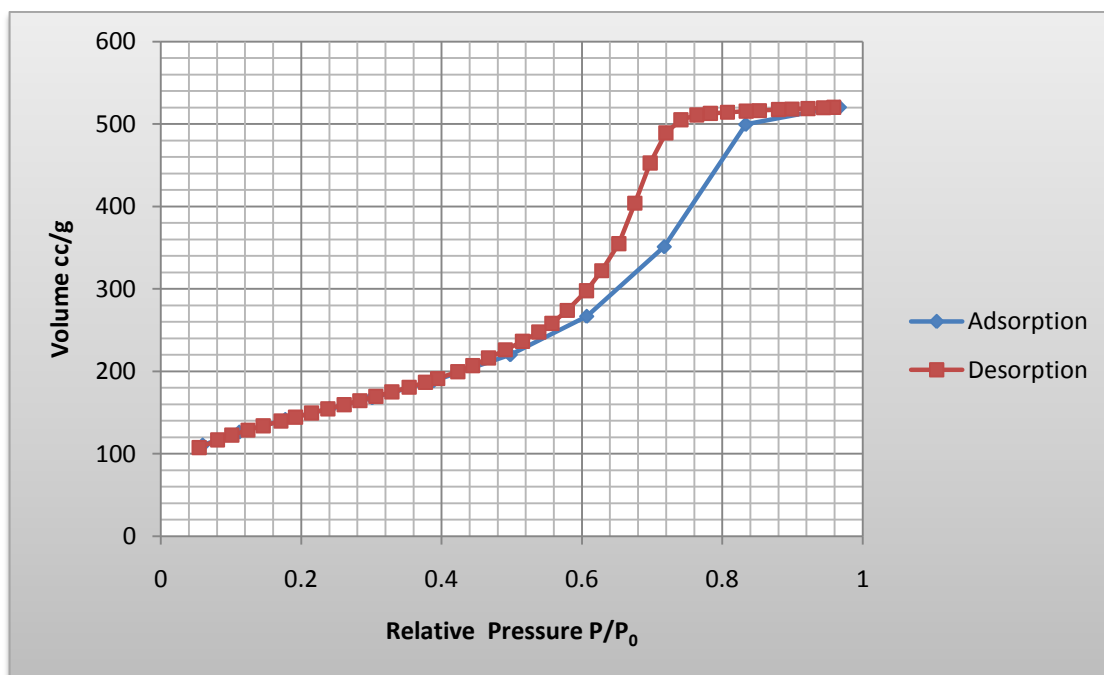


**Figure 2.2** Sorption isotherm for silica-60

Further to this the pore size distribution of silica-60 was also obtained. This revealed the pore sizes to range largely between 50-75 Å, with an overall distribution ranging from 30-90 Å (**Figure 2.3**).

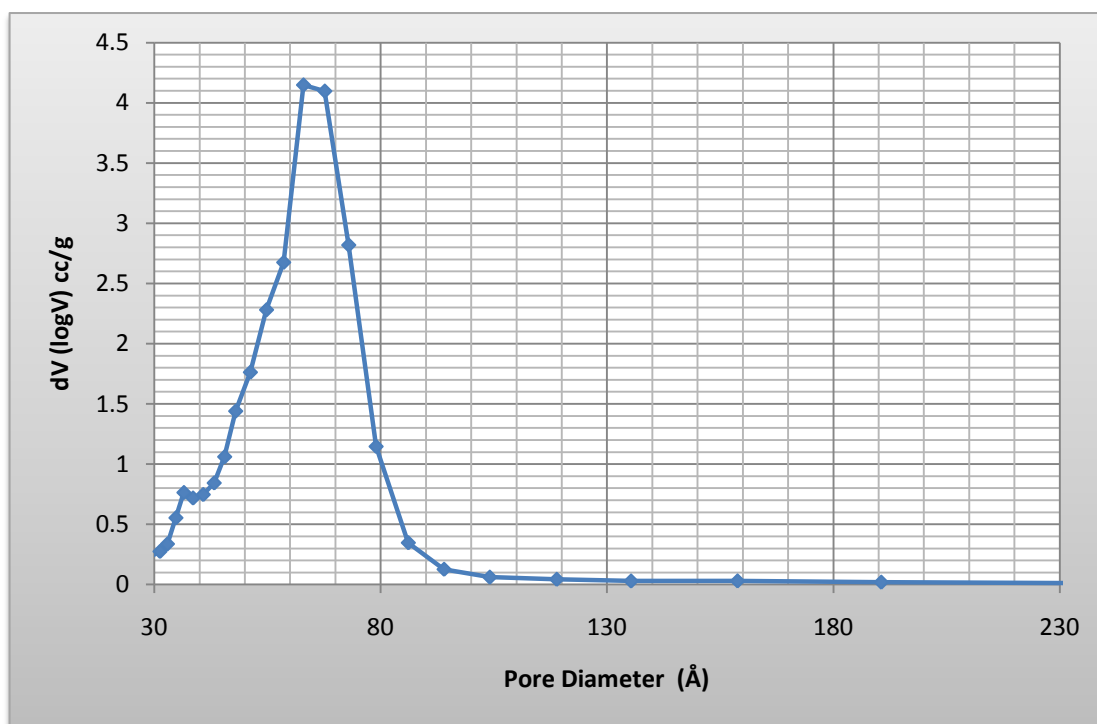


**Figure 2.3** Pore size distribution chart for silica-60

### 2.2.2. Determination of silanol groups in silica-60Å

The quantification of silanol groups on silica-60Å was determined by following a procedure from Sierra *et al.*<sup>5</sup> The nature and concentration of silanol groups present on unmodified silica-60Å was studied by exposing the material to pyridine vapours and then analysing the materials by thermogravimetric analysis (TGA) (**Appendix 3**). Silica-60Å was dried overnight at 200 °C in an oven to ensure the sample was dry before being exposed to pyridine vapours. In addition, during the experiment, the silica particles were spread out to maximise contact between the silica particles and the pyridine vapours. The TGA graph of silica-60 Å after pyridine adsorption is shown below (**Figure 2.4**).

As reported by Harnes *et al.*, the TGA graph for amorphous silica shows two pyridine desorption peaks in the range of 50-170 °C.<sup>6</sup> The first peak, seen at 50-100 °C is associated with pyridine interacting with hydrogen-bonded SiOH groups. The second peak, observed at 120-170 °C is associated with pyridine desorbed from free SiOH groups. In the TGA graph below we can see desorption in the temperature range at 50 °C to 170 °C. The first and second steps correspond to pyridine desorption from hydrogen bonded SiOH groups and free SiOH groups respectively. The tailing of the desorption is inherent to this type of material, as desorption of pyridine is occurring from a range of pore sizes.



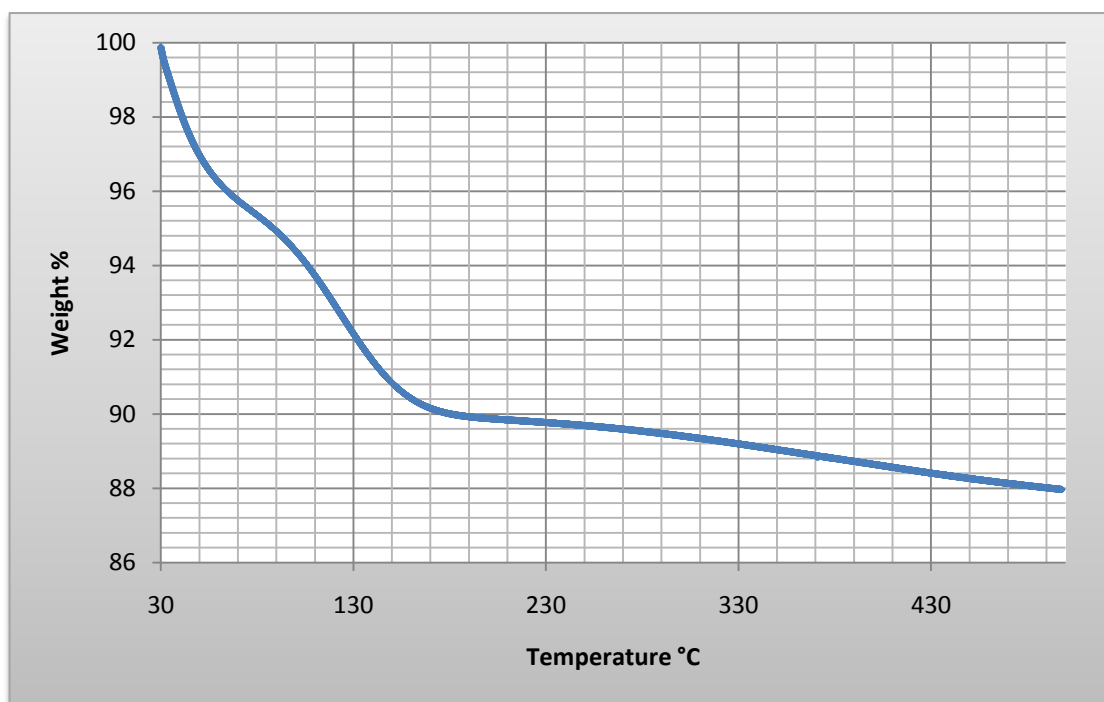


**Figure 2.4.** TGA graph for silica-60Å after pyridine adsorption total 10% loss

If the assumption is made that one pyridine interacts with one silanol group, the number of surface hydroxyl groups can be calculated. From the TGA graph, a total of 10% weight loss is observed. The total loading of silanol groups on silica-60Å was calculated as 1.5 mmol/g, with approximately 0.65 mmol/g of the hydroxyl groups being hydrogen bonded SiOH groups and 0.85 mmol/g of the hydroxyl groups from free SiOH groups. The experiment was run a second time, taking less silica (0.1 g instead of 1 g), in order to ensure maximum exposure to the pyridine atmosphere. The loading of the silanol groups was calculated as 1.5 mmol/g, which is similar to that from the first experiment. For further notes see **Appendix 3**.

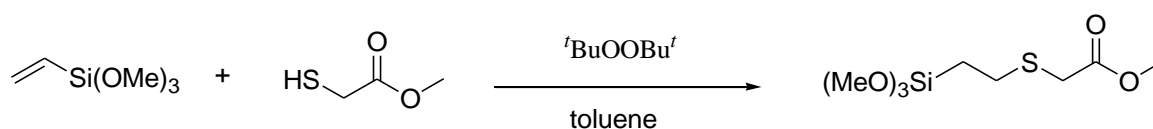
## 2.3. Synthesis and characterisation of silica immobilised sulfur based ligands

### 2.3.1. Synthesis of silica ethyl thioglycolic acid, silica-60-G<sub>1</sub>

The first of the silica supported sulfur based ligand materials developed was silica ethyl thioglycolic acid, **silica-60-G<sub>1</sub>**. The thioglycolic acid moiety was selected firstly because of the high affinity that sulfur atoms display for precious metals such as Pd. In addition the carboxylate moiety provides further coordination sites that can lead to a five membered ring

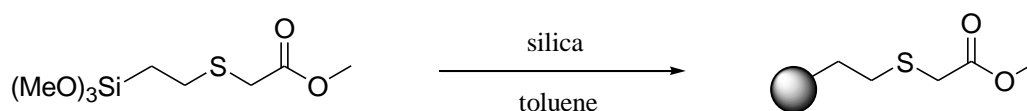
chelate. Indeed thioglycolate coordination compounds are known to have this type of metal to ligand interaction.<sup>7</sup>

The first step in the synthesis of **silica-60-G<sub>1</sub>** was to form the linker compound with the thioglycolate fragment, formally trimethoxysilylethylsulfanyl-acetic acid methyl ester, as shown in **Scheme 2.3**. This was achieved relatively easily. Trimethoxyvinylsilane was reacted with methyl thioglycolate in toluene with the addition of di-*tert*-butyl peroxide by a radical reaction. The reaction mixture was heated to 115 °C under an atmosphere of nitrogen for 1 hour to give the desired product.



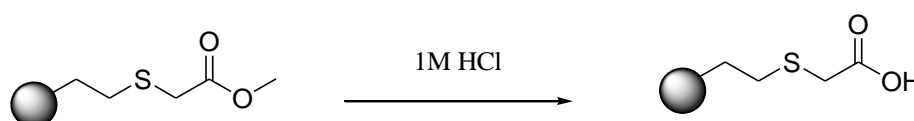
**Scheme 2.3.** Free radical reaction of vinyl trimethoxysilane and methyl thioglycolate

The next step involved tethering trimethoxysilyl compound to the silica surface, **Scheme 2.4**. This was done by stirring trimethoxysilylethylsulfanyl-acetic acid methyl ester and silica in toluene at the reflux temperature. After cooling, the solid was filtered and washed thoroughly with methanol.



**Scheme 2.4.** Synthesis of methylthioglycolate silica.

Further modification of the silica supported thioglycolate fragment to the corresponding acid was achieved by stirring this material in hydrochloric acid (1M) at the reflux temperature for 2 hours, after which it was filtered, washed well with distilled water, methanol and ether to give **silica-60-G<sub>1</sub>** (**Scheme 2.5**).



**Scheme 2.5.** Synthesis of **silica-60-G<sub>1</sub>**

The immobilisation of the thioglycolic acid ligand on silica was confirmed by solution state  $^1\text{H}$  NMR, solid state  $^{13}\text{C}$  and  $^{29}\text{Si}$  NMR as well as IR spectroscopy and elemental analysis.

### 2.3.2 Solution state $^1\text{H}$ NMR silica-60-G<sub>1</sub>

A simple method allowed solution phase  $^1\text{H}$  NMR to be used to determine the presence of the organic functionality on the modified silica framework. A sample for this analysis was prepared by taking a small amount of the solid material **silica-60-G<sub>1</sub>** (*ca* 30 mg) and adding 3 drops of NaOD/D<sub>2</sub>O (20 wt%) and *ca* 1 mL D<sub>2</sub>O. This was heated (to promote siloxane bond cleavage and formation of lower molecular weight oligomers) until a clear solution was formed. NMR analysis of this dispersion was carried out immediately. Herein for a sample of **silica-60-G<sub>1</sub>** three proton environments were present; 0.51 ppm (SiCH<sub>2</sub>), 2.47 ppm (CH<sub>2</sub>S) and 3.07 ppm (SCH<sub>2</sub>C(O)). The splitting pattern demonstrated by the SiCH<sub>2</sub> and CH<sub>2</sub>S proton environments is a good indication of the immobilisation of the thioglycolic acid on to the silica. Similar splitting patterns and chemical shifts have been observed for SiCH<sub>2</sub> proton environments found for the precursor alkoxy silane.

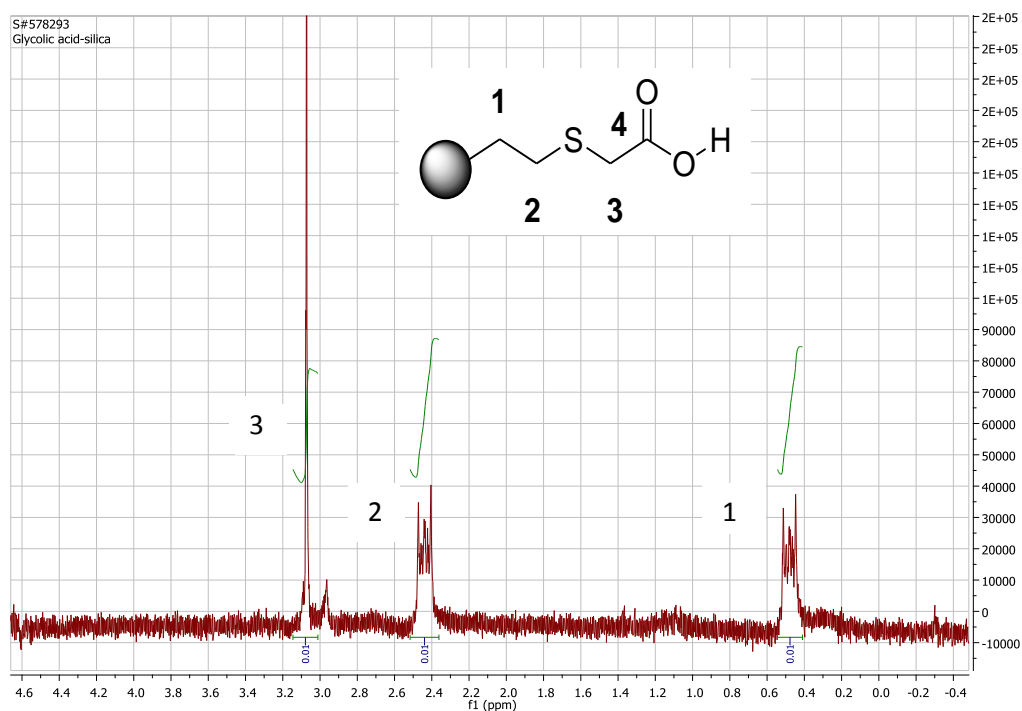


Figure 2.5  $^1\text{H}$  NMR (NaOD/ D<sub>2</sub>O) of silica-60-G<sub>1</sub>

Solid state  $^{13}\text{C}$  and  $^{29}\text{Si}$  MAS NMR were also used to characterise and confirm immobilisation of the thioglycolic acid fragment on the silica support and proved to be a very useful technique.

### 2.3.3 $^{13}\text{C}$ CP MAS NMR silica-60-G<sub>1</sub>

Four distinct carbon environments are found in the  $^{13}\text{C}$  CP MAS NMR of **silica-60-G<sub>1</sub>**; 16.9 (SiCH<sub>2</sub>), 30.3 (CH<sub>2</sub>S), 36.3 (CH<sub>2</sub>C(O)) and 177.0 (CO<sub>2</sub>H) ppm. A further peak is found at 54.77ppm would suggest that conversion of the thioglycolate ester to the corresponding acid was incomplete.

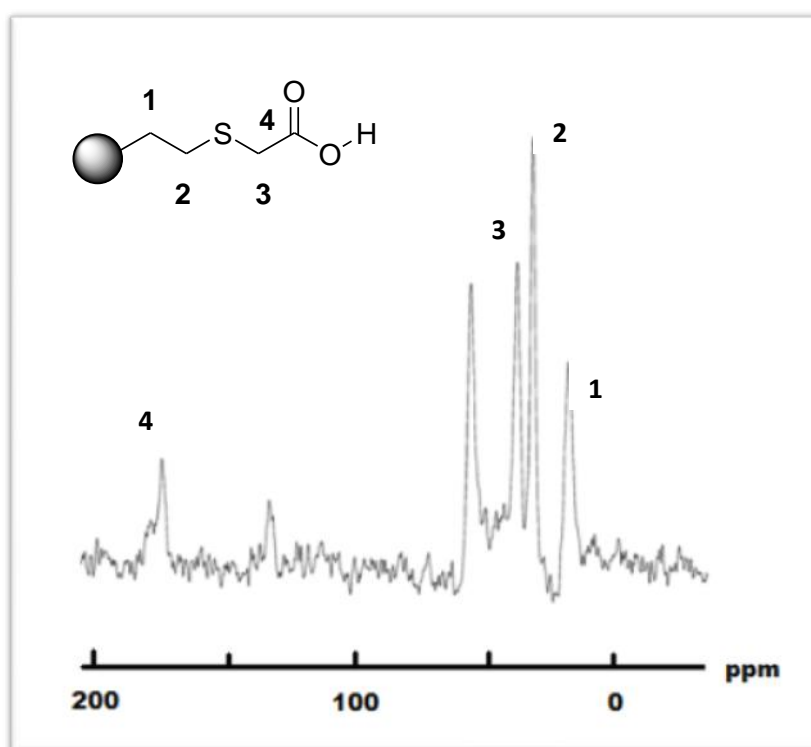
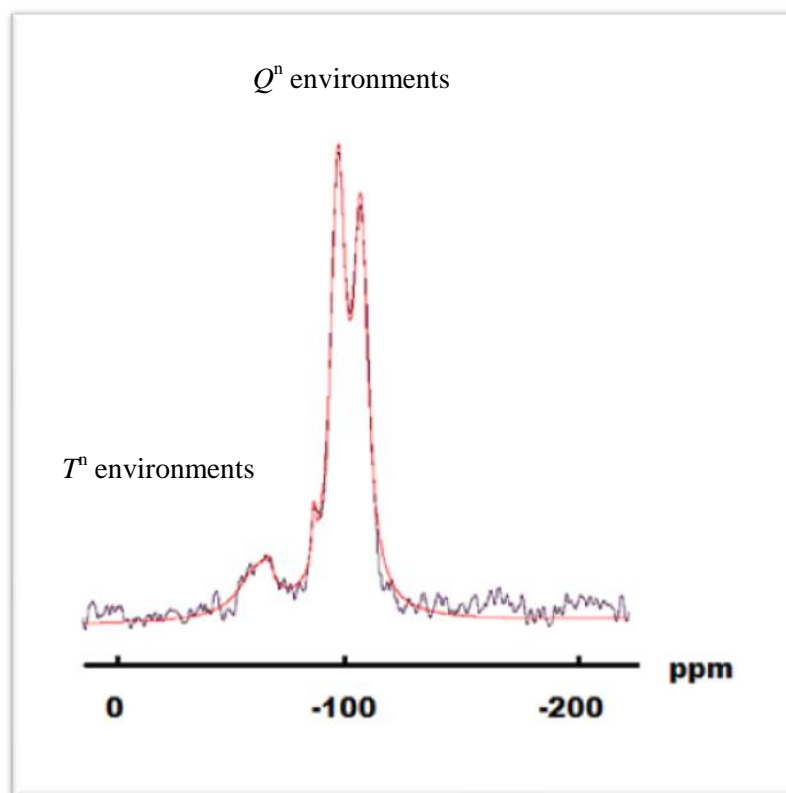


Figure 2.6  $^{13}\text{C}$  CP MAS NMR of **silica-60-G<sub>1</sub>**

### 2.3.5 $^{29}\text{Si}$ MAS NMR and Elemental Analysis of silica-60-G<sub>1</sub>

The  $^{29}\text{Si}$  MAS NMR spectrum shows two distinct environments, one corresponding to the T<sup>n</sup> functionalities at -64ppm, and the other corresponding to the Q<sup>n</sup> environments within the material, with peaks at -87, -98, -107 ppm. From the Gaussian fitting of the  $^{29}\text{Si}$  MAS NMR, a T:Q ratio of 1:7 is found (13% T environment and 87% Q). From this, the functional group loading is calculated as 1.6 mmol/g. Ligand loading was also determined from elemental analysis. Elemental analysis revealed 4.06% S present in **silica-60-G<sub>1</sub>** which would imply that the functional group loading was 1.3 mmol/g.



**Figure 2.7**  $^{29}\text{Si}$  MAS NMR of silica-60-G<sub>1</sub> with Gaussian fitting

The ligand loading as well as the presence of a large proportion of T<sup>2</sup> environment in the  $^{29}\text{Si}$  MAS NMR suggests that all the silanol groups of silica-60 have reacted. In addition, the methoxy peak observed in the  $^{13}\text{C}$  NMR can be attributed to both residual methoxysilyl as well as thioglycolate methyl ester groups.

### 2.3.5 IR Spectroscopy of silica-60-G<sub>1</sub>

Further confirmation of the immobilisation of the thioglycolic acid on the silica support was provided by IR spectroscopy. Herein peaks corresponding to the vibrations of C-S bonds at  $800\text{ cm}^{-1}$  and vibrations due to the C=O bond at  $1732\text{ cm}^{-1}$  were observed. In addition bands corresponding to the Si-O-Si bending vibrations were found at  $473\text{ cm}^{-1}$  and  $811\text{ cm}^{-1}$ . The peak at  $1101\text{ cm}^{-1}$  corresponds to the Si-O stretching vibration and a strong broad peak was also found at  $3436\text{ cm}^{-1}$  corresponding to carboxylic O-H stretch. In addition, a shoulder peak found at  $1276\text{ cm}^{-1}$  is ascribed to Si-C stretching.<sup>8</sup>

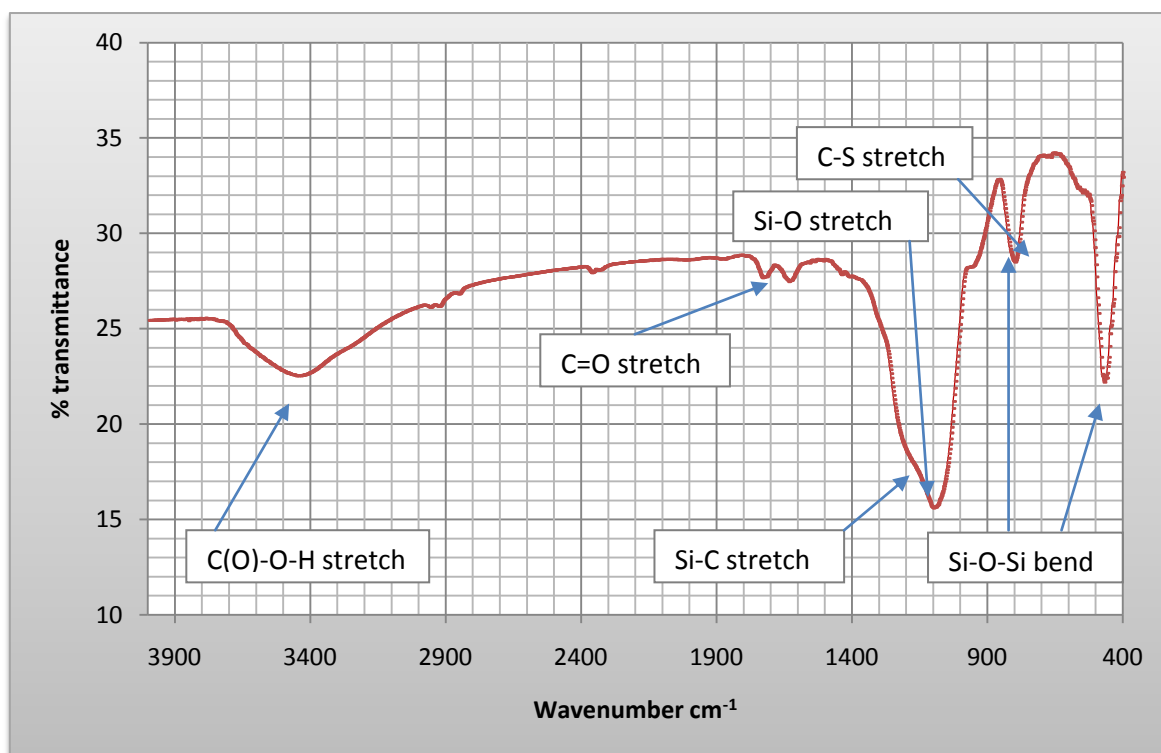


**Figure 2.8** Solid state IR spectroscopy of **silica-60-G<sub>1</sub>**

### 2.3.6 T<sub>1</sub> measurements

Spin lattice relaxation times were obtained from an inversion-recovery sequence experiment following the procedure described by Torchia.<sup>9</sup> **Figure 2.9** shows the plots of amplitude height (a.u.) versus time for T<sub>1</sub> measurements generated by **silica-60-G<sub>1</sub>**. Through analysis of the relaxation times of a given chemical environment, the relative degree of localised motion in an anchored chain can be determined (See **Appendix 3** for experimental). Such an experiment was carried out with **silica-60-G<sub>1</sub>** to see if the carbon environments were differentiated with distance from the silica framework. From the T<sub>1</sub> measurements of this material all the CH<sub>2</sub> environments were found to have slightly different T<sub>1</sub> values. The CH<sub>2</sub> closest to the silicon framework was found to have a slightly lower R<sub>1</sub> (relaxation rate) than that adjacent to the S. If we compare the correlation times of the two environments as in **Table 2.1**, the CH<sub>2</sub> closest to the silicon framework has a shorter correlation time which suggests greater mobility. This environment would be expected to show less mobility due to the rigidity of the silica framework but here it is found that the presence of the terminal carboxylic acid group gives less mobility to those methylene groups further away from the silica framework, in which case these measured T<sub>1</sub> times are shorter and correlation times longer.

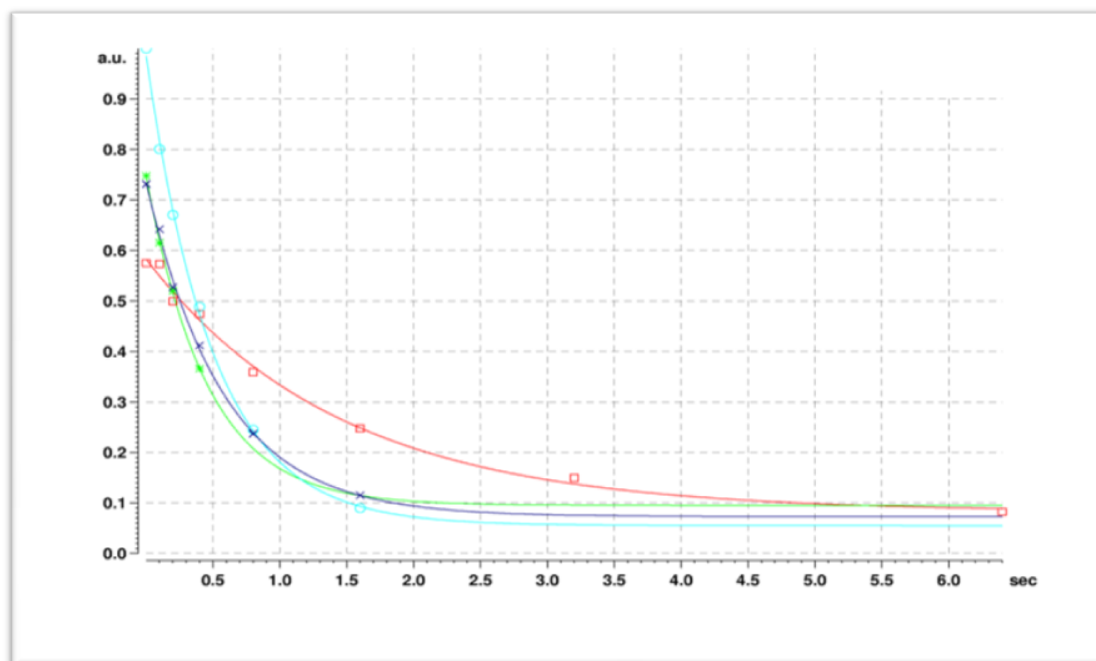
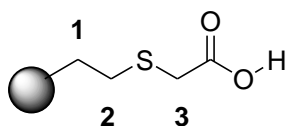


**Figure 2.9**  $T_1$  measurements for **silica-60-G<sub>1</sub>** with a dephasing time delay of 120 seconds

**Table 2.1** Calculated spin relaxation times  $T_1$  and correlation times  $\tau_c$  for material **silica-60-G<sub>1</sub>**



Key	$^{13}\text{C}$ $\delta$ ppm	Carbon position	$T_1$ (s)	$R_1$ ( $\text{s}^{-1}$ )	$\tau_c$ ( $\times 10^{-11}$ s)
× —	16.56	1	0.58	1.73	4.07
○ —	30.24	2	0.50	2.03	4.72
* —	36.42	3	0.46	2.19	5.16
□ —	55.25	Residual methoxy	1.45	-	-

Spin lattice relaxation derives from fluctuating magnetic fields that are in part a result of modulated dipolar spin-spin coupling. The time dependence of local fields is induced at a nucleus by neighbouring magnetic dipoles and hence modulation of the dipolar coupling is due to motional changes affecting the angle  $\theta$  in a component of the equation governing the strength of dipolar interactions.

The  $T_1$  values obtained from **silica-60-G<sub>1</sub>** can be compared to literature  $T_1$  values for organic compounds, for example decanoic acid in solution (**Figure 2.10**).

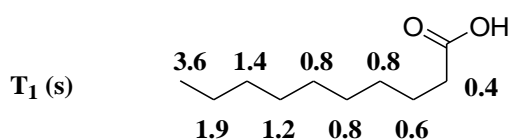


**Figure 2.10**  $T_1$  values of decanoic acid

Here it can be seen that the mobility of the carbon environments decrease going from the methyl, CH<sub>3</sub> end, towards the carboxylic acid end. The carbons are said to become less flexible towards the carboxylic acid end. In comparison to the silica supported glycolic acid material, the  $T_1$  measurements for the methylene groups also indicate increasing mobility with distance from the carboxylic acid moiety.

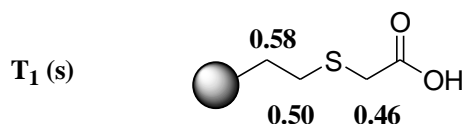


**Figure 2.11**  $T_1$  values of **silica-60-G<sub>1</sub>**

The rationale for this pattern of mobility in decanoic acid and related systems depends on hydrogen bonded dimer formation at the carboxylic acid terminus. With regard to **silica-60-G<sub>1</sub>** a range of H-bonded interactions involving carboxylic acid termini located on the silica pore walls can be envisaged given the likely presence of surface Si-OH groups or adsorbed water in addition to the possibility of functional groups being within H-bonding range themselves. However it should be noted that the difference in correlation times are relatively small.



### 2.3.7 Dipolar dephasing

Dipolar Dephasing experiments employ pulse sequences which result in the suppression of non-quaternary centres with the exception of those that are highly mobile. This type of experiment was used to estimate the percentage of mobile species in the material through comparison of  $^{13}\text{C}$  signal intensities with and without proton decoupling.

The dipolar dephasing experiment for **silica-60-G<sub>1</sub>** is shown in the figure below. Here, a small reduction in the peak intensities is observed. This suggests that only a small percentage, *ca* 10% of the ligand sites are in restricted environments, while the majority of the ligand sites are inhabiting pore environments where rotation with respect to their Si-C, C-C and C-S bonds is relatively less restricted.

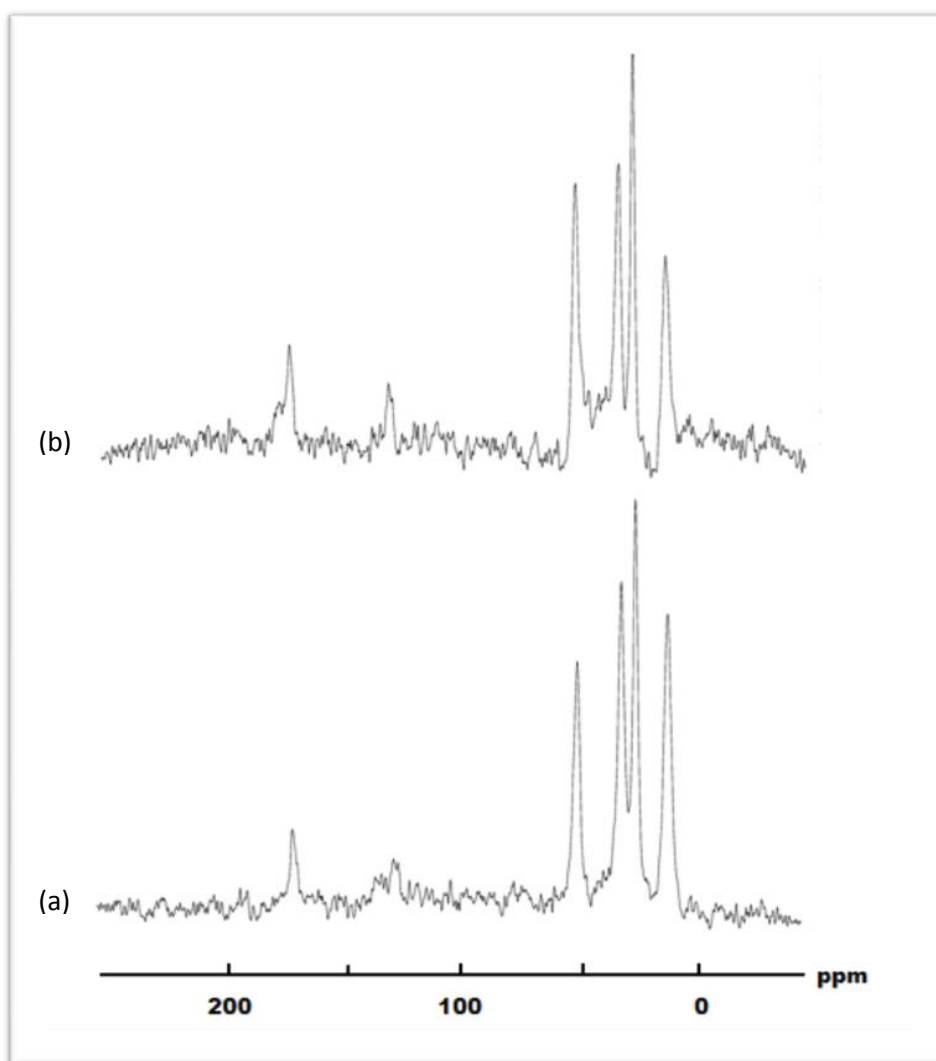


**Figure 2.12** Dipolar dephasing experiment for **silica-60-G<sub>1</sub>** (a) normal spectrum (b) dipolar dephasing experiment

### 2.3.8 Transmission Electron Microscopy (TEM) and Energy Dispersive X-ray Spectroscopy (EDS)

TEM analysis was also carried out on **silica-60-G<sub>1</sub>**. **Figure 2.13** reveals the material to have agglomerated spherically shaped particles of irregular size. The aggregated particulate structure of the material is evident and the light grey patches are believed to be pores. Alongside the TEM analysis, EDS was performed, this revealed the distribution of the thioglycolic acid ligand to be varied. In some regions the ratio of Si: S was found to be as high as 26:1 and in other regions very low ligand loadings were found with a Si: S ratio of 193:1. The distribution of the organic component upon the silica surface is found to be non-homogeneous.

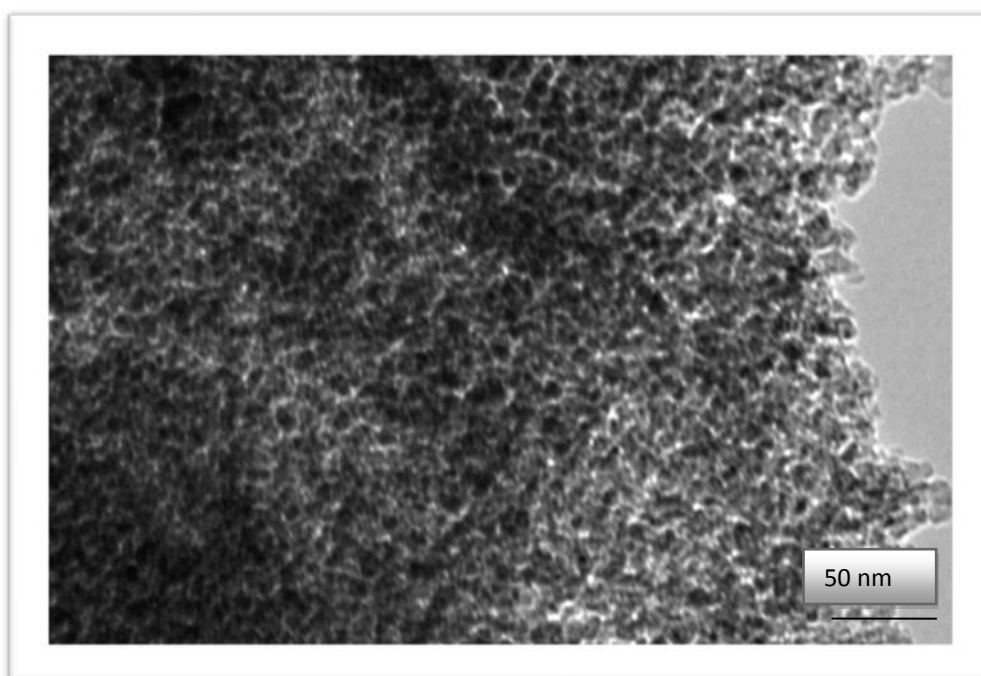


**Figure 2.13** TEM image of **silica-60-G<sub>1</sub>** at 100k

The image below at higher magnification shows a rough sponge like texture displayed by material **silica-60-G<sub>1</sub>**.

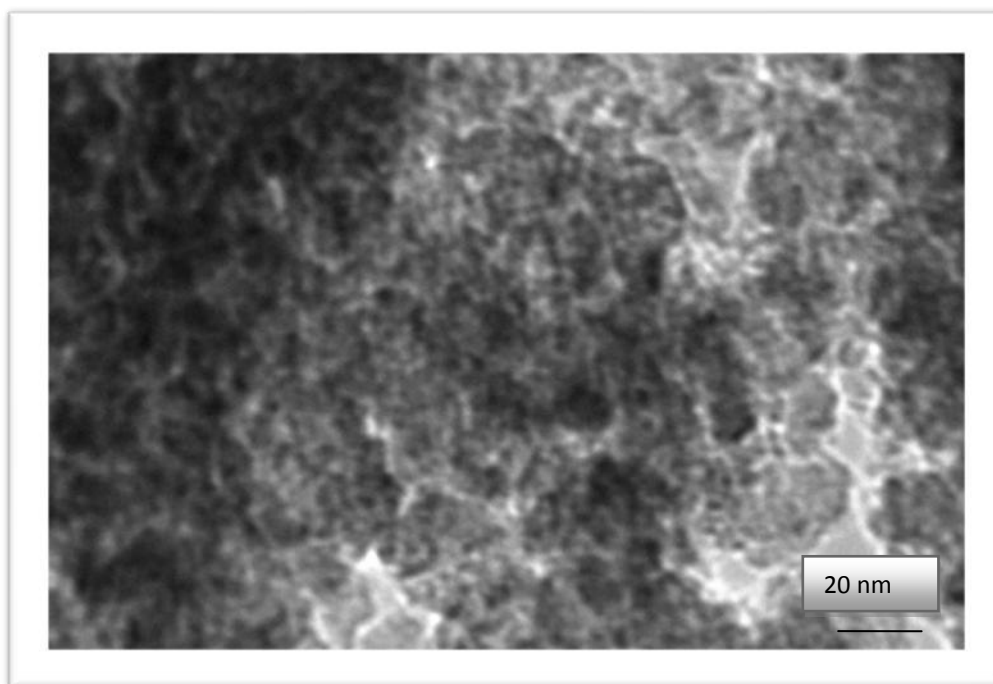


**Figure 2.14** TEM image of **silica-60-G<sub>1</sub>** at 200k

An image of the thioglycolic acid modified silica particles was also captured. This reveals silica particles of irregular shape, with a small range in the particle size. Post modification with the thioglycolate ligand shows a small reduction in the size of the silica particles.

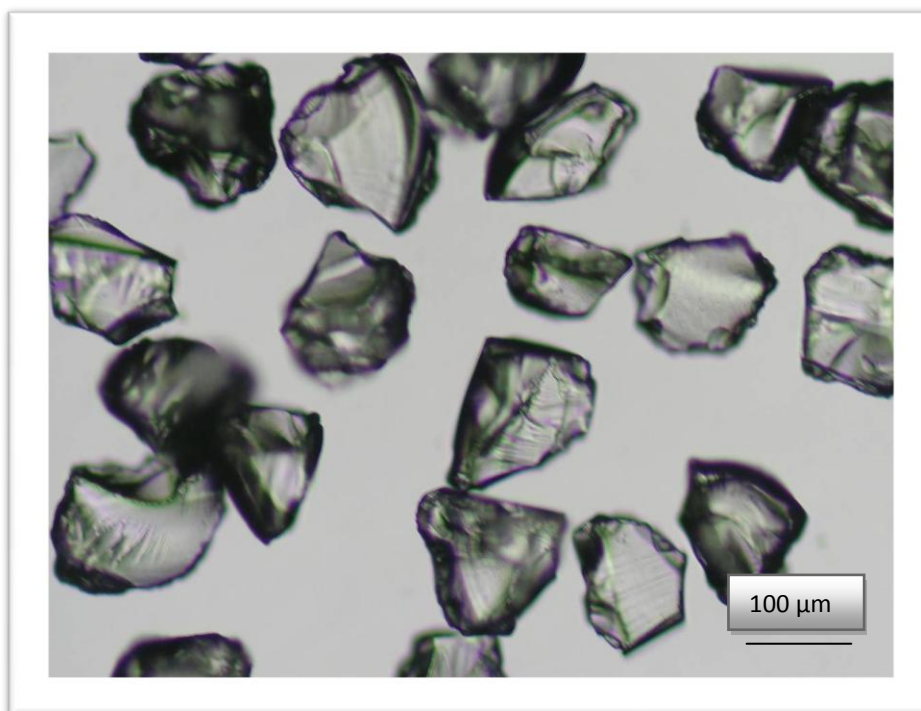


**Figure 2.15** Image of **silica-60-G<sub>1</sub>** particles

### 2.3.9 Summary

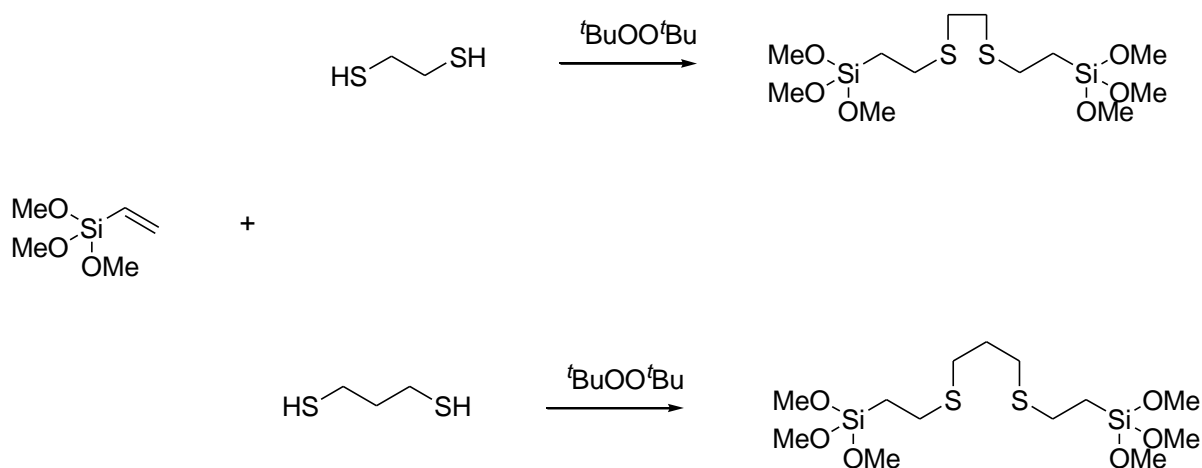
In the actions above, the easy synthetic procedure to **silica-60-G<sub>1</sub>** has been described. Characterisation of this material by solution state <sup>1</sup>H and solid state <sup>13</sup>C and <sup>29</sup>Si NMR confirm immobilisation of the thioglycolic acid onto the silica surface. Further confirmation was provided by IR spectroscopy and elemental analysis from which a high ligand loading of 1.3 mmol/g was calculated. From the <sup>29</sup>Si MAS NMR it can be seen that the majority of the ligand sites are in T<sup>2</sup> environments. This is further supported by the dipolar dephasing experiment and T<sub>1</sub> measurements wherein it is revealed that a small percentage, *ca* 10%, of the ligands are immobilised in fairly rigid environments and that the carbon atoms adjacent to the silica framework are fairly flexible. TEM and EDS analysis revealed **silica-60-G<sub>1</sub>** to have a non homogeneous distribution of functionality. Porosimetry studies were also carried out for **silica-60-G<sub>1</sub>**; these are described later on in the chapter.

## 2.4 Synthesis and characterisation of silica- bis(alkyldithio)alkanes

### 2.4.1 Synthesis of silica - bis(alkyldithio)alkanes, silica-60-C<sub>2</sub> and silica-60-C<sub>3</sub>

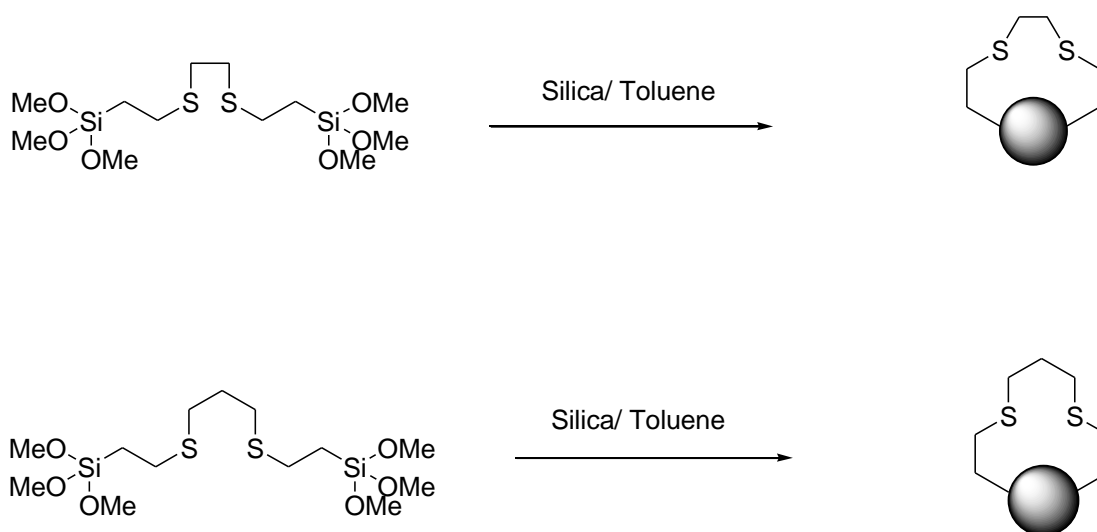
Organosilica materials bearing bidentate sulfur based ligands silica-1,2-bis(ethylthio) ethane, **silica-60-C<sub>2</sub>** and silica-1,3-bis(ethylthio) propane, **silica-60-C<sub>3</sub>** were also developed and characterised. The design choice of these materials was based on three key aspects; firstly the bidentate nature of ligands in **silica-60-C<sub>2</sub>** and **silica-60-C<sub>3</sub>** could ensure effective metal binding. Secondly, soft acids like sulfur display high affinity for heavy metals and such a system could resist leaching of the metal. Thirdly, capturing of the metal by the dithioalkane ligands would produce a stable five or six membered ring system which might aid in shifting the equilibrium towards the silica supported metal ligand complex.

The first step of the synthesis of **silica-60-C<sub>2</sub>** and **silica-60-C<sub>3</sub>** involved addition of the dithiols, 1,2 ethanedithiol and 1,3 propanedithiol to the vinylsilanes to give compounds 1,2-bis(trimethoxysilylethylthio)ethane and 1,3-bis(trimethoxysilylethylthio)propane in high yields (99% for both respectively) (**Scheme 2.6**).



**Scheme 2.6** Synthesis of compounds 1,2-bis(trimethoxysilylethylthio)ethane and 1,3-bis(trimethoxysilylethylthio)propane

Anchoring of these compounds on to the silica support was achieved by refluxing compounds 1,2-bis(trimethoxysilylethylthio)ethane or 1,3-bis(trimethoxysilylethylthio)propane in toluene with commercial silica for 8 hours. After cooling, the mixture was filtered, washed with ethanol and diethyl ether and then dried *in vacuo* to give white powders, **silica-60-C<sub>2</sub>** and **silica-60-C<sub>3</sub>** (Scheme 2.7).



**Scheme 2.7** Synthesis of **silica-60-C<sub>2</sub>** and **silica-60-C<sub>3</sub>**

It is anticipated that both sulfur ligand sites are anchored on to the silica support and so give **silica-60-C<sub>2</sub>** and **silica-60-C<sub>3</sub>** as plausible structural depictions. Characterization of the **silica-60-C<sub>2</sub>** and **silica-60-C<sub>3</sub>** was achieved by solid state <sup>13</sup>C and <sup>29</sup>Si NMR, IR spectroscopy and elemental analysis and this confirmed the immobilisation of the sulfur ligand.

#### 2.4.2 Solution state <sup>1</sup>H NMR of silica-60-C<sub>2</sub> and silica-60-C<sub>3</sub>

Solution state <sup>1</sup>H NMR (NaOD/ D<sub>2</sub>O) was used to determine the presence of organic functionality on the silica framework. In the solution state <sup>1</sup>H spectrum for **silica-60-C<sub>2</sub>**, three proton environments are found to be present; 0.58 ppm (SiCH<sub>2</sub>), 2.56 ppm (CH<sub>2</sub>S) and 2.65 ppm (SCH<sub>2</sub>). Three proton environments are also found in the solution state <sup>1</sup>H NMR spectrum for **silica-60-C<sub>3</sub>**; 0.38 ppm (SiCH<sub>2</sub>), 1.54 ppm (CH<sub>2</sub>S) and 2.31-2.36 ppm (SCH<sub>2</sub>CH<sub>2</sub>CH<sub>2</sub>S).

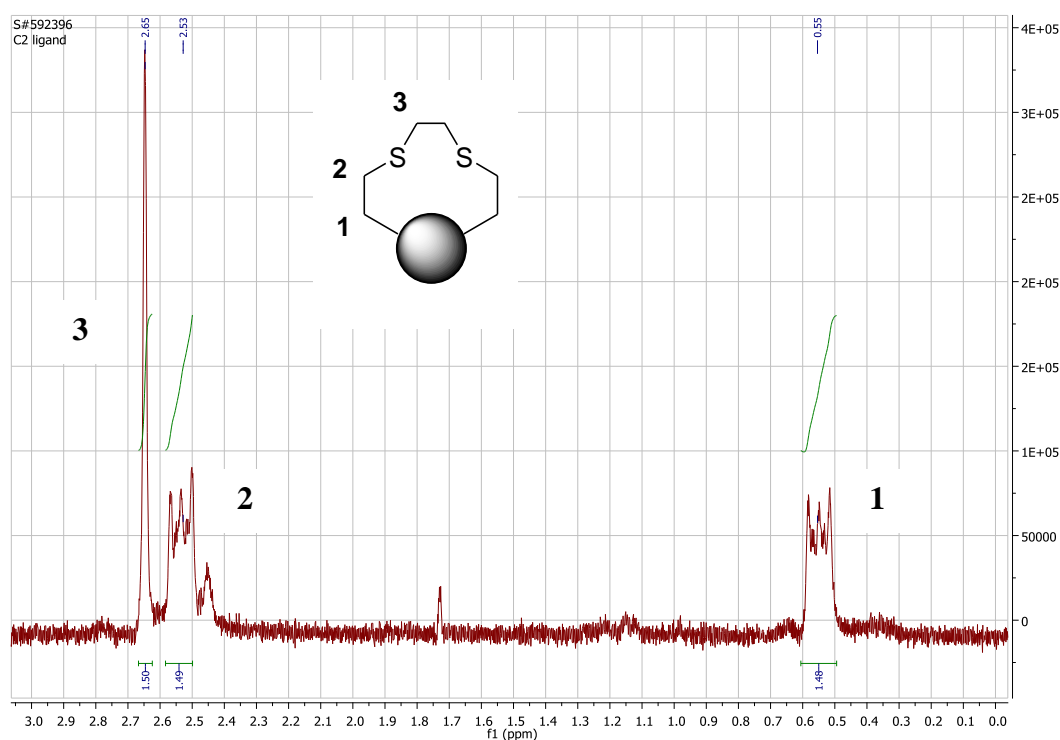


Figure 2.16 <sup>1</sup>H NMR spectrum of silica-60-C<sub>2</sub>

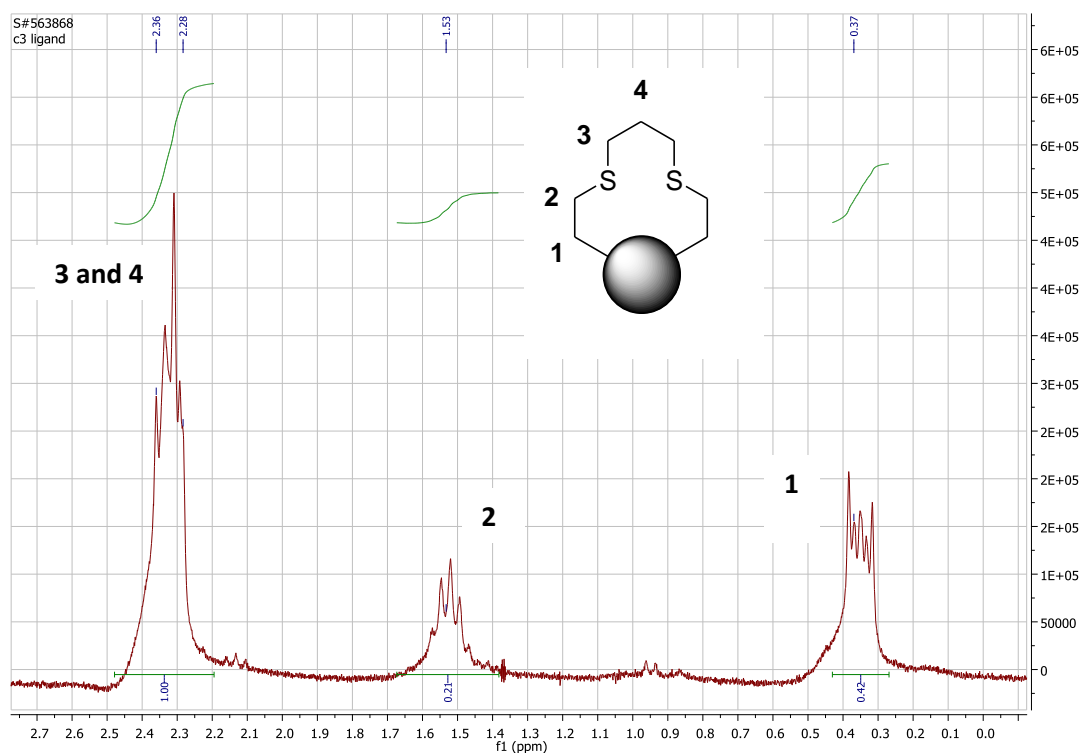
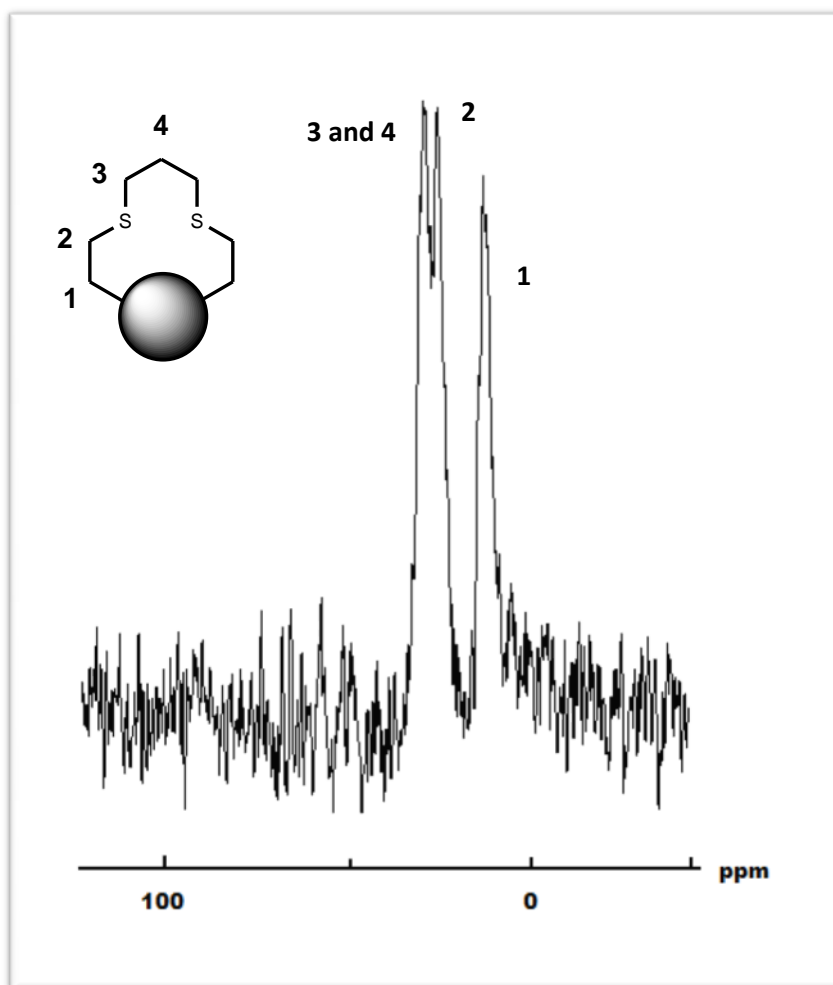


Figure 2.17  $^1\text{H}$  NMR of silica-60-C<sub>3</sub>

#### 2.4.3 $^{13}\text{C}$ CP MAS NMR of silica-60-C<sub>2</sub> and silica-60-C<sub>3</sub>

$^{13}\text{C}$  CP MAS NMR further confirmed immobilisation of the dithioalkane ligands on the silica supports. The NMR spectrum for silica-60-C<sub>2</sub> shows three resonance peaks as expected at 12.1, 25.5 and 37.7 ppm which correspond to the SiCH<sub>2</sub>, CH<sub>2</sub>S and SCH<sub>2</sub> carbon environments. The  $^{13}\text{C}$  CP MAS NMR spectrum of silica-60-C<sub>3</sub> is shown below and also shows three chemical environments at 13.5 (SiCH<sub>2</sub>), 26.2 (CH<sub>2</sub>S) and 29.1 ppm (SCH<sub>2</sub>CH<sub>2</sub>CH<sub>2</sub>S).



**Figure 2.18**  $^{13}\text{C}$  CP MAS NMR of **silica-60-C<sub>3</sub>**

#### 2.4.4 $^{29}\text{Si}$ MAS NMR of **silica-60-C<sub>2</sub>** and **silica-60-C<sub>3</sub>**

The T: Q ratio (that is the ratio of functional group silicon: framework silicon) was estimated from the Gaussian fitted  $^{29}\text{Si}$  MAS NMR spectra. In the  $^{29}\text{Si}$  NMR spectrum of **silica-60-C<sub>2</sub>** two distinct environments are observed; the  $\text{Q}^n$  environments within the material are found to give peaks at -86.3, -97.8 and -106.6 ppm with a relative area of 92% from the Gaussian fitting. The peaks found at -64.1 and -68.3 ppm correspond to the  $\text{T}^n$  environments with relative area of 8%. From here a T: Q ratio of 1:11.5 is calculated, and this corresponds to a T loading (functional group loading) of 0.7 mmol/g.



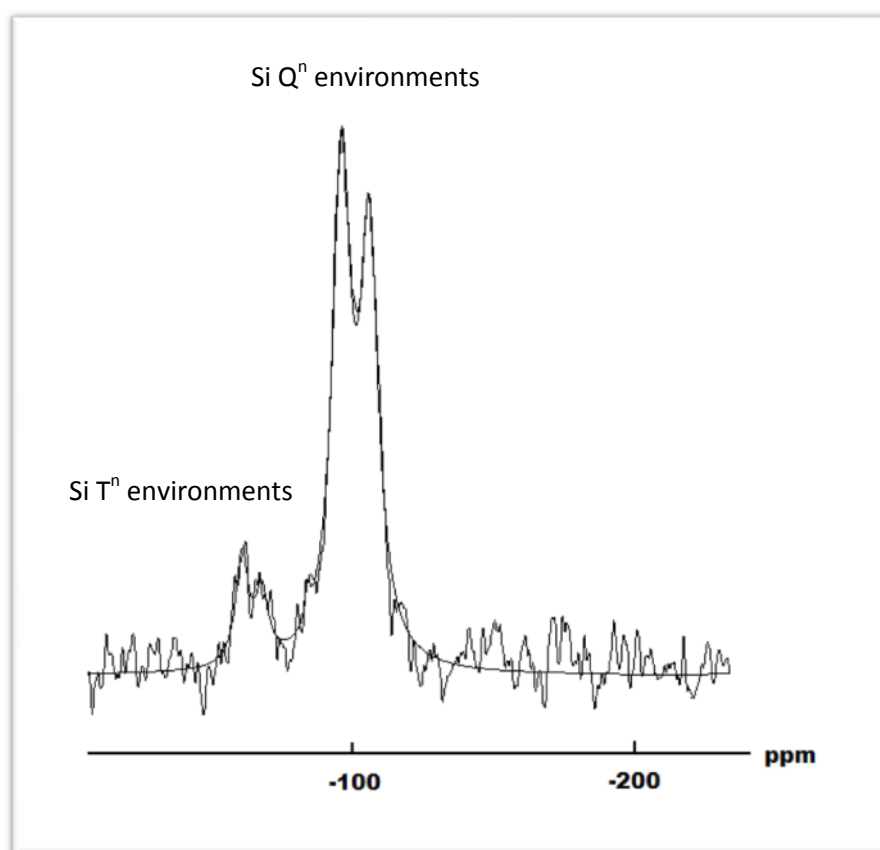


**Figure 2.19**  $^{29}\text{Si}$  MAS NMR of silica-60-C<sub>2</sub> with Gaussian fitting.

The  $^{29}\text{Si}$  NMR spectrum of silica-60-C<sub>3</sub> also shows two distinct chemical environments. The peaks found at -98, -108 and -117 ppm correspond to the presence of Q<sup>n</sup> environments within the material, with percentage area of 88%. The peaks present at -70 ppm and -76 ppm correspond to T<sup>n</sup> environments within the material, and this is shown to have 12% area from the Gaussian fitting. From here, a T: Q ratio of 1:7 is calculated, which corresponds to a T loading of 0.90 mmol/g.

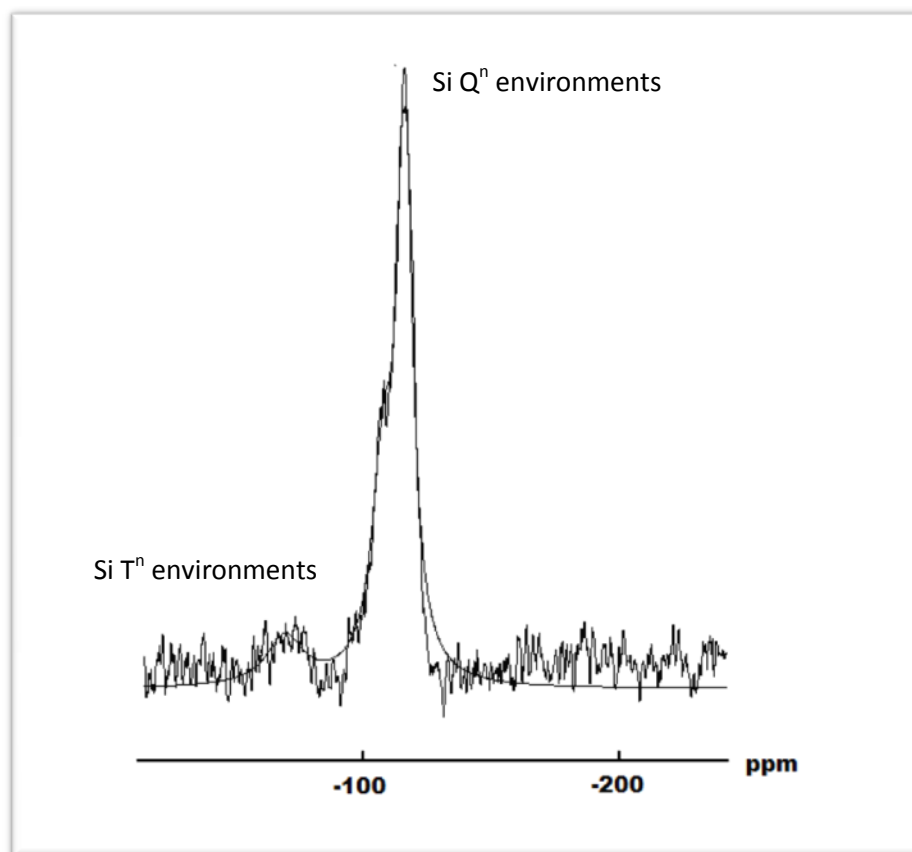


**Figure 2.20**  $^{29}\text{Si}$  MAS NMR of **silica-60-C<sub>3</sub>** with Gaussian fitting.

#### 2.4.5 Elemental analysis of silica-60-C<sub>2</sub> and silica-60-C<sub>3</sub>

Sulfur analysis revealed **silica-60-C<sub>3</sub>** to have 3.29 % S present and material **silica-60-C<sub>2</sub>** to have 3.62 % S present. From here the amount of loaded ligand upon the silica framework can be calculated; our calculations show that a ligand loading of 0.51 mmol/g and 0.56 mmol/g are found for **silica-60-C<sub>3</sub>** and **silica-60-C<sub>2</sub>** respectively. For this work the ligand loadings as measured from sulfur analysis will be used.

#### 2.4.6 IR Spectroscopy of silica-60-C<sub>2</sub> and silica-60-C<sub>3</sub>

Further confirmation of the immobilisation of the dithioalkane ligands was confirmed by IR spectroscopy. Characteristic Si-O-Si bending vibrations are visible at  $470\text{cm}^{-1}$  and  $813\text{cm}^{-1}$  for both **silica-60-C<sub>2</sub>** and **silica-60-C<sub>3</sub>**. A peak is also found at  $802\text{cm}^{-1}$  which corresponds to stretching vibrations of the C-S bonds. The Si-O stretching vibration is found at  $\sim 1100\text{cm}^{-1}$

and the shoulder peak found at  $\sim 1270\text{ cm}^{-1}$  is attributed to Si-C stretch. A broad peak at  $\sim 3400\text{ cm}^{-1}$  can be attributed to some hydroxyl groups on the surface of the silica.

#### 2.4.7 Dipolar Dephasing Experiment

Dipolar dephasing experiments were conducted for both **silica-60-C<sub>2</sub>** and **silica-60-C<sub>3</sub>** materials. As shown in the figures below, a great suppression in the carbon environments of material **silica-60-C<sub>3</sub>** is observed, *ca* 70%, suggesting the remaining 30% are in less restrictive environments. A lower degree of suppression is found in material **silica-60-C<sub>2</sub>**, *ca* 50%.

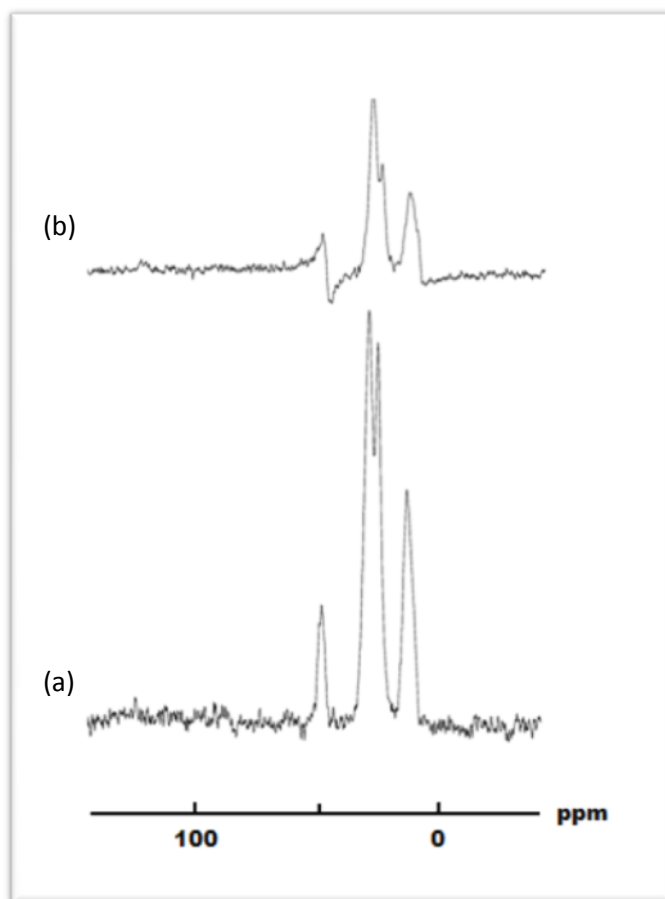


**Figure 2.21** Dipolar dephasing for **silica-60-C<sub>3</sub>** (a) normal spectrum (b) spectrum run with time delay of 180 seconds

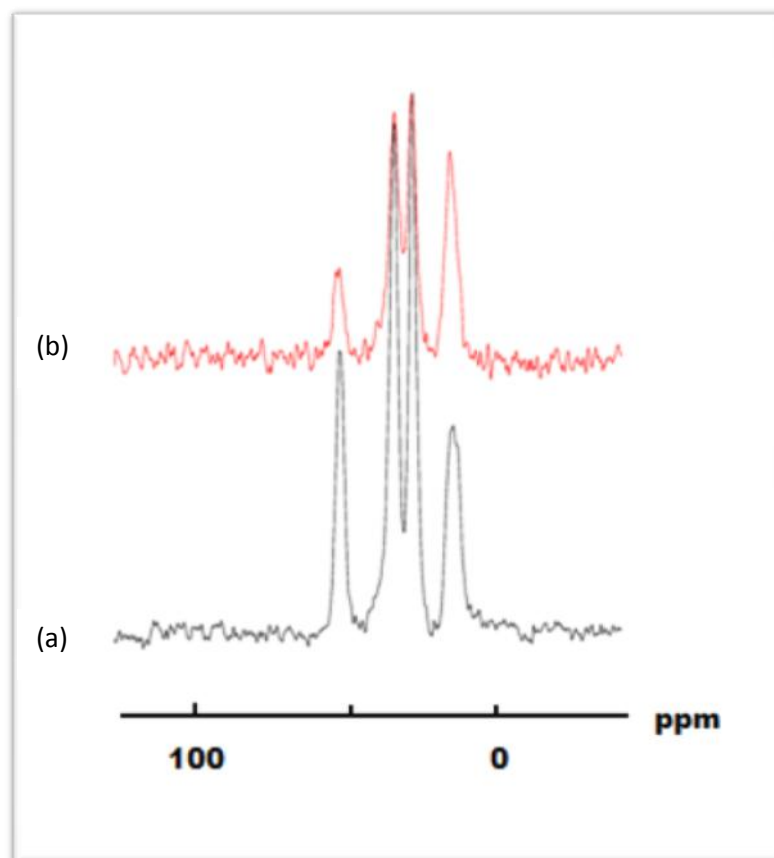


**Figure 2.22** Dipolar dephasing for **silica-60-C<sub>2</sub>** (a) normal spectrum (b) spectrum run with time delay of 180 seconds

#### 2.4.8 $T_1$ measurements

The  $T_1$  measurements revealed a similar pattern to those observed for **silica-60-G<sub>1</sub>** with mobility of the methylene groups decreasing with distance from the silica framework. As with **silica-60-G<sub>1</sub>** the differences are relatively small but the pattern is striking and indicative of Van der Waals or H-bonded interactions varying in strengths.

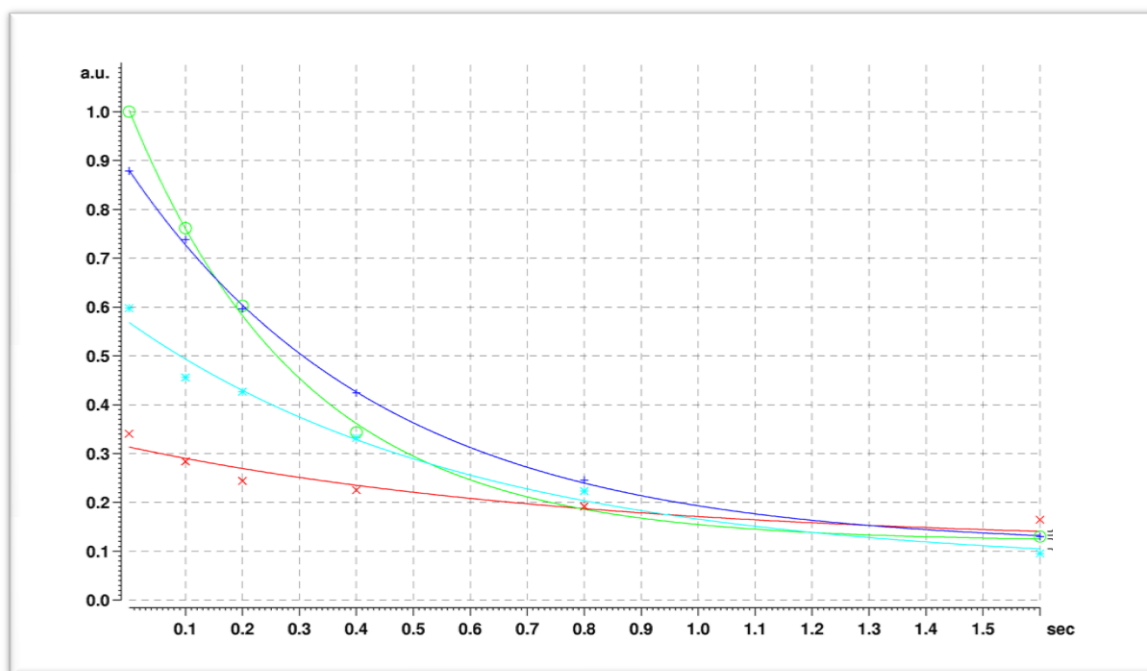
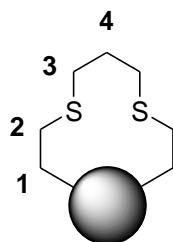
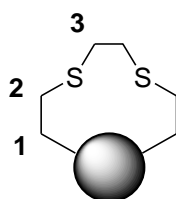


Figure 2.23  $T_1$  measurements for silica-60-C<sub>3</sub>

Table 2.2 Calculated correlation times for material silica-60-C<sub>3</sub>



Key	$^{13}\text{C}$ $\delta$ ppm	Carbon position	$T_1$ (s)	$R_1$ ( $\text{s}^{-1}$ )	$\tau_c$ ( $\times 10^{-11}$ s)
	13.04	1	0.61	1.64	3.86
	25.69	2 and 3	0.45	2.23	5.26
	29.64	4	0.31	3.25	7.67
	49.89	Residual OMe	0.80	-	-

**Table 2.3**  $T_1$  measurement,  $R_1$  and  $\tau_c$  measurements calculated for silica-60-C<sub>2</sub>

$^{13}\text{C}$ $\delta$ ppm	C position	$T_1$ /s	$R_1$ /s <sup>-1</sup>	$\tau_c$ /x10 <sup>-11</sup> s <sup>-1</sup>
13.34	1	3.60	0.28	0.65
24.45	2	0.61	1.65	3.89
37.6	3	0.58	1.72	4.05

#### 2.4.9 Microscopy Studies of silica-60-C<sub>2</sub> and silica-60-C<sub>3</sub>

TEM images were recorded for **silica-60-C<sub>3</sub>** and as shown in the picture below the porous nature of the material is observed.

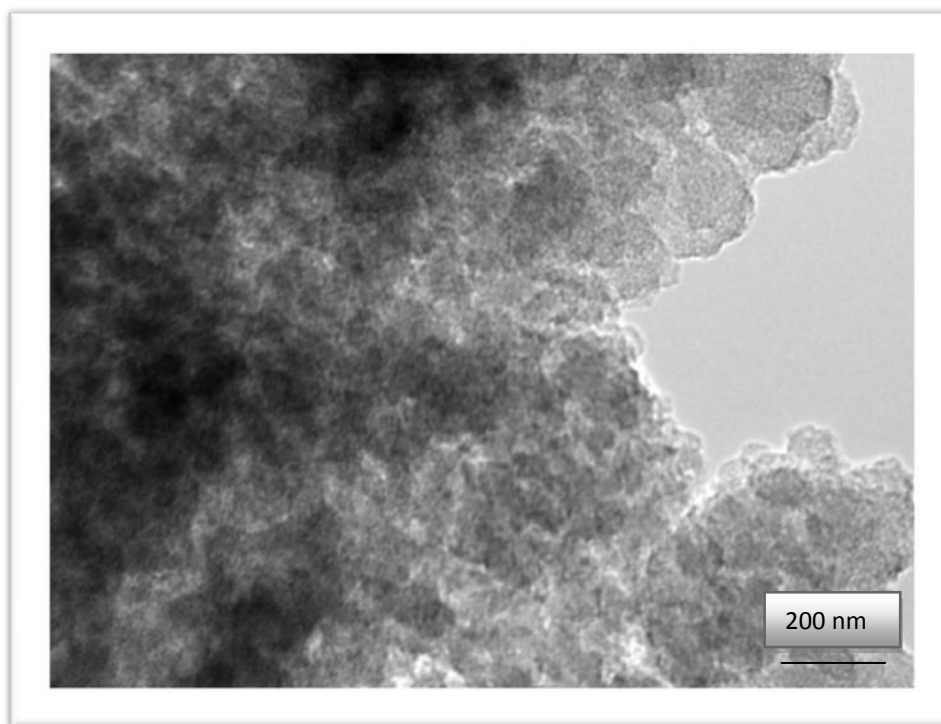


**Figure 2.24** TEM analysis of **silica-60-C<sub>3</sub>** reveals particles with spherical like shape

#### 2.4.10 Synthesis and characterisation of silica-90-C<sub>3</sub> and silica-150-C<sub>3</sub>

For comparative pore size work, **silica-90-C<sub>3</sub>** and **silica-150-C<sub>3</sub>** were also prepared from silica of average pore sizes 90 and 150Å respectively following the same synthetic procedure used to prepare **silica-60-C<sub>3</sub>**. Solution state <sup>1</sup>H NMR confirmed the presence of the sulfur ligands on the silica support. As expected, characteristic resonances corresponding to the three hydrogen environments were found at 0.39, 1.52 and 2.30-2.34 ppm. The ligand loadings were calculated from weight difference and found to be 0.66 and 0.52 mmol/g for **silica-90-C<sub>3</sub>** and **silica-150-C<sub>3</sub>** respectively.

$^{13}\text{C}$  CP MAS NMR of silica-90-C<sub>3</sub>

$^{13}\text{C}$  CP MAS NMR for **silica-90-C<sub>3</sub>** further confirmed immobilisation of the dithioalkane ligand onto the silica support. As shown in the NMR spectrum below, three resonance peaks are found as expected at 14.4, 26.3 and 32.2 ppm which correspond to the SiCH<sub>2</sub>, CH<sub>2</sub>S and SCH<sub>2</sub> carbon environments. An additional peak observed at 49.16 ppm suggests that some residual methoxy is present within the material.

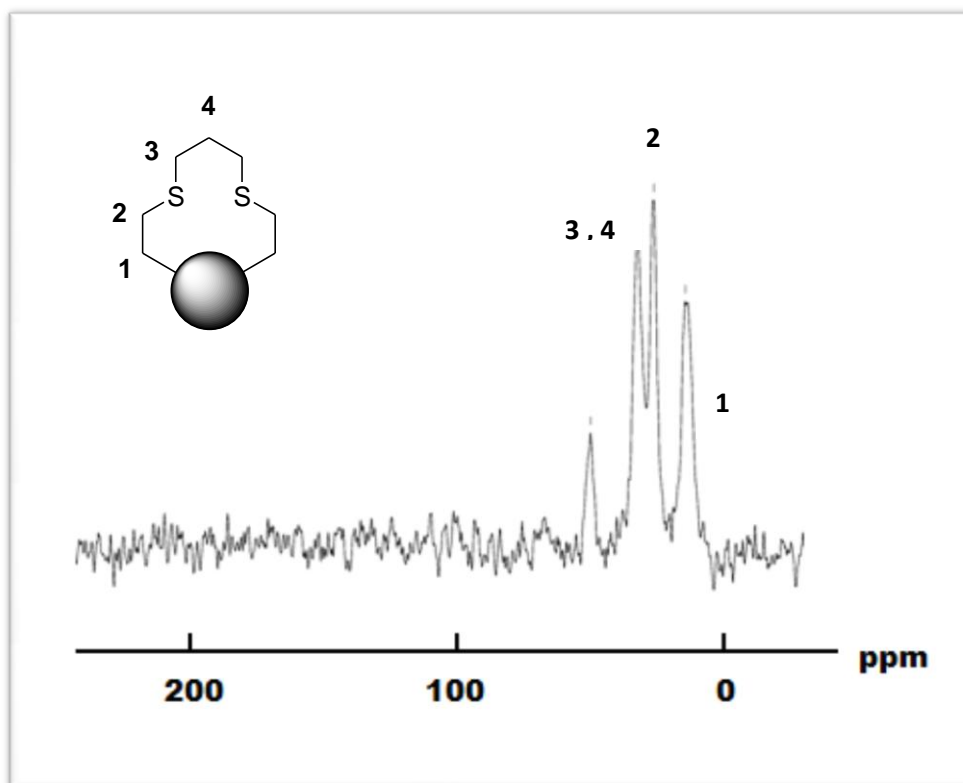
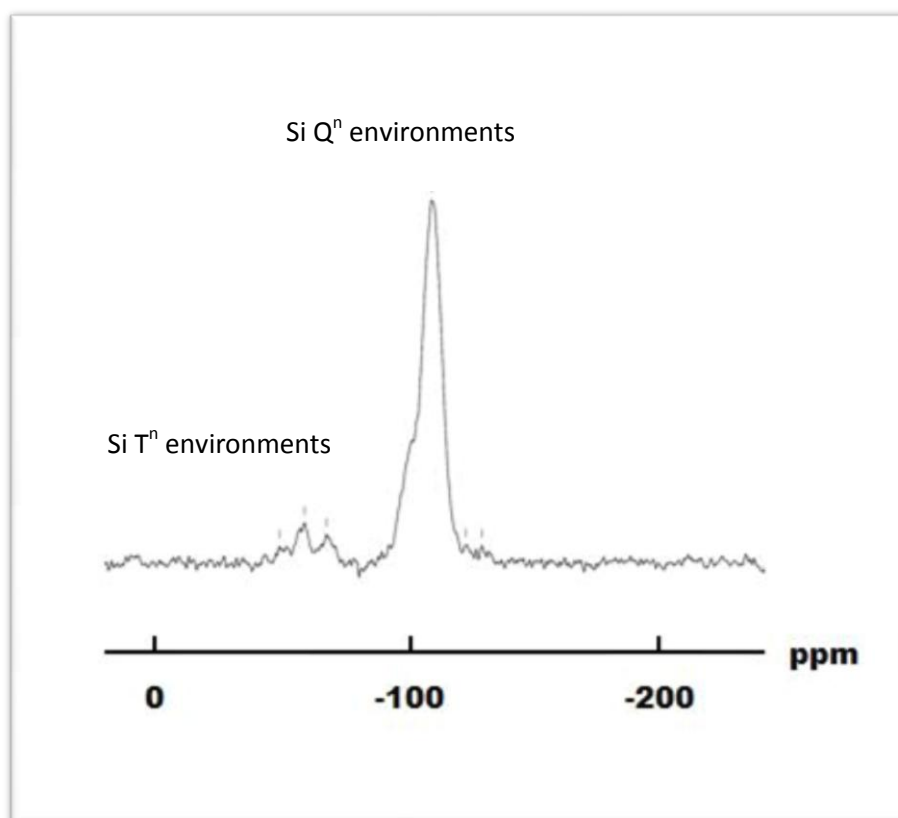


Figure 2.25  $^{13}\text{C}$  CP MAS NMR of **silica-90-C<sub>3</sub>**

 $^{29}\text{Si}$  MAS NMR of silica-90-C<sub>3</sub>

The confirmation of ligand immobilisation on **silica-90-C<sub>3</sub>** is further provided by  $^{29}\text{Si}$  MAS NMR. Herein, two distinct environments are observed, one corresponding to the T<sup>n</sup> environments (-48.7, -56.5 and -65.5 ppm) and the Q<sup>n</sup> environments at -107 ppm.





**Figure 2.26**  $^{29}\text{Si}$  MAS NMR of **silica-90-C<sub>3</sub>**

#### 2.4.10 Summary

Herein the immobilisation of sulfur ligands onto silica-60 has been described in a simple synthetic procedure to give materials **silica-60-C<sub>2</sub>** and **silica-60-C<sub>3</sub>**. The confirmation of the ligand immobilization is strongly provided by  $^1\text{H}$  solution state NMR as well as solid state  $^{13}\text{C}$  and  $^{29}\text{Si}$  NMR. Further NMR experiments such as dipolar dephasing and  $T_1$  measurements reveal a large proportion of the ligands to be residing in more restrictive environments. Interestingly,  $T_1$  measurements found the most flexible environments to be found at the carbon atoms adjacent to the silica framework. TEM and EDS analysis revealed a homogeneous distribution of ligands on the surface.

The immobilization of dithioalkanes to silica of larger pore sizes to give materials **silica-90-C<sub>3</sub>** and **silica-150-C<sub>3</sub>** was also confirmed by solution state  $^1\text{H}$  NMR and solid state  $^{13}\text{C}$  and  $^{29}\text{Si}$  NMR. The appearance of a methoxy peak in the  $^{13}\text{C}$  CP NMR of **silica-90-C<sub>3</sub>** suggests that this material has some T<sup>1</sup> and T<sup>2</sup> character. This is further confirmed by the  $^{29}\text{Si}$  NMR where clear peaks corresponding to T<sup>1</sup>, T<sup>2</sup> as well as T<sup>3</sup> environments are found. This observation is not found in the case of **silica-60-C<sub>3</sub>**. As the dipolar dephasing experiments

suggest 70 % of the ligand environments are in more restrictive environments, this would most probably correspond to the T<sup>3</sup> ligand sites. Further it can be deduced that 0.1 mmol/g of Si-OH groups remain on **silica-60-C<sub>3</sub>**.

In the case of **silica-60-C<sub>2</sub>**, it is evident from <sup>29</sup>Si NMR that there is T<sup>2</sup> and T<sup>3</sup> organosilicon environments. A large proportion of T<sup>2</sup> is in fact observed, further to this dipolar dephasing experiment conducted support this as 50% of the ligand sites are found in restricted environments. It can be deduced that within this material relatively more silanol groups reside, approximately 0.2 mmol/g.

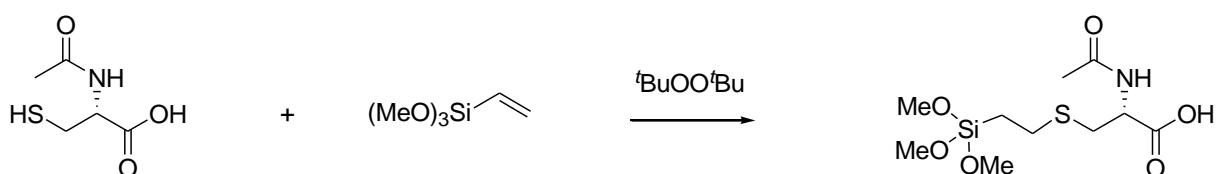
Porosimetry data has also been obtained for these materials and these are explained later on in the chapter.

## 2.5 Chiral Sulfur based ligands immobilised on silica

Stereochemistry in chemical interactions is vitally important in several fields of chemistry, including pharmaceutical, biological, agricultural, fragrance and materials chemistries. For example, in the context of drug receptor interactions, host biological targets are chiral entities.<sup>10</sup> Thus there is an enormous demand to produce practical methods for preparing chiral catalysts for the preparation of chiral compounds as single enantiomers. It is this demand that drives the field of asymmetric catalysis. The research area of asymmetric catalysis is dedicated to the development and applications of enantioenriched catalysts to transform prochiral and racemic substances into valuable enantioenriched synthetic building blocks. It was in the early 1960s, when William Knowles and his colleagues in Monsanto demonstrated that rhodium complexes containing chiral phosphine ligands were able to catalyse the enantioselective addition of hydrogen to one of the faces of the prochiral olefinic substrate generating a chiral C-H centre with high enantioselectivity.<sup>11</sup> Soon, this process was commercialised to produce the anti Parkinson drug, *L*-Dopa, followed by the generation of many other processes, as well as laboratory scale syntheses, to generate enantiomerically enriched compounds. A variety of organometallic and organocatalysts have been identified as asymmetric catalysts. These catalysts not only produce high levels of enantioselectivity but are also functional group tolerant. In 2001, Knowles shared the Nobel Prize for chemistry with Ryoji Noyori for his work on asymmetric catalytic hydrogenation and K. Barry Sharpless for his work on asymmetric catalytic oxidation. With all the work having been done in the field, there is an incredible demand for a catalytic transformation that would proceed 100% and provide complete chemo, regio and stereocontrol.

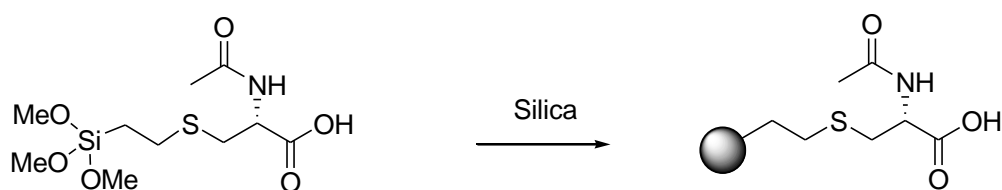
## 2.5.1 Synthesis of silica-60-N-acetyl-L-cysteine

In keeping with sulfur based ligands, N-derivatised-*L*-cysteine compounds were synthesised and then immobilised onto silica. The presence of the acid group was convenient as this might aid in binding to a metal atom. The first of the materials synthesized was **silica-N-acetyl-L-cysteine**. **Silica-60-N-acetyl-L-cysteine** was formed by first combining commercially available N-acetyl-*L*-cysteine with vinyl trimethoxysilane with the addition of di-*tert*-butyl peroxide. A total reflux time of 8 hours ensured complete conversion to the trimethoxysilylethyl derivative (**Scheme 2.8**). This reaction was monitored by  $^1\text{H}$  NMR



**Scheme 2.8** Synthesis of S-ethyltrimethoxysilyl-N-acetyl-L-cysteine

The addition of S-ethyltrimethoxysilyl-N-acetyl-*L*-cysteine to silica was carried out at reflux temperature in toluene with a total reaction time of 6 hours. Due to the high viscosity of trimethoxysilyl-S-ethyl-N-acetyl-*L*-cysteine, it was introduced to the silica in methanol. The methanol was subsequently removed with a Dean-Stark apparatus. Water had to be added after 4 hours to aid the co-condensation reaction between the surface silanol groups of the silica and the alkoxy groups of S-ethyltrimethoxysilyl-N-acetyl-*L*-cysteine.



**Scheme 2.9** Synthesis of **silica-60-N-acetyl-L-cysteine**

**Silica-60-N-acetyl-L-cysteine** was characterised in a number of ways to confirm and study the immobilisation of the chiral ligand to the silica support including solution state  $^1\text{H}$  NMR, solid state  $^{13}\text{C}$  CP MAS and  $^{29}\text{Si}$  MAS NMR, dipolar dephasing and  $T_1$  measurements.

## 2.5.2 Solid state NMR of silica-60-N-acetyl-L-cysteine

The  $^{13}\text{C}$  CP MAS NMR of **silica-60-N-acetyl-L-cysteine** is shown in the **Figure 2.27** below. The spectrum shows seven peaks at 15.3 ( $\text{SiCH}_2$ ), 24.2 ( $\text{CH}_2\text{S}$ ), 29.9 ( $\text{SCH}_2$ ), 36.3 ( $\text{C(O)CH}_3$ ), 65.6 ( $\text{CHNH}$ ), and 177.1 ppm ( $\text{C(O)OH}$ ) ( $\text{NHC(O)}$ ) as expected. The peak at 55.82 ppm corresponds to residual methoxysilyl moieties. Comparison of these chemical shifts to those found in the  $^{13}\text{C}$  NMR of N-acetyl-L-cysteine reveals that the signals for  $\text{SCH}_2$  and  $\text{SCH}_2\text{CH}$  of the silica bound material are found at higher ( $\sim 5$  ppm) fields which may be due to the shielding these carbon environments experience from the silica framework.

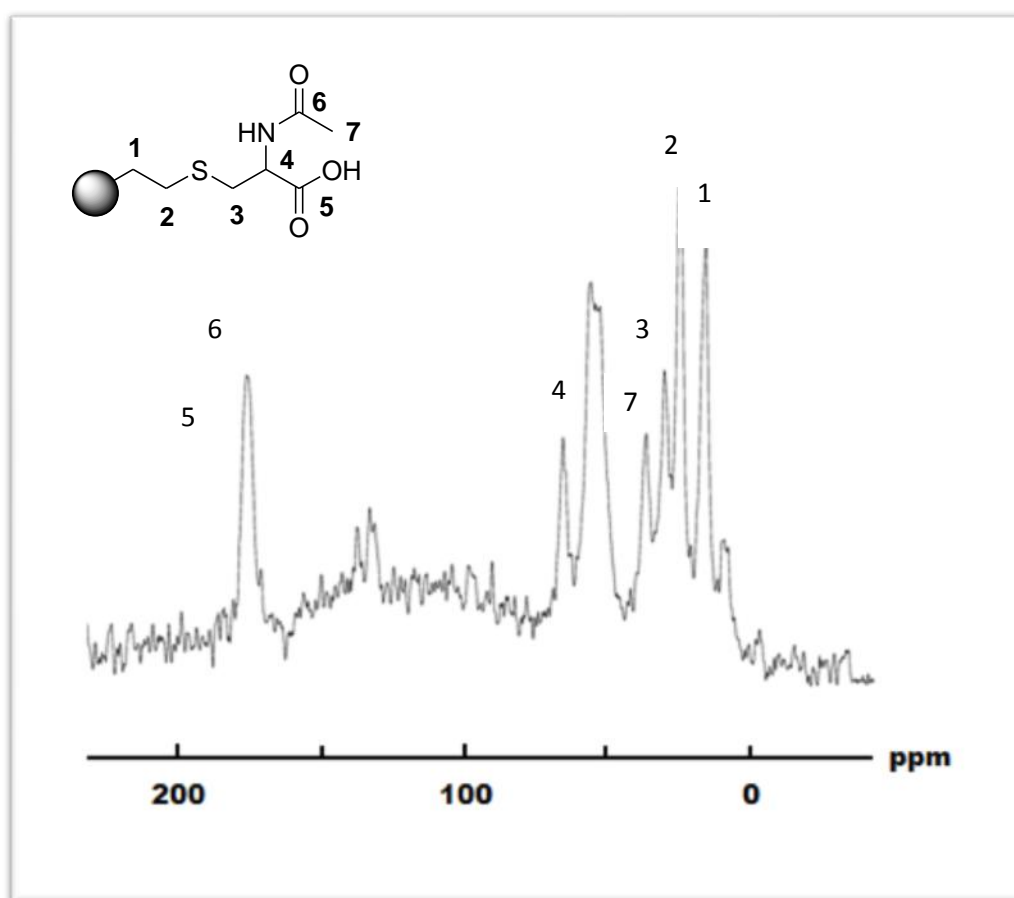


**Figure 2.27**  $^{13}\text{C}$  CP MAS NMR of **silica-60-N-acetyl-L-cysteine**

$^{29}\text{Si}$  MAS NMR also proved to be a useful tool to characterise **silica-60-N-acetyl-L-cysteine**. Resonant peaks found at -64.9 ppm correspond to the T functionality within the material and resonant peaks found at -98.4ppm and -107.8ppm corresponds to the Q environments. From the Gaussian fitting of the graph a total T environment of 4 % is calculated and a total Q environment of 96 %. This suggests a T: Q ratio of 1:24 which corresponds to a ligand loading of 0.58 mmol/g. The ligand loading of **silica-60-N-acetyl-L-cysteine** was also

calculated from titration with HCl which revealed a ligand loading of 1.25 mmol/g to be present. Sulfur analysis revealed total sulfur contribution to be 1% in the sample which corresponds to 0.31 mmol/g. This method of calculating ligand loading was in closer agreement with the mass increase of the silica after grafting of the ligand.

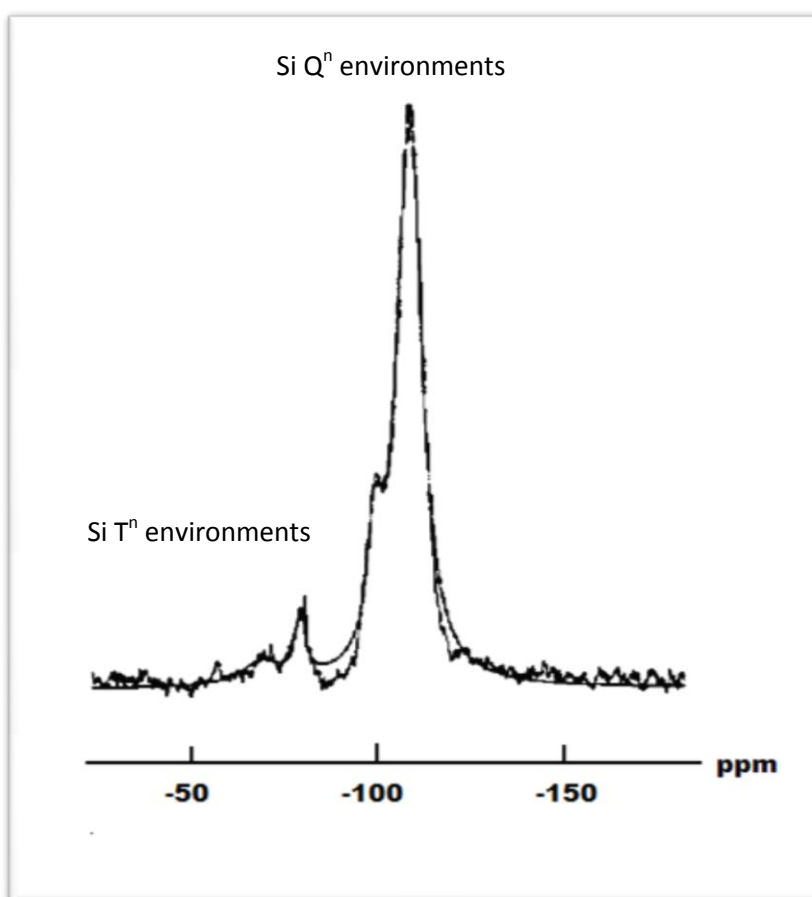


**Figure 2.28**  $^{29}\text{Si}$  MAS NMR of **silica-60-N-acetyl-L-cysteine** with Gaussian fitting

### 2.5.3 Dipolar Dephasing

Dipolar dephasing experiments of material **silica-60-N-acetyl-L-cysteine** reveals rather interestingly a large proportion of the ligand sites to be in restricted environments. Suppression of almost 80% of the resonant peaks in the  $^{13}\text{C}$  CP MAS NMR reveals that the ligand is highly confined. (**Figure 2.29**).

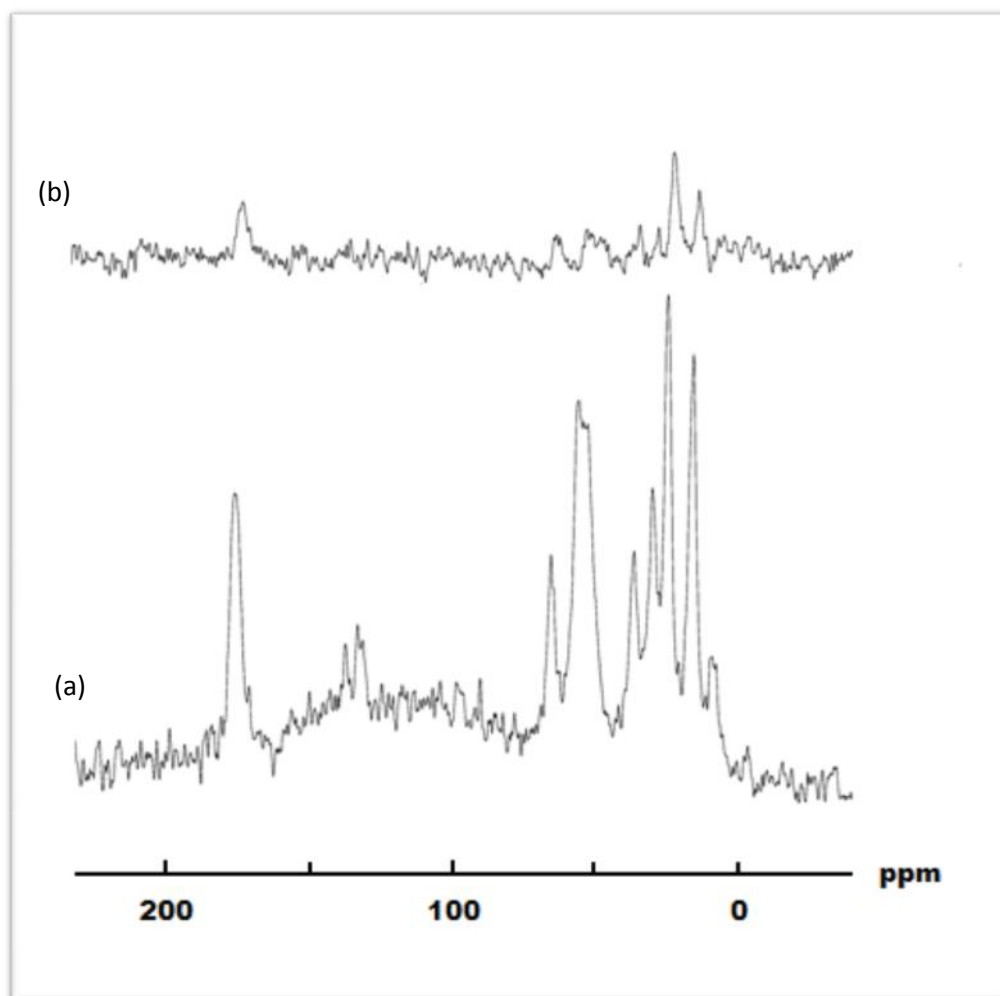


**Figure 2.29** Dipolar dephasing experiment for **silica-60-N-acetyl-L-cysteine** (a) is the normal experiment. (b) run with time delay of 180s.

#### 2.5.4 $T_1$ measurements

Immobilised N-acetyl-L-cysteine was also characterised by  $T_1$  measurements. The results are tabulated in **Table 2.4**.  $T_1$  measurements reveal that the most flexible environment measured for **silica-60-N-acetyl-L-cysteine** is the methylene group  $\beta$  to the silica framework (4.27s). Interestingly, in comparison to the  $T_1$  measurements of solution phase decanoic acid, **silica-60-N-acetyl-L-cysteine** reveals to have carbon environments with similar flexibility as carbons atoms  $\gamma$  to the carboxylic acid moiety.

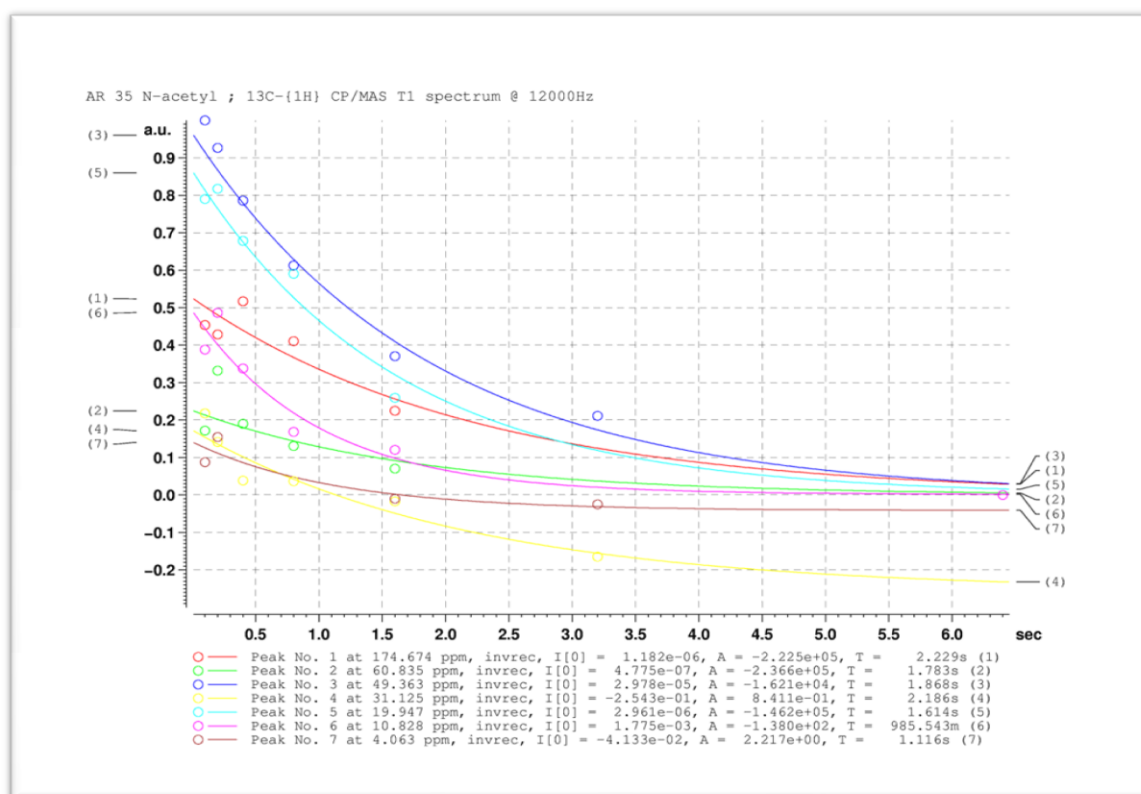
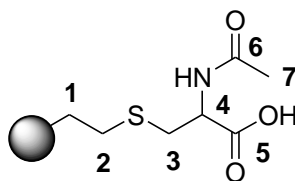


**Figure 2.30**  $T_1$  measurements for **silica-60-N-acetyl-L-cysteine** with a Dephasing time delay of 120 seconds

**Table 2.4** Calculated correlation times for material **silica-60-N-acetyl-L-cysteine**

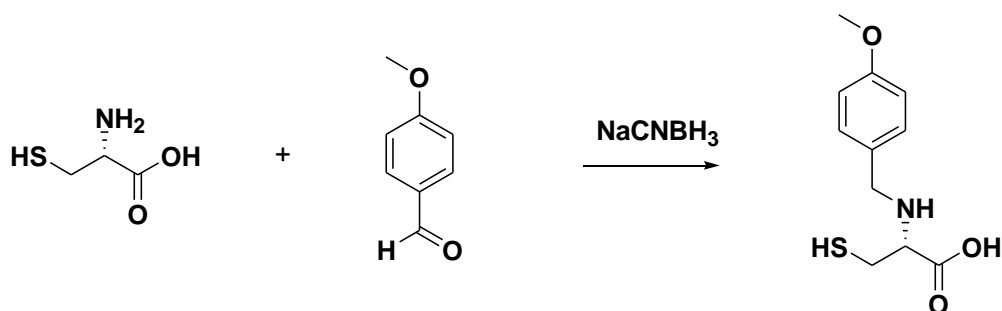


$^{13}\text{C}$ $\delta$ ppm	C position	$T_1$ /s	$R_1$ /s $^{-1}$	$\tau_c$ /x10 $^{-11}$ s $^{-1}$
4.06	1	1.12	0.896	2.11
10.83	2	0.985	1.01	2.39
19.95	3	1.61	0.62	1.46
60.84	4	1.78	0.561	2.64
174.68	5	2.23	0.449	-
49.36	7	2.19	0.457	0.718

### 2.5.5 Synthesis of Silica-*N*-4-methoxybenzyl-*L*-cysteine

Following the same procedure, the immobilisation of *N*-4-methoxybenzyl-*L*-cysteine onto silica via the grafting method was explored. It was anticipated that the substitution of 4-methoxybenzyl on the nitrogen atom would allow a greater discrimination between the two faces of the chiral carbon atom.

The first step involved modifying *L*-cysteine. This was done by reductive elimination with the corresponding aldehyde to give *N*-4-methoxybenzyl-*L*-cysteine.



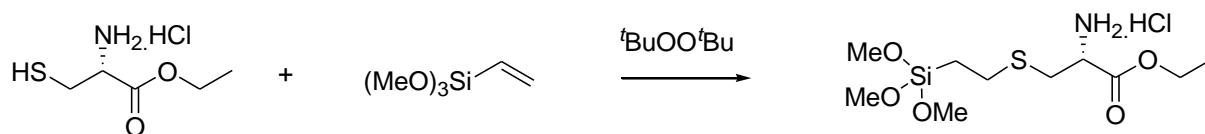
**Scheme 2.10** Synthesis of *N*-4-methoxybenzyl-*L*-cysteine

*N*-4-methoxybenzyl-*L*-cysteine was then added to vinyltrimethoxysilane and refluxed in toluene for 6 hours with the addition of di-*tert*-butyl peroxide. The consumption of vinyltrimethoxysilane was monitored by the disappearance of the vinyl peaks at 5.8-6.0ppm in the <sup>1</sup>H NMR. In this case, after the given time vinyl peaks remained, suggesting limited conversion.

The reaction was repeated, with a greater excess of *N*-4-methoxybenzyl-*L*-cysteine and the total reflux time was 8 hours. This product was dissolved in methanol and added to silica, following the same procedure as described for synthesizing **silica-60-*N*-acetyl-*L*-cysteine**. Unfortunately using this method solid state <sup>13</sup>C CP NMR revealed a large proportion of vinyl peaks to be present.

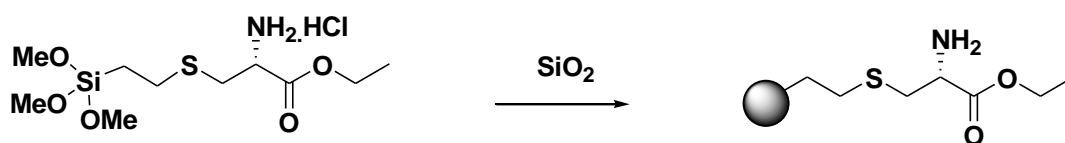
Therefore in a new synthetic route, ethyl-*L*-cysteine hydrochloride (0.043 mol) in *p*-xylene was heated and then reacted with vinyltrimethoxysilane (0.031 mol). Di-*tert*-butyl peroxide was also added and the mixture heated further for four hours before cooling. <sup>1</sup>H NMR analysis revealed consumption of all the vinyltrimethoxysilane (i.e. no vinyl peaks were present at 5.8-6.0ppm in <sup>1</sup>H NMR run in CDCl<sub>3</sub>).





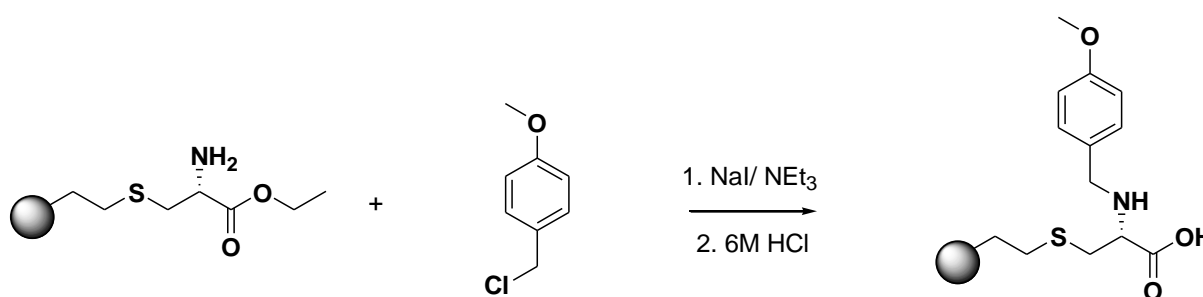
**Scheme 2.11** Synthesis of S-trimethoxysilyl-ethyl-L-cysteine hydrochloride

S-trimethoxysilyl-ethyl-L-cysteine hydrochloride was then dissolved in methanol and introduced to silica slurried in toluene. After refluxing for four hours, the mixture was cooled to room temperature, washed with methanol and then added to a solution of 0.35M NaOH and stirred for 20 minutes to reach pH 9.8.  $^1\text{H}$  NMR confirmed the immobilisation of *L*-cysteine on to silica and titration with 0.2M HCl revealed a ligand loading of 1.6 mmol/g.



**Scheme 2.12** Synthesis of silica-60-*L*-cysteine-ethyl ester

Post modification of the amine group was done by stirring silica-60-*L*-cysteine-ethyl ester in toluene and 4-methoxybenzylchloride. The filtered solid obtained was further hydrolysed in 6M HCl at the reflux temperature for 4 hours before being filtered, washed and dried to yield **silica-60-*N*-4-methoxybenzyl-*L*-cysteine**.



**Scheme 2.13** Synthesis of silica-60-*N*-4-methoxybenzyl-*L*-cysteine

### 2.5.6 Solution state NMR of silica-60-*N*-4-methoxybenzyl-*L*-cysteine

The confirmation of the loaded material came from  $^1\text{H}$  solution state (NaOD/  $\text{D}_2\text{O}$ ) NMR. This confirmed the presence of eight proton environments; 0.44 ( $\text{SiCH}_2$ ), 2.29 ( $\text{SCH}_2$ ), 2.60 ( $\text{CH}_2\text{S}$ ), 2.87 ( $\text{CH}_2\text{CH}$ ), 3.09 ( $\text{NHCH}$ ), 3.32 ( $\text{OCH}_3$ ), 6.92 and 7.08 (aromatic  $\text{CH}$ 's). Comparison to the  $^1\text{H}$  NMR of *N*-4-methoxybenzyl-*L*-cysteine shows an upfield shift in the resonance peak of  $\text{SCH}_2$  from 3.31 ppm to 2.29 ppm in the silica supported material. Interestingly the aromatic protons are also found to have shifted to higher field, from 7.08 and 6.74 ppm in *N*-4-methoxybenzyl-*L*-cysteine to 6.92 and 6.58 ppm in **silica-60-*N*-4-methoxybenzyl-*L*-cysteine**.

### 2.5.7 IR spectroscopy of silica-60-*N*-para-methoxybenzyl-*L*-Cysteine

The IR spectrum of **silica-60-*N*-4-methoxybenzyl-*L*-cysteine** (KBr) is shown in **Figure 2.31** below. A strong broad peak is observed at  $3489\text{ cm}^{-1}$  corresponding to the stretching vibrations of carboxylic O-H. The sharp peak found at  $1120\text{ cm}^{-1}$  corresponds to the Si-O-Si vibrations, the sharp band present at  $474\text{ cm}^{-1}$  corresponds to Si-C bend. A strong band at  $801\text{ cm}^{-1}$  corresponding to C-S bond vibrations is also found. Additionally, the band present at  $1656\text{ cm}^{-1}$  corresponds to C=O peak of the carboxylic acid and peaks corresponding to the aromatic C=C vibrations can be found at  $1585$  and  $1434\text{ cm}^{-1}$  (weaker).

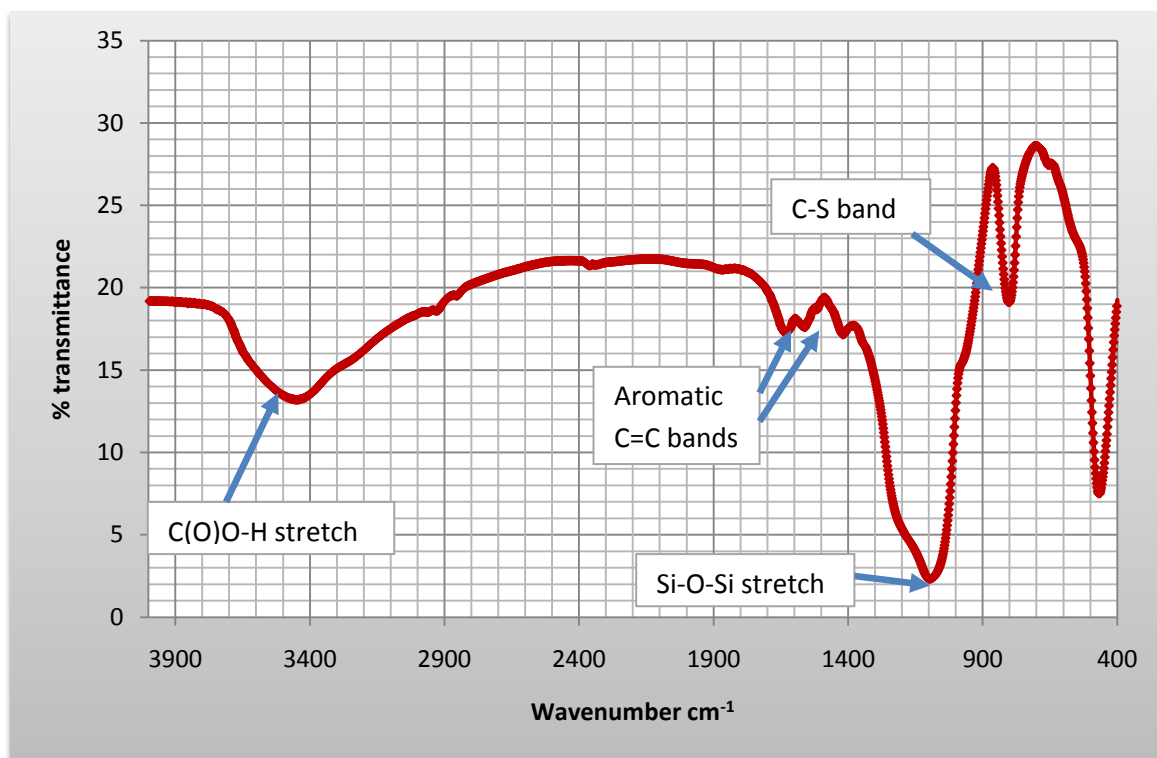


**Figure 2.31** IR spectrum of **silica-60-N-4-methoxybenzyl-L-cysteine**

### 2.5.8 Ligand loading of silica-60-N-4-methoxybenzyl-L-cysteine

The ligand loading of **silica-60-N-4-methoxybenzyl-L-cysteine** was calculated from titration experiment with HCl. This revealed a ligand loading of 1.25 mmol/g. Ligand loading from difference in weight equated to 0.8 mmol/g.

### 2.5.9 Summary

The immobilisation of N-derivatised-*L*-cysteine ligands on silica has been described in a relatively simple procedure. The immobilisation of these ligands is supported by solution state <sup>1</sup>H NMR as well as solid state <sup>13</sup>C and <sup>29</sup>Si NMR. Further to this, from <sup>29</sup>Si NMR of **silica-60-N-acetyl-L-cysteine** it is observed that a large proportion of T<sup>3</sup> character exists. This is further supported by the dipolar dephasing and T<sub>1</sub> measurements which show 80% of the ligand sites in restricted environments and the relatively reduced flexibility around the carbon adjacent to the silica framework. In addition, the low ligand loading of 0.31 mmol/g as calculated from sulfur analysis reveals that in this material approximately 0.6 mmol/g of silanol groups are residing on the surface.

In the case of **silica-60-N-4-methoxybenzyl-L-cysteine**, the relatively high ligand loading suggests that there exists more T<sup>2</sup> character than T<sup>3</sup> character.

Porosimetry work has also been carried out for **silica-60-N-acetyl-L-cysteine** and **silica-60-N-4-methoxybenzyl-L-cysteine**; these are described later in the chapter.

## 2.6 Palladium derivatised organosilica materials; synthesis and characterisation

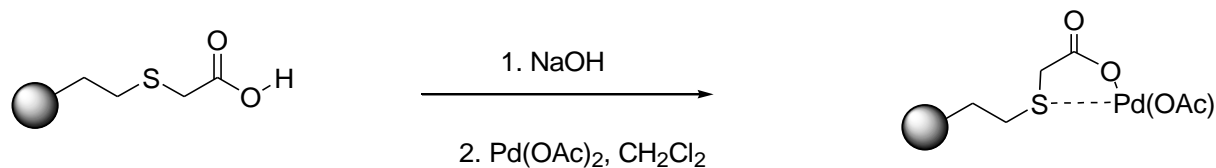
Preparation of the metal derivatised organically modified silica followed a general procedure. The metal complexed catalysts were prepared by stirring the appropriate organically modified silica and metal salt in dichloromethane at room temperature for 24 hours. A strong change in colour, white to orange, was a good indication of metal immobilisation onto the silica support.

Palladium derived catalysts have become the most important catalysts for a huge array of synthetic manipulations in basic feed stocks, to fine chemicals through to more elaborate, often complicated, natural products.<sup>12</sup> The general synthetic applications of palladium have expanded immensely in the last 15 years. This area has grown to become a powerful tool for the synthetic chemist, providing innumerable versatile transformations, in such a way that affords exclusive control in the conversion of simple starting materials, into often rather complex target molecules. Further, selectivity is a key facet in Pd-mediated synthesis, for example in chemo, regio and stereoselective processes that often result. Thus, synthetic chemists are able to assemble some of the intricate synthetic targets, which was not possible by traditional methods.<sup>12</sup>

### 2.6.1 Synthesis of silica-60-G<sub>1</sub>-Pd(OAc)

The first step in this reaction was to prepare the sodium salt of the thioglycolate (**Scheme 2.14**). This was achieved by the dropwise addition of 1M NaOH to a slurry of **silica-60-G<sub>1</sub>** (1g) in distilled water (15 mL) until pH 8.5 was attained. The sodium thioglycolate salt formed was then filtered and washed until the washings were neutral. The solid was further washed with ethanol and ether. The white solid was then dried under vacuum at 120 °C overnight. The immobilisation of palladium acetate to give **silica-60-G<sub>1</sub>-Pd(OAc)** was rapid as was indicated by the fast colouration of the solid in contact with the palladium acetate in solution. This was achieved by stirring the silica material (2g) in a solution of Pd(OAc)<sub>2</sub> (0.32g) in dichloromethane (20 mL) for 24 hours at room temperature. The mixture was then

filtered and washed with dichloromethane until the washings were clear. The dark orange solid obtained was then dried under vacuum at 50 °C overnight.



**Scheme 2.14** Synthesis of **silica-60-G<sub>1</sub>-Pd(OAc)**

### 2.6.1 <sup>13</sup>C CP MAS NMR of silica-60-G<sub>1</sub>-Pd(OAc)

Immobilisation of the palladium by the supported thioglycolate was confirmed by solid state <sup>13</sup>C NMR. The spectrum showed line broadening of all the resonances after introduction of palladium acetate. A 1:1 Pd:ligand binding ratio would give rise to additional peaks in the solid state <sup>13</sup>C NMR due to the PdOAc from fragments such as SiCH<sub>2</sub>CH<sub>2</sub>SCH<sub>2</sub>C(O)<sub>2</sub>PdOAc. However, these peaks would be very close to the acetate of the supported ligand. Thus, the line broadening observed is consistent with the presence of Pd-free ligand and PdOAc complexed ligand.

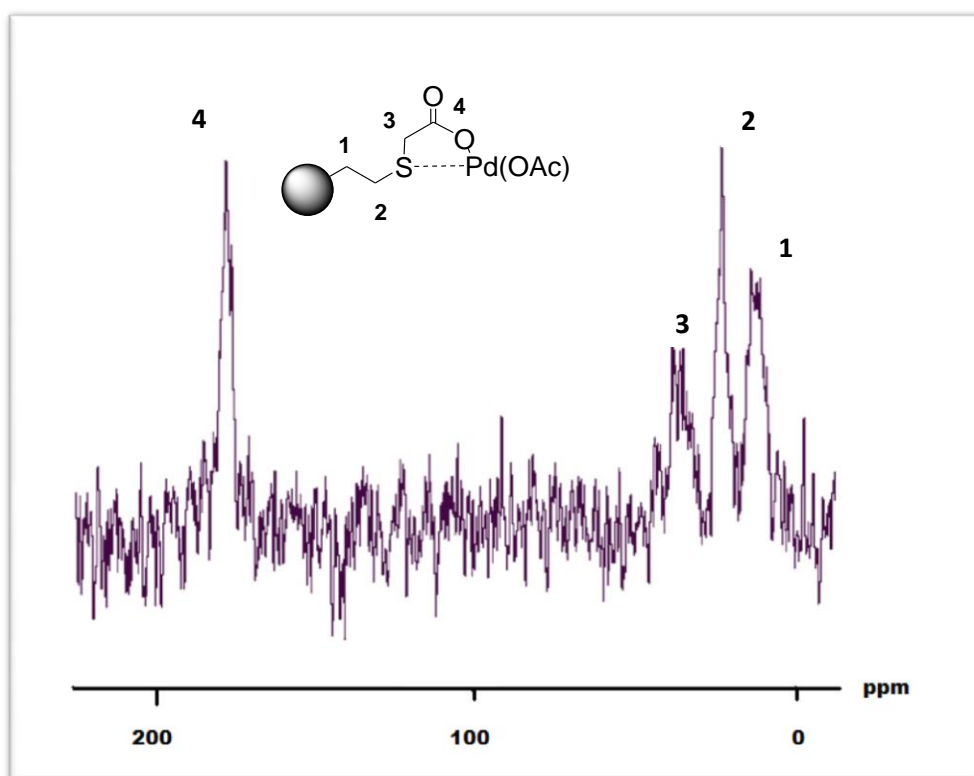


**Figure 2.32** <sup>13</sup>C CP MAS NMR of **silca-60-G<sub>1</sub>-Pd(OAc)**

### 2.6. 3 Solid state IR spectroscopy for silica-60-G<sub>1</sub>- Pd(OAc)

Further support of the presence of Pd(OAc) is provided by IR spectroscopy of the Pd loaded solid (**Figure 2.33**). The IR spectrum shows the major bands associated with the network Si-O-Si vibrational modes at 472, 810 and 1220  $\text{cm}^{-1}$  along with Si-O stretching vibration at 964  $\text{cm}^{-1}$  and a Si-OH stretching vibration at about 3400  $\text{cm}^{-1}$ . The appearance of an additional shoulder at 1190  $\text{cm}^{-1}$  in the Si-O-Si stretching region (1000-1200  $\text{cm}^{-1}$ ) indicates the presence of Si-C.<sup>13</sup> The IR spectrum also shows two sharp peaks at 1606 and 1440  $\text{cm}^{-1}$  which are related to the C=O and C-O vibrational modes; these peaks are also found in the organically modified silica, but with lower intensity.<sup>14</sup>

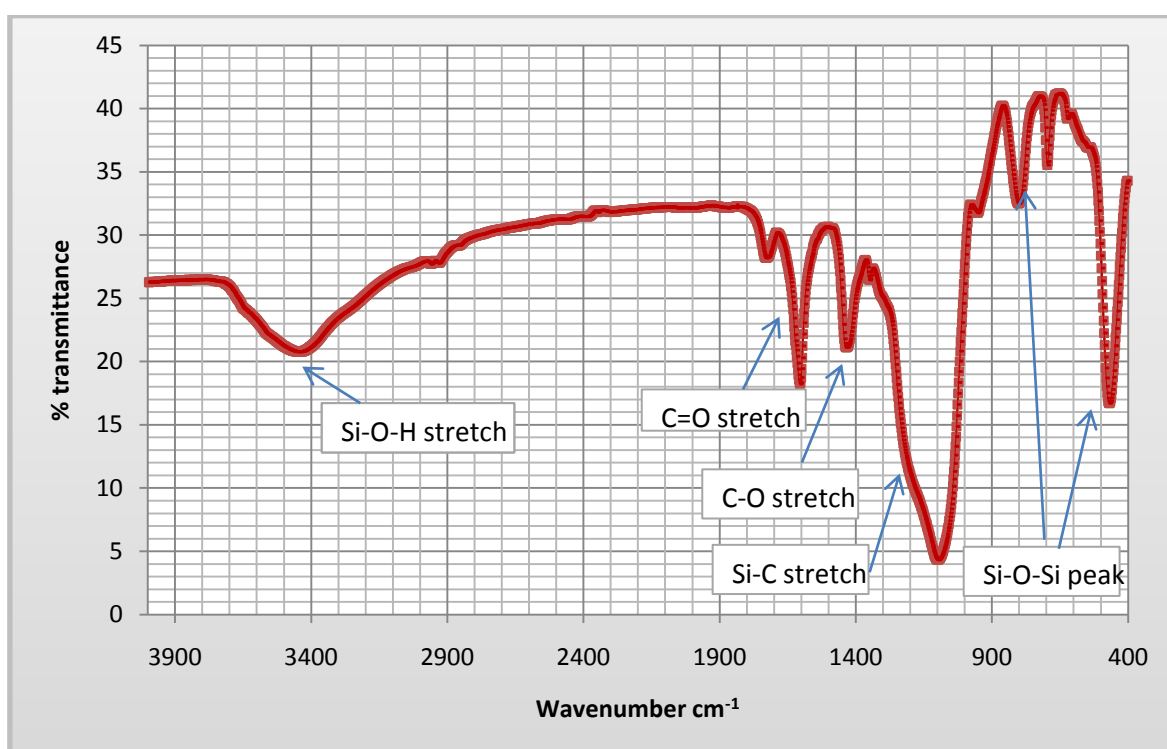


**Figure 2.33** Solid state IR spectroscopy of **silica-60-G<sub>1</sub>-Pd(OAc)**

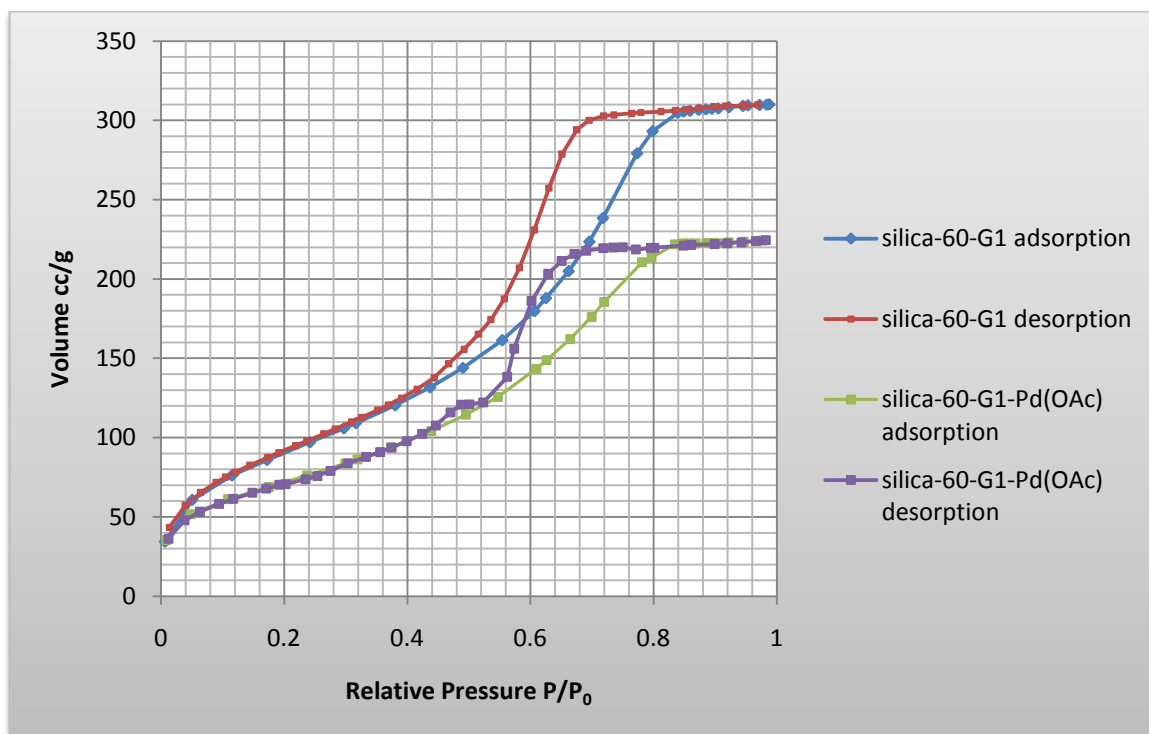
### 2.6.4 Porosimetry Studies of silica-60-G<sub>1</sub>-Pd(OAc)

Porosimetry studies were also carried out for **silica-60-G<sub>1</sub>-Pd(OAc)**. As with the organic modification, a small reduction in surface area, total pore volume and average pore diameter is observed upon introduction of the palladium. Even so the mesoporosity and surface area are still relatively high.

**Table 2.5** Porosimetry data for **silica-60-G<sub>1</sub>** and **silica-60-G<sub>1</sub>- Pd(OAc)**

	Surface area m <sup>2</sup> /g	Average Pore volume cc/g	Average Pore Diameter Å
<b>silica-60-G<sub>1</sub></b>	388.39	0.482	54.89
<b>silica-60-G<sub>1</sub>- Pd(OAc)</b>	287.89	0.347	47.88

Further, the sorption isotherms obtained for **silica-60-G<sub>1</sub>** and **silica-60-G<sub>1</sub>-Pd(OAc)** correspond to type IV according to the IUPAC classification. Both isotherms show the same hysteresis shape indicative of ink bottle shape pores being retained after modification both with ligand and with palladium. For **silica-60-G<sub>1</sub>-Pd(OAc)**, a shift in the adsorption branch towards lower pressures reveals a decrease in the pore size. This is further illustrated in the pore size distribution chart, **Figure 2.34**, for both materials.

**Figure 2.34** Isotherm graph for **silica-60-G<sub>1</sub>** and **silica-60-G<sub>1</sub>-Pd(OAc)**

The pore size distribution chart reveals sharp peaks in the mesoporous region, with the majority of pore sizes falling between 45 and 55 Å for **silica-60-G<sub>1</sub>-Pd(OAc)** and between 45 and 65 Å for **silica-60-G<sub>1</sub>**. The average pore size as calculated by the BJH method was found to decrease from 54.9 to 47.9 Å.

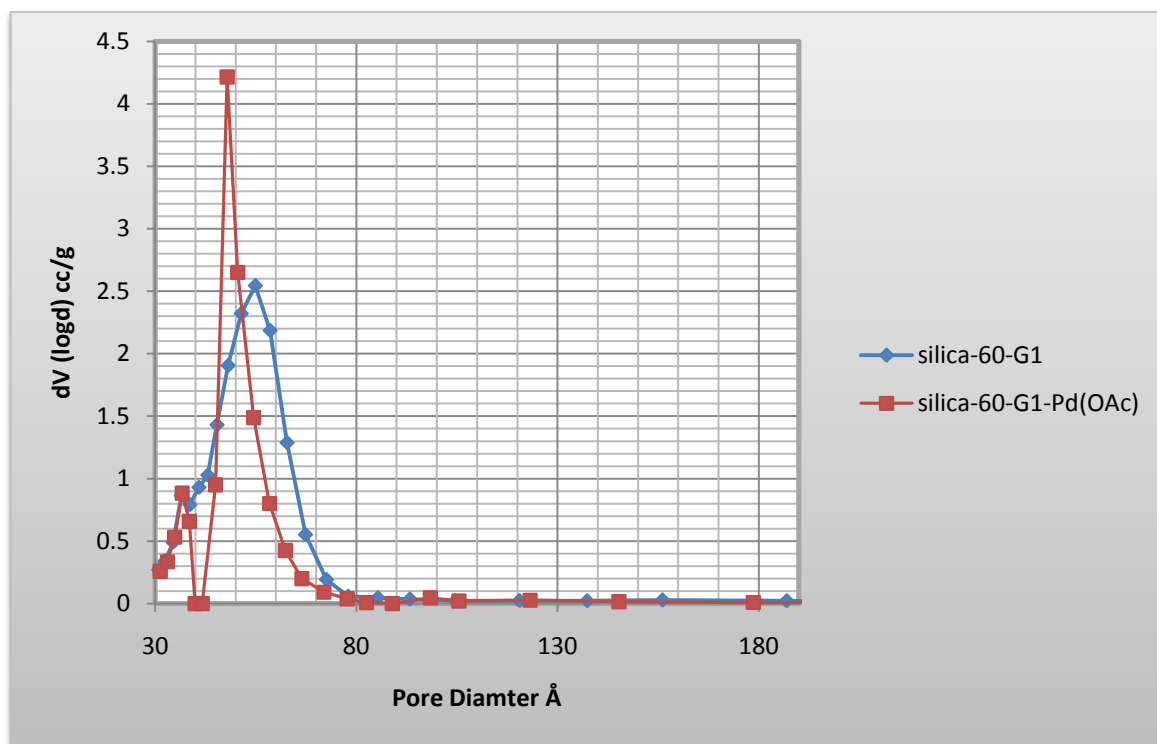


**Figure 2.35** Pore Size distribution chart for **silica-60-G<sub>1</sub>** and **silica-60-G<sub>1</sub>-Pd(OAc)**

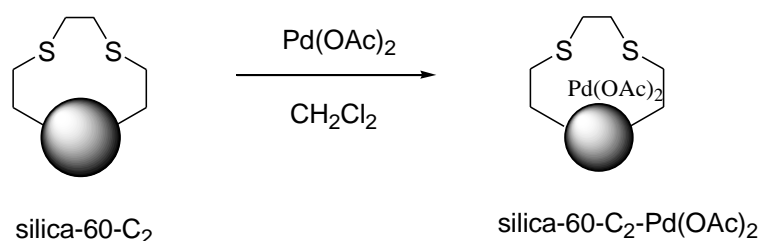
### 2.6.5 Palladium analysis in silica-60-G<sub>1</sub>-Pd(OAc)

The Pd content within the material was determined by stirring a known weight of **silica-60-G<sub>1</sub>-Pd(OAc)** in a solution of concentrated nitric acid under reflux for 6 hours. The solid was filtered and the digested metal in solution was measured by ICP-OES. The metal loading was found to be 0.8 mmol/g. Assuming 1:1 metal:thioglycolate binding this would suggest that approximately 60% of the ligand sites are occupied with 40% metal free. The solid filtered was a white solid indicating that all the palladium had been removed from the support. A further important point to make is that the harsh conditions needed to liberate the palladium reflect the high affinity the ligand has for the metal.

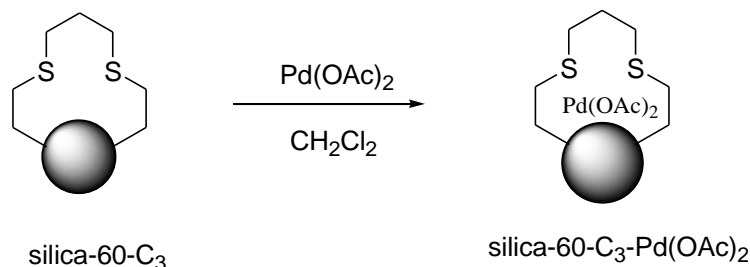


### 2.6.6 Synthesis of silica-60-C<sub>2</sub>-Pd(OAc)<sub>2</sub> and silica-60-C<sub>3</sub>-Pd(OAc)<sub>2</sub>

The complexation of palladium by these materials was relatively straightforward, **Schemes 2.15** and **2.16**. This was achieved by stirring **silica-60-C<sub>2</sub>** or **silica-60-C<sub>3</sub>** (2g) in a solution of Pd(OAc)<sub>2</sub> (0.32g) in dichloromethane (20 mL) for 24 hours at room temperature. The solid was then filtered, washed with dichloromethane until the washings were clear before being dried under vacuum at 60 °C overnight. The change in colour from a white powder to a strong orange colour was a good indication of metal complexation at immobilised ligand sites.



**Scheme 2.15** Synthesis of **silica-60-C<sub>2</sub>-Pd(OAc)<sub>2</sub>**



**Scheme 2.16** Synthesis of **silica-60-C<sub>3</sub>-Pd(OAc)<sub>2</sub>**

The structural depiction as shown in the **schemes 2.15** and **2.16** above between the Pd and the bis(dithio)alkane ligands is featured in a number of palladium complexes listed on the Cambridge Crystallographic database.<sup>15, 16</sup>

2.6.7  $^{13}\text{C}$  CP MAS NMR of silica-60- $\text{C}_2\text{-Pd}(\text{OAc})_2$  and silica-60- $\text{C}_3\text{-Pd}(\text{OAc})_2$ 

Further confirmation of the immobilisation of the metal complex onto the sulfur ligands came from  $^{13}\text{C}$  CP MAS NMR spectra of **silica-60- $\text{C}_2\text{-Pd}(\text{OAc})_2$**  and **silica-60- $\text{C}_3\text{-Pd}(\text{OAc})_2$** . This revealed line broadening of all resonances in both systems relative to the  $^{13}\text{C}$  CP MAS NMR of **silica-60- $\text{C}_2$**  and **silica-60- $\text{C}_3$** . This would suggest metal complexation to the ligand and/or the presence of bound and unbound ligand sites within the material giving rise to overlapping resonances. Further, in the  $^{13}\text{C}$  CP MAS spectrum of **silica-60- $\text{C}_3\text{-Pd}(\text{OAc})_2$** , a new peak at 90 ppm may be assigned to the quaternary carbon of the bidentate acetate. Additionally  $^{29}\text{Si}$  MAS NMR for **silica-60- $\text{C}_3\text{-Pd}(\text{OAc})_2$**  revealed a slight shift in the  $\text{T}^n$  environment, from -76ppm to -71ppm.

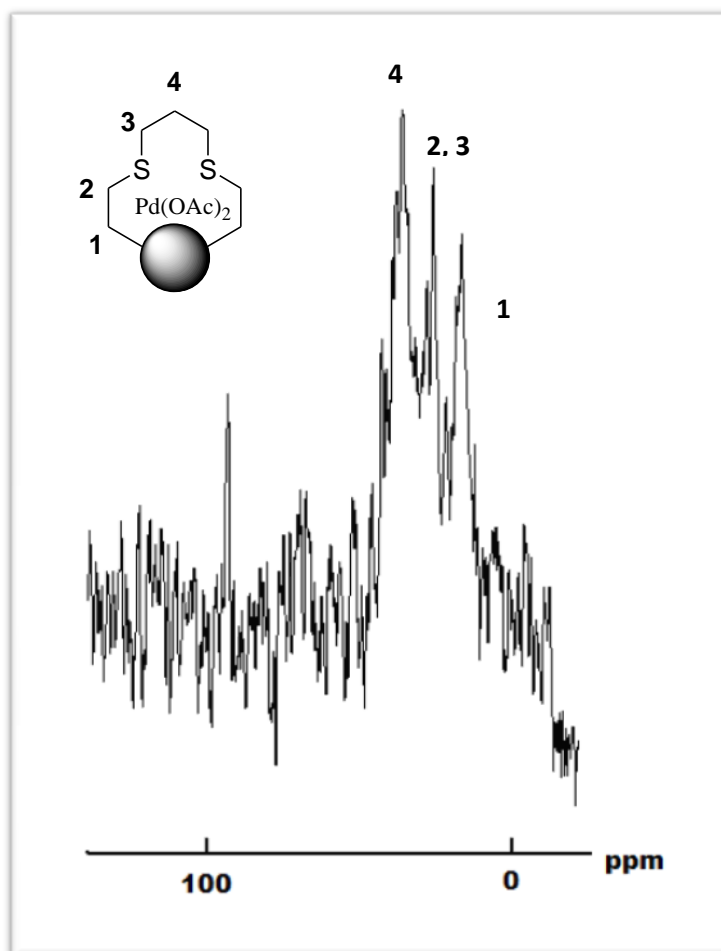


**Figure 2.36**  $^{13}\text{C}$  CP MAS NMR for **silica-60- $\text{C}_3\text{-Pd}(\text{OAc})_2$**

### 2.6.8 IR spectroscopy of silica-60-C<sub>2</sub>-Pd(OAc)<sub>2</sub> and silica-60-C<sub>3</sub>-Pd(OAc)<sub>2</sub>

Solid state IR spectroscopy was also carried out to characterise these palladium complexed catalysts. The samples were measured as KBr discs. The IR spectrum of **silica-60-C<sub>2</sub>-Pd(OAc)<sub>2</sub>** showed distinct peaks at 1449 cm<sup>-1</sup> and 1620 cm<sup>-1</sup> corresponding to the acetate peaks as well as the bands seen in silica-60-C<sub>2</sub> corresponding to the silica framework. Confirmation of the immobilisation of the Pd(OAc)<sub>2</sub> onto the silica-60-C<sub>3</sub> was also provided by IR spectroscopy. In addition to the bands corresponding to Si-O-Si bending vibrations at 472 cm<sup>-1</sup> and the Si-O stretching vibration at 1200 cm<sup>-1</sup>, as well as the band corresponding to the C-S bond at 801 cm<sup>-1</sup>, new peaks are found at 1429 cm<sup>-1</sup> and 1647 cm<sup>-1</sup>. These correspond to C-O and C=O stretches of the acetate group (**Figure 2.37**).

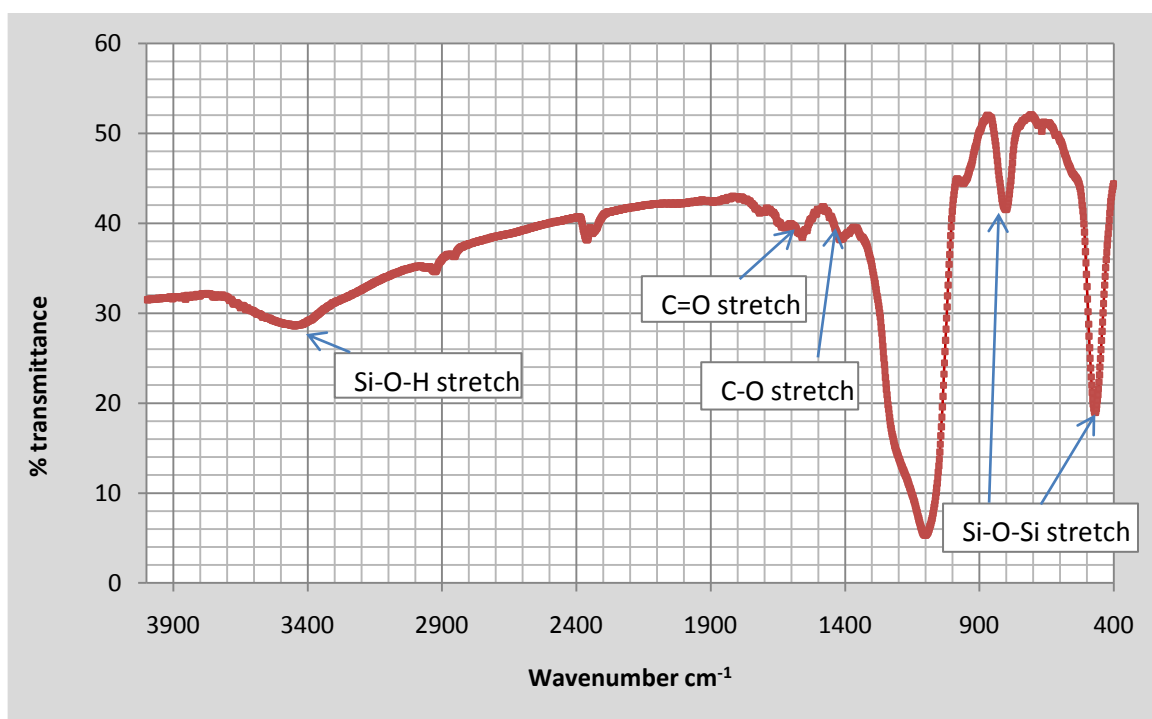


**Figure 2.37** Solid state IR spectrum for **silica-60-C<sub>3</sub>-Pd(OAc)<sub>2</sub>**

### 2.6.9 Porosimetry for silica-60-C<sub>2</sub>-Pd(OAc)<sub>2</sub> and silica-60-C<sub>3</sub>-Pd(OAc)<sub>2</sub>

Porosimetry studies were carried out for both **silica-60-C<sub>2</sub>-Pd(OAc)<sub>2</sub>** and **silica-60-C<sub>3</sub>-Pd(OAc)<sub>2</sub>**. An obvious drop in the pore volume is seen from the shape of the isotherm recorded before and after metal complexation. The physisorption isotherm shape was of type IV which is commonly seen for mesoporous materials. For **silica-60-C<sub>2</sub>-Pd(OAc)<sub>2</sub>** the shape

of the hysteresis loop (**Figure 2.38**) shows the pore shapes to have changed from ink bottle to more slit shaped pores, type H3, according to the IUPAC classification, after palladium uptake.

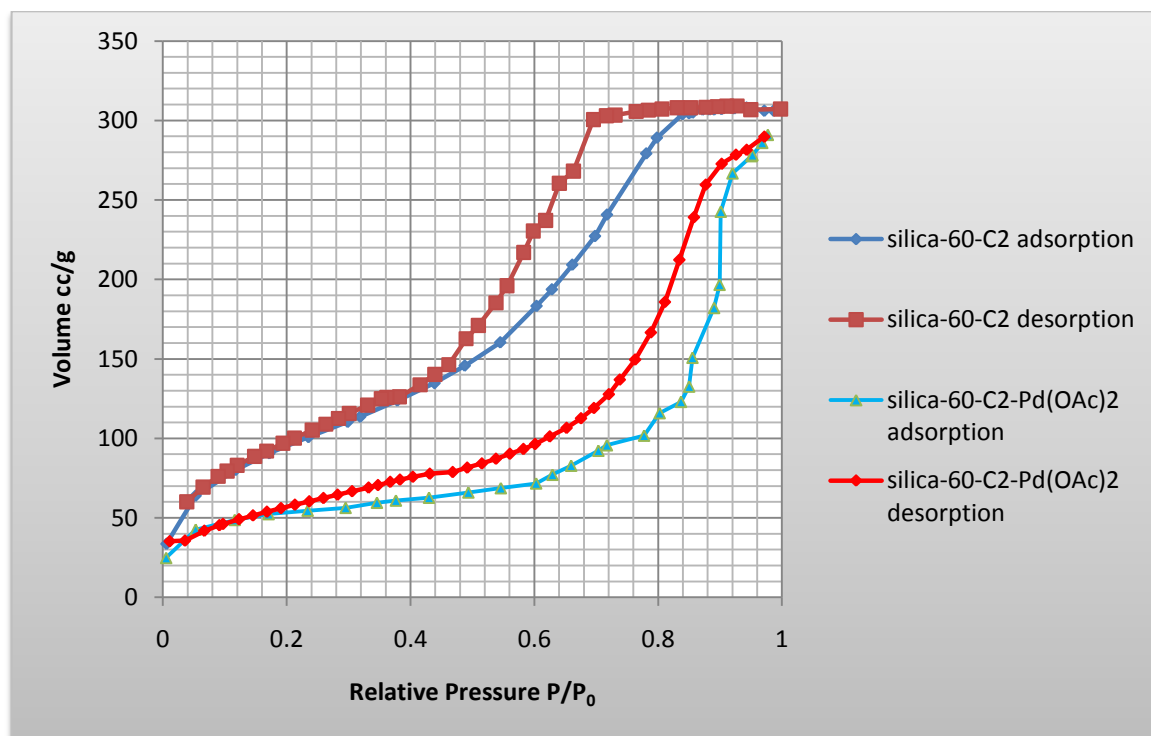


**Figure 2.38** Isotherm graph for **silica-60-C<sub>2</sub>** and **silica-60-C<sub>2</sub>-Pd(OAc)<sub>2</sub>**

A drop in surface area, from 377.61 m<sup>2</sup>/g to 170 m<sup>2</sup>/g was observed after modification of **silica-60-C<sub>2</sub>** with Pd complex. A much smaller change is observed from the average pore diameter and pore volumes.

**Table 2.6** Porosimetry values for **silica-60-C<sub>2</sub>** using BJH method

	Surface Area m <sup>2</sup> /g	Average Pore volume cc/g	Average Pore Diameter Å
<b>Silica-60-C<sub>2</sub></b>	377.61	0.469	56.7
<b>Silica-60-C<sub>2</sub>-Pd(OAc)<sub>2</sub></b>	170.7	0.425	78.6

The pore size distribution after palladium uptake is considerably broader and the average diameter increased from 56 Å to 78 Å. This could reflect a degree of blocking of the smaller pores by palladium with the consequence of skewing the distribution towards the larger pores.

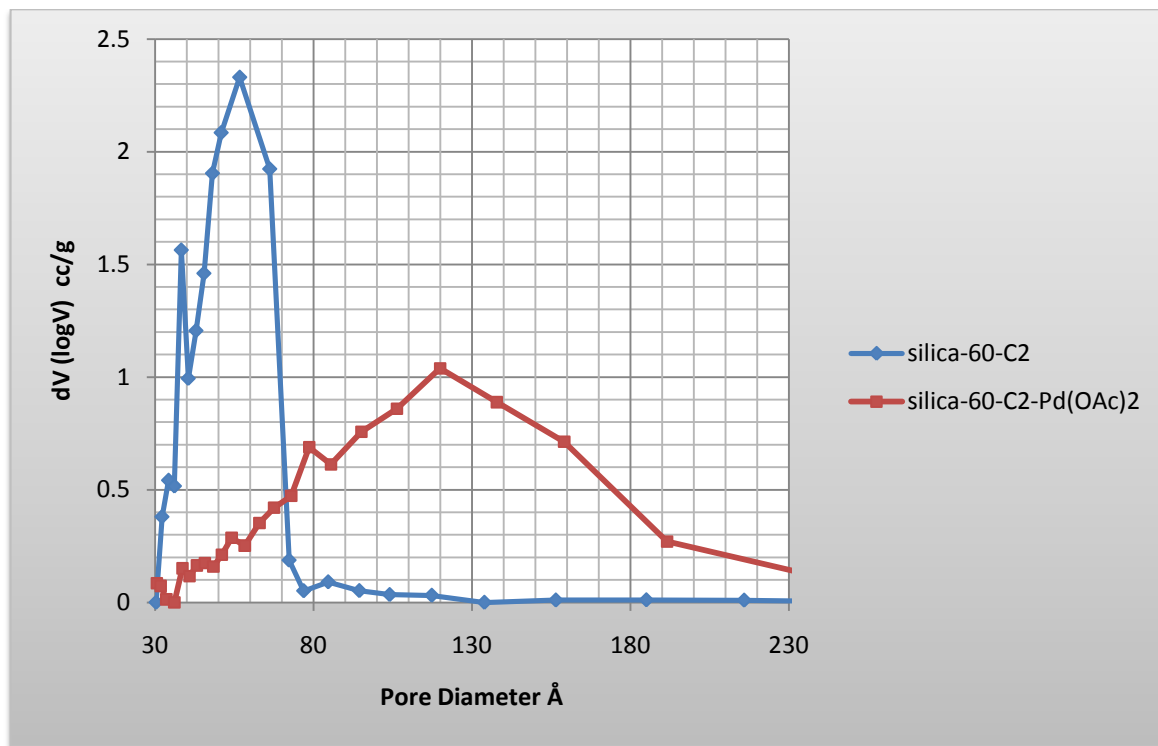


**Figure 2.39** Pore size distribution chart **silica-60-C<sub>2</sub>** and **silica-60-C<sub>2</sub>-Pd(OAc)<sub>2</sub>**

Porosimetry data was also recorded for **silica-60-C<sub>3</sub>** and **silica-60-C<sub>3</sub>-Pd(OAc)<sub>2</sub>**. A first look at the isotherm graph shows a clear drop in the pore volume after introduction of palladium. In addition a slight shift of the hysteresis loop towards lower relative pressures reveals a decrease in average pore size. The shape of the hysteresis loop indicates ink bottle shaped pores are present after both modification with organic ligand and metal.

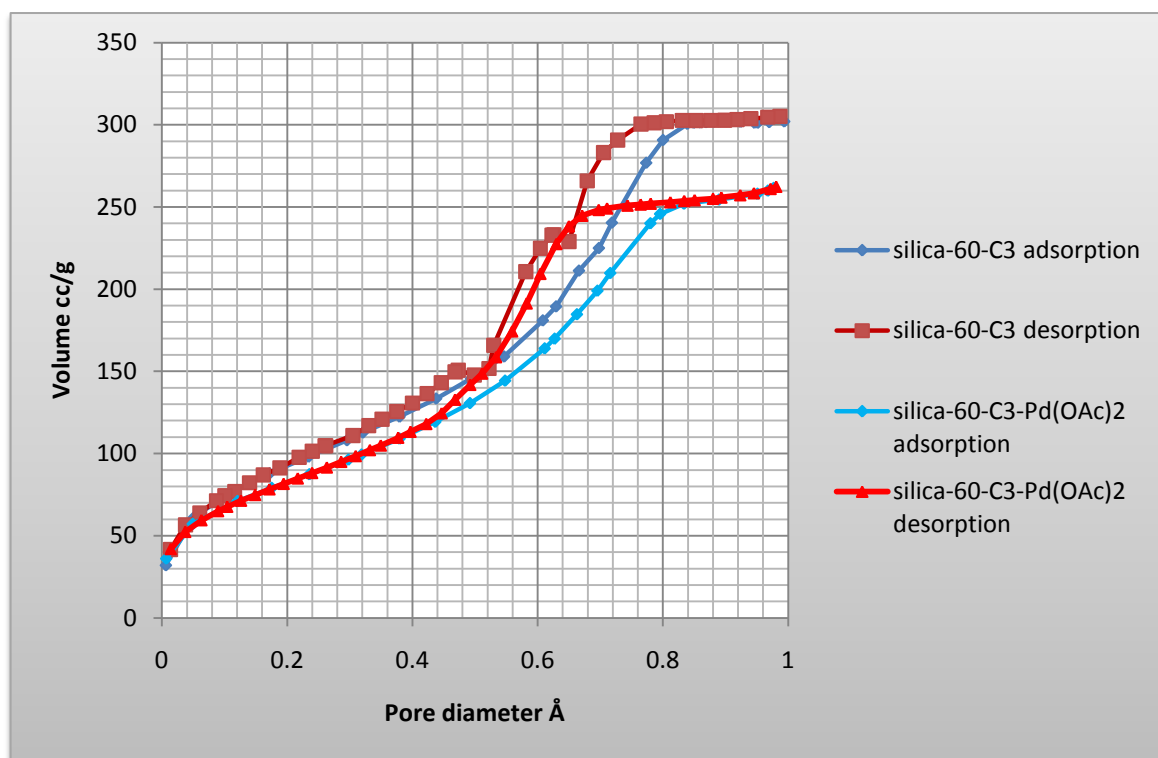


**Figure 2.40** Isotherm graph for **silica-60-C<sub>3</sub>** and **silica-60-C<sub>3</sub>-Pd(OAc)<sub>2</sub>**

In addition, despite the small drop in surface area and average pore volume observed upon palladium complexation, the mesoporosity and surface area are still high.

**Table 2.7** Porosimetry Data for chart **silica-60-C<sub>3</sub>** and **silica-60-C<sub>3</sub>-Pd(OAc)<sub>2</sub>**

	Surface Area m <sup>2</sup> /g	Average Pore Volume cc/g	Average Pore Diameter Å
<b>Silica-60-C<sub>3</sub></b>	371.3	0.479	43.1
<b>Silica-60-C<sub>3</sub>-Pd(OAc)<sub>2</sub></b>	319.9	0.39	51.3

As shown in the figure below, the pore size distribution for **silica-60-C<sub>3</sub>** is bimodal and covers the mesoporous range. The distribution appears more monomodal after modification of **silica-60-C<sub>3</sub>** with Pd(OAc)<sub>2</sub> but there is less obvious evidence of pore blocking compared to **silica-60-C<sub>2</sub>** with Pd(OAc)<sub>2</sub>.

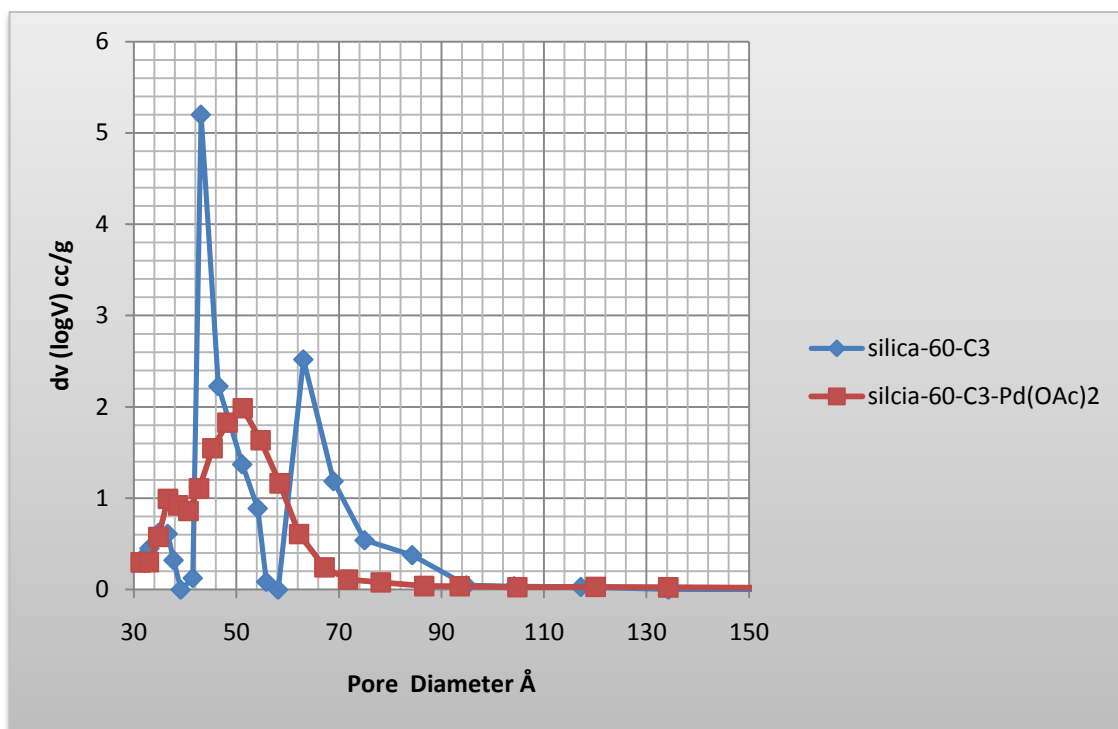


**Figure 2.41** Pore size distribution chart for **silica-60-C<sub>3</sub>** and **silica-60-C<sub>3</sub>-Pd(OAc)<sub>2</sub>**

#### 2.6.10 Palladium analysis in silica-60-C<sub>3</sub> and silica-60-C<sub>3</sub>-Pd(OAc)<sub>2</sub>

Determination of the palladium content was carried out as previously described by digesting the solid in concentrated nitric acid. The uptake of Pd acetate by **silica-60-C<sub>2</sub>** and **silica-60-C<sub>3</sub>** was extremely rapid as indicated by the fast colourisation of the organically modified materials. The measured Pd loadings were 0.26 mmol/g and 0.41 mmol/g respectively. Assuming a 1:1 metal binding, this suggests that approximately 46 and 80 % of the ligand sites are bound to Pd in **silica-60-C<sub>2</sub>-Pd(OAc)<sub>2</sub>** and **silica-60-C<sub>3</sub>-Pd(OAc)<sub>2</sub>** respectively. Porosimetry indicated some irregularities in the pore structure of the **silica-60-C<sub>2</sub>** material which may be correlated with the lower palladium uptake in this material.

### 2.6.11 TEM analysis for silica-60-C<sub>3</sub>-Pd(OAc)<sub>2</sub>

TEM coupled with EDS was carried out on **silica-60-C<sub>3</sub>-Pd(OAc)<sub>2</sub>**. This revealed a mostly homogeneous distribution of the Pd on the surface. The image below shows the material to have maintained its textural properties with respect to the palladium free parent (**Figure 2.42**).

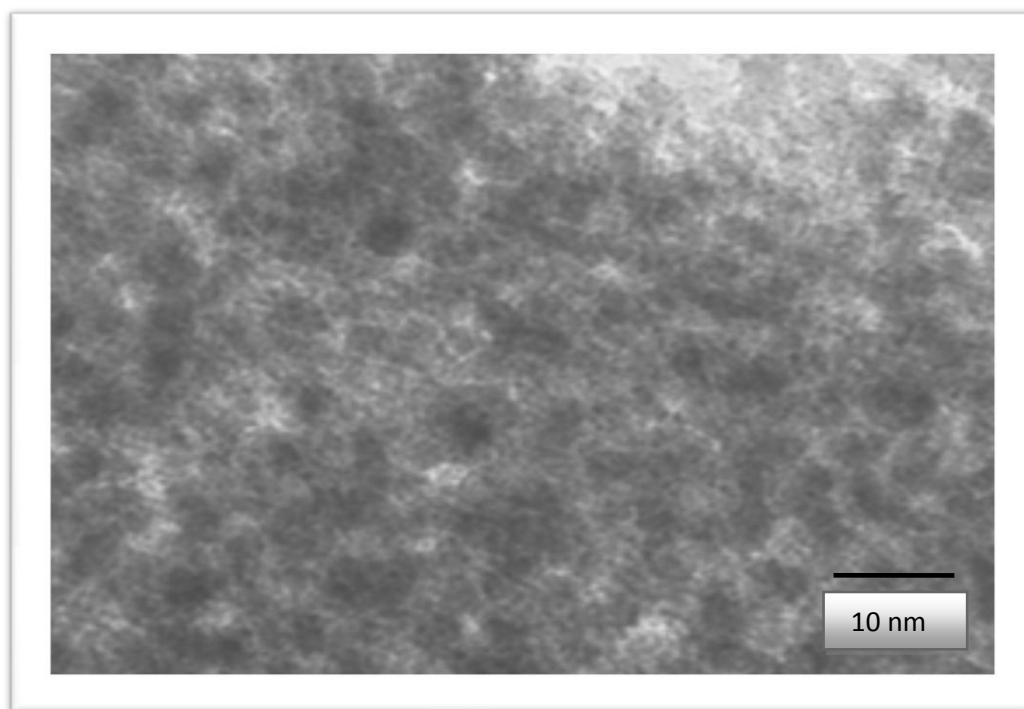


**Figure 2.42** TEM image of **silica-60-C<sub>3</sub>-Pd(OAc)<sub>2</sub>**

EDS analysis revealed varying ratios of Pd:S from as great as 1:3 to as little as 1:10. Furthermore, areas with higher sulfur content did not correlate with the highest Pd loading suggesting that Pd was more unvaryingly distributed.

### 2.6.12 Porosimetry studies of silica-90-C<sub>3</sub>-Pd(OAc)<sub>2</sub> and silica-150-C<sub>3</sub>-Pd(OAc)<sub>2</sub>

Catalysts silica-90-C<sub>3</sub>-Pd(OAc)<sub>2</sub> and silica-150-C<sub>3</sub>-Pd(OAc)<sub>2</sub> were synthesised in the same way as silica-60-C<sub>3</sub>-Pd(OAc)<sub>2</sub>. These materials were characterised by porosimetry and Pd analysis. The adsorption isotherms below show mesoporosity has been maintained for both materials after introduction of palladium. The isotherm shape of **silica-90-C<sub>3</sub>** seems to be type IV, which is indicative of mesoporous materials. The hysteresis loop formed can be



described as type H2 which is said to be associated with ink bottle neck pores. The isotherm graph shape of **silica-150-C<sub>3</sub>** can be described as type IV with the hysteresis shape type H1, which is associated with open ended cylindrical pores; often these materials have a narrow distribution of pore sizes.

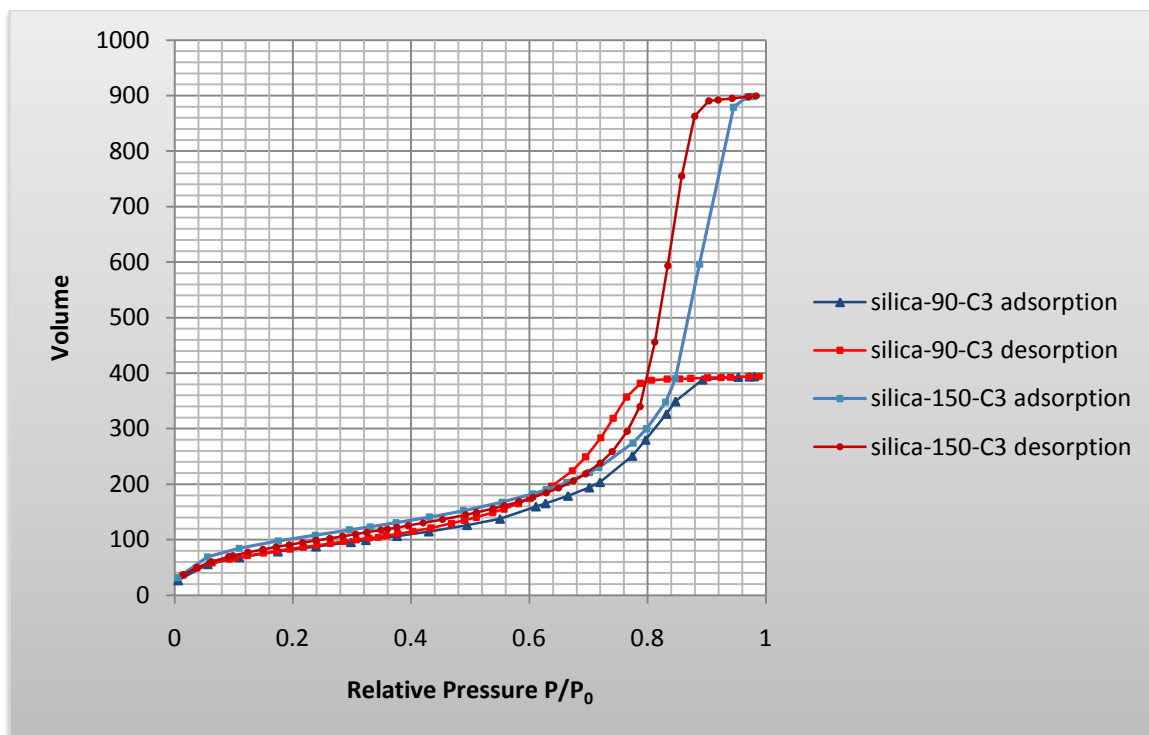


**Figure 2.43** Sorption isotherms for **silica-90-C<sub>3</sub>** and **silica-150-C<sub>3</sub>**

The table below shows the change in porosimetry data in both materials following palladium uptake. A huge reduction is seen in the surface areas of both **silica-90-C<sub>3</sub>-Pd(OAc)<sub>2</sub>** and **silica-150-C<sub>3</sub>-Pd(OAc)<sub>2</sub>**. In the case of **silica-90-C<sub>3</sub>**, a reduction from 379 m<sup>2</sup>/g to 278 m<sup>2</sup>/g is reported. A large reduction in the average pore volume is also observed, from 0.629 cc/g to 0.469 cc/g. The average pore size distribution of catalyst **silica-90-C<sub>3</sub>-Pd(OAc)<sub>2</sub>** is also found to reduce, from 79 Å to 72 Å.

**Table 2.8** The calculated porosimetry data from the BJH method for materials **silica-90-C<sub>3</sub>** and **silica-150-C<sub>3</sub>** before and after metal introduction.

	Surface Area m <sup>2</sup> /g	Average Pore volume cc/g	Average Pore Diameter Å
<b>silica-90-C<sub>3</sub></b>	378.8	0.629	79.3
<b>silica-90-C<sub>3</sub>-Pd(OAc)<sub>2</sub></b>	278.1	0.469	72.42
<b>silica-150-C<sub>3</sub></b>	497.3	1.47	120.2
<b>silica-150-C<sub>3</sub>-Pd(OAc)<sub>2</sub></b>	238.2	0.71	137.0

In the case of **silica-150-C<sub>3</sub>**, we find a huge reduction in the surface area from 497 to 238 m<sup>2</sup>/g. Similarly, the average pore volume is also found to decrease quite significantly as well from 1.47 cc/g to 0.71 cc/g. Even so, the calculated surface area, average pore size and average pore diameter are still relatively high and such physical properties are features of successful catalysts.

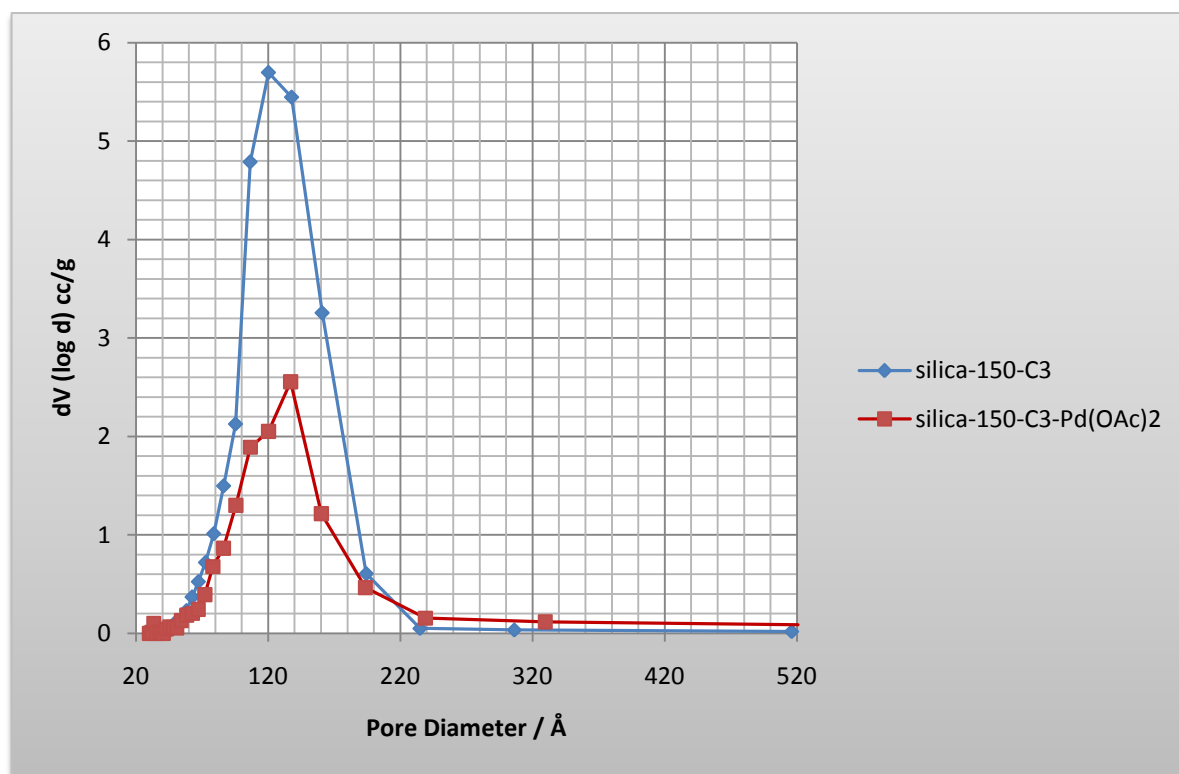


**Figure 2.44** Pore size distribution graph for **silica-150-C<sub>3</sub>** and **silica-150-C<sub>3</sub>-Pd(OAc)<sub>2</sub>**

Porosimetry studies for **silica-150-C<sub>3</sub>** after treatment with palladium showed a huge reduction in the surface area, from 497m<sup>2</sup>/g to 238 m<sup>2</sup>/g, greater than was observed for **silica-90-C<sub>3</sub>**. The average pore volume was also shown to decrease from 1.47 cc/g to 0.71 cc/g. As shown in the pore size distribution chart above, a change in average pore diameter seems to be rather insignificant and in contrast to the silica-60-C<sub>3</sub>-Pd(OAc)<sub>2</sub> there is no evidence of pore blocking.

#### 2.6.14 Palladium analysis

Palladium analysis for both **silica-90-C<sub>3</sub>** and **silica-150-C<sub>3</sub>** was carried as described previously and ICP-OES analysis revealed **silica-90-C<sub>3</sub>-Pd(OAc)<sub>2</sub>** and **silica-150-C<sub>3</sub>-Pd(OAc)<sub>2</sub>** to have 0.59 and 0.54 mmol/g of palladium respectively. This would suggest that approximately 90 % of the ligand sites are bound to Pd metal for **silica-90-C<sub>3</sub>** and for **silica-150-C<sub>3</sub>** complete metal complexation of the ligand sites is indicated.

### 2.6.15 Synthesis of silica-60-C<sub>3</sub>-PdCl<sub>2</sub>

Catalyst **silica-60-C<sub>3</sub>-PdCl<sub>2</sub>** was prepared using a similar procedure to that described earlier for **silica-60-C<sub>3</sub>-Pd(OAc)<sub>2</sub>**. This was achieved by stirring **silica-60-C<sub>3</sub>** in a solution of PdCl<sub>2</sub> in THF for 24 hours at room temperature. After this the solid was filtered, washed well with THF and then dried under vacuum to give an orange coloured powder.

### 2.6.16 Porosimetry studies of silica-60-C<sub>3</sub>-PdCl<sub>2</sub>

Porosimetry was used to characterise the catalyst **silica-60-C<sub>3</sub>-PdCl<sub>2</sub>**. Herein, a drop in average pore volume, average pore diameter and surface area was observed with the introduction of PdCl<sub>2</sub> to silica-60-C<sub>3</sub> (**Table 2.9**). From the isotherm graph it can be seen that the mesoporous nature of the catalyst remains as well as a high surface area.

**Table 2.9** Porosity values for **silica-60-C<sub>3</sub>-PdCl<sub>2</sub>** as calculated from the BJH method.

	Surface area m <sup>2</sup> /g	Average Pore Volume cc/g	Average Pore Diameter A
<b>Silica-60-C<sub>3</sub></b>	345.6	0.51	54.5
<b>Silica-60-C<sub>3</sub>-PdCl<sub>2</sub></b>	325.8	0.43	89.9

The sorption isotherm graph obtained corresponds to type IV isotherms. In addition, the IUPAC classification describes hysteresis shapes as shown by **silica-60-C<sub>3</sub>-PdCl<sub>2</sub>** to be of the slit shaped pores.

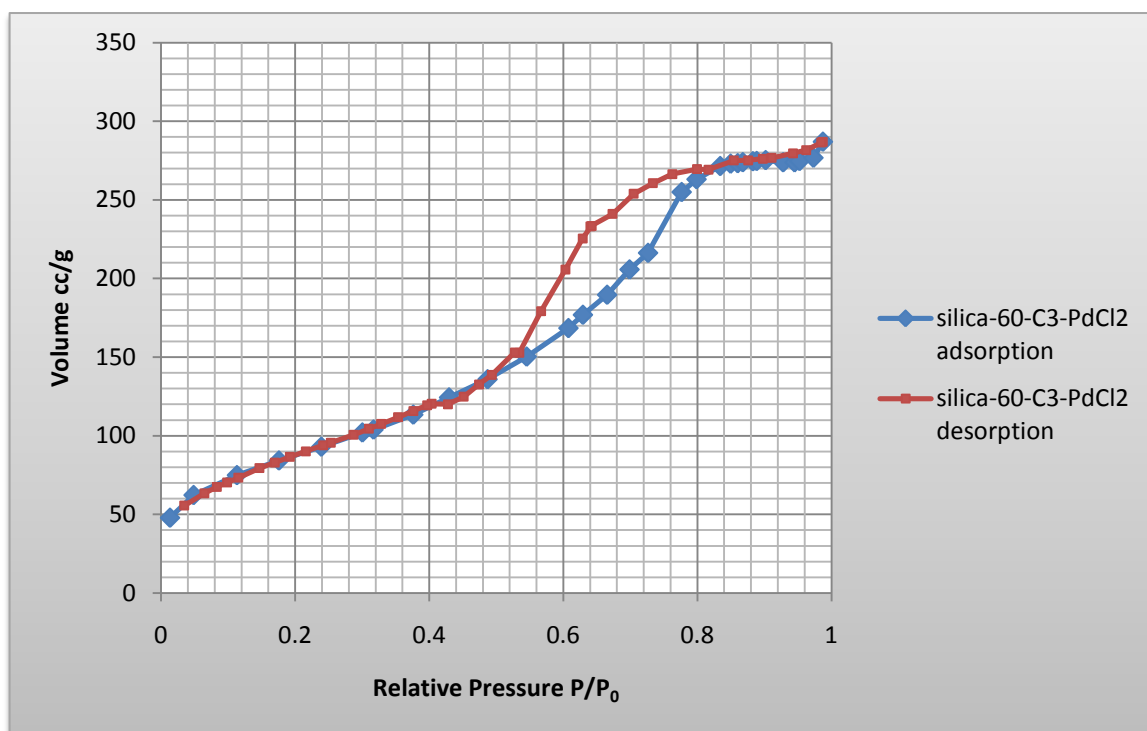


Figure 2.45 Isotherm graph for silica-60-C<sub>3</sub>-PdCl<sub>2</sub>

The pore size distribution chart revealed that the majority of pore sizes fall between 40-60 Å, with a small proportion of larger pores (Figure 2.46).

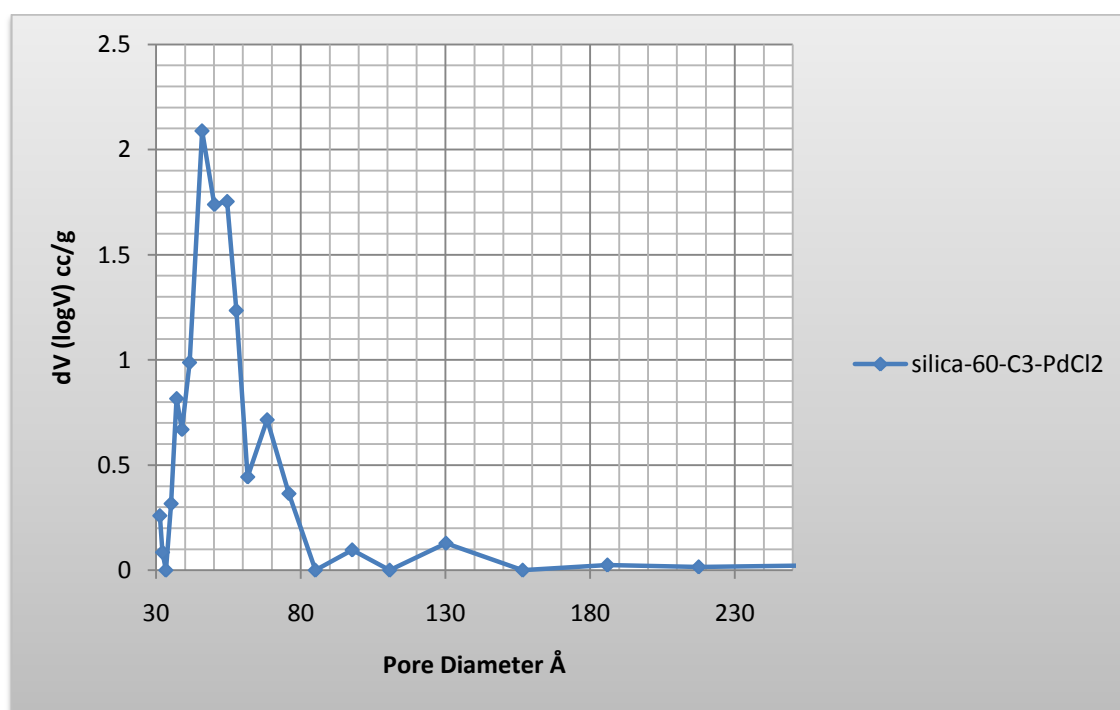


Figure 2.46 Pore Size distribution graph for silica-60-C<sub>3</sub>-PdCl<sub>2</sub>

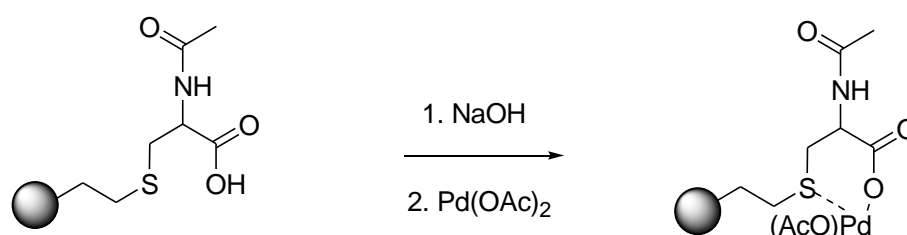
### 2.6.17 Palladium analysis of silica-60-C<sub>3</sub>-PdCl<sub>2</sub>

The palladium content was determined as before using ICP-OES. The metal loading for silica-60-C<sub>3</sub>-PdCl<sub>2</sub> was found to be 0.48 mmol/g suggesting that approximately 90% of the ligand sites are complexed to metal.

## 2.7 Pd derivatised cysteine materials; synthesis and characterisation

### 2.7.1 Synthesis and characterisation of silica-60-N-derivatised-L-cysteine-Pd(OAc)

Preparation of **silica-60-N-acetyl-L-cysteine-Pd(OAc)** and **silica-60-N-4-methoxybenzyl-L-cysteine-Pd(OAc)** followed the same procedure as described for **silica-60-G<sub>1</sub>-Pd(OAc)**. Here, **silica-60-N-derivatised-cysteine** (1g) was added to a 1M solution of NaOH (30 mL) and stirred for 15 minutes. The solid was then filtered, washed with methanol and dried under reduced pressure.



**Scheme 2.17** Preparation of **silica-60-N-acetyl-L-cysteine-Pd(OAc)**

The immobilisation of palladium to give **silica-60-N-acetyl-L-cysteine-Pd(OAc)** and **silica-60-N-4-methoxybenzyl-L-cysteine-Pd(OAc)** was rapid as was indicated by the fast colouration of the solid in contact with the palladium acetate in solution. This was achieved by stirring the sodium salt materials (2g) in a solution of Pd(OAc)<sub>2</sub> (0.32g) in dichloromethane (20mL) for 24 hours at room temperature. The mixture was then filtered and washed with dichloromethane until the washings were clear. The dark orange solid obtained was then dried under vacuum at 50 °C overnight.

Characterization of the new catalyst systems was carried out by solid state <sup>13</sup>C spectroscopy, IR spectroscopy, porosimetry and analysis of the metal loading.

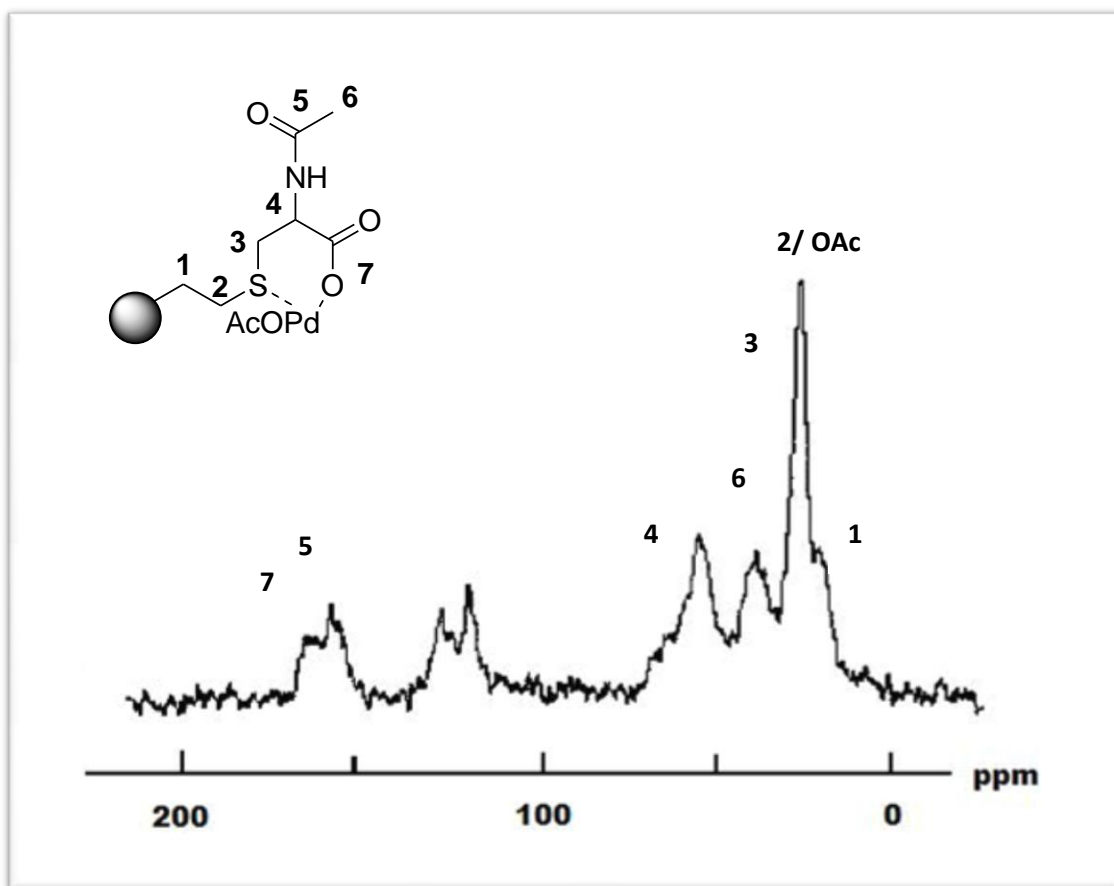
2.7.2  $^{13}\text{C}$  CP MAS NMR Spectroscopy

Figure 2.47  $^{13}\text{C}$  CP MAS NMR of silica-60-N-acetyl-L-cysteine-Pd(OAc)

The  $^{13}\text{C}$  CP MAS spectrum of **silica-60-N-acetyl-L-cysteine-Pd(OAc)** confirms immobilisation of the Pd metal onto the modified silica. Extensive line broadening is observed and this would suggest both metal complexed ligand sites as well as metal free ligand sites.

## 2.7.3 IR spectroscopy

IR spectroscopy further confirms the immobilisation of metal to **silica-60-N-acetyl-L-cysteine**. Herein, peaks corresponding to the silica framework, such as Si-O-Si bending vibrations and Si-O stretching vibrations were found at 799, 950 and 1050  $\text{cm}^{-1}$  respectively. An additional shoulder peak at 1210  $\text{cm}^{-1}$  corresponds to Si-C stretching vibrations while C=O vibrations are found at 1650  $\text{cm}^{-1}$ . A broad O-H stretch found at 3400  $\text{cm}^{-1}$  would

suggest some residual silanol groups are present on the surface of **silica-60-N-acetyl-L-cysteine**.

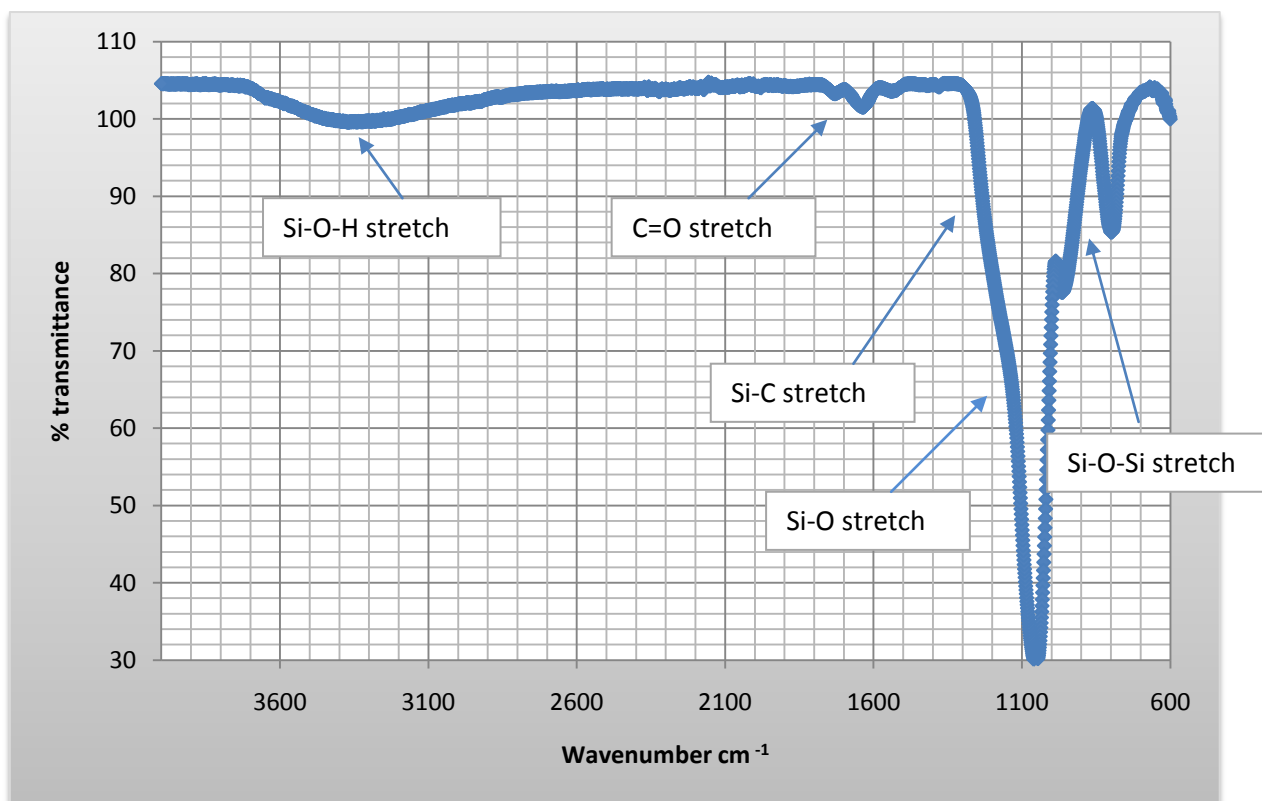


**Figure 2.48** IR spectroscopy for **silica-60-N-acetyl-L-cysteine-Pd(OAc)**

#### 2.7.4 Porosimetry

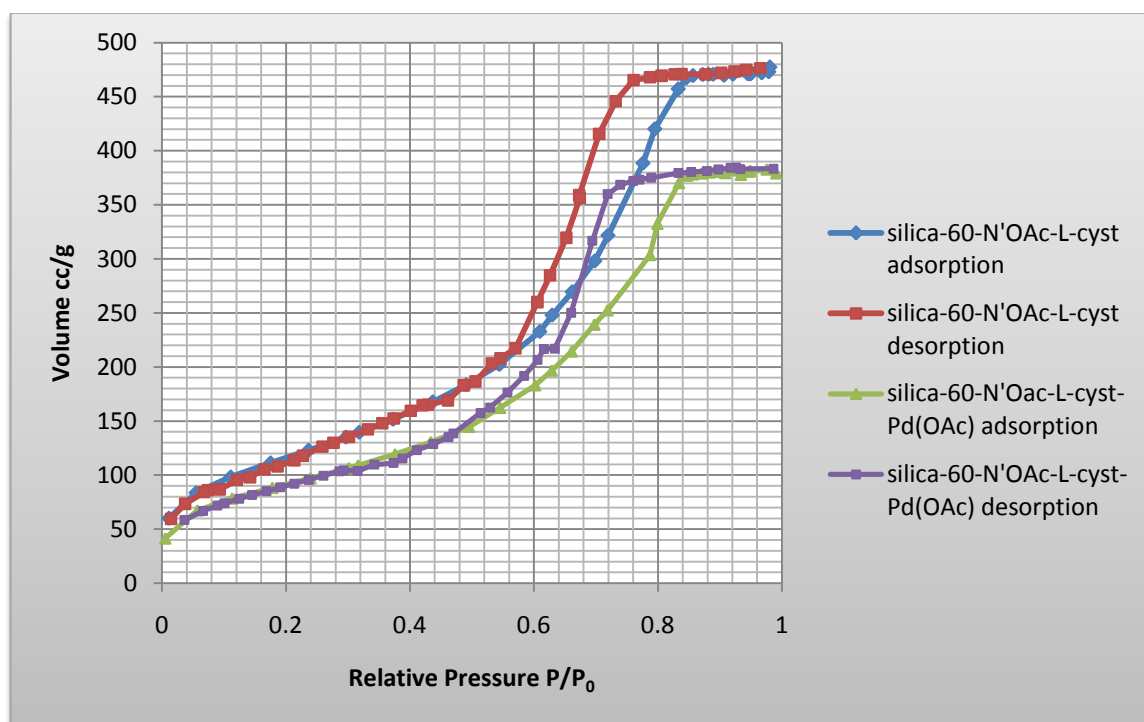
Porosimetry measurements were also taken for **silica-60-N-acetyl-L-cysteine-Pd(OAc)**. This revealed a relatively high surface area, pore volume and pore diameter to be retained after the complexation of palladium.



**Table 2.10** Porosimetry Data for **silica-60-N-acetyl-L-cysteine** and **silica-60-N-acetyl-L-cysteine-Pd(OAc)** as calculated from BJH method.

	Surface Area m <sup>2</sup> /g	Average Pore Diameter Å	Average Pore volume cc/g
<b>silica-60-N-acetyl-L-cyst</b>	524.7	64.8	0.769
<b>silica-60-N-acetyl-L-cyst-Pd(OAc)</b>	452.5	65.7	0.650

The sorption isotherm obtained for **silica-60-N-acetyl-L-cysteine** and **silica-60-N-acetyl-L-cysteine-Pd(OAc)** reveals mesoporosity is retained after both ligand and metal modification of the silica. Further to this a clear drop in the total volume is indicative of metal modification on the surface. The hysteresis shape as shown by these materials **silica-60-N-acetyl-L-cysteine** and **silica-60-N-acetyl-L-cysteine-Pd(OAc)** indicate pore shapes to be of a more ink bottle shaped nature.

**Figure 2.49** Isotherm graph for **silica-60-N-acetyl-L-cysteine** and **silica-60-N-acetyl-L-cysteine-Pd(OAc)**

The pore size distribution chart as shown in the figure below shows little difference in the pore size range for **silica-60-N-acetyl-L-cysteine** and **silica-60-N-acetyl-L-cysteine-Pd(OAc)** and no evidence of pore blocking. Both observations are consistent with the low level of palladium loading in the material.

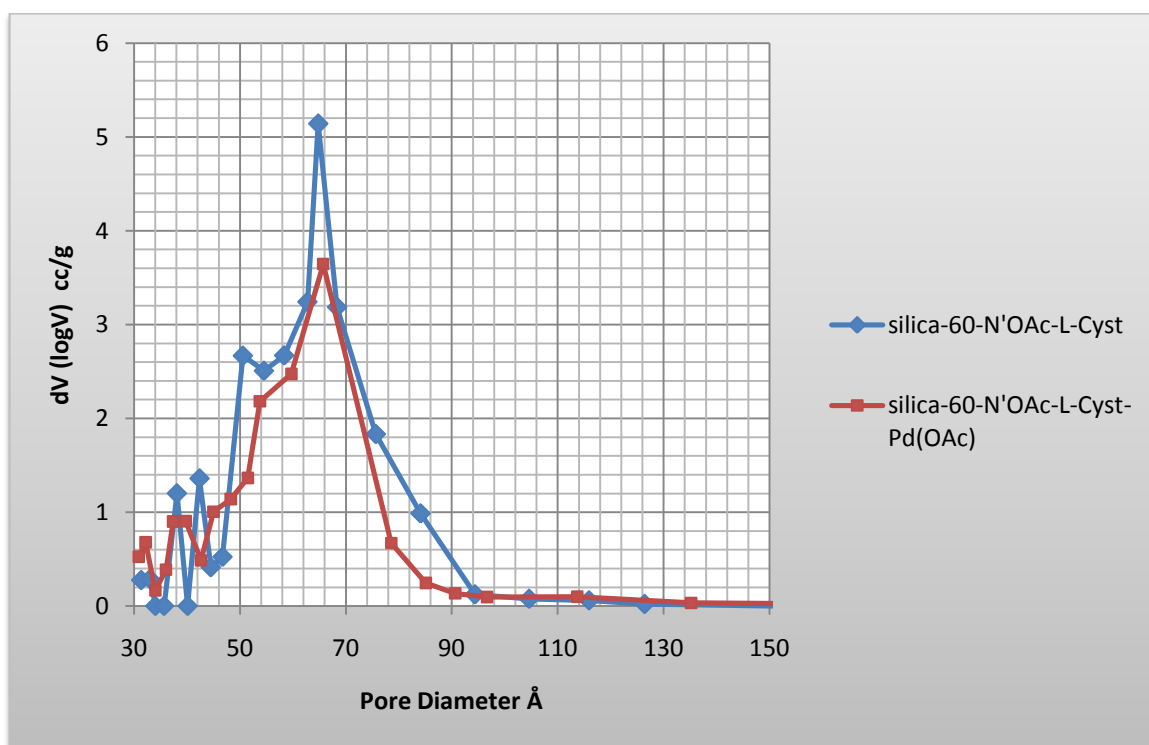


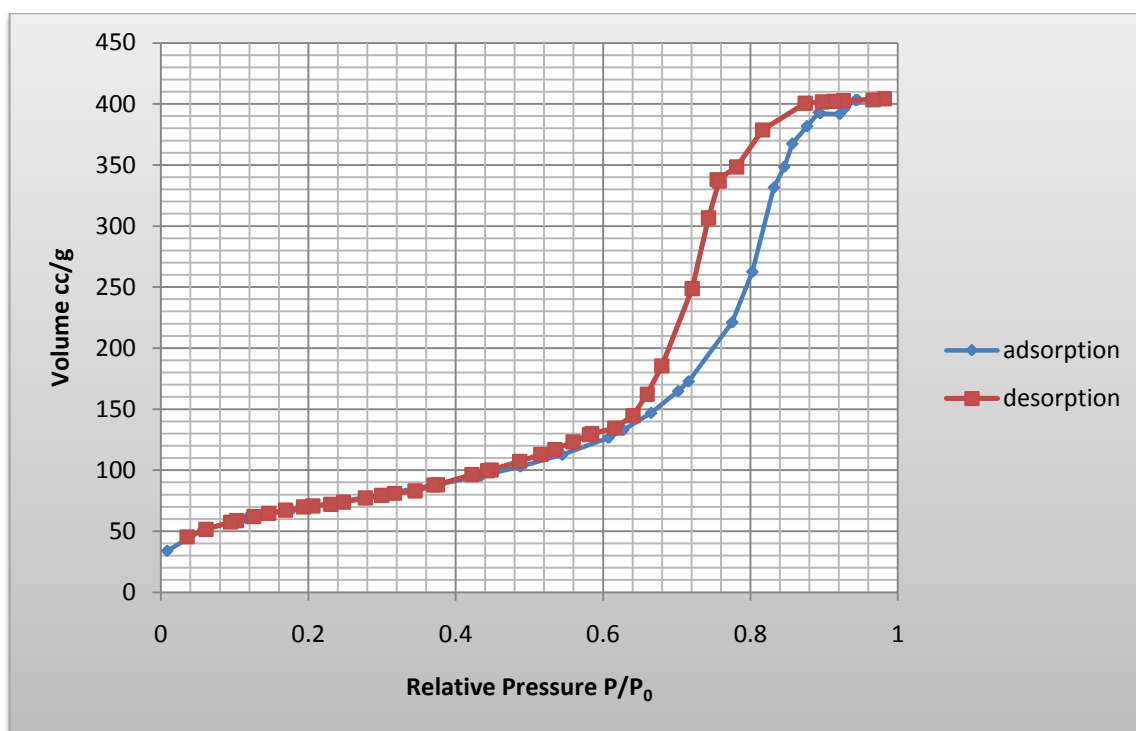
**Figure 2.50** Pore Size distribution chart for **silica-60-N-acetyl-L-cysteine** and **silica-60-N-acetyl-L-cysteine-Pd(OAc)**

The porosimetry data obtained for **silica-60-N-4-methoxybenzyl-cysteine-Pd(OAc)** shows the material to have relatively high surface area, average pore diameter and pore volume. The organically modified silica, **silica-60-N-4-methoxybenzyl-cysteine** was prepared using silica with average pore diameter of 60Å. The observation of larger average pore size for **silica-60-N-4-methoxybenzyl-cysteine-Pd(OAc)** may be due to the blocking of small pores which could skew the distribution of pore sizes towards larger pores.

**Table 2.11** Porosimetry data for **silica-60-N-4-methoxybenzyl-L-cysteine-Pd(OAc)** as calculated from the BJH method

	Surface area $\text{m}^2/\text{g}$	Average pore diameter $\text{\AA}$	Average pore volume $\text{cc/g}$
<b>silica-60-N-4-methoxybenzyl-L-cysteine-Pd(OAc)</b>	354.18	82.3	0.70

The shape of the hysteresis of the sorption isotherm of **silica-60-N-4-methoxybenzyl-L-cysteine-Pd(OAc)** reveals it to have ink bottle shaped pores which are quite cylindrical like as the pore diameters are relatively large. This is also found to be the case for **silica-60-N-acetyl-L-cysteine**.

**Figure 2.51** Isotherm graph for **silica-60-N-4-methoxybenzyl-cysteine-Pd(OAc)**

The pore size distribution chart as shown below demonstrates the pore size range to fall mainly between 70 to 85  $\text{\AA}$ . Approximately 20% of the pore sizes are of the range 90 to 170  $\text{\AA}$ .

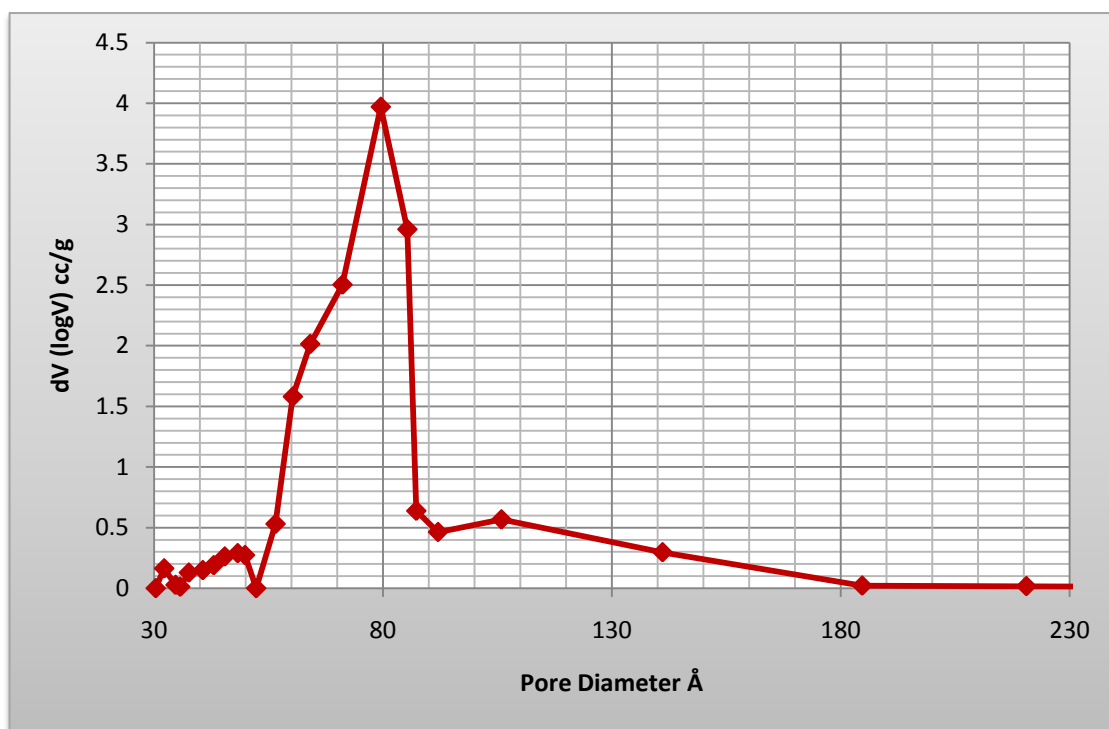


**Figure 2.52** Pore size distribution chart for **silica-60-N-4-methoxybenzyl-L-cysteine-Pd(OAc)**

### 2.7.5 Palladium analysis

The palladium loadings for **silica-60-N-acetyl-L-cysteine-Pd(OAc)** and **silica-60-N-4-methoxybenzyl-L-cysteine-Pd(OAc)** from ICP-OES analysis were found to be 0.23 and 0.25 mmol/g respectively. In comparison to the determined ligand loadings we find a large proportion of the ligand sites within **silica-60-N-acetyl-cysteine-L-Pd(OAc)** are occupied by metal, more than 80%. In the case of **silica-60-N-4-methoxybenzyl-L-cysteine-Pd(OAc)**, approximately 20% of the ligand sites are complexed to metal.

### 2.8. Comparative palladium binding studies

Having prepared these heterogeneous palladium catalysts it was of interest to evaluate the relative palladium affinity of the parent materials. To do this, samples of organically modified silica (200 mg) were exposed to palladium acetate (for a range of supported ligand: Pd ratios) in 2 mL dichloromethane. The mixtures were stirred for 24 hours at room temperature before being filtered and washed with 2mL of dichloromethane. The Pd content

in the combined filtrate and washings was measured by ICP-OES. In addition to binding studies being performed for **silica-60-G<sub>1</sub>**, **silica-60-C<sub>2</sub>** and **silica-60-C<sub>3</sub>**, a fourth material was prepared for comparison. This material, **silica-60-SC<sub>3</sub>SH**, differs from silica-60-C<sub>3</sub> in having one untethered thio group and was prepared relatively simply from 1,3-propanedithiol and one equivalent of vinyltrimethoxysilane. The organoalkoxysilane product was then grafted onto silica.

The graph below shows the % Pd uptake by the different materials with varying Pd/ligand ratio, in the range 0.5 to 1. Whilst all of the materials displayed very good Pd uptake performance in this window, that is >98%, the material **silica-60-C<sub>3</sub>SSH** gave the best results with >99% uptake for all ratios studied. The experiment shows that for the other materials, a Pd:ligand ratio of <0.7 should be employed to ensure >99% immobilisation.

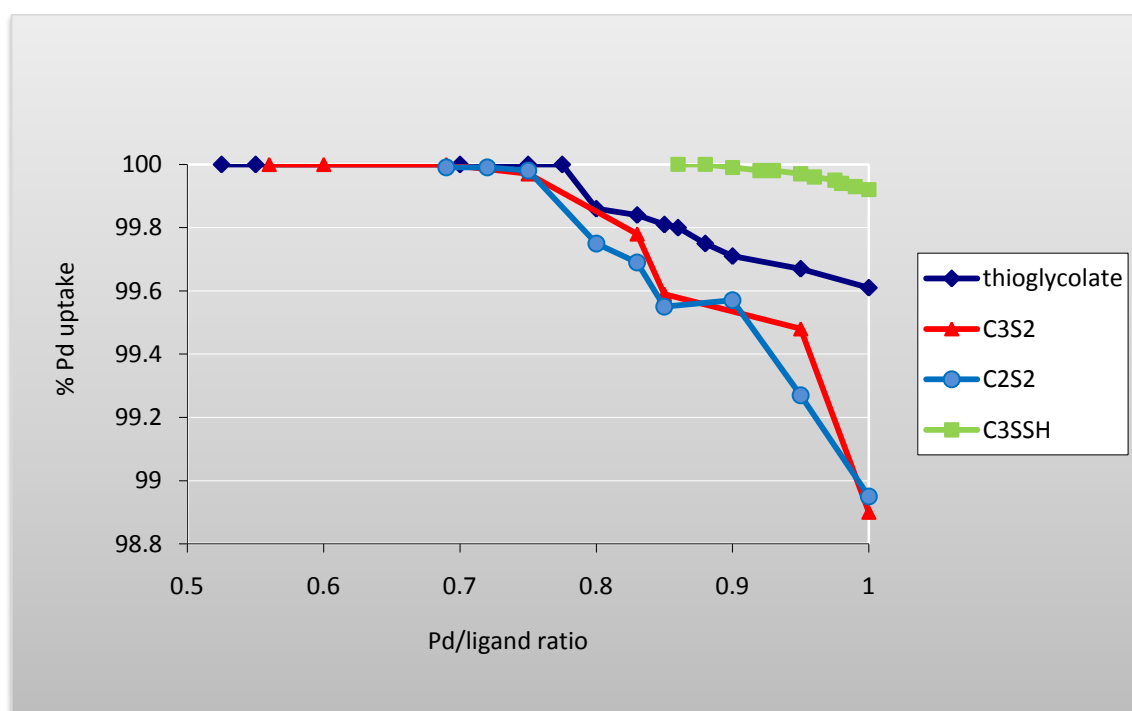


**Figure 2.53** Comparative uptake of Pd(OAc)<sub>2</sub> at different Pd/Ligand ratios for materials **silica-60-G<sub>1</sub>**, **silica-60-C<sub>2</sub>**, **silica-60-C<sub>3</sub>** and **silica-60-C<sub>3</sub>SSH**

The near quantitative uptake of palladium indicated in these relative binding studies contrasts with the uptake measured for the larger scale preparations discussed earlier where uptake was

60% **silica-60-G<sub>1</sub>**, 46% **silica-60-C<sub>2</sub>** and 90% **silica-60-C<sub>3</sub>**. Contact time is likely to be an important factor that should be varied with scale and this could account for the differences observed.

To further test the stability of the metal – support interaction, catalysts prepared as above from varying ratios of Pd/Ligand were stirred at room temperature in dichloromethane for 24 hours. The solids were then filtered, washed thoroughly with dichloromethane and the palladium content measured in solution – herein, for all ratios tested no palladium was detectable.

An additional experiment was carried out at higher temperatures, wherein **silica-60-C<sub>3</sub>** was treated with different concentrations of Pd(OAc)<sub>2</sub> in trichloroethane at Pd: ligand ratios 0.8 to 1 for 24h. This experiment revealed no measurable palladium in solution up to a ratio of 1:1, suggesting that all the ligand sites had been complexed to metal.

A final experiment to test the binding strength of the catalysts was carried out by taking some **silica-60-C<sub>3</sub>-Pd(OAc)<sub>2</sub>** (0.25g) catalyst and stirring it in a solution of cysteine (1g) in methanol. Cysteine was chosen because it offers many competing binding sites for the palladium. The catalyst was refluxed for several hours and then the solution filtered. The solution was then made up to 10% HNO<sub>3</sub> (10 mL) volumetric and measured for its Pd content by ICP-OES analysis. This showed no Pd had been leached from the support. Thus supporting the high affinity the sulfur supports displays for palladium.

## 2.9 Conclusions

The heterogeneous sulfur based silica catalysts modified with palladium metal are potential catalysts for a number of organic transformations. These materials retain their mesoporosity after palladium complexation. In addition, the calculated high surface area, relatively large pore diameters and pore volumes make these systems very attractive. TEM analysis reveals a homogenous distribution of Pd metal on the surface and NMR studies and Pd analysis reveal that there are some ligand sites which are Pd free.

Interestingly, the pore shapes are shown to be of ink bottle shaped when silica-60 is modified to **silica-60-C<sub>3</sub>** and **silica-60-C<sub>3</sub>-Pd(OAc)<sub>2</sub>**, while modification of larger pore sizes are shown to have more cylindrical shaped pores. **Silica-60-C<sub>2</sub>** has demonstrated to have a large T<sup>2</sup>

character and porosimetry data reveals the material to have ink bottle shaped pores. This shape of the pores is slightly altered after modification with metal as **silica-60-C<sub>2</sub>-Pd(OAc)<sub>2</sub>** shows more slit like shaped pores. The silica-N-derivatised-*L*-cysteine materials showed to have more cylindrical like ink bottle shaped pores, with no change in average pore diameters after modification with metal.

## 2.10 References

- <sup>1</sup> M. Jurado-Gonzalez, A. C. Sullivan, J. R. H. Wilson, *Tet. Lett.*, 2004, **45**, 4465-4468;
- <sup>2</sup> E. Fisset, M. Al-Hashimi, J. R. H. Wilson, A. C. Sullivan, *Tet. Lett.*, 2006, **46**, 801; M. Al-Hashimi, G. Roy, J. R. H. Wilson, A. C. Sullivan, *Tet. Lett.*, 2005, **46**, 4365-4368;
- <sup>3</sup> A. Bugrayev, N. Al-Haq, R. A. Okopie, A. Qazi, M. Suggate, A. C. Sullivan, J. R. H. Wilson, *J. Mol. Catal. A:Chemical*, 2008, **280**, 96-101;
- <sup>4</sup> J. D. Wright and N. A. J. M. Sommerdijk, *Sol gel materials: Chemistry and Applications*, Gordon and Breach Science Publishers, Amsterdam, 2001;
- <sup>5</sup> A. Ramirez, B. L. Lopez, and L. Sierra, *J. Phys. Chem. B*, 2003, **107**, 9275-9280;
- <sup>6</sup> I. Harmes, D. Gillis, I. Corneliessens, I. K.C. Vrancken, P. Van der Voort, E. F. Vansant, *J. Chem. Soc., Faraday Trans.*, 1992, **88**, 723; X. S. Zhao, G. Q. Lu, A. K. Whitalaker, G. J. Millar, H. Y. Zhu, *J. Phys. Chem. B.*, 1997, **101**, 6525;
- <sup>7</sup> M. Basato, A. Cardinale, M. Zecca, G. Vale, *Inorg. Chim. Acta*, 2000, **303**, 1100; M. W. Esterhuysen, R. Brull, H. G. Raubenheimer, C. Esterhuysen, G. J. Kruger, *J. Organomet. Chem.*, 2001, **69**, 164; B. Wenzel, P. Lonneck, M. Stender, E. Hey-Hawkins, *Dalton Trans.*, 2002, 248;
- <sup>8</sup> H. J. Kim, Q. Shao and Y-H. Kim, *Surf. Coat. Technol.*, 2003, **171**, 39-45;
- <sup>9</sup> D. A. Torchia, J. A. Lyerla Jr., and A. J. Quattrone, *Biochem.*, 1975, **14**, 887;
- <sup>10</sup> J. McConarthy and M. J. Owens, *J. Clin. Psychiatry*, 2003, **5**, 5, 70-73; S. B. Singh, D. L. Zink, B. Heimbach, O. Genilloud, A Teran, K. C. Silverman, R. B. Lingham, P. Felock, D. J. Hazuda; *Org. Lett.*, 2002, **4**, (7), 1123-1126;
- <sup>11</sup> H. U. Blaseer, E. Schmidt, *Asymmetric Catalysis on Industrial Scale: Challenges, Approaches and Solutions*, Wiley-VCH, Verlag, 2004;
- <sup>12</sup> J. Tsuji, *Palladium Reagents and Catalysts: New Perspectives for the 21<sup>st</sup> Century*, Wiley & Sons, Chichester, 2004; J. G. De Vries, A. H. M. De Vries, C. E. Tucker, J. A. Miller, *Chemical Technology, Innovations in Pharmaceutical Technology*, 125-130;
- <sup>13</sup> H. J. Kim, Q. Shao and Y-H Kim, *Surf. Coat. Technol.*, 2003, **171**, 39-45; U. Vijayalakshmi, A. Balamurugan and S. Rajeswari, *Trends Biomater. Artif. Organs.*, 2005, **18** (2), 101;
- <sup>14</sup> <http://www.chem.ucla.edu/~webspectra/irtable.html>
- <sup>15</sup> B.E. Mann, P.M. Bailey, P.M. Maitlis, *J. Am. Chem. Soc.* 1975, **97**, 1275; N.V. Kaminskaia, I.A. Guzei, N.M. Kostic, *J. Chem. Soc., Dalton Trans.*, 1998, 3879;



<sup>16</sup> F. Fernandez, M. Gomez, S. Jansat, G. Muller, E.Martin, L. Flores-Santos, P.X. Garcia, A. Acosta, A. Aghmiz, M. Gimenez-Pedros, A.M. Masdeu-Bulto, M. Dieguez, C. Claver, M.A. Maestro, *Organometallics*, 2005, **24**, 3946; C. Drexler, H. Paulus, H. Elias, *Inorg. Chem.* 1991, **30**, 1297;

## Chapter 3

### Organosilica Supported Palladium Catalyzed Cross Coupling Reactions

#### 3.1 Cross coupling reactions

In 1845 Kolbe reported on the first ever synthesis of a carbon-carbon bond in the synthesis of acetic acid. Ever since, carbon-carbon bond formations play an important role and have become central to shaping many chemical syntheses.<sup>1</sup> The Grignard, Diels Alder and Wittig reactions are prominent examples of reactions forming carbon-carbon bonds. However, in the last 25 years, a new class of carbon-carbon bond forming reactions based on transition metal catalysts has evolved as a powerful tool in organic synthesis. In particular, Pd catalysed cross coupling reactions are the most prominent. Palladium catalyzed reactions have become an important tool in organic synthesis due to their high efficiency, possibility of transformations involving complex substrates and tolerance of many functional groups. Mizoroki-Heck,<sup>2</sup> Suzuki-Miyaura,<sup>3</sup> Stille,<sup>4</sup> Sonagashira<sup>5</sup> and Buchwald-Hartwig are the predominantly used reactions catalysed by palladium catalysts.

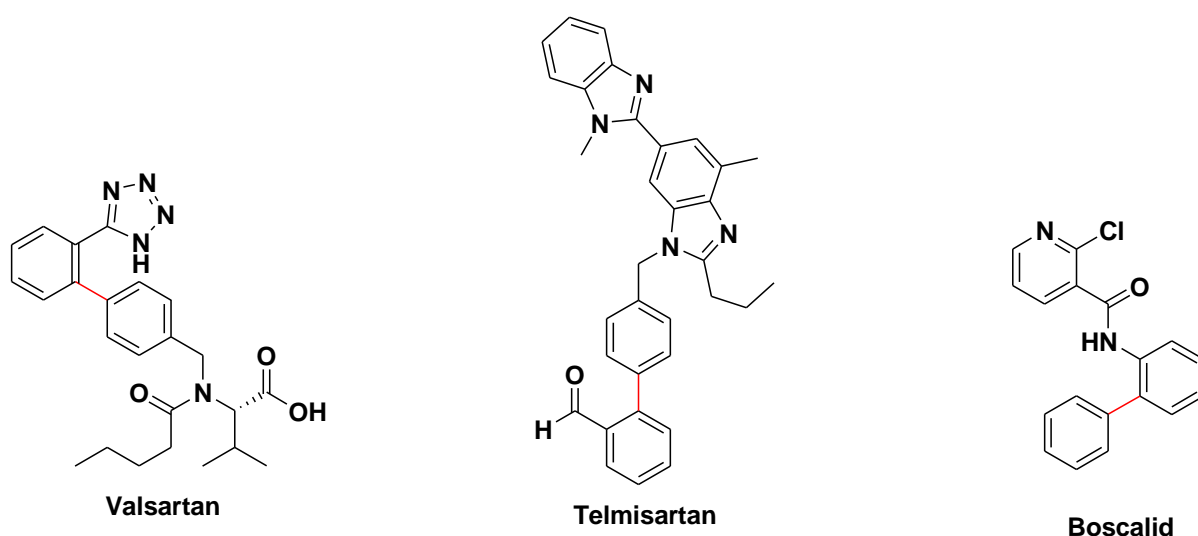
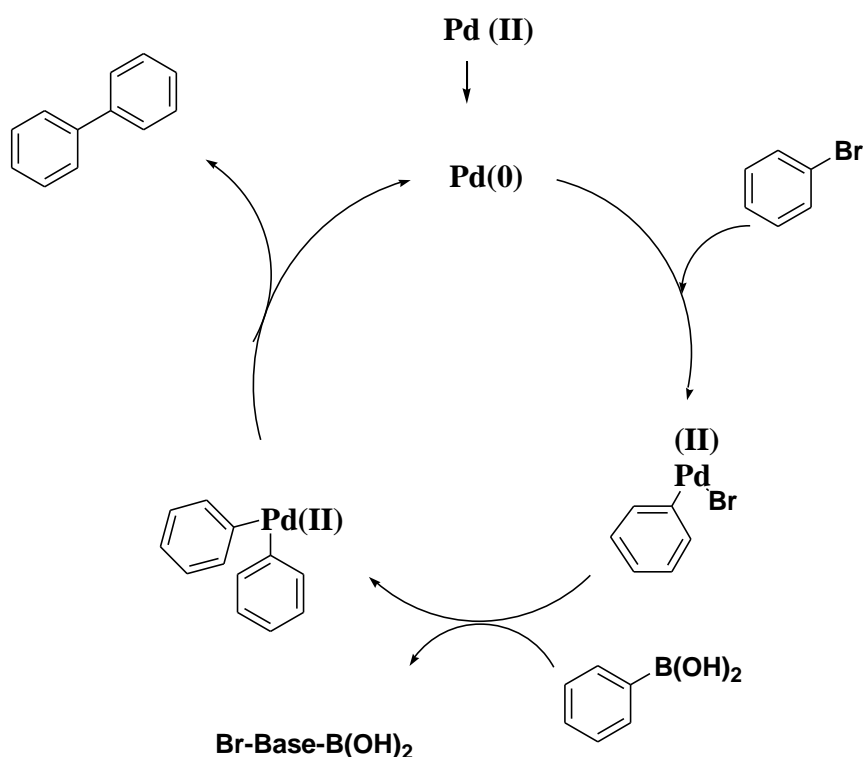


**Figure 3.1** Examples of macromolecules where the bond formed by the Suzuki-Miyaura reaction is shown in red.

The Suzuki-Miyaura reaction involves the formation of carbon-carbon bonds via the cross coupling reaction between an aryl halide and aryl boronic acid. This reaction was first published by Akira Suzuki<sup>3</sup> in 1979 and since has become hugely popular in the

pharmaceutical industry and has been utilised in the synthesis of Valsartan <sup>6</sup> and Telmisartan <sup>7</sup> and in the agrochemicals sector the key step in the synthesis of Boscalid <sup>8</sup> is the formation of a biaryl substructure (**Figure 3.1**).

The Suzuki-Miyaura reaction has become the most widely reliable and widely applied palladium catalysed cross coupling reaction in total synthesis, where it has an important role. The ease of synthesis of the organoboron starting materials and their stability to air/moisture makes this cross coupling reaction attractive. In addition, relatively mild reaction conditions are often used and the by-products formed are non toxic. These advantages make the Suzuki-Miyaura reaction valuable for organic synthesis.



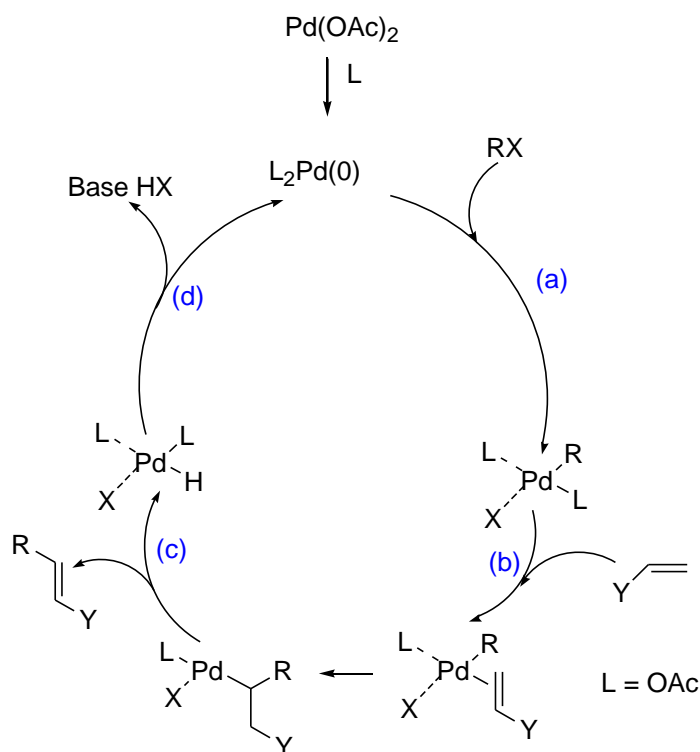
**Scheme 3.1** Textbook catalytic cycle for Suzuki-Miyaura reaction

The standard textbook catalytic cycle for the Suzuki-Miyaura reaction sees the palladium catalysts cycling between Pd(0) and Pd(II) oxidation states. Most commonly a Pd(II) precatalyst is used, such as palladium acetate and this is believed to be reduced to Pd(0) *in situ* consequently allowing it to oxidatively add the aryl halide forming a Pd(II) intermediate as shown in the scheme above. The Pd(II) complex then binds onto the arylboronic acid with loss of the halide from the palladium. A new carbon-carbon bond is then formed and Pd(0)

catalyst regenerated. In this mechanism, the base is presumed to form a salt with the boronic acid and halide.

The Mizoroki-Heck reaction involves the formation of a new carbon-carbon bond in a single transformation via the arylation, alkylation or vinylation of various alkenes through coupling with alkyl or aryl halide substrates. These palladium catalysed reactions are attractive due to their simplicity and applicability to a wide range of functional groups. The Mizoroki-Heck reaction is used in the synthesis of multifunctional derivatives,<sup>9</sup> such as bioactive compounds, natural products,<sup>10</sup> high performance materials and pharmaceuticals.<sup>11</sup> The first example of this reaction was reported independently by Mizoroki in 1971 and then in an improved form by Heck in the 1972.<sup>12</sup> More than a decade after the first reports, this reaction received much attention and contribution from the scientific community and its broad application was investigated. It was in the late 1980's, catalytic asymmetric Heck reactions were developed and thus led to a resurgence of interest in the reaction. In industry, this method is used in the synthesis of fine chemicals. The growing interest in Mizoroki-Heck reactions in both academia and industry is largely because of broad tolerance of solvent and functional groups on the substrates, high selectivity and relatively moderate toxicity levels of by-products.

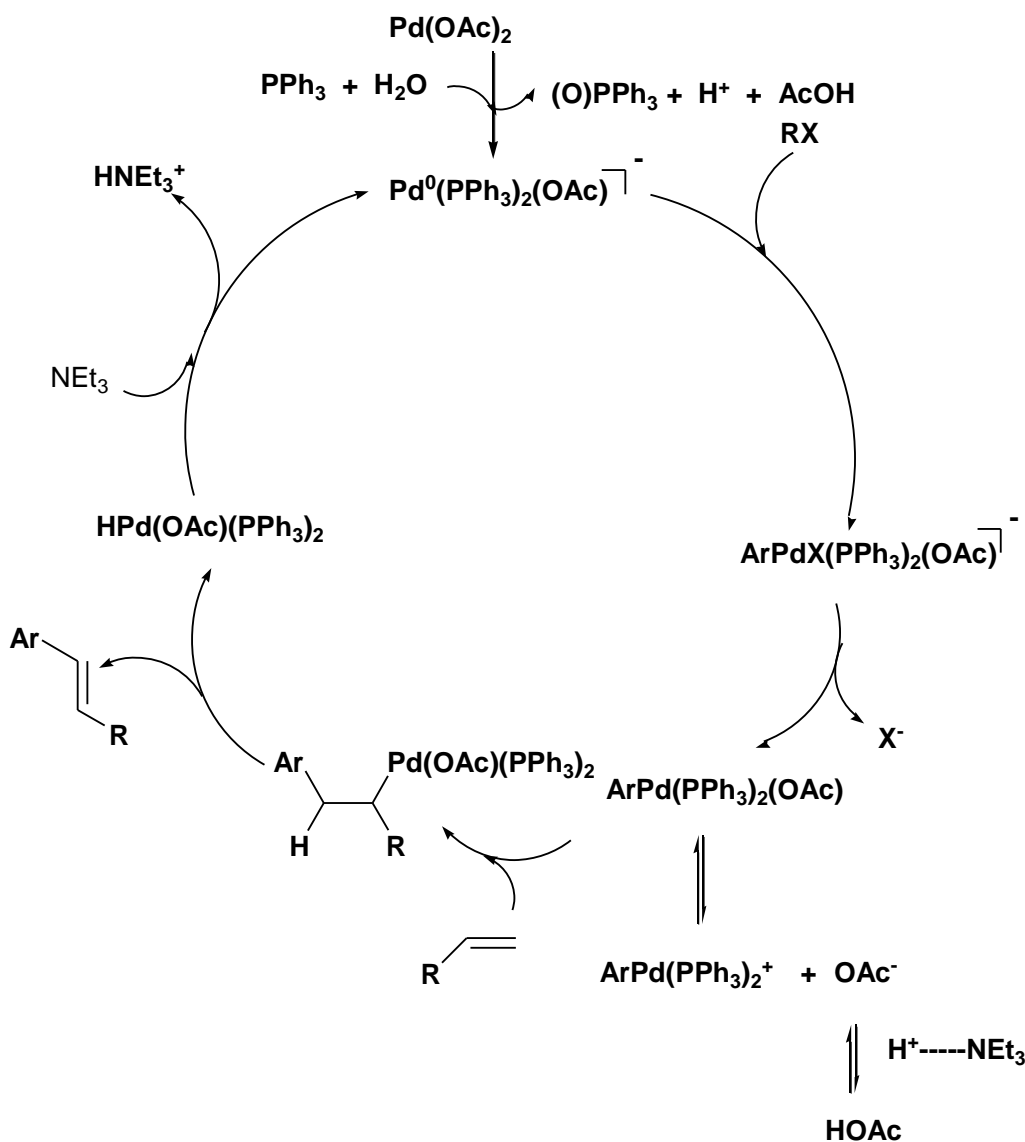
The typical textbook catalytic cycle for the Mizoroki-Heck reaction involves a postulated molecular, homogeneous Pd catalyst that cycles between Pd(II) and Pd(0) oxidation states (**Scheme 3.2**). Similar to the Suzuki-Miyaura reaction, a precatalyst in the Pd(II) oxidation state is used and this is reduced *in situ* to Pd(0). This reduction step is only postulated as there are no strong reducing agents present in the reaction mixture. In phosphine free systems however, the base is assumed to assist in the reduction to Pd(0). As shown in the scheme below there are four main stages in the mechanistic cycle of a Mizoroki-Heck reaction. The most important step is the oxidative addition of the aryl halide (Ar-X) to the palladium complex to yield [Ar-Pd-X], which subsequently complexes to the alkene. After this, insertion into the Ar-Pd bond occurs and then  $\beta$ -hydride elimination yields the desired coupled product and Pd(0) is regenerated.



**Scheme 3.2** Standard textbook mechanism for the Mizoroki-Heck reaction

A more widely accepted proposed mechanistic catalytic pathway has been reported by Amatore and Jutland (**Scheme 3.3**).<sup>13</sup> They report that the commonly postulated Pd(0)L<sub>2</sub> catalytic system is not formed as a main intermediate. In its place, a reactive anionic species is produced in which Pd(0) is ligated by a halide [Pd(0)L<sub>2</sub>X]<sup>−</sup> or by an acetate ion [Pd(0)L<sub>2</sub>(OAc)]<sup>−</sup>. The rate of the oxidative addition of the aryl halide depends strongly on the anion ligated to the Pd(0) and this rate is further increased by cations or protons (through anionic pairing or acid-base reaction with the X<sup>−</sup> or OAc<sup>−</sup> respectively).

Further, postulated *trans*-ArPdXL<sub>2</sub> complexes are not formed as a main intermediate. Instead, Amatore and Jutland report on the formation of penta-coordinated anionic complexes [ArPdX(OAc)(PPh<sub>3</sub>)<sub>2</sub>]<sup>−</sup> from the neutral complex [ArPd(OAc)(PPh<sub>3</sub>)<sub>2</sub>] in which an acetate anion remains ligated to the aryl Palladium (II) species produced in the cycle and conditions the intrinsic stability of the palladium species and its reactivity with nucleophiles.<sup>13</sup>



**Scheme 3.3** Mechanism for Pd catalyzed Heck reactions involving anionic intermediates

Palladium catalysts cross coupling reactions are used in the synthesis of many Active Pharmaceutical Ingredients (APIs). Typically 25-100kg of waste is produced for every kg of API manufactured.<sup>14</sup> This causes a huge environmental burden and a significant associated disposal cost. Many pharmaceutical syntheses involve the use of homogeneous catalysts, which are difficult to separate from the products and this in turn leads to palladium contamination of APIs. Contamination of these products poses a serious concern in the pharmaceutical industry. The use of heterogeneous catalysts in place of the homogeneous catalysts offers greater stability, cheaper production methods and easier catalyst separation from the products. This can involve simple filtration or decantation or the use of flow

systems. However, the selectivity and activity of these systems are often lower than homogeneous catalysts.

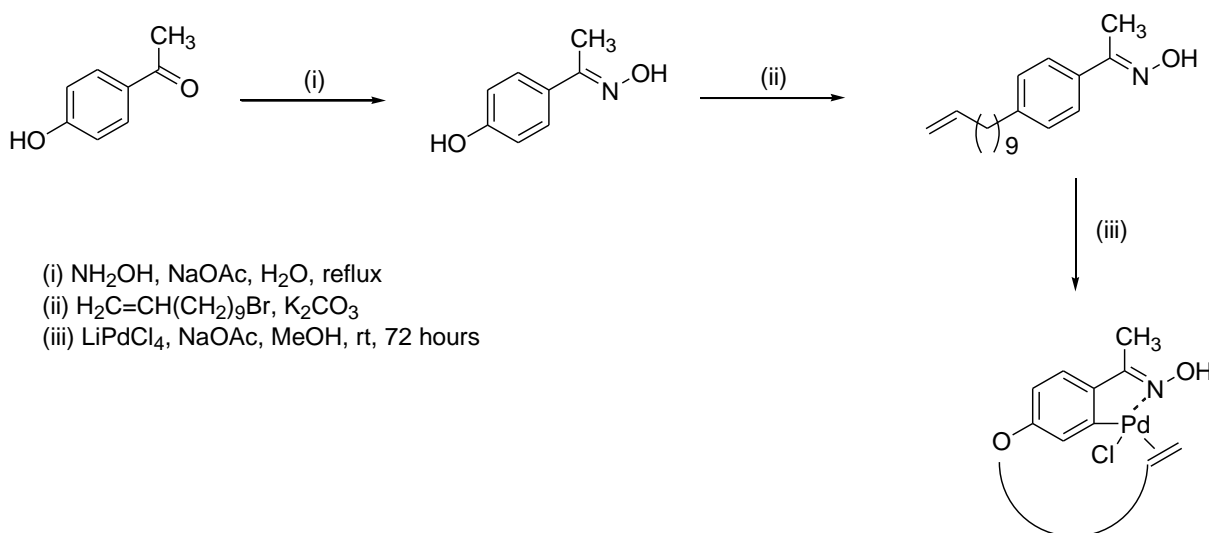
Thus there is a huge interest in developing efficient heterogeneous catalysts. Immobilisation of homogeneous systems onto suitable supports would allow for ease of catalyst recovery and reuse, minimise generation of waste and additional purification processes making it of further interest to the development of environmentally friendly processes. Scientists have developed many heterogeneous catalysts. Palladium can be found to be supported on carbon, zeolites, silicates and polymers for catalytic applications. Shimizu *et al.* findings reveal that palladium supported on the conventional supports such as zeolite or carbon tends to aggregate and so form less active particles or clusters. In comparison, silica immobilised sulphur ligands are shown to form more stable supported palladium complexes.<sup>15</sup> Silica supports are attractive as they can be easily modified with a variety of ligands and metals with a choice of pore sizes. In addition unlike polymer supports, no pre swelling is required and most importantly these systems have been found to be highly stable. Recently, organic reagents grafted onto silica gels have attracted much attention, with industries seeking more environmentally friendly chemical manufacturing processes.<sup>15</sup>

Much of the work in this thesis concerns organically functionalised (ligand) modified silicas where the ligand contains sulfur donor atoms and the development and activity of corresponding silica supported palladium catalysts. Related reported work on use of silica supported palladium catalysts often concerns nitrogen or sulfur based ligand modified silicas. For this reason literature reports on ligand modified silicas where the supported ligand contains nitrogen or sulfur donor atoms, and the activity of these in Suzuki-Miyaura and Mizoroki-Heck reactions is reviewed in this chapter. Systems where the sulfur is not explicitly coordinated to the palladium metal are included for completeness.

### 3.2 The Suzuki-Miyaura reaction catalyzed by silica-60-G<sub>1</sub>-Pd(OAc), silica-60-C<sub>2</sub>-Pd(OAc)<sub>2</sub> and silica-60-C<sub>3</sub>-Pd(OAc)<sub>2</sub>

#### 3.2.1 Background literature

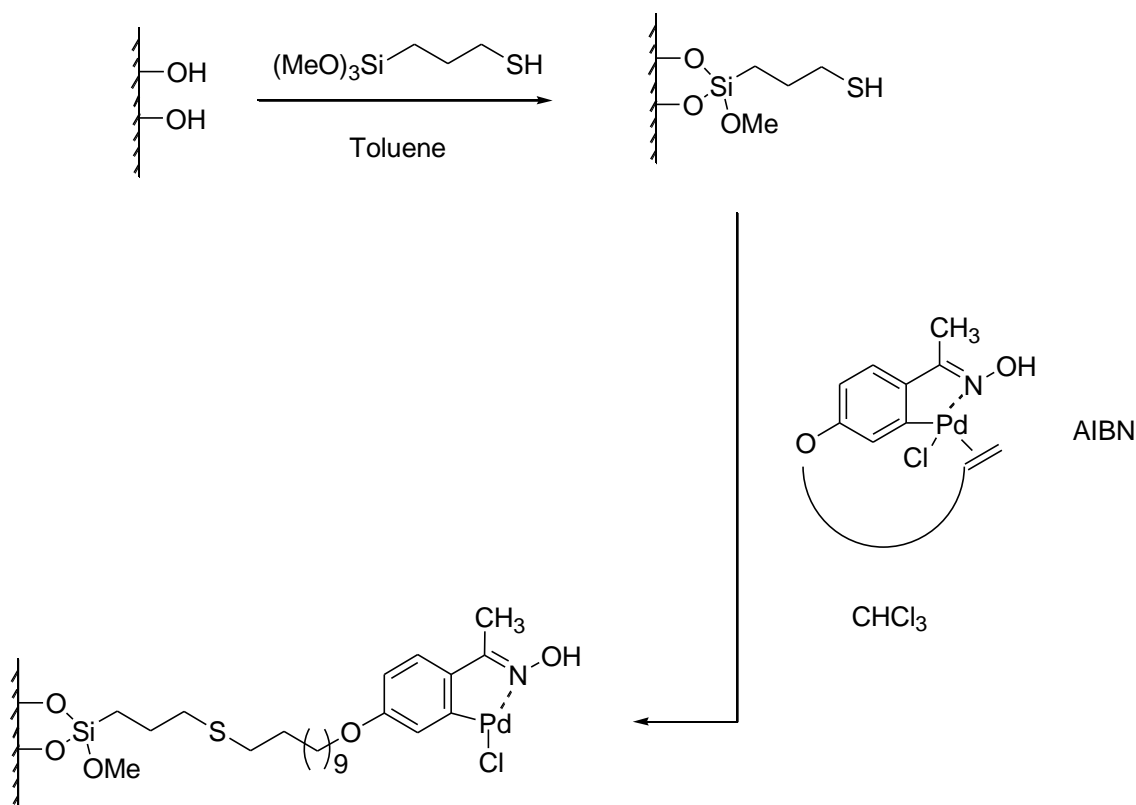
As mentioned earlier, the anchoring of active homogeneous catalysts onto a solid support, poses the advantage of easy separation as well as demonstrating activity comparable to its homogeneous counterpart. One such example was demonstrated by Corma and Garcia. In 2003, they reported on anchoring an oxime carbapalladacycle, which is known to be an extremely active homogeneous catalyst for the Suzuki-Miyaura reaction in water, onto SiO<sub>2</sub>.<sup>16</sup> Preparation of so called **PdL@SiO<sub>2</sub>** is depicted in **Schemes 3.4** and **3.5**. The palladium complex was prepared in a three step synthesis starting from 4-hydroxy-acetophenone. The presence of a double bond in the oxime carbapalladacycle enables the anchoring of this complex on to the silica support relatively easily.



**Scheme 3.4** Synthesis of Corma and Garcia's carbapalladacycle<sup>16</sup>

The palladium complex was anchored to 3-mercaptopropyl modified silicas via a radical chain mechanism. Modification of the silica was achieved by reacting, 3-mercaptopropyl trimethoxysilane with silica silanol groups. Characterization studies suggested firstly that the Pd complex survived the anchoring procedure and secondly that half the mercaptopropyl groups of the modified silica reacted with the palladium complex.





**Scheme 3.5** Synthesis of Corma and Garcia's catalyst PdL@SiO<sub>2</sub> via grafting route

With water as a solvent, and potassium carbonate as a base, this catalyst **PdL@SiO<sub>2</sub>** was tested in the Suzuki-Miyaura coupling of various aryl halides. Excellent yields were achieved with aryl bromides and iodides as well as with aryl chlorides, although longer reaction times were needed for chlorides. In the cross coupling of bromoacetophenone and phenyl boronic acid, quantitative conversions were achieved in 10 minutes and the cross coupling of chloroacetophenone gave 91% conversion in 2 hours. Recycling of the catalyst in the coupling of 4-chloroacetophenone and phenyl boronic acid showed no loss in activity in eight consecutive runs, further demonstrating the high activity of these catalysts. Interestingly, in the cross coupling of 4-chlorotoluene (73%, 6 hours) and 2-nitrochlorobenzene (99%, 48 hours) along with high conversions, the reactions were marred by the production of unwanted biphenyl product, arising from homocoupling of phenyl boronic acid.

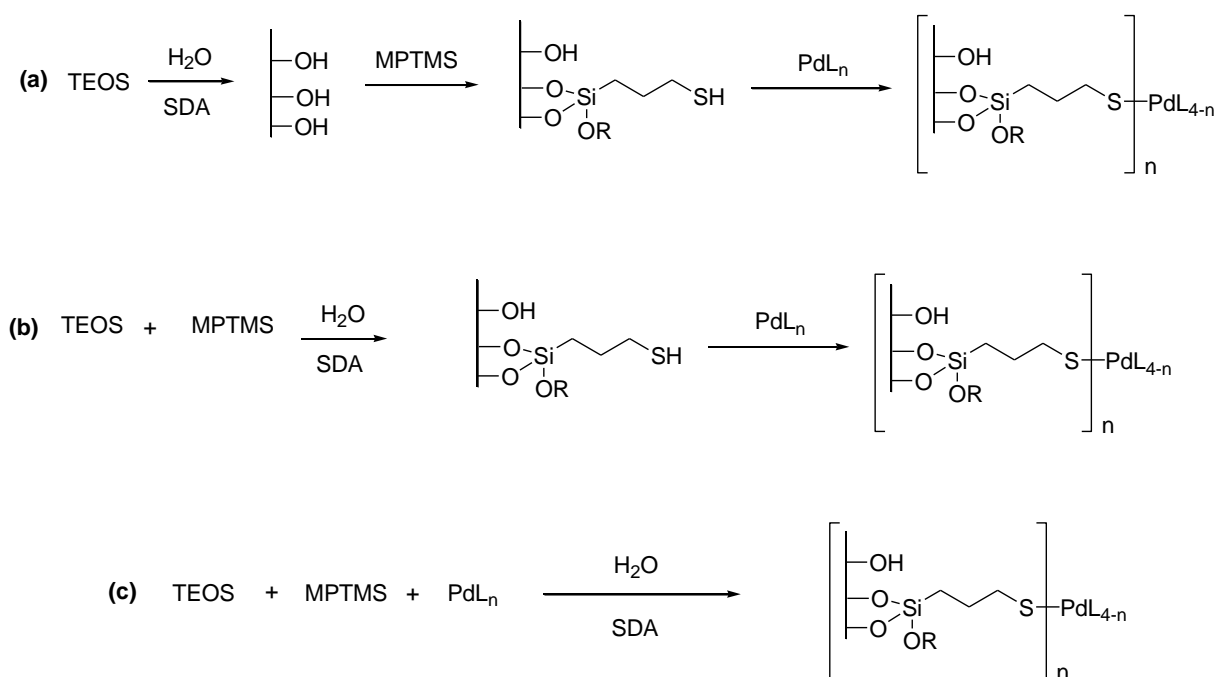
Hot filtration tests showed palladium to be retained by the support, additionally chemical analysis of the Pd content after eight runs showed it to have the same metal content as fresh catalyst. Further to this, three phase tests were also carried out to determine whether Pd was leaching from the support during the reaction. Immobilisation of 4-chloroacetophenone onto a

silica support showed no coupled product produced thus supporting a heterogeneous nature of **PdL@SiO<sub>2</sub>**.

In 2004 Shimizu *et al.* reported on the successful catalytic activity of mesoporous silica (FSM-16)-supported mercaptopropyl palladium (II) complex, **Pd-SH-FSM** in both the Mizoroki-Heck and the Suzuki-Miyaura cross coupling reactions.<sup>15</sup> The silica support for this catalyst was prepared from Kanemite (NaHSi<sub>2</sub>O<sub>5</sub>.H<sub>2</sub>O) using C<sub>16</sub>H<sub>33</sub>NMe<sub>3</sub>Cl as a template. Introduction of the thiol ligand to the support was carried out by a postmodification method. Subsequently the material was stirred in a solution of Pd(OAc)<sub>2</sub> in acetone to yield the new **Pd-SH-FSM** catalyst. In addition to this, Shimizu *et al.* report on the synthesis of another catalyst **Pd-SH-SiO<sub>2</sub>**, wherein the thiol ligand 3-mercaptopropyl was also loaded onto silica *via* method of sol gel processing.

Characterization of **Pd-SH-FSM** and **Pd-SH-SiO<sub>2</sub>** showed both systems to display similar loadings of metal and sulfur ligand. Shimizu *et al.* reported on the use of these catalysts in the Suzuki Miyaura cross coupling of 4-bromoanisole and phenyl boronic acid with KOAc as a base and DMP as a solvent. With the excellent activity shown (79% with **Pd-SH-FSM** and 73% with **Pd-SH-SiO<sub>2</sub>**), these catalysts were then employed in the Mizoroki-Heck reaction and again were found to be highly active (92 and 84% respectively). These catalysts showed excellent activity with minimal Pd leaching (<0.01%). Hot filtration tests revealed a heterogeneous mode of action for the catalysts and recycles of up to five times were conducted without loss in activity.

In 2008, Crudden *et al.* reported on the activity of Pd complexes immobilized on mercapto functionalised SBA-16 and KIT-16 in the Suzuki-Miyaura reaction.<sup>17</sup> The preparation of the solid support KIT-16 and SBA-16 was via soft templating methods.<sup>18</sup> These silica supports were then modified with 3-mercaptopropyl by the three methods; grafting (a), chemical adsorption (b) and single step (c) **Scheme 3.6**. In the first method, grafting, the SBA-16 or KIT-16 was refluxed in dry toluene and 3-mercaptopropyltrimethoxysilane (MPTMS) for eighteen hours. The solid product formed was then filtered and excess MPTMS was removed by soxhlet extraction with ethanol. The material was then added to a solution of the appropriate palladium precursor and stirred at room temperature for six hours. These catalysts were then filtered, washed with DMF, THF and then vacuum dried.



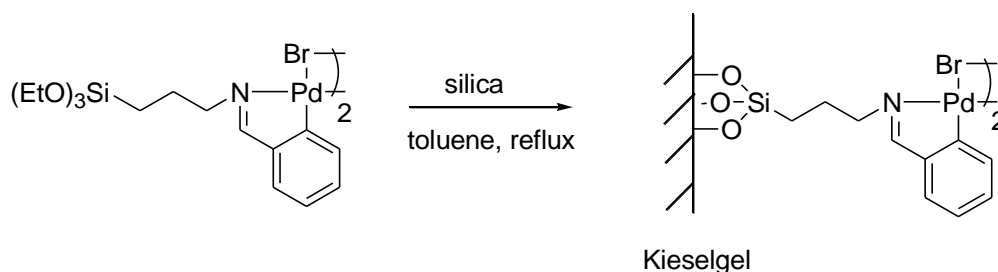
**Scheme 3.6** Preparation methods of silica modified mercaptopropyl Pd catalysts: (a) grafting (b) Pd complex adsorption (c) single step.  $\text{PdL}_n = \text{Pd(0)}$  or  $\text{Pd(II)}$

Palladium catalysts prepared by complex adsorption involved addition of the palladium complex to the preformed mercaptopropyl modified silica, and after filtration, the catalysts were washed further by refluxing in ethanol, toluene and acetonitrile in order to remove any physisorbed palladium species. These materials were loaded with  $\text{Pd(OAc)}_2$  or  $\text{Pd(PPh}_3)_4$ . All catalysts showed high activity in the Suzuki coupling reaction of bromoacetophenone and pinol ester of phenyl boronic acid. Crudden *et al.* report that of the methods employed to prepare these thiol modified silicas, those prepared by chemical adsorption displayed the highest activity.

With reaction times of 12 hours and 1 mol % Pd employed, quantitative conversions were achieved for catalysts **Ph<sub>3</sub>P-Pd-SH-SBA** and **Ph<sub>3</sub>P-Pd-SH-KIT-6** respectively as prepared by the chemical adsorption method. A solvent mixture of DMF/H<sub>2</sub>O (20:1) and potassium carbonate as a base was employed in these reactions at 80 °C. In the case of catalysts prepared by single step method, long reaction times were required to achieve good yields. The authors speculate that this may be due to the consequences of the harsh conditions needed for a one

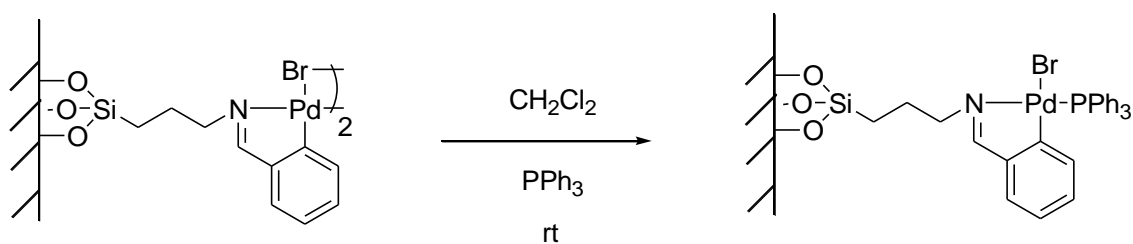
step synthesis which resulted in this catalyst lacking an ordered porous structure. Leaching tests showed Pd in solution to be <0.1 mol % which is still significant however recycling of these catalysts showed no loss in activity up to the third run.

Many research groups have also reported on the high activity of Pd loaded silica supported nitrogen based ligands in the Suzuki-Miyaura reaction such as Bedford *et al.* Bedford *et al.* reported on the catalytic activity of silica supported imine palladacycle catalysts in the Suzuki coupling of aryl bromides with phenyl boronic acid. Preparation of the catalyst, **SiO<sub>2</sub>-Imine-palladacycle** is shown in **Schemes 3.7** and **3.8** below. This catalyst was prepared via method of grafting. **SiO<sub>2</sub>-Imine-palladacycle** gave 69% yield in the cross coupling of 4-bromoanisole and phenyl boronic acid in 6 hours.<sup>19</sup> Recycling of the catalysts showed a huge drop in activity (11%, 19 hours).



**Scheme 3.7** Preparation of Bedford *et al.* catalyst SiO<sub>2</sub>-Imine-palladacycle.<sup>19</sup>

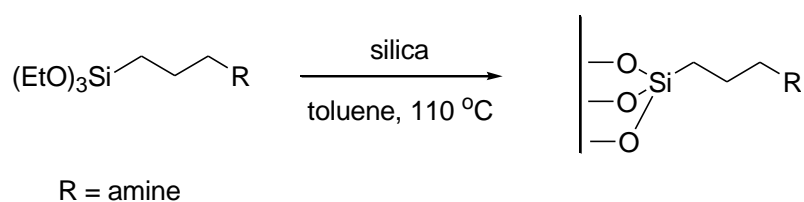
Further investigation of **SiO<sub>2</sub>-Imine-palladacycle** by treatment with a solution of triphenylphosphine gave catalyst **SiO<sub>2</sub>-Imine-PdPPh<sub>3</sub>**. This showed higher activity than **SiO<sub>2</sub>-Imine-palladacycle**. However, in recycling this catalyst was in fact less active than catalyst **SiO<sub>2</sub>-Imine-palladacycle**, with complete loss in activity being observed between the first and second runs. Bedford *et al.* report that small Pd(0) clusters are likely to be the active catalysts in these reactions with catalysts **SiO<sub>2</sub>-Imine-palladacycle** and **SiO<sub>2</sub>-Imine-PdPPh<sub>3</sub>**.



**Scheme 3.8** Preparation of Bedford *et al.* catalyst SiO<sub>2</sub>-Imine-PdPPh<sub>3</sub>.<sup>19</sup>

In a more recent contribution, Bedford *et al.* reported on the immobilisation of various amine functionalities on silica supports with encapsulated nanoparticulate palladium. These catalytic systems were then utilised in the Suzuki-Miyaura reaction of aryl bromides with phenyl boronic acid.<sup>20</sup>

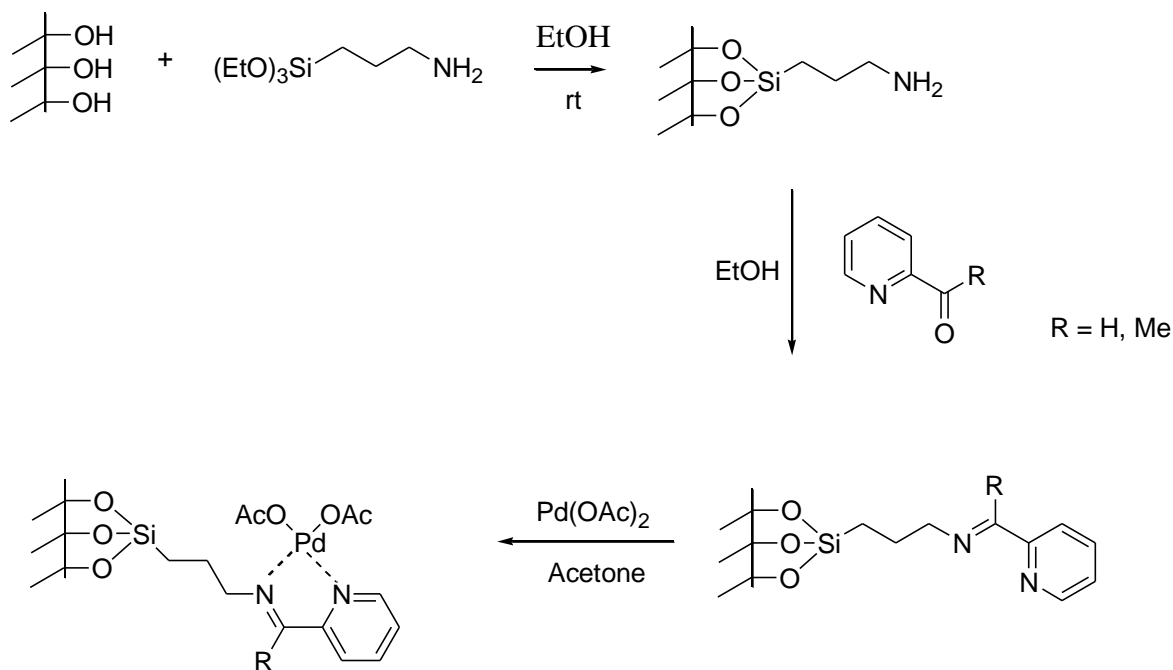
The synthesis of these catalytic systems was also investigated by the method of grafting. Previously Bedford *et al.* had shown that nanoparticulate palladium stabilized by TBAB (tetrabutylammonium bromide), in the presence of water, can couple deactivated aryl bromide and chloride substrates. In this report, the authors discuss the advantages of supporting this system on a silica support. Bedford *et al.* report on preparing a range of organosiloxane-modified silica, containing various amine functionalities, ranging from primary to quaternary centres. These were tethered and used to encapsulate Pd(OAc)<sub>2</sub> to give new catalysts.



**Scheme 3.9** Synthesis of covalently modified silica by Bedford *et al.*<sup>20</sup>

Bedford *et al.* reported the use of potassium phosphate as a base and toluene as a solvent to be optimal conditions for these catalytic systems. Initial studies of the Suzuki-Miyaura reaction of 4-bromoanisole and phenyl boronic acid revealed that of the catalysts synthesised catalysts **G3** (R=diethylamine) and **H3** (R= diethylenetriamine) were found to give the most promising results (94 and 98 % conversion respectively). Recycles of these catalysts showed them to retain high activity up to the third run, after which both catalysts displayed significant loss in activity and leaching of Pd into solution. TEM analysis showed that the nanoparticulate structure of catalyst **G3** remains, however for catalyst **H3**, this was not the case. Catalyst **G3** was then further tested in the Suzuki-Miyaura reaction of substituted aryl bromides and phenyl boronic acid. Essentially quantitative yields were achieved for the cross coupling of phenyl boronic acid with 4-bromoanisole (95% conversion) and 4-bromotoluene (90% conversion). The cross coupling of more difficult aryl bromides such as 2-bromotoluene with phenyl boronic acid also gave good conversions (78% conversion).

Clark *et al.* also reported on the synthesis of novel silica supported Pd complexes incorporating nitrogen containing ligands.<sup>21</sup> These catalysts were prepared by initially modifying silica with a substituted propylamine with subsequent imine formation prior to addition of Pd(OAc)<sub>2</sub>. Clark *et al.* reported good conversions were achieved when 0.4 mol% Pd was employed with potassium carbonate as a base and *o*-xylene as a solvent at 110 °C.



R = CH<sub>3</sub>, **SiO<sub>2</sub>-Propyl-(1-pyridin-2-yl-ethylidene)-amine**<sup>21</sup>

R = H, **SiO<sub>2</sub>-Propyl-pyridin-2-ylmethylene-amine**<sup>21</sup>

**Scheme 3.10** Synthetic pathway of Clark *et al.* catalysts<sup>21</sup>

The higher activity of catalyst R = CH<sub>3</sub> compared to R = H (**Scheme 3.10**) was suggested to arise from an increased electron density around the Pd atom due to the presence of the methyl group. Further, analysis of the catalyst surface and thermal analysis revealed no change in the catalyst structure, even when the catalyst was used several times.

### Summary

The literature reports summarised here demonstrate that there is still much work needed in the area of silica supported palladium catalysts for successful Suzuki-Miyaura reactions. Although some catalysts showed excellent activity, such as Bedford *et al.*'s ethylenediamine

modified silica palladium catalysts, these were marred by significant leaching of the metal. In other reports where catalysts were resistant to leaching, such as Corma and Garcia's immobilised palladacycle systems, activity of the catalysts was rather sluggish requiring a total reaction time of 48 hours to achieve good conversions. The work carried out by Crudden *et al.* and Shimizu *et al.* is very promising; however preparation of these catalytic systems is quite demanding. With each passing year, research groups are reporting on their contribution to the Suzuki-Miyaura reaction with shorter reaction times, lower levels of leaching, higher activity and even simpler preparation methods to previous reports. This is an area of research which is developing very fast. Even so, little is understood about the truly active species involved. In addition, the characterisation of such systems has also proven to be difficult. Thorough characterization and activity studies as well as mechanistic studies of the catalyst may pave the way for highly active heterogeneous Pd catalysts which can be used in the Suzuki-Miyaura reaction.

Palladium is known to form rather stable complexes with a variety of sulfur and nitrogen donor ligands. Using Pearson's Soft Hard rules it would be anticipated that the soft acid like palladium would have a higher binding affinity to softer sulfur ligands than to the harder oxygen or nitrogen based ligands. Palladium's preference for sulfur groups can also be seen from comparison of the affinities of palladium for a series of simple ligand systems, such as amino acids.<sup>22</sup> The affinity for cysteine is much greater than for glutamic acid or histidine. The large binding preference of palladium (II) to sulfur (and other heavy-atom donors) is due largely to the metal-ligand  $\pi$  bond overlap of filled metal *d*-orbitals with empty *d*-orbitals of the heavy atom.<sup>23</sup>

In addition, phosphine free catalysts have recently generated great interest as less complicated, environmentally friendly and cheaper alternatives to phosphine-containing systems.<sup>24</sup> Conversely, these systems are often disadvantaged by their low stability and low catalytic activity due to the formation of usually catalytically inactive 'palladium black'. The challenge remains to develop efficient catalytic systems, wherein the catalytic activity of these solid supported systems mirrors that of their homogeneous counterparts. With this in mind the palladium catalysts described in Chapter 2 were assessed and the results are discussed below.

### 3.3 Results and Discussion

#### 3.3.1 Suzuki-Miyaura reaction at high temperature with silica-60-G<sub>1</sub>-Pd(OAc), silica-60-C<sub>2</sub>-Pd(OAc)<sub>2</sub> and silica-60-C<sub>3</sub>-Pd(OAc)<sub>2</sub>

The catalytic activity of material **silica-60-G<sub>1</sub>-Pd(OAc)**, was initially assessed in the Suzuki-Miyaura reaction. This catalyst was fully characterized and details of its synthesis and properties were given in Chapter 2.

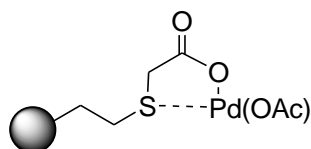


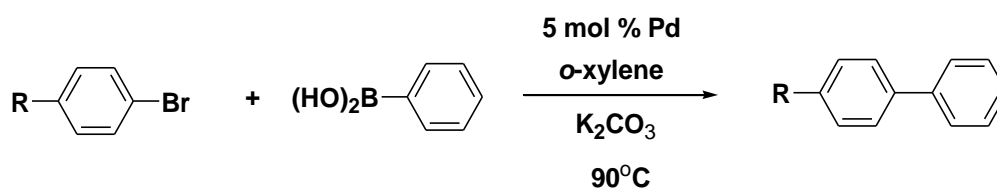
**Figure 3.2 silica-60-G<sub>1</sub>-Pd(OAc)**

The conditions chosen for this reaction were those commonly reported in literature.<sup>24, 25</sup> In a typical reaction, aryl halide (1 mmol), phenyl boronic acid (1.5 mmol) and potassium carbonate (2.0 mmol) were combined. To this was added solvent *o*-xylene and the silica catalyst and the reaction mixture heated to 90 °C. The amount of palladium employed was typically 5 mol % of the aryl halide. This corresponded to 60mg of **silica-60-G<sub>1</sub>-Pd(OAc)**. Recycles were achieved through filtration of the supernatant from the catalyst, washing with *o*-xylene and then transferring to a clean flask followed by addition of fresh substrates, solvent and base.

As shown in **Table 3.1**, all catalysts were found to rapidly cross couple the different substituted aryl bromides with phenyl boronic acid in excellent conversions. The coupling of bromobenzene and phenylboronic acid was achieved in 2 hours with quantitative yields. For this reaction no significant loss in activity is observed in subsequent runs, **Entry 1**. In the cross coupling of bromoanisole, catalyst **silica-60-G<sub>1</sub>-Pd(OAc)**, gave quantitative yields in runs 1 and 2 and then in run 3 a drop in activity to 90% was found, **Entry 2**. By allowing further reaction time of an hour, quantitative conversions are achieved for this reaction. A drop in activity is found to be repeated in the cross coupling of 4-bromotoluene and 4-bromochlorobenzene with phenyl boronic acid in the second run (**Entry 3 and 4**). This drop in activity could be due to substrate transport limitations.



To further test the activity of this catalyst, the cross coupling reaction of the more difficult chloroanisole and phenyl boronic acid was tested with precatalyst **silica-60-G<sub>1</sub>-Pd(OAc)**. This gave 18% conversion in 6 hours; a total reaction time of 48 hours gave 99% conversion.

**Table 3.1** Suzuki-Miyaura reaction of aryl bromides with phenyl boronic acid catalysed by **silica-60-G<sub>1</sub>-Pd(OAc)**

Entry	Substrate	Time (hours)	% conversion (cycle 1, 2 and 3)
1		2	99, 99, 90
2		1.5	99, 99, 90 (99, 2.5Hrs)
3		1.5	97, 90 (97, 4.5 Hrs), 90 (94, 6 hrs)
4		2.5	97, 90 (94, 3.5 Hrs), 90
5		6	18 (99, 47 hrs)

**Conditions:** Taken 1.5 mmol phenyl boronic acid, 1.0 mmol aryl halide, 1.5 mmol  $\text{K}_2\text{CO}_3$ , 60 mg of catalyst and 7mL of *o*-xylene. % conversion was determined by  $^1\text{H}$  NMR or GC.

The promising results of precatalyst **silica-60-G<sub>1</sub>-Pd(OAc)**, in the Suzuki-Miyaura reaction led to the development of bidentate sulfur palladium catalysts **silica-60-C<sub>2</sub>-Pd(OAc)<sub>2</sub>** and

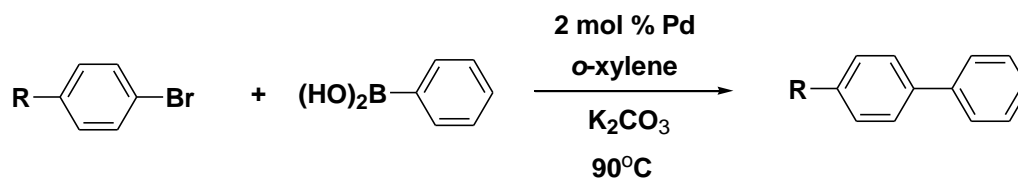
**silica-60-C<sub>3</sub>-Pd(OAc)<sub>2</sub>**. These materials were prepared via a grafting method which has been described in detail in chapter two. Just to note, precatalyst **silica-60-C<sub>3</sub>-Pd(OAc)<sub>2</sub>** was shown to have a higher palladium loading than **silica-60-C<sub>2</sub>-Pd(OAc)<sub>2</sub>** although the latter material has a higher ligand loading.



**Figure 3.3** Catalysts **silica-60-C<sub>2</sub>-Pd(OAc)<sub>2</sub>** (*S* loading 0.56 mmol/g , Pd loading 0.26 mmol/g) and **silica-60-C<sub>3</sub>-Pd(OAc)<sub>2</sub>** (*S* loading 0.50 mmol/g , Pd loading 0.42 mmol/g).

The catalytic activity of these materials was assessed in the Suzuki-Miyaura reaction of aryl bromides with phenyl boronic acid. Typical reaction conditions were as described before for **silica-60-G<sub>1</sub>-Pd(OAc)** wherein aryl bromide (1.0 mmol), phenyl boronic acid (1.5 mmol), potassium carbonate (2.0 mmol) and dry *o*-xylene were added to the reaction. The amount of catalyst used was 50mg which corresponds to 1.3 and 2.1 mol % of Pd for **silica-60-C<sub>2</sub>-Pd(OAc)<sub>2</sub>** and **silica-60-C<sub>3</sub>-Pd(OAc)<sub>2</sub>** respectively, and a reaction temperature of 90 °C was used. Recycles were achieved through filtration of the supernatant from the catalyst, washing with *o*-xylene and then transferring to a clean flask followed by addition of fresh substrates, solvent and base.

Both catalysts showed high activity in the substrates screened. Both activated and deactivated aryl bromides coupled to phenyl boronic acids rapidly (**Table 3.2**). The coupling of bromobenzene gave 99% conversion for both catalysts in 2 hours. Further, recycles of the catalysts gave quantitative conversions as well for both systems (99% run 1, 99% run 2, 99 % run 3). Direct comparison of the activity of catalysts **silica-60-C<sub>2</sub>-Pd(OAc)<sub>2</sub>** and **silica-60-C<sub>3</sub>-Pd(OAc)<sub>2</sub>** shows that **silica-60-C<sub>3</sub>-Pd(OAc)<sub>2</sub>** precatalyst gives faster kinetics in the cross coupling of 4-bromotoluene and 4-bromochlorobenzene with phenyl boronic acid (**Entry 3** and **4**). This is most probably due to the higher Pd loading of **silica-60-C<sub>3</sub>-Pd(OAc)<sub>2</sub>**.

**Table 3.2** Suzuki-Miyaura cross coupling of phenyl boronic acid and aryl halides catalysed by **silica-60-C<sub>2</sub>-Pd(OAc)<sub>2</sub>** and **silica-60-C<sub>3</sub>-Pd(OAc)<sub>2</sub>**

Entry	Substrate	Catalyst	Time (hours)	% conversion (cycle 1, 2 and 3)
1		C2	2	99, 99, 99
		C3		99, 99, 99
2		C2	2	99, 98, 95
		C3		99, 97, 97
3		C2	6	97, 97, 92
		C3	4	99, 98, 90 (97, 4.5hrs)
4		C2	6	99, 96, 90
		C3	4	99, 99, 90 (99, 6hrs)
5		C2	24	4
		C3	24	6

**Conditions:** Taken 1.5 mmol phenyl boronic acid, 1.0 mmol aryl halide, 1.5 mmol K<sub>2</sub>CO<sub>3</sub>, 50 mg of catalyst and 7mL of *o*-xylene. % conversion was determined by <sup>1</sup>H NMR or GC.

To further test the activity of these catalysts, the cross coupling of the more difficult chloroanisole and phenyl boronic acid was assessed. Unfortunately, both catalysts **silica-60-C<sub>2</sub>-Pd(OAc)<sub>2</sub>** and **silica-60-C<sub>3</sub>-Pd(OAc)<sub>2</sub>** were found to be inert in these conditions.

### 3.3.2 Palladium leaching tests

Is the Pd in these ligand modified Silica supported Palladium catalysts engaged in a heterogeneous or homogeneous process? There is a common concern in the scientific community about the nature of the catalyst in the cross coupling reactions whereby it is important to question whether the catalysis is truly heterogeneous involving palladium particles bound to a solid support, or whether leached palladium into solution is also active for the cross coupling. In a system where palladium is leached into solution, to what extent does this contribute to the overall catalysis? Furthermore, what about a mixed system where active palladium particles are supported on the solid and there is leached palladium in solution both contributing to the catalysis.<sup>26</sup> There are several common methods developed to distinguish homogeneous catalysis from heterogeneous catalysis for cross coupling reactions over palladium supported on solid supports. Catalyst poisoning,<sup>27</sup> 3-phase tests,<sup>28</sup> hot filtration (split) tests<sup>29</sup> and correlation between reaction rate and Pd concentration in solution<sup>30</sup> are the most commonly applied techniques.

#### Catalyst Poisoning

Catalyst poisoning involves introduction of a poison for any leached Pd from the support. This method is less practiced as it can alter the influence of the solid support on leached soluble Pd particles and so influence the reaction rate in the liquid phase which may deviate from the actual situation.<sup>31</sup>

#### Three Phase tests

Three-phase tests involve anchoring one of the substrates, usually the aryl halide onto a solid support and monitoring the reaction. If coupled product is formed this suggests that Pd particles have leached into solution and catalysed the reaction and if it has not then it supports a truly heterogeneous mode of action for the catalyst. It is well reported that only a small amount of leached Pd is required to catalyse a reaction. Although the three-phase test can provide strong evidence for the nature of the catalyst, regardless of the amount of the Pd leached, it still has restrictions.<sup>13</sup> In more difficult reactions such as the coupling of aryl chlorides, this test may give ambiguous evidence for the occurrence of heterogeneous catalysis. This is because a decrease of active palladium concentrations in the liquid phase through leached palladium reattaching to the support, can give a low reaction rate suggesting a heterogeneous mode of action of the catalyst.

### Hot filtration tests

In this study hot filtration tests were carried out with all catalysts for the reaction between phenyl boronic acid and bromotoluene. After reaction time of 2 hours, a conversion of 44% was observed in the case of **silica-60-C<sub>3</sub>-Pd(OAc)<sub>2</sub>**. The solid catalyst was filtered and the filtrate was then transferred to a new reaction flask with a new magnetic stirrer. To this, fresh base was added and the reaction left to stir for a further four hours. After this reaction time, no further conversion was observed. Further to this analysis, the filtrate was analysed by ICP-OES and it was found that no palladium was present in the filtrate. Similar results were found with catalyst **silica-60-G<sub>1</sub>-Pd(OAc)** and **silica-60-C<sub>2</sub>-Pd(OAc)<sub>2</sub>**. These findings would suggest strong binding of palladium to the sulfur ligand modified silica supports. Additionally, recycling of the catalysts in which there was no significant loss in activity suggests that all the palladium is recovered by the support at the end of a reaction. Only a very small amount of homogeneous palladium (0.0001 mol %) is required to catalyse these cross coupling reactions.<sup>32</sup>

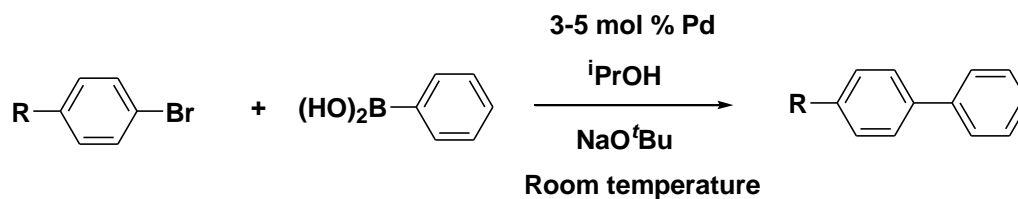
Assuming the sulfur ligand: Pd ratio in these materials in 1:1 then palladium and sulfur analysis suggests that for **silica-60-G<sub>1</sub>-Pd(OAc)** approximately 85% of the ligand sites would be coordinated to palladium and for **silica-60-C<sub>2</sub>-Pd(OAc)<sub>2</sub>** and **silica-60-C<sub>3</sub>-Pd(OAc)<sub>2</sub>** 68 % and 90% of the ligand sites would be coordinated to palladium respectively. This presence of excess free ligand sites in the company of any solution phase free palladium could facilitate its rebinding at the end of a reaction.

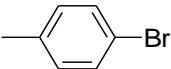
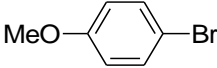
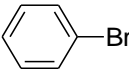
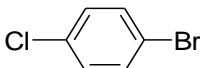
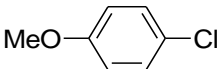
### 3.3.3. Suzuki Miyaura reactions catalysed by silica-60-G<sub>1</sub>-Pd(OAc), silica-60-C<sub>2</sub>-Pd(OAc)<sub>2</sub> and silica-60-C<sub>3</sub>-Pd(OAc)<sub>2</sub> at room temperature

The need to make synthetic procedures more environmentally friendly has been discussed in Chapter 1. There are a large number of parameters to be considered in the Suzuki reaction; palladium source, solvent, temperature, base etc. In this work it desirable to explore milder reaction conditions so the use of catalysts **silica-60-G<sub>1</sub>-Pd(OAc)**, **silica-60-C<sub>2</sub>-Pd(OAc)<sub>2</sub>** and **silica-60-C<sub>3</sub>-Pd(OAc)<sub>2</sub>** in the Suzuki-Miyaura cross coupling reaction carried out at room temperature were studied. Successful Suzuki-Miyaura cross coupling reactions carried out at room temperature have previously been reported by Fu *et al.*, Lipshutz *et al.* as well as Nolan

*et al.*<sup>33</sup> In 2002, Fu and *et al.* reported on the cross coupling of phenyl boronic acid and substituted bromides with 5 mol % Pd(OAc)<sub>2</sub> and phosphine ligands (10 mol %). They reported that high conversions were achieved when potassium-*tert*-butoxide was used as a base and *t*-amyl-alcohol as a solvent.<sup>34</sup> More recently, Lipshutz *et al.* reported on the efficient cross coupling of aryl boronic acids with a wide array of aryl halides also carried out at room temperature.<sup>35</sup> These reactions were carried out with Pd(dtbpf)Cl<sub>2</sub> (0.02 mol%) and ammonia as a base. Apart from the examples discussed above the use of silica supported catalysts in room temperature Suzuki-Miyaura reactions of aryl bromides would appear to be relatively rare.

In this work room temperature Suzuki-Miyaura cross coupling reactions of aryl bromides and phenyl boronic acids wherein isopropanol was used as a solvent and sodium *tert*-butoxide as a base were explored. These reducing conditions had previously been used by Nolan *et al.* in studies using homogeneous Pd catalysts. The amount of catalyst used in these reactions corresponded to 3 mol % for catalysts **silica-60-C<sub>2</sub>-Pd(OAc)<sub>2</sub>** and **silica-60-C<sub>3</sub>-Pd(OAc)<sub>2</sub>** and 5 mol% for **silica-60-G<sub>1</sub>-Pd(OAc)**. As before, aryl halide (1.0 mmol), phenyl boronic acid (1.5 mmol), sodium *tert*-butoxide (1.2 mmol) and isopropanol (4 mL) were added to the reaction flask and stirred. To this was then added catalyst and the reaction mixture left to stir for the required time. Recycles were performed by separation of the solid catalyst from the reaction media by filtration and washing with isopropanol.

**Table 3.3** The Suzuki-Miyaura reaction catalyzed by **silica-60-G<sub>1</sub>-Pd(OAc)**, **silica-60-C<sub>2</sub>-Pd(OAc)<sub>2</sub>** and **silica-60-C<sub>3</sub>-Pd(OAc)<sub>2</sub>** at room temperature

Entry	Aryl Halide	Catalyst	% conversion
1		G <sub>1</sub> Pd(OAc)	95, 92, 92
		C <sub>2</sub> Pd(OAc) <sub>2</sub>	88, 86, 88
		C <sub>3</sub> Pd(OAc) <sub>2</sub>	[95 (3h)] 99, 99, 99
2		G <sub>1</sub> Pd(OAc)	96, 94, 94
		C <sub>2</sub> Pd(OAc) <sub>2</sub>	95, 94, 94
		C <sub>3</sub> Pd(OAc) <sub>2</sub>	[83 (3h)] 99, 99, 99
3		C <sub>2</sub> Pd(OAc) <sub>2</sub>	98, 95, 95
		C <sub>3</sub> Pd(OAc) <sub>2</sub>	[90 (3h)] 99, 99, 95
4		G <sub>1</sub> Pd(OAc)	99, 89, 90
		C <sub>2</sub> Pd(OAc) <sub>2</sub>	76, 76, 74
		C <sub>3</sub> Pd(OAc) <sub>2</sub>	[83 (3h)], 99, 90, 87
5		G <sub>1</sub> Pd(OAc)	4
		C <sub>3</sub> Pd(OAc) <sub>2</sub>	5
		C <sub>3</sub> Pd(OAc) <sub>2</sub>	8

**Conditions:** Taken 1.0 mmol aryl halide, 1.5 mmol phenyl boronic acid, 1.2 mmol NaO<sup>t</sup>Bu, (100 mg **silica-60-C<sub>2</sub>-Pd(OAc)<sub>2</sub>** or 70 mg **silica-60-G<sub>1</sub>Pd(OAc)** or 70 mg **silica-60-C<sub>3</sub>-Pd(OAc)<sub>2</sub>**) catalyst and Isopropanol (4mL). % conversion calculated from <sup>1</sup>H NMR for 4-Bromotoluene, 4-Bromoanisole and Chloroanisole. % conversion calculated from GC for Bromobenzene and 4-Bromochlorobenzene.



High conversions coupled with consistent recycles were achieved with supported catalyst **silica-60-C<sub>3</sub>-Pd(OAc)<sub>2</sub>** (Table 3.3). In comparison, the activity of supported catalyst **silica-60-C<sub>2</sub>-Pd(OAc)<sub>2</sub>** was found to be slower in the case of cross coupling bromotoluene and bromochlorobenzene (entries 1 and 4). However, no loss in activity is found in subsequent runs. A slight decrease in activity is found in the recycle of the cross coupling of bromochlorobenzene using **silica-60-C<sub>3</sub>-Pd(OAc)<sub>2</sub>**. The results of catalyst **silica-60-G<sub>1</sub>-Pd(OAc)** were found to be comparable to **silica-60-C<sub>3</sub>-Pd(OAc)<sub>2</sub>**, and for both a drop in activity was observed in the recycles of the coupling of bromochlorobenzene with phenyl boronic acid. The finding may be a result of substrate effects to these conditions.

### 3.3.4 Kinetic Studies

A closer look at the kinetics of the cross coupling reaction of 4-bromochlorobenzene and bromobenzene with phenyl boronic acid is illustrated in Figures 3.4 and 3.5 for **silica-60-C<sub>2</sub>-Pd(OAc)<sub>2</sub>** and **silica-60-C<sub>3</sub>-Pd(OAc)<sub>2</sub>**. For bromobenzene there is a clear difference in rate of conversion for the two catalysts where the profile for **silica-60-C<sub>3</sub>-Pd(OAc)<sub>2</sub>** indicates a faster rate of conversion. The faster conversion for bromobenzene by **silica-60-C<sub>3</sub>-Pd(OAc)<sub>2</sub>** may simply be a reflection of the higher Pd loading (factor of 1.5 ). Data were only collected after the first hour and there is no obvious induction period beyond this point. The same batches of catalysts were employed in both experiments and several points were repeated a number of times which excludes the possibility of inaccuracies associated with the conversion measurements.

A similar finding is observed on the rate of conversion for the more deactivated 4-bromochlorobenzene. As expected both catalysts show a faster rate of conversion for bromobenzene in comparison to 4-bromochlorobenzene.

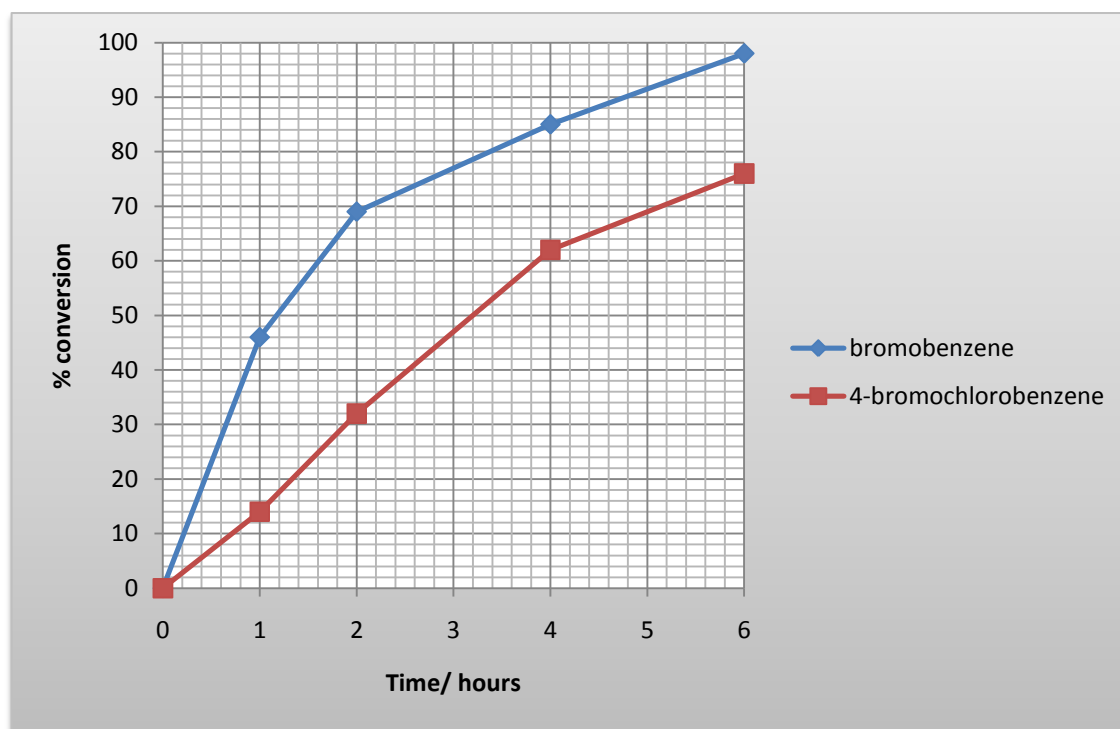


**Figure 3.4** Kinetic profile for the Suzuki-Miyaura reaction of 4-chlorobromobenzene and bromobenzene with phenylboronic acid at room temperature catalysed by **silica-60-C<sub>2</sub>Pd(OAc)<sub>2</sub>**.

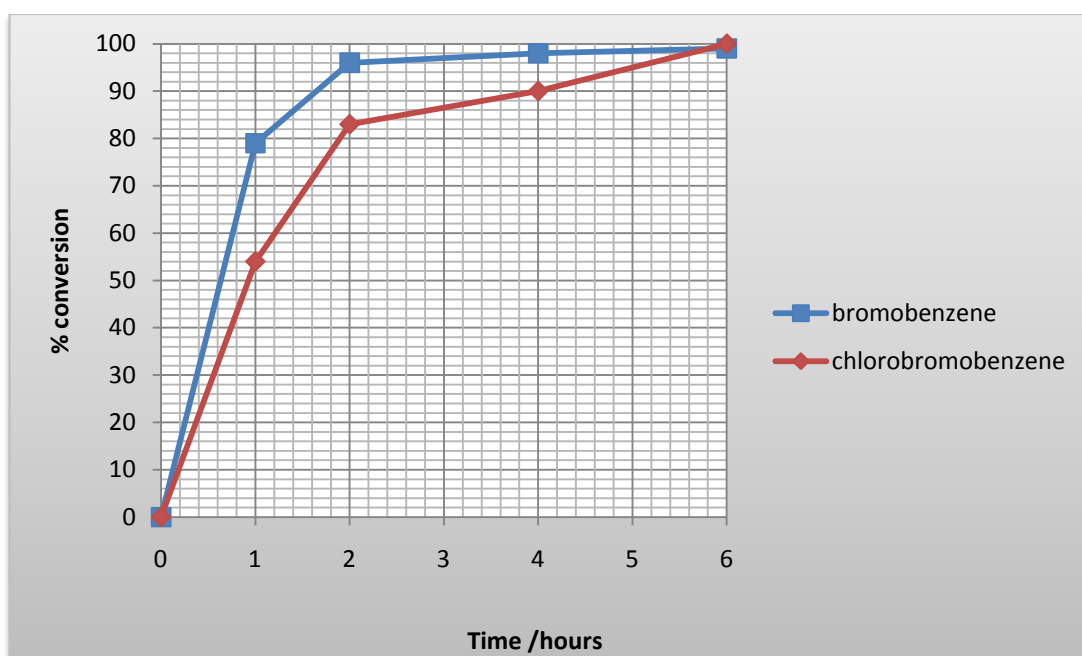


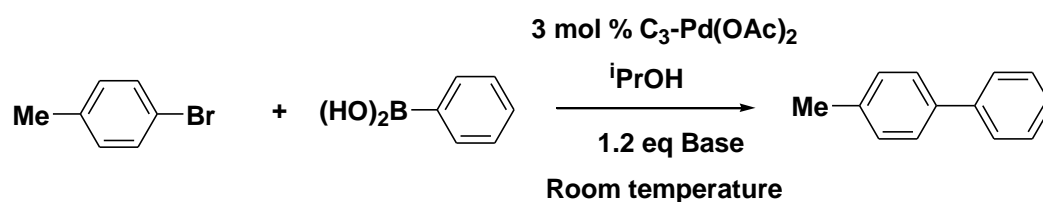
**Figure 3.5** Kinetic profile for the Suzuki-Miyaura reaction of 4-chlorobromobenzene and bromobenzene with phenylboronic acid at room temperature catalysed by **silica-60-C<sub>3</sub>-Pd(OAc)<sub>2</sub>**.

### 3.3.5 Suzuki-Miyaura reaction with low Pd loading **silica-60-C<sub>3</sub>-Pd(OAc)<sub>2</sub>**

An additional catalytic run was carried out in which 2 mol % of Pd was taken in these mild conditions. The catalyst was prepared by reacting a 1:0.5 mole ratio of **silica-60-C<sub>3</sub>**: palladium acetate to give a new catalyst with a high ligand: Pd ratio. The measured Pd loading for this catalyst was 0.23 mmol/g, suggesting that 30 % of the ligand sites are occupied by metal. This material was light yellow in colour in comparison to the strong orange colour displayed by **silica-60-C<sub>3</sub>-Pd(OAc)<sub>2</sub>**. This new catalyst was screened in the reaction of bromotoluene with phenylboronic acid in isopropanol with sodium *tert* butoxide as a base. High conversions as well as successful recycles (cycle 1 (93%), cycle 2 (92%), cycle 3 (93%)) were observed and its performance was found to be comparable to catalysts **silica-60-G<sub>1</sub>-Pd(OAc)**, **silica-60-C<sub>2</sub>Pd(OAc)<sub>2</sub>** and **silica-60-C<sub>3</sub>Pd(OAc)<sub>2</sub>**. This finding is particularly interesting as this suggests that the required amount of Pd does not need to be high and that balance between free ligand sites and occupied ligand sites needs to be found.

### 3.3.6 Suzuki-Miyaura reaction **silica-60-C<sub>3</sub>-Pd(OAc)<sub>2</sub>** and different bases

Further studies were carried out to determine the most suitable base for these room temperature reactions. Catalyst **silica-60-C<sub>3</sub>Pd(OAc)<sub>2</sub>** was tested in the cross coupling reaction of bromotoluene and phenyl boronic acid in isopropanol with different bases. Caesium carbonate was found to be a little more effective than sodium *tert* butoxide with almost quantitative conversion in 3 hours (see **Table 3.4**). However, other bases including sodium methoxide and sodium acetate were found to be less effective.

**Table 3.4** Suzuki-Miyaura reaction with the use of different bases

Entry	Base <sup>a</sup>	Time/ hours	% Conversion <sup>b</sup>
1	Potassium carbonate	3	66
2	Cesium carbonate	3	94
3	Triethylamine	3	21
4	Sodium methoxide	3	23
5	Sodium acetate	3	26

Taken 1.0 mmol 4-bromotoluene, 1.5 mmol phenyl boronic acid, 1.2 mmol base, 70 mg catalyst and isopropanol (4mL) and stirred at room temperature. <sup>b</sup>. % conversion calculated from <sup>1</sup>H NMR

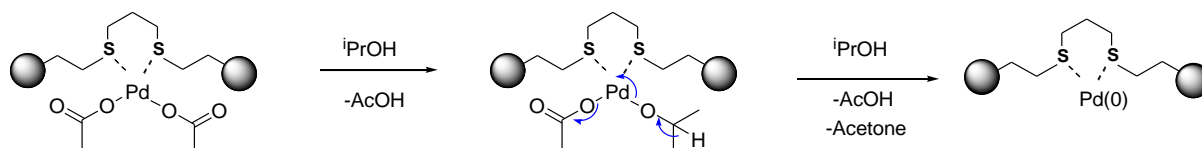
### 3.3.7 Palladium leaching tests

Leaching tests were carried out with all catalysts for the reaction between phenyl boronic acid and bromotoluene in mild conditions. After reaction was run for 2 hours, a conversion of 44% was observed in the case of **silica-60-C<sub>3</sub>Pd(OAc)<sub>2</sub>**. The solid catalyst was filtered and the filtrate was then transferred to a new reaction flask with a new magnetic stirrer. To this fresh base was added and the reaction left to stir for a further four hours. After this reaction time, no further conversion was observed. Further to this analysis, the filtrate was analysed by ICP-OES and it was found that no palladium was present in the filtrate. Similar results were found with catalyst **silica-60-G<sub>1</sub>Pd(OAc)** and **silica-60-C<sub>2</sub>Pd(OAc)<sub>2</sub>**. This finding suggests that the active catalysts are heterogeneous.

As mentioned already, the presence of free ligand sites in these catalysts, in the company of any solution phase free palladium facilitates its rebinding at the end of a reaction. This ambiguity in the reaction pathway led to further mechanistic studies.

3.3.8 TEM of silica-60-G<sub>1</sub>-Pd(OAc), silica-60-C<sub>2</sub>-Pd(OAc)<sub>2</sub> and silica-60-C<sub>3</sub>-Pd(OAc)<sub>2</sub>

Further probing of the mechanistic route of these reactions started with TEM images of the catalyst before and after reaction at room temperature. Before catalysis, catalyst **silica-60-C<sub>3</sub>Pd(OAc)<sub>2</sub>** shows a homogeneous distribution of palladium particles on the silica surface. Interestingly after catalysis, regions of high palladium content are observed (**Figure 3.6**), suggesting movement of the palladium during reaction and redeposition onto the supported ligand as clusters once the reaction was stopped. Assuming this is reduced palladium, Pd(0), reduction can be owed to the conditions used at room temperature. It is proposed that the solvent isopropanol may facilitate the reduction of Pd(II) to Pd(0) via the formation of acetic acid and acetone.



**Scheme 3.11** Mechanistic proposal for the reduction of Pd(II) to Pd(0)

TEM images of catalyst **silica-60-G<sub>1</sub>-Pd(OAc)** before and after catalysis in high temperature Suzuki-Miyaura reactions show homogeneous distribution of Pd metal on the silica surface (**Figure 3.7**). It would seem that the (less reducing) conditions used when the reaction is carried out at high temperatures prevent the agglomeration of Pd. In addition, the binding of the Pd to the thioglycolate system might be stronger thus inhibiting Pd dissociation and formation of colloidal particles. It is also worth noting that while porosimetry showed evidence for pore blocking by palladium in the **silica-60-C<sub>3</sub>Pd(OAc)<sub>2</sub>** material there was no such indication for **silica-60-G<sub>1</sub>-Pd(OAc)** and this fits nicely with the TEM observations where we see clustering of palladium for **silica-60-C<sub>3</sub>Pd(OAc)<sub>2</sub>** but not for **silica-60-G<sub>1</sub>-Pd(OAc)**.

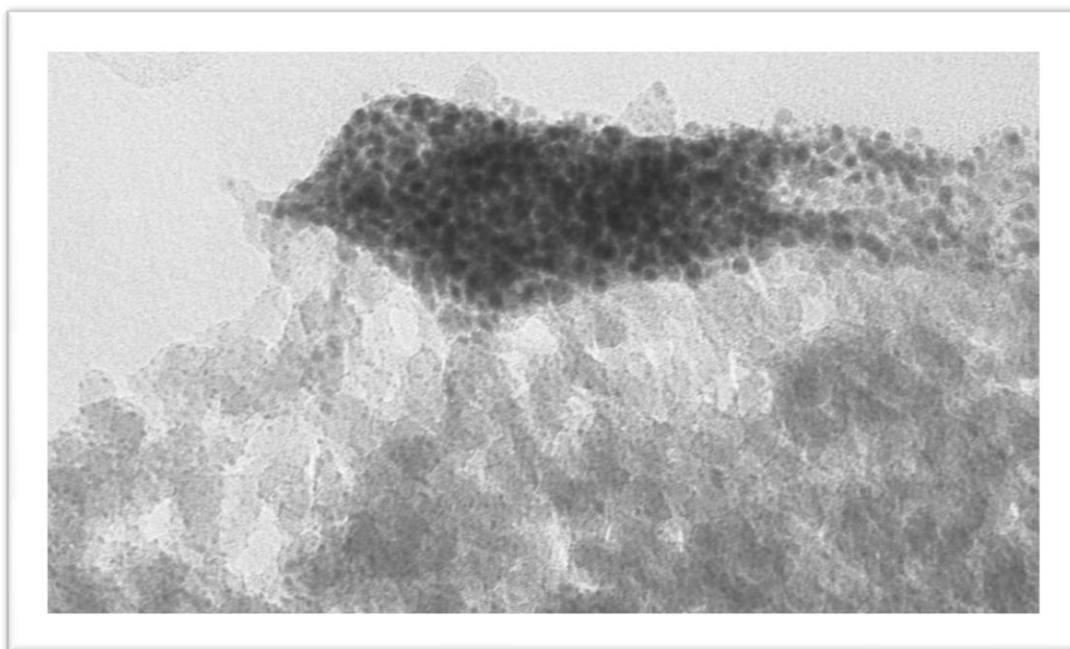


**Figure 3.6** TEM image of **silica-60-C<sub>3</sub>-Pd(OAc)<sub>2</sub>** after catalysis at room temperature showing Pd clustering

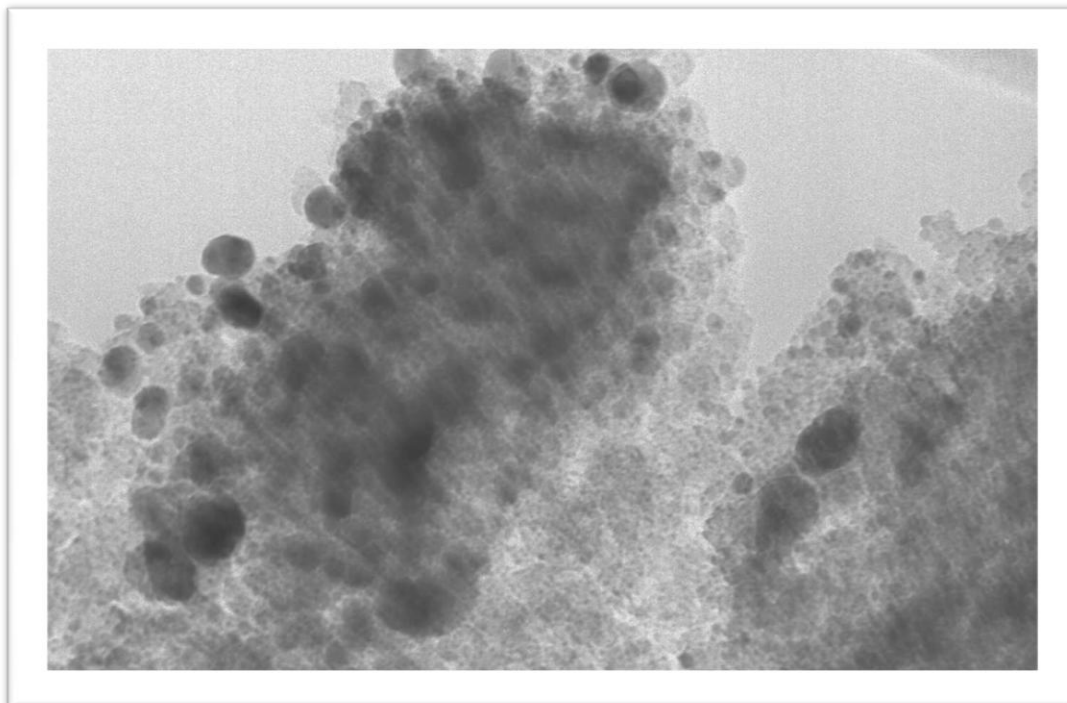


**Figure 3.7** TEM image of **silica-60-G<sub>1</sub>-Pd(OAc)** after catalysis at high temperature showing a homogeneous distribution of Pd

It is important to note that TEM analysis does not provide quantitative information of all palladium species in a sample whereas a technique such as XPS provides potentially average structural information of all Pd species in the sample.

### 3.3.9 X-ray Photoelectron Studies of silica-60-G<sub>1</sub>-Pd(OAc), silica-60-C<sub>2</sub>-Pd(OAc)<sub>2</sub> and silica-60-C<sub>3</sub>-Pd(OAc)<sub>2</sub>

To gain more insight into the mechanistic nature of these catalysts in the Suzuki-Miyaura reactions, XPS measurements were performed on catalysts **silica-60-C<sub>2</sub>-Pd(OAc)<sub>2</sub>**, **silica-60-C<sub>3</sub>-Pd(OAc)<sub>2</sub>**, **silica-60-G<sub>1</sub>-Pd(OAc)** before and after catalysis. From TEM and EDS analysis, the formation of palladium clusters in catalyst **silica-60-C<sub>3</sub>-Pd(OAc)<sub>2</sub>** was observed after use at room temperature with isopropanol; this suggests that this reaction follows a Pd(II)/(0) pathway. In addition, the likely pathway for reduction of Pd(II) to Pd(0) by isopropanol further supports this suggestion. In the case of reactions carried out at higher temperatures in *o*-xylene, the absence of an obvious reduction pathway for Pd(II) to Pd(0), as well as the homogeneous distribution of Pd metal on the surface as observed from TEM and EDS analysis after catalysis suggests this reaction may occur via a Pd(IV)/(II) mechanistic pathway. The Pd 3d XPS spectrum obtained from these catalysts were characterized by peaks with binding energies around 336.5 for 3d<sub>5/2</sub> and 342.8 eV for 3d<sub>3/2</sub>, both distinctive for palladium (**Figure 3.8**). The line shape of the high resolution Pd 3d<sub>5/2</sub> peak reveals that there are three different types of valent states. As shown in the figure below, the minor component of the binding energy of Pd 3d<sub>5/2</sub> is 335.0 eV which corresponds to zerovalent states of Pd, while major components at 336.2 and 337.4 eV are assigned to non-zerovalent states.

Zerovalent palladium complexes show unique reactivity in a number of organic transformations. The use of Pd(0) catalysts is known to be difficult because of its instability to air and moisture. Catalysts **silica-60-C<sub>2</sub>-Pd(OAc)<sub>2</sub>**, **silica-60-C<sub>3</sub>-Pd(OAc)<sub>2</sub>**, **silica-60-G<sub>1</sub>-Pd(OAc)** reveal some Pd(0) character before catalysis, approximately 5, 5.5 and 10% respectively. The presence of Pd(0) on these catalysts before use suggests that some Pd(II) species may have been reduced to Pd(0) under the conditions used to prepare them. Interestingly, an increase of the Pd(0) content is observed after use, in some cases doubling. An increase of 30% in Pd(0) content is seen in catalyst **silica-60-C<sub>3</sub>-Pd(OAc)<sub>2</sub>** after use in high temperature conditions. Just to note, after catalysis, a change in the colour of the catalyst

from a deep orange to an earthy brown colour further suggests that the reduction of some of the starting Pd(II) complex to the lower valent state, Pd(0) has occurred.

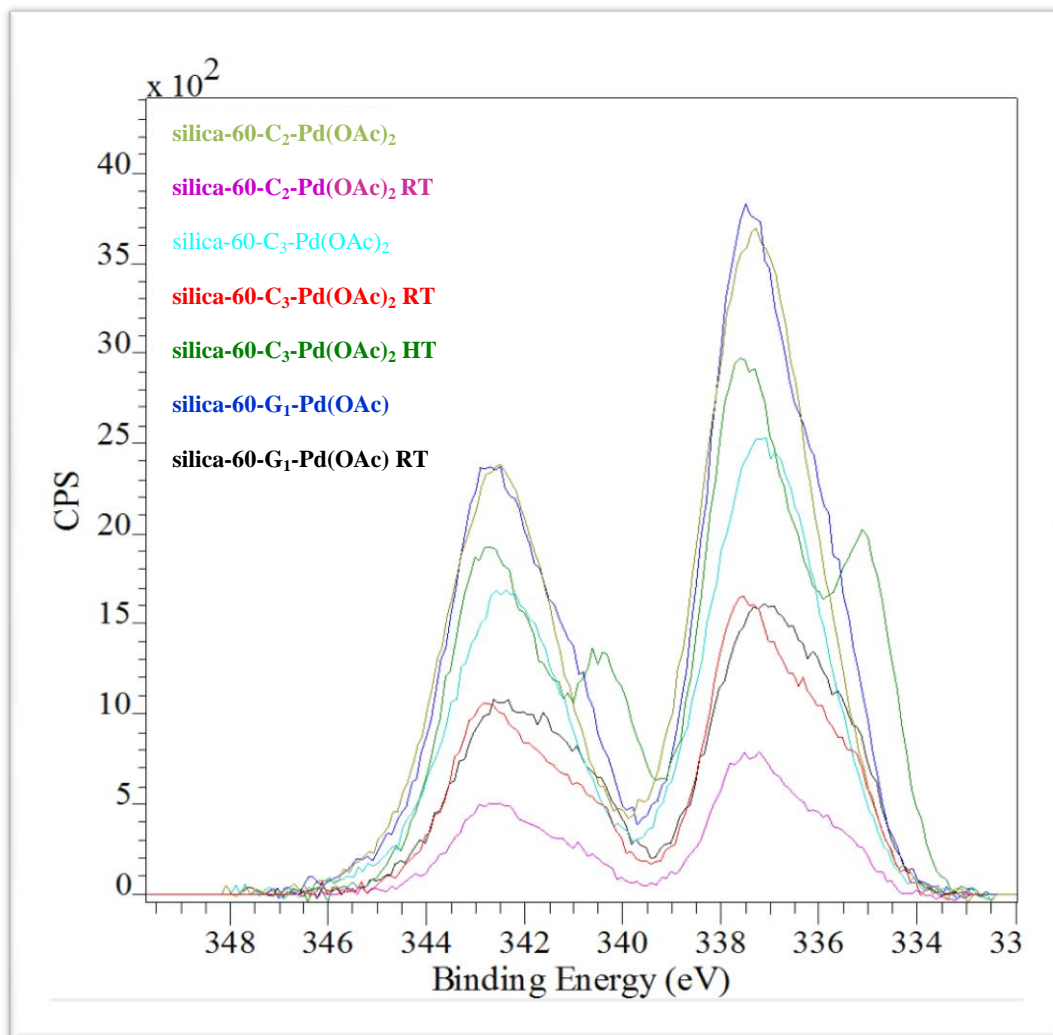


**Figure 3.8** XPS of catalysts **silica-60-C<sub>2</sub>-Pd(OAc)<sub>2</sub>**, **silica-60-C<sub>3</sub>-Pd(OAc)<sub>2</sub>**, **silica-60-G<sub>1</sub>-Pd(OAc)** before and after catalysis.

The binding energies with peak maxima ranging from 335.3 to 335.5 eV are assigned to Pd(0), which is in agreement with the binding energy of Pd metal (335.0 eV).<sup>36</sup> The binding energy of Pd(OAc)<sub>2</sub> is reported to be 336.6 eV. The binding energies at 336.2 eV is assigned to Pd(II) for catalysts **silica-60-C<sub>2</sub>-Pd(OAc)<sub>2</sub>**, **silica-60-C<sub>3</sub>-Pd(OAc)<sub>2</sub>**, **silica-60-G<sub>1</sub>-Pd(OAc)**. The Pd binding energies depend strongly on the nature of the ligands co-ordinating



to the metal. The binding energy found at 337.4 eV is also assigned to Pd(II), however the metal here is in a different chemical environment.

**Table 3.5** % Composition of Pd(0) and Pd(II) in catalysts **silica-60-C<sub>2</sub>-Pd(OAc)<sub>2</sub>**, **silica-60-C<sub>3</sub>-Pd(OAc)<sub>2</sub>**, **silica-60-G<sub>1</sub>-Pd(OAc)** before and after use in the Suzuki-Miyaura reaction.

	<b>Pd(0)</b> 335.0 eV	<b>Pd(II)</b> 336.2 eV	<b>Pd(II)</b> 337.4 eV
<b>silica-60-C<sub>2</sub>-Pd(OAc)<sub>2</sub></b>	5.4	29.5	65.1
<b>silica-60-C<sub>2</sub>-Pd(OAc)<sub>2</sub> RT</b>	9.5	31.1	59.4
<b>silica-60-C<sub>3</sub>-Pd(OAc)<sub>2</sub></b>	5.2	37.2	57.6
<b>silica-60-C<sub>3</sub>-Pd(OAc)<sub>2</sub> RT</b>	16.0	27.3	56.7
<b>silica-60-C<sub>3</sub>-Pd(OAc)<sub>2</sub> HT</b>	33.9	10.6	55.5
<b>silica-60-G<sub>1</sub>-Pd(OAc)</b>	10.5	29.2	60.3
<b>silica-60-G<sub>1</sub>-Pd(OAc) RT</b>	17.8	36.2	46.1

**RT** – after reaction at room temperature; **HT** – after reaction at high temperature

Alvarez *et al.* report that in the XPS studies of Pd nanoparticles dispersed on silica, a small shoulder occurring at 337.3 eV in the XPS spectrum can be assigned to the Pd 3d<sub>5/2</sub> of Pd (II) and Pd (IV) resulting from the oxidation of metallic Pd during XPS sample preparation.<sup>37</sup> In the case of all the catalysts the peaks around 337.4 are very significant and unlikely to be wholly attributed to oxidation of Pd metal (see **Table 3.5** for % content). Additionally, the presence of a large amount of Pd (IV) prior to catalyst use seems unlikely. In the case of **silica-60-C<sub>2</sub>-Pd(OAc)<sub>2</sub>** and **silica-60-C<sub>3</sub>-Pd(OAc)<sub>2</sub>**, it may be that the Pd metal is complexed to one of the sulfur ligands. In the case of **silica-60-G<sub>1</sub>-Pd(OAc)**, from the <sup>13</sup>C NMR of silica-60-G<sub>1</sub> it is evident that there exists thioglycolate ester immobilised on the silica surface.

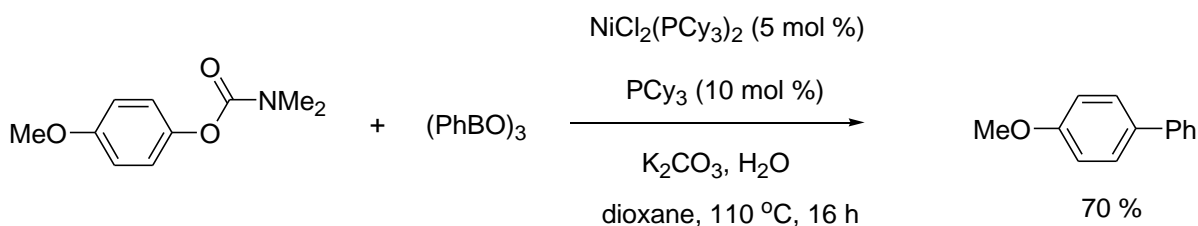
Interaction of the Pd metal to these weaker binding sites could give rise to these higher binding energies found.

A closer look at the Pd  $3d_{5/2}$  peak, shows a shift of the peak for **silica-60-C<sub>3</sub>-Pd(OAc)<sub>2</sub>** at lower binding energies, with a difference of 0.4 eV from catalysts **silica-60-C<sub>2</sub>-Pd(OAc)<sub>2</sub>** and **silica-60-G<sub>1</sub>-Pd(OAc)**. Clark *et al.* reported that lower binding energies of Pd catalysts reflect higher activity in cross coupling reactions.<sup>38</sup> Interestingly, in the Suzuki-Miyaura reactions, catalyst **silica-60-C<sub>3</sub>-Pd(OAc)<sub>2</sub>** showed higher activity than catalysts **silica-60-C<sub>2</sub>-Pd(OAc)<sub>2</sub>** and **silica-60-G<sub>1</sub>-Pd(OAc)**. Another important point, a shift in binding energies is observed after reaction for all three catalysts suggests that some alteration to the catalyst after use has occurred. For example, the palladium may detach from the support during the reaction such as in the case of catalyst **silica-60-C<sub>3</sub>-Pd(OAc)<sub>2</sub>**, TEM studies reveal the formation of Pd clusters after use in the Suzuki-Miyaura reaction at room temperature.

These silica bound Pd(II)/Pd(0) complexes are very stable to air and moisture, possibly due to the isolation/confinement of the active species by the silica framework. As a result, the catalysts show excellent longevity and can be stored for long periods and are thus very convenient to use.

#### 3.3.10 Suzuki-Miyaura reaction at room temperature with silica-60-C<sub>3</sub>-Ni(OAc)<sub>2</sub>

Focus was also turned to the use of cheaper, more abundant metals to carry out the Suzuki-Miyaura reaction. In 2006, Fu *et al.* reported on the Suzuki cross coupling of alkyl halides with phenyl boronic acid catalysed by Ni/amino alcohol catalyst.<sup>39</sup> The authors reported 80% conversion in the cross coupling of 4-chlorocyclohexane and phenyl boronic acid employing isopropanol as a solvent and KHMDS as a base. Reaction times were not reported. Most recently, in 2010, nickel catalysed Suzuki coupling of aryl carbamates and phenyl boronic acids have been reported by Shi *et al.*<sup>40</sup> With dioxane as a solvent and potassium carbonate as base, almost quantitative conversions were achieved for a variety of substituted aryl carbamates (**Scheme 3.12**).



**Scheme 3.12** Nickel catalysed Suzuki-Miyaura coupling of aryl carbamates with phenyl boroxines

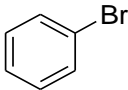
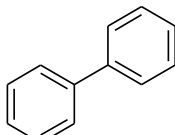
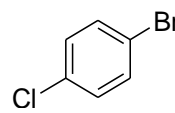
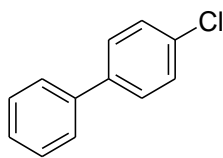
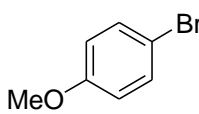
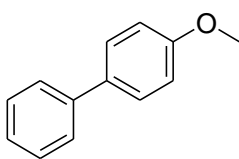
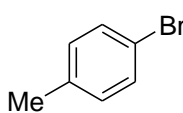
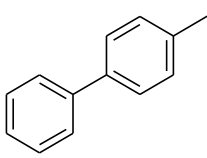
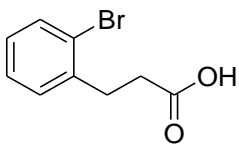
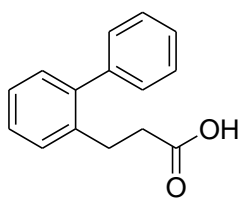
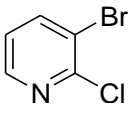
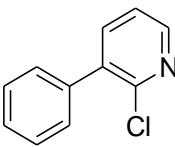
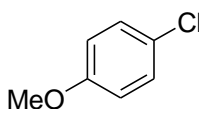
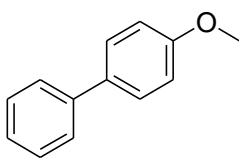
Heterogeneous Ni/C has also been reported to successfully catalyse the Suzuki-Miyaura reaction and mirror the performance of homogeneous Ni(0) catalysts.<sup>41</sup> Leaching tests revealed some nickel to be released from the charcoal during coupling process. To date silica immobilised nickel catalysts have not been reported. With the success of the homogeneous nickel catalysts in the Suzuki-Miyaura reaction and the leaching problems associated with Ni/C catalysts, we immobilized nickel and cobalt salts onto our silica-60-C<sub>3</sub> material. The uptake of Ni(OAc)<sub>2</sub> was carried out as previously described for Pd(OAc)<sub>2</sub>. This catalyst was first used employing conditions used for the palladium analogues, at room temperature and unfortunately it was found that this catalytic system was inactive with these conditions. The catalyst loading was thereby increased to 5 mol% and the cross coupling of bromoanisole and phenyl boronic acid was studied. No coupled product was obtained. We also immobilised Co(OAc)<sub>2</sub> onto silica-60-C<sub>3</sub> and found this immobilised cobalt catalyst to also be inactive, even at higher temperatures. It would seem that for these particular ligands, palladium remains to be the metal of choice for this transformation.

### 3.3.11 Microwave assisted Suzuki-Miyaura coupling with silica-60-C<sub>3</sub>-Pd(OAc)<sub>2</sub>

The drive for more environmentally benign synthetic protocols in the field of organic chemistry is more prominent than before. The use of microwave assisted transformations has emerged as a useful technique for a variety of organic transformations. Microwave assisted transformations have received great attention due to the high reaction rates and purity of the end products.<sup>42</sup> As a powerful and easily controllable power source, the results obtained from microwave irradiation are found to be more consistent than conventional heating source.<sup>43</sup> With this in mind, attention was then turned to utilising the **silica-60-C<sub>3</sub>-Pd(OAc)<sub>2</sub>** catalyst in microwave assisted Suzuki-Miyaura reactions. For these reactions isopropanol and sodium *tert*-butoxide were employed as solvent and base using 1.0 mmol substrates and 1.2 mol % of

catalyst (30mg). With a total reaction time of 6 minutes, quantitative conversions were achieved for bromobenzene and 4-bromotoluene (Table 3.6)

**Table 3.6** Microwave assisted Suzuki-Miyaura reaction with 1.2 mol % silica-60-C<sub>3</sub>-Pd(OAc)<sub>2</sub>

Entry	Aryl Halide	Product	% conversion (cycle 1, 2)
1			97, 95
2			85, 67
3			97, 95
4			97, 94
5			74,
6			64
7			6

**Conditions:** Taken 1.5 mmol Phenyl boronic acid, 1.0 mmol aryl halide, 1.2 mmol NaO<sup>t</sup>Bu, 30 mg catalyst and 5mL Isopropanol. Microwave (600 W), 6 minutes at 140 °C. % conversion determined by <sup>1</sup>H NMR and GC-MS.

Recycling of the catalyst found activity to be retained. The activity of more complex aryl bromides was also tested. The coupled products of sterically hindered 2-(bromophenyl)propionic acid and 2-bromochloropyridine with phenyl boronic acid were formed in good conversions (74 and 64% respectively). The cross coupling of the more difficult aryl chloride 4-chloroanisole was also attempted in these conditions and unfortunately the catalyst was found to be inactive.

### 3.3.12 Suzuki-Miyaura reaction with silica-60-C<sub>3</sub>-Pd( $\eta^3$ -allyl)chloride

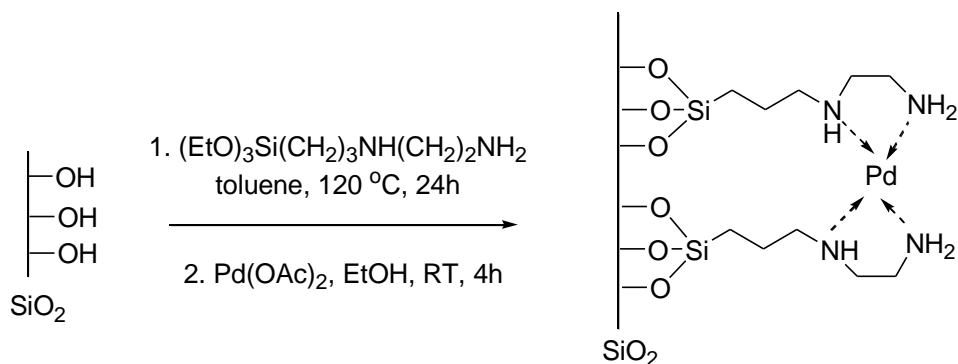
In choosing a suitable palladium compound for immobilisation two different types were considered and tried. Initial studies of the Suzuki-Miyaura reaction with these ligand systems were carried out with immobilised Pd( $\eta^3$ -allyl)chloride. In these reactions it was found that Pd had a higher tendency for Pd black formation. The colour of the reaction mixture was notably changed very quickly from light brown to black at room temperature and the Pd black was visually observed. Despite these observations reactions were carried out for prolonged periods to counteract any long induction period but conversion was repeatedly low ~ 3%. These reactions were also carried out under nitrogen but what seemed to be Pd black formed once again. Our attention was then turned to immobilising other Pd salts like Pd(OAc)<sub>2</sub> and PdCl<sub>2</sub> onto these sulfur based ligands and so these became choice sources of Pd metal.

## 3.4 Mizoroki-Heck reactions catalysed by Silica supported Pd catalyst

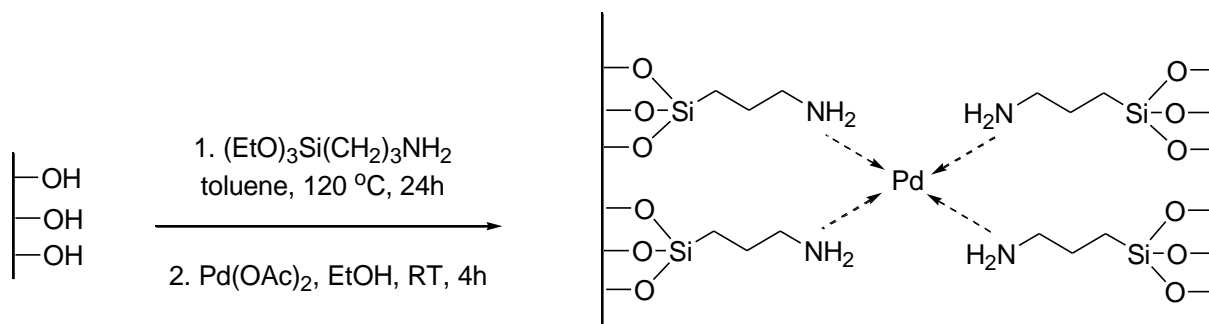
### 3.4.1 Background literature

Many palladium complexes supported on silica have been reported including Pd(II)-pincer complexes, Pd(II) Schiff base complexes, Pd(II)-carbon metallated palladacycle complexes and Pd-thiol complexes which catalyse Mizoroki-Heck reactions in excellent yield with negligible leaching of the palladium. In addition functionalized silica-Pd, sol gel entrapped palladium and palladium nanoparticles in silica have also been reported to show high activity for Heck reactions. Recently Wang *et al.* reported on the preparation of highly active 3-[(2-aminoethyl)amino]propyl-functionalized silica immobilized palladium (silica-AAPTS-Pd) and 3-aminopropyl functionalized silica (silica APTS) and their subsequent use as efficient

and recyclable catalysts in the Mizoroki-Heck reaction.<sup>44</sup> These catalysts were prepared in a two step synthesis (**Scheme 3.13**) by treatment of silica gel with [(2-aminoethyl)amino]propyl-triethoxysilane (AAPTS) or (3-aminopropyl)triethoxysilane (APTS) in dry toluene for 24 hours at 120 °C and afforded silica-AAPTS or silica-APTS (**Scheme 3.14**).



**Scheme 3.13** Preparation of silica-AAPTS-Pd

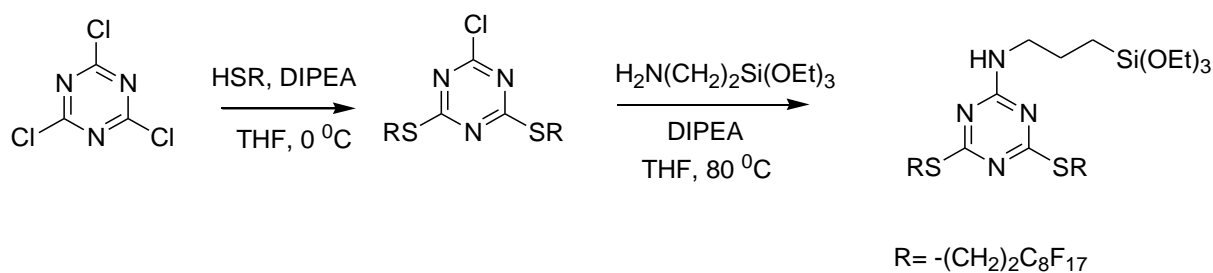


**Scheme 3.14** Preparation of silica-APTS-Pd

The functionalised silica materials were then reacted with palladium acetate in ethanol at room temperature for four hours to generate the corresponding silica-supported palladium catalysts, **silica-AAPTS-Pd** and **silica-APTS-Pd**. These catalysts were tested in the Mizoroki-Heck olefination of styrene with iodoarenes and bromoarenes containing electron rich and electron poor substituents. Good conversions were obtained when iodobenzene was reacted with styrene in DMF using potassium carbonate as a base, 96% and 88% with **silica-AAPTS-Pd** and **silica-APTS-Pd** respectively. In the cross coupling of bromobenzene and styrene 96% conversion was reported when **silica-AAPTS-Pd** catalyst was used and 83% when **silica-APTS-Pd** catalyst was used. The catalyst **silica-AAPTS-Pd** was further used in the cross coupling of iodoarenes with ether vinyl substrates, such as ethyl acrylate (99% with iodobenzene, 94% with 4-nitro-iodobenzene) and acrylonitrile (93% with iodotoluene) and

the authors report excellent conversions. In these conditions, chloroarenes coupled in good yields, although a longer reaction time was required (45 %, 24 hours). Further recycles of up to ten times in the reaction of iodobenzene and styrene were performed without any loss in activity. Most importantly, leaching tests revealed low levels of Pd, 0.02ppm, were present in solution.

In 2008, Niembro and Alibes reported on the preparation of Pd nanoparticles supported on a silica framework embedded within a fluoruous agent.<sup>45</sup> This catalyst was prepared by sol gel methods and showed excellent activity in the Mizoroki-Heck reactions. To prepare this catalyst trichlorotriazine was reacted with the fluorinated thiol,  $\text{HSCH}_2\text{CH}_2\text{C}_8\text{F}_{17}$ , in THF at 0 °C to give a disubstituted intermediate in good yield. Subsequent reaction of this compound with silylated amine in THF at 80 °C gave the desired product in 63% yield (**Scheme 3.15**). This product was then carried through the sol gel process to give the silica supported system. Solid state  $^{13}\text{C}$  and  $^{29}\text{Si}$  NMR and elemental analysis confirmed the incorporation of the fluoruous stabilizer into the material. This material was then loaded with Pd nanoparticles to give a black solid, catalyst **Pd<sub>n</sub>-6b**.

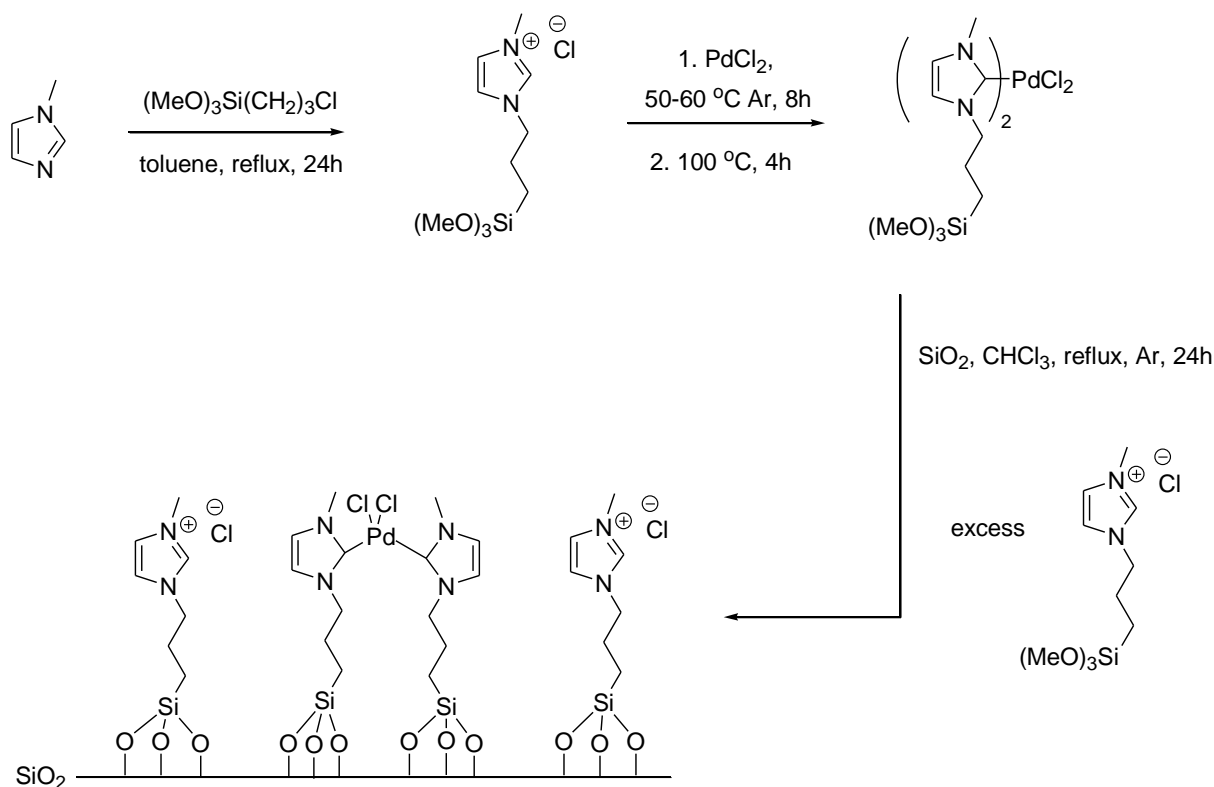


**Scheme 3.15** Synthesis of trialkoxysilane intermediate

The authors report on the high catalytic activity of **Pd<sub>n</sub>-6b** employing microwave irradiation. The coupling of iodobenzene with butyl acrylate was achieved in 3 hours at 130 °C and 150W initial power and using 2 mol % Pd (99%, 24 hours). The catalyst was reused five times without any appreciable loss in activity. Shorter reaction times at higher temperatures gave faster kinetics, however this was coupled with a loss in activity in recycles. Unfortunately this catalyst was found to be inactive in the cross coupling of aryl bromides. Leaching tests revealed 6ppm of Pd to be present in crude mixtures which is relatively significant.

In 2006, Karimi and Enders reported on the use of N-heterocyclic carbene ligands (NHC) as an alternative to phosphine ligands in the Mizoroki Heck reaction of a variety of haloarenes.<sup>46</sup> The silica supported NHC-Pd catalyst (preparation shown in scheme below) was tested in the Pd catalyzed arylation of olefins and with a variety of aryl halides under two different sets of conditions.

They report on the coupling of aryl iodides with substituted olefins in DMF with potassium carbonate/triethylamine as a base in excellent yields. The silica supported NHC-Pd catalyst failed to couple bromobenzene and methyl acrylate, however, a change of solvent to NMP and the use of sodium acetate as a base found the reaction to go to completion with 0.01 mol% Pd.



**Scheme 3.16** Preparation of Karimi and Enders silica supported NHC-Pd catalyst.<sup>46</sup>

Recycling of the catalyst in the Heck reaction of bromobenzene and methyl acrylate showed no considerable loss in activity (cycle 1, 2, 3 and 4; 95, 90, 92 and 89%). Karimi and Enders further reported that hot filtration tests showed no Pd had leached from the catalyst. Unfortunately chloroarenes failed to convert.



Clark *et al.* also reported on the high activity of bidentate iminopyridine ligands grafted onto mesoporous silica with Pd(II) in the Heck coupling of aryl iodides and olefins with triethylamine as the base and acetonitrile as a solvent..<sup>47</sup> The most notable conversion was from iodobenzene and methyl acrylate (82 % conversion in 24 hours).

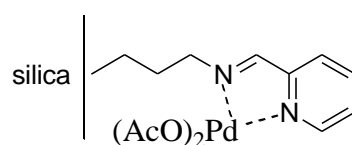
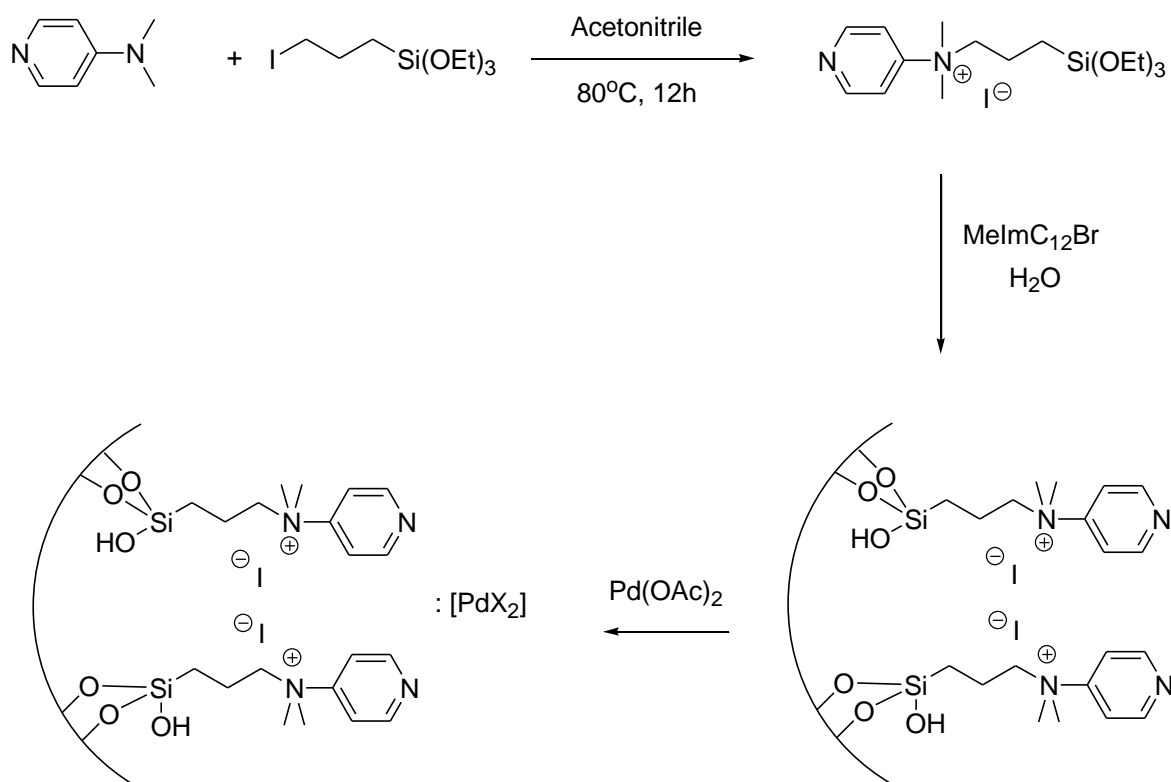


**Figure 3.8** Clark *et al.* amino modified silica Pd catalyst.

Recycles of the catalysts, showed no loss in activity up to run five. Interestingly, a close look at the reaction rate showed that an induction period existed in the first run and in consecutive runs no induction period was observed. Clark *et al.* suggested the finding may be due to some catalyst restructuring occurring after the first run. Leaching tests revealed 0.1 ppm of palladium in solution, and further to this the authors report that hot filtration tests revealed continued activity in the solution separated from the catalyst. In a later report, Clark *et al.* reported that this was clearly not the case for this catalyst in the Suzuki-Miyaura reaction, whereby no leaching was observed and hot filtration tests revealed no activity in the solid free reaction.

In 2007 Polshettiwar *et al.* reported on the synthesis and characterisation of nanostructured silica with trialkyl-(4-pyridyl)-ammonium binding sites, **I-Pd**, and studied its activity in the Mizoroki-Heck reaction.<sup>48</sup> The design of the catalyst focuses on the metal-ligand interactions of the palladium and the ammonium and pyridine binding sites and an ionic interaction between ionic species covalently grafted to the silica support and ionic palladium species. Catalyst **I-Pd** was prepared by method of nanocasting and the schematic of the preparation is shown below.



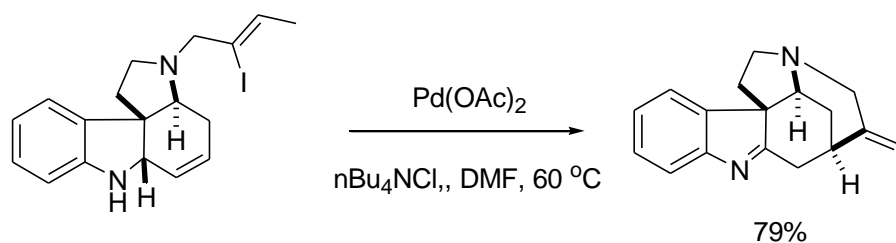
**Scheme 3.17** Preparation of Imidazolone based Pd catalyst **I-Pd** (Polshettiwar *et al.*).<sup>48</sup>

Electron microscopy revealed catalyst **I-Pd** to have nanostructured morphology with a high degree of regularity. The cross coupling reaction of methyl acrylate and various aryl halides catalysed by **I-Pd** were studied. Polshettiwar *et al.* found that using triethylamine as a base and acetonitrile as a solvent were the most efficient conditions when using this catalyst. At high temperatures, taking 10 mol % **I-Pd** gave excellent yields in the Mizoroki-Heck cross coupling of aryl bromides and iodides with methyl acrylate and styrene (iodobenzene and methyl acrylate, 90% conversion(24 hours); bromobenzene and styrene, 70% conversion (24 hours)). More complex substrates such as 2-iodothiophene were also successfully coupled to methyl acrylate (93 % conversion) and styrene (84 % conversion). Unfortunately the cross coupling of aryl chlorides with methyl acrylate was not achieved.

Leaching tests revealed a significant amount of Pd to have leached into solution, 0.9 ppm; the authors report this amount of leached Pd overall contributes to 0.08% of the initially added Pd. Interestingly, re-use of the catalyst showed it to be very active after 5 runs (run 1, 90% conversion; run 5, 89% conversion). Polshettiwar *et al.* report that the high activity displayed

by catalyst **I-Pd** is owed to the nanostructured morphology of the material which provides a strong interaction between the substrates and the solid catalyst.

Mizoroki-Heck reactions have contributed enormously to the field of total synthesis by way of fragment couplings, ring closure reactions and polyene construction.<sup>49</sup> In 1993, Rawal *et al.* reported on the total synthesis of alkaloid dehydrotubifoline which employed the Mizoroki-Heck reaction.<sup>50</sup> In the final step of the synthesis, the Mizoroki-Heck reaction was employed to cast the final ring of the polycyclic structure to give the target molecule in 79% yield.



**Scheme 3.18** Intramolecular Mizoroki-Heck reaction in the total synthesis of (±)-dehydrotubifoline (Rawal *et al.*)<sup>50</sup>

To date, the formation of this alkaloid still stands out with the key step in its formation being final Mizoroki-Heck coupling. Total synthesis has benefitted enormously from the Mizoroki-Heck reaction, being applied to intramolecular and intermolecular compounds. Here is just one example of the Mizoroki-Heck reaction applied in total synthesis but there are many others. In a recent review by Nicolaou *et al.*, many examples including Danishefsky *et al.* report on the synthesis of Taxol were reported.<sup>51</sup> Nicolaou *et al.* reported that such Pd catalysed cross coupling reactions such as the Mizoroki-Heck reaction will soon imitate the ability to construct very complex molecules just as the Grignard, Diels Alder and Wittig reactions have.<sup>37</sup>

### Summary

There is a real challenge set for researchers to address key issues affecting silica supported palladium catalysts utilised in the Mizoroki Heck reaction. A review of the literature shows that, leaching of the expensive palladium metal remains to be a problem with some heterogeneous systems. In addition the coupling of more difficult aryl chlorides in high yields

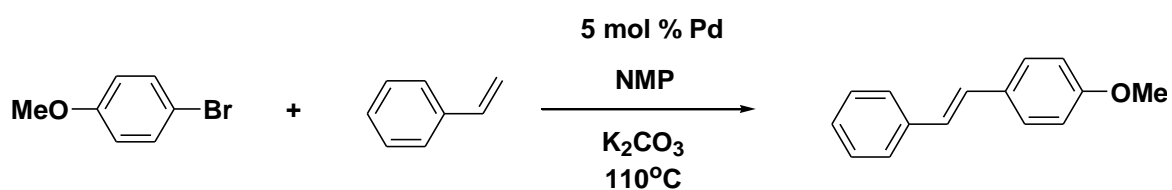
are also yet to be met as well as using a low catalytic amount of palladium in these reactions. Unfortunately, most heterogeneous catalysts found in the literature that successfully couple difficult substrates in the Mizoroki-Heck reaction are marred by lengthy synthetic procedures or lengthy reaction times, for example the cross coupling of chloroarenes requires 24 hours as reported by Wang *et al.* by Pd loaded silica supported amine catalysts. In cases where the reaction times are short, leaching of expensive metal is a real problem, as found with Pd loaded silica supported triazine thio fluoro tagged catalysts as reported by Niembro and Alibes and in a separate contribution by Polshettiwar *et al.* There are still many obstacles to be overcome for silica supported Pd catalysts before they can mirror the activity of its homogeneous counterparts. The need for supported ligands with high palladium affinity is required to ensure that palladium is retained by the solid support at the end of a reaction. New catalysts need to be highly active and successfully couple the more difficult aryl bromide and chloride substrates. In addition, the required amounts of palladium to carry out the reaction needs to be low as well as reaction times need to be shorter.

### 3.4.2 Results and discussion

A real challenge remains in developing a new Heck reaction heterogeneous catalyst with higher activity towards deactivated aryl bromides and eventually toward the more readily available aryl chlorides. With the success in using catalysts **silica-60-C<sub>2</sub>-Pd(OAc)<sub>2</sub>** and **silica-60-C<sub>3</sub>-Pd(OAc)<sub>2</sub>** in Suzuki-Miyaura reactions, attention was given to using these catalysts in the more difficult cross coupling reactions of Mizoroki-Heck. Given the desirability of employing reaction conditions which are less energy demanding or more 'green', these Mizoroki-Heck reactions were first carried out at room temperature. By using isopropanol as a solvent there is an obvious pathway to the reduction of immobilized Pd(II) to Pd(0) which is a key step in the Heck reaction. No conversion was observed however, and so the reaction temperature was raised to 80 °C. Herein it was assumed that the rise in temperature and the reducing conditions of isopropanol would facilitate the coupling of an aryl halide with styrene, however the catalysts were found to be inert in this instance too. Attention was then turned to carrying out these reactions in conditions as found in literature reports.

Subsequent studies were carried out using 4-bromobenzene, styrene, potassium carbonate and N-methylpyrrolidinone at 110 °C. The quantity of catalyst material used corresponded to 5

mol%. In these reactions, both catalysts were found to be rather inert. The slightly more active performance of the **silica-60-C<sub>3</sub>-Pd(OAc)<sub>2</sub>** however led us to explore different palladium precursors. PdCl<sub>2</sub> has been reported as an excellent precatalyst in the Mizoroki-Heck reaction. Catalyst **silica-60-C<sub>3</sub>-Pd(dba)** was also prepared for comparison to catalyst **silica-60-C<sub>3</sub>-PdCl<sub>2</sub>**. The best result was for the catalyst **silica-60-C<sub>3</sub>-PdCl<sub>2</sub>** (**Table 3.7**) for bromoanisole with styrene with 79% conversion in 24 hours. In these reaction conditions, there does not seem to be an obvious pathway to reduce Pd(II) to Pd(0). In this case, it could be proposed that the catalytic cycle proceeds via Pd(II)/(IV) pathway. The slower kinetics of Pd(dba) could be due to the presence of the dibenzylideneacetone ligands around the Pd atom whereby the oxidative addition of the aryl halide may be more difficult in the presence of these bulky groups forming a six co-ordinate palladium intermediate.

**Table 3.7** The Mizoroki-Heck reaction of Bromoanisole and Styrene

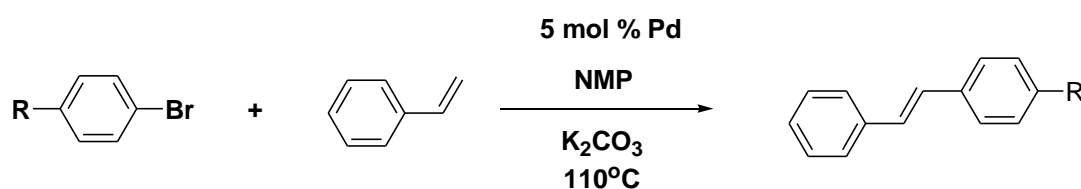
Entry	Catalyst	Time (hours)	% conversion
1		36	8
2		24	5
3		24	35
4		24	79

**Conditions:** Taken 1.0 mmol 4-bromoanisole, 1.5 mmol styrene, 2.0 mmol K<sub>2</sub>CO<sub>3</sub>, 5 mol % catalyst (100 mg silica-60-C<sub>3</sub>-PdCl<sub>2</sub>/silica-60-C<sub>3</sub>-Pd(dba)<sub>3</sub>; 120 mg silica-60-C<sub>2</sub>-Pd(OAc)<sub>2</sub>; 100 mg silica-60-C<sub>3</sub>-PdCl<sub>2</sub> catalyst and NMP (5 mL). % conversion determined by <sup>1</sup>H NMR.

3.4.2.1 Mizoroki-Heck reaction with silica-60-C<sub>3</sub>-PdCl<sub>2</sub>

This scoping work led to further exploration of the **silica-60-C<sub>3</sub>-PdCl<sub>2</sub>** catalyst with different aryl bromides and styrene. The coupling of non activated aryl bromides such as bromochlorobenzene with styrene proceeded more slowly (**Table 3.8, Entry 3**) than activated aryl bromides such as bromotoluene (**Entry 4**). Most interestingly, recycles showed no drop in activity in cycles 2 and 3 of any of the substrates employed. This would suggest that in these reactions there is no substrate diffusion limitation, or perhaps the use of a polar solvent like NMP could help facilitate movement of substrates and coupled product.

**Table 3. 8 Mizoroki-Heck reactions with silica-60-C<sub>3</sub>-PdCl<sub>2</sub>**



Entry	Substrate	Time (hours)	% conversion
1		24	81, 81, 79
2		24	79, 77, 77
3		24	67, 68, 65
4		24	84, 85, 85

**Conditions:** Taken 1.0 mmol aryl halide, 1.5 mmol styrene, 2.0 mmol K<sub>2</sub>CO<sub>3</sub>, 100 mg catalyst and NMP (5 mL). % conversion calculated from <sup>1</sup>H NMR for Bromoanisole and Bromotoluene. % Conversion calculated from GC for Bromobenzene and Bromochlorobenzene.

Leaching tests were performed on **silica-60-C<sub>3</sub>-PdCl<sub>2</sub>** in these reactions. After a reaction time of 10 hours, the conversion was 45% for the coupling of bromotoluene and styrene, the solid catalyst was separated from the liquid reaction media by filtration. After transfer of the filtrate to a new reaction flask with a new stirrer bar and fresh base, the reaction was allowed to continue for a further 10 hours. Analysis of the reaction mixture showed no further conversion of the aryl bromide to the coupled product. Additionally, analysis of the reaction media by ICP-OES showed no palladium thus suggesting that the active catalyst is likely to be heterogeneous.

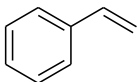
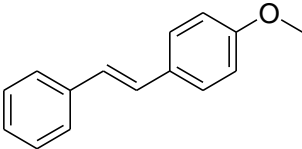
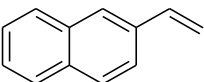
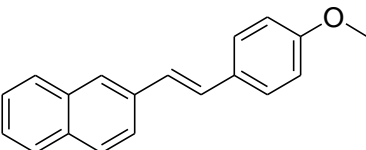
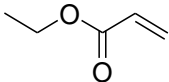
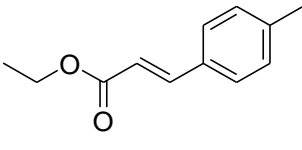
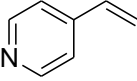
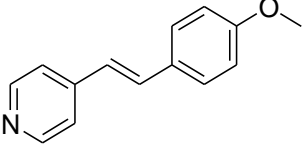
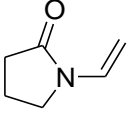
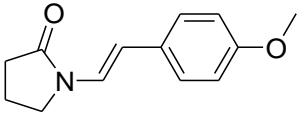
The cross coupling reaction of the more difficult and highly desired aryl chlorides was also attempted with this catalyst. Chloroanisole and styrene were reacted in NMP and unfortunately no activity was observed when catalyst **silica-60-C<sub>3</sub>-PdCl<sub>2</sub>** was employed.

### 3.4.2.2 Microwave assisted Mizoroki-Heck reactions with silica-60-C<sub>3</sub>-PdCl<sub>2</sub>

Microwave –assisted Mizoroki-Heck reactions were also carried out using catalysts **silica-60-C<sub>3</sub>-PdCl<sub>2</sub>**. The Mizoroki-Heck reaction of styrene and 4-bromoanisole was used as a test reaction employing NMP and potassium carbonate as solvent and base and 1.5mmol of aryl halide and alkene respectively. Initially, 1.5 mol % Pd was employed and reactions were carried out at 200 °C for 7 minutes. This gave 20% conversion. The catalyst loading was then increased to 3 mol % which corresponded to 70 mg. A reaction time of 10 minutes in the microwave at 220 °C gave 56% conversion. Finally a reaction time of 20 minutes, at 200 °C with **silica-60-C<sub>3</sub>-PdCl<sub>2</sub>** (3 mol % Pd) gave almost quantitative conversion to the coupled product. The Mizoroki-Heck cross coupling of more difficult substrates was tested under these conditions. Excellent conversions were achieved with this catalyst with a variety of substituted alkenes and aryl bromides.



**Table 3.9 Microwave assisted Mizoroki-Heck reactions with 3 mol % silica-60-C<sub>3</sub>-PdCl<sub>2</sub>**

Entry	Vinyl	Coupled Product	% conversion
1			76
2			98
3			99
4			76
5			75

**Conditions:** Taken 1.5 mmol alkene, 1.0 mmol aryl halide, 2.0 mmol K<sub>2</sub>CO<sub>3</sub>, 70 mg catalyst and 4mL NMP. Microwave, 20 minutes at 200 °C. % conversion determined by <sup>1</sup>H NMR and GC-MS.

Microwave-assisted Mizoroki-Heck coupling of 4-chloroanisole with styrene was also screened, and unfortunately this failed to couple using **silica-60-C<sub>3</sub>-PdCl<sub>2</sub>** as a catalyst, even when the reaction time was increased to 30 minutes, the coupled product failed to form.

### 3.5 Conclusions

In these carbon-carbon cross coupling reactions it is found that these catalysts, **silica-60-C<sub>2</sub>-Pd(OAc)<sub>2</sub>**, **silica-60-C<sub>3</sub>-Pd(OAc)<sub>2</sub>** and **silica-60-G<sub>1</sub>-Pd(OAc)** displayed very good activity as well as resistance to leaching in the Suzuki-Miyaura reaction in both high temperature and milder room temperature conditions. In the more difficult Mizoroki-Heck reactions good conversions were obtained in the cross coupling of various aryl bromides and styrene when catalyst **silica-60-C<sub>3</sub>-PdCl<sub>2</sub>** was employed. In microwave assisted reactions these catalysts can be used in relatively low mol % and have the ability to couple more difficult aryl bromides. Recycling of the catalysts was also found to be promising as the activity was largely retained by the systems. Unfortunately the catalysts were found to be inactive in the cross coupling of aryl chlorides. A number of positive points can be mentioned. Firstly, in comparison to those catalysts described in the literature for Suzuki-Miyaura reactions, the preparation of these heterogeneous systems, **silica-60-G<sub>1</sub>-Pd(OAc)** and **silica-60-C<sub>2</sub>-Pd(OAc)<sub>2</sub>**, **silica-60-C<sub>3</sub>-Pd(OAc)<sub>2</sub>** and **silica-60-C<sub>3</sub>-PdCl<sub>2</sub>** is rather simple and convenient from commercially available starting materials. Secondly, the reaction conditions employed to achieve quantitative conversions were relatively mild, with reactions carried out without the need of an inert atmosphere. Temperatures did not exceed 110 °C and in the Suzuki-Miyaura reactions, these reactions even proceeded at room temperature. Thirdly, the solid catalysts were separated from the reaction mixture easily by filtration and reused successfully without loss in activity suggesting all the metal was retained by the support at the end of a reaction.

Lastly, and perhaps most importantly, hot filtration tests reveal no palladium to be detected to the ppb level in the filtrate solutions of these reactions further confirming the palladium metal to be retained by the support. In addition, these catalysts were resistant to the formation of inactive palladium metal particles, i.e. palladium black, which further demonstrates the stability of these catalytic systems in Suzuki-Miyaura and Mizoroki-Heck reactions.

Initial mechanistic studies support a catalytic pathway for the Suzuki-Miyaura reaction at room temperature with isopropanol that proceeds via a Pd(0)/(II) pathway. TEM images

reveal the formation palladium clustering at room temperature whereas reactions carried out at high temperature reveal the homogeneous distribution of palladium. XPS studies reveal some Pd(0) to be present on catalysts **silica-60-C<sub>2</sub>-Pd(OAc)<sub>2</sub>**, **silica-60-C<sub>3</sub>-Pd(OAc)<sub>2</sub>** and **silica-60-G<sub>1</sub>-Pd(OAc)** before catalysis; this increases after catalysis, although the major component in these systems remains to be Pd(II). A large increase of Pd(0) is found in reactions carried out at high temperature, from 5 to 35% and this would suggest that this reaction also proceeds via a Pd(0)/(II) catalytic pathway. In this case, as regularly reported in the literature the precatalyst Pd(II) species is likely reduced to the active Pd(0) by the base. Further work needs to be carried out in order to shed more light on the mechanistic nature of the Mizoroki-Heck reaction as catalysed by **silica-60-C<sub>3</sub>-PdCl<sub>2</sub>**.

### 3.6 References

- <sup>1</sup> K. C. Nicolau, P. G. Bulger and D. Sarlah, *Angew. Chem. Int. Ed.*, 2005, **44**, 4442-4409;
- <sup>2</sup> R. F. Heck and J. P. Nolly, *J. Org. Chem.*, 1972, **37**, 2320;
- <sup>3</sup> N. Miyaura, K. Yamada and A. Suzuki, *Tet. Lett.*, 1979, 3437;
- <sup>4</sup> J. K. Stille, *Angew. Chem. Int. Ed.*, 1986, **25**, 208;
- <sup>5</sup> K. Sonogashira, Y. Tohda and N. Hagihara, *Tet. Lett.*, 1975, 4467;
- <sup>6</sup> C. X. Zhang, G. J. Zheng, F. Q. Bi and Y. L. Li; *Chinese Chem. Lett.*, 2008, **19** (7), 759;
- <sup>7</sup> A. S. Kumar, S. Ghosh and G. N. Mehta; *Arch. Appl. Sci. Res.*, 2010; **2** (5), 135-141;
- <sup>8</sup> A. M. Rouhi, *Chem. & Eng. News*, 2004, **82** (36), 49-58;
- <sup>9</sup> I. P. Beletskaya and A. P. Cheprakov, *Chem. Rev.*, 2000, **100**, 3009 and references therein;
- <sup>10</sup> S. J. Danishefsky, J. J. Masters, W. B. Young, J. T. Link, L. B. Snyder, T. V. Magee, D. K. Jung, R. C. A. Isaacs, W. G. Bornmann, C. A. Alaimo, C. A. Coburn, and M. J. Di Grandi; *J. Am. Chem. Soc.*, 1996, **118**, 2843;
- <sup>11</sup> S. C. Stinson, *Chem. Eng. News*, 1999, **77** (10), 63;
- <sup>12</sup> T. Mizoroki, K. Mori and A. Ozaki, *Bull Chem. Soc. Jpn.*, 1971, **44**, 581; R. F. Heck, J. P. Nolley Jr, *J. Org. Chem.*, 1972, **37**, 2320-2322;
- <sup>13</sup> C. Amatore and A. Jutland, *J. Organomet. Chem.* 1999, **576**, 254;
- <sup>14</sup> T. Hara "Innovation in the Pharmaceutical Industry: The process of drug discovery and development", Edward Elgar Publishing Ltd., Cornwall, 2003;
- <sup>15</sup> K-I. Shimizu, S. Koizumi, T. Hatamachi, H. Yoshida, S. Komai, T. Kodama and Y. Kitayama, *J. Catal.*, 2004, **228**, 141;
- <sup>16</sup> C. Beleizao, A. Corma, H. Garcia, A. Leyva, *J. Org. Chem.*, 2004, **69**, 439-446;
- <sup>17</sup> B. Nohair, S. MacQuarrie, C. M. Crudden and S. Kaliaguine; *J. Phys. Chem. C.*, 2008, **112**, 6065-6072;
- <sup>18</sup> C. O. Gobin, Q. Huang, H. G. Vinh-Thang, F. Kleitz, M. Eic and S. Kaliaguine; *J. Phys. Chem. C* **2007**, *111*, 3059;
- <sup>19</sup> R. Bedford, C. S. J. Cazin, M. B. Hursthouse, M. E. Light, K. J. Pike and S. Wimperis, *J. Organomet. Chem.*, 2001, **633**, 173;
- <sup>20</sup> R.B. Bedford, U.G. Singh, R. I. Walton, R. T. Williams and S.A. Davis, *Chem. Mater.*, 2005, **17**, 701;
- <sup>21</sup> S. Paul and J.H. Clark, *Green Chem.* 2003, **5**, 635;
- <sup>22</sup> M. L. J. Reiner, J. B. Westmore and M. Das, *J. Chem. Soc.*, 1994, **72**, 1302;

- <sup>23</sup> F. R. Hartley, "The chemistry of Platinum and Palladium", Applied Science Publishers Ltd, 1965, pg 13-21;
- <sup>24</sup> A. F. Schmidt and V. V. Smirnov, *J. Mol. Catal. A: Chem*, 2003, **203**, 75;
- <sup>25</sup> O. Vassilyer, J. Chen., A. P. Panarello and J. G. Khinast, *Tet. Lett.*, 2005, **46**, 6865; C Balaizao, A. Corma, G. Hermenegildo and A. Leyva, *J. Org. Chem.*, 2004, **69**, 439;
- <sup>26</sup> N. T. S. Phan, M. Van der Sluys and C. W. Jones, *Adv. Synth. Catal.*, 2006, **348**, 609
- <sup>27</sup> R. Rebek, *Tetrahedron*, **35**, 723;
- <sup>28</sup> J. P. Collman, K. M. Kosydar, M. Bressan, W. Lamanna and T. Garrett, *J. Am. Chem. Soc.*, 1984, **106**, 2569;
- <sup>29</sup> F. Y. Zhao, B. M. Bhanage, M. Shirai and M. Arai, *Chem. Eur. J.*, 2000, **6**, 843; F. Y. Zhao, K. Murakami, M. Shirai, M. Arai, *J. Catal.*, 2000, **154**, 39; F. Y. Zhao, M. Shirai and M. Arai, *J. Mol. Catal. A: Chem.*, 2000, **154**, 39;
- <sup>30</sup> K. Kohler, R. G. Heindenweich, J. G. E. Kranter and M. Pietsch, *Chem. Eur. J.*, 2002, **8**, 622;
- <sup>31</sup> C. S. Consorti, F. R. Flores, J. Dupont, *J. Am. Chem. Soc.*, 2005, **127**, 12054; G. C. Georgiades and P. A. Sermon, *J. Chem. Soc. Chem. Commun.*, 1985, 975;
- <sup>32</sup> A. Corma and H. Garcia, *Top. Catal.*, 2008, **48**, 8
- <sup>33</sup> O. Navarro, H. Kaur, P. Mahjoor and S. P. Nolan, *J. Org. Chem.*, 2004, **69**, 3173-3180;
- <sup>34</sup> J. H. Kirchhoff, M. R. Netherton, I. D. Hills, and G. C. Fu, *J. Am. Chem. Soc.*, 2002, **124** (46), 13662-13663;
- <sup>35</sup> B. H. Lipshutz, T. B. Petersen and A. R. Abela, *Org. Lett.*, 2008, **10**, 1333-1336;
- <sup>36</sup> M. Zhong Cai, J. Zhou, H. Zhao and C-S Song, *J. Chem. Research*, 2002, 76-78; k. Y. Lee, H-S. Byeon, J-K. Yang, G-W. Cheong and S. W. Han, *Bull. Korean Chem. Soc.*, 2007, **28**, 5, 880; C. Ming-Zhong, Z. Hong and H. Wen-Ying, *Chin. J. Chem.*, 2005, **23**, 443-447;
- <sup>37</sup> M. O. Nutt, K. N. Heck, P. Alvarez and M. S. Wong, *Appl. Catal. B*, 2006, **69**, 115-125
- <sup>38</sup> S. Paul and J. Clark, *J. Mol. Catal A: Chemical*, 2004, **215**, 107-111;
- <sup>39</sup> F. G. Bobes and G. Fu, *J. Am. Chem. Soc.*, 2006, **128**, 5360;
- <sup>40</sup> L. Xu, B. Li, Z. Wu, X. Lu, B. Guan, B. Wang, K. Zhao and Z. Shi, *Org. Lett.*, 2010, **12**, 4, 884;
- <sup>41</sup> B. H. Lipshutz, J. A. Sclafani and P. A. Blongren, *Tetrahedron*, 2000, **56**, 2139-2144;

- <sup>42</sup> P. Lidstrom, J. Tierney and B. Watney, *Tetrahedron.*, 2001, **57**, 9225; L. Perreux, A. Loupy, *Tetrahedron.*, 2001, **57**, 9199; J. Yan, Z. S. Zhou and M. Zhu, *Chin. Chem. Lett.*, 2006, **17**, 4, 473-476;
- <sup>43</sup> B. L. Hayes, "Microwave synthesis: Chemistry at the speed of light", CEM Publishing: Matthews, 2002;
- <sup>44</sup> H. Li, L. Wang, P. Li, *Synthesis*, 2007, **11**, 1635; L. Zhang, L. Wang, P. Li and H. Li, *Synth. Commun.*, 2008, **38**, 1498;
- <sup>45</sup> S. Niembro, A. Shafir, A. Vallribera and R. Alibes, *Org. Lett.*, 2008, **10** (15) 3215-3218;
- <sup>46</sup> B. Karimi and D. Enders, *Org. Lett.*, 2006, **8**, 1237;
- <sup>47</sup> J. H. Clark, D. J. Macquarrie and E. B. Mobufu, *Green Chem.*, 2000, **2**, 53;
- <sup>48</sup> V. Polshettiwar, V. Hesemann and J. J. E. Moreau, *Tetrahedron*, 2007, **63**, 6784;
- <sup>49</sup> K. C. Nicolaou, P. G. Bulger and D. Sarlah, *Angew. Chem. Int. Ed.*, 2005, **44**, 4442-4489;
- <sup>50</sup> V. H. Rawal, C. Michoud and R. F. Monestel, *J. Am. Chem. Soc.*, 1993, **115**, 3030-3031; V. H. Rawal and C. Michoud, *Org. Chem.*, 1993, **58**, 5583-5584;
- <sup>51</sup> S. J. Danishefsky, J. J. Masters, W. B. Young, J. T. Link, L. B. Synder, T. V. Magee, D. K. Jung, R. C. A. Isaacs, W. G. Barnmann, C. A. Alaimo, C. A. Coburn and M. J. Di Grandi, *J. Am. Chem. Soc.*, 1996, **118**, 2843-2859.

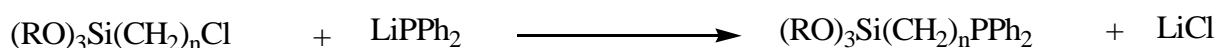
## Chapter 4

### Hydrogenation Reactions with Organosilica Supported Palladium Catalysts

#### 4.1. Background literature

In the pharmaceutical and fine chemicals industry, hydrogenations are found to be involved in over 25 % of the organic chemistry steps during multiple-stage synthesis. Heterogeneous catalytic hydrogenations are ideal as the reaction can be fine tuned for optimal activity and selectivity, as well as recovery of the catalyst at the end of the reaction. The optimization of the hydrogenation reaction requires selection of multiple parameters such as ideal catalyst, solvent, temperature, pressure and substrate to catalyst ratio.<sup>1, 2</sup> The background literature review will focus on hydrogenation of various functional groups (groups discussed will indicated in bold type in the text below) by supported metal catalysts.

Diosady *et al.* reported on the preparation of ruthenium catalysts immobilised on silica with methylene, ethylene and propylene spacer chains and the activity of these catalysts in the hydrogenation of **alkenes**.<sup>3</sup> The catalysts were prepared by first preparing alkoxy-silyl substituted phosphines from reaction of alkyloxysilyl substituted alkyl halogenides with diphenylphosphino lithium in THF (**Scheme 4.1**).

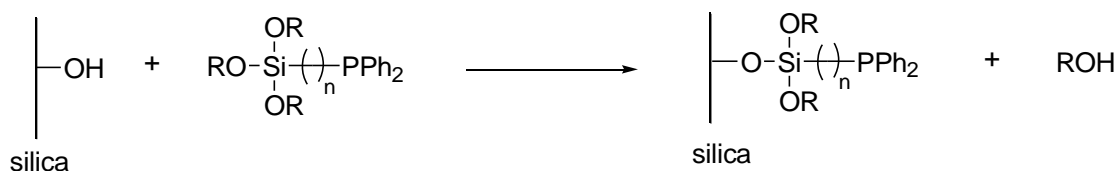


**Scheme 4.1** Synthesis of alkoxy-silyl substituted phosphines

The preparation of the modified silica ensued with reaction of silica gel with alkoxy-silyl substituted phosphines in xylene at reflux temperature under nitrogen (**Scheme 4.2**). Finally immobilisation of the ruthenium complex to the silica support was achieved by the addition of the modified silica to a stirred solution of the ruthenium complex in toluene (**Figure 4.1**). After a total reflux time of 4 hours, the solid catalysts formed was filtered and dried under vacuum for three days.

These catalysts were found to display excellent activity in the hydrogenation of alkenes. In the hydrogenation of 1-hexene carried out in hexanol at 130 °C and 5 bar H<sub>2</sub> pressure, TOFs between 0.786-0.0995 s<sup>-1</sup> were reported. The higher activity was displayed by catalysts prepared with shorter spacer chains. The authors speculate that this may be a result of

increased flexibility of the longer spacer ligands resulting in interaction of the silylethoxy groups with the Ru metal centre and so inhibiting catalytic activity. Leaching tests revealed that for these reactions, a significant amount of ruthenium was found in solution, approximately 15% and in the case of catalysts with propylene spacer chains, leaching of metal increased to 96%.



**Scheme 4.2** Synthesis of phosphine modified silica

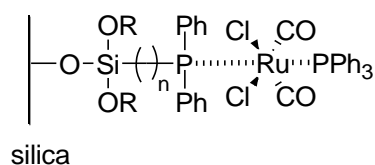
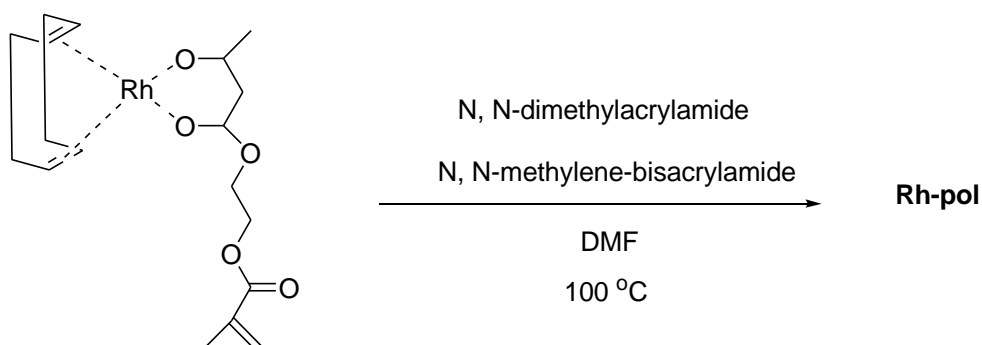


**Figure 4.1** Diosady *et al.* silica supported Ru catalyst.<sup>3</sup>

Mastrorilli *et al.* recently reported on the successful hydrogenation of a number of **alkenes** and other functionalities with a hybrid rhodium based catalyst.<sup>4</sup> The authors reported on the anchorage of a rhodium complex onto an organic polymer matrix by co-polymerizing Rh(cod)(aaema) with N,N'-methylene bisacrylamide and N,N'-dimethylacrylamide in DMF to give Rh-pol (**Scheme 4.3**).



**Scheme 4.3** Synthesis of **Rh-pol**.<sup>4</sup>

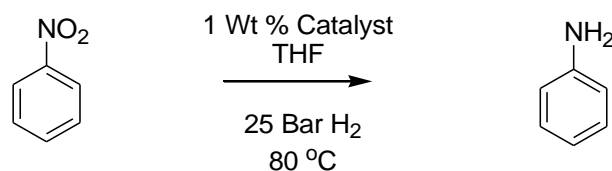
The hydrogenation of cyclohexene at room temperature and H<sub>2</sub> pressure gave complete conversion to cyclohexane in 2 hours. Recycling of Rh-pol revealed no loss in activity up to



cycle 5. Further the hydrogenation of 1-heptene under the same reaction conditions gave complete conversion in 4 hours. The authors report employing a substrate/ Rh of 160 mmol/ 1 mmol for these reactions. Leaching tests revealed that these hybrid rhodium complex organic matrixes showed no metal was detectable in solution.

Aminoaromatics are an important class of intermediates for agrochemicals, pharmaceuticals, dyestuffs and other industrially important products.<sup>5</sup> These materials are produced by the hydrogenation of corresponding **nitro** precursors. A commonly used catalyst for this reaction is Raney nickel which exists as a dark grey powder or cubic crystals, derived by leaching aluminium from an alloy of aluminium and nickel with caustic soda solution.<sup>6</sup> However, not only is this catalyst moisture sensitive but also pyrophoric and so the search for a more successful catalyst is a challenge. Palladium on carbon is also known to catalyse this reaction but aside from the expense of the catalyst, it is found to leach into the final product.<sup>7</sup> This latter problem leads to additional steps being taken to remove the palladium from the hydrogenated product, usually by use of metal scavengers.<sup>8</sup> A great number of other catalysts have also been employed in this type of hydrogenation, including heterogeneous mono- and bi-metallic palladium –or platinum complexes as well as polymer-anchored anthranilic acid complexes.<sup>9</sup> However, low turnover numbers and hydrogen-transfer media, frequent need for involvement of a suitable base (usually pyridine) in the catalytic cycle, with the requirement of reflux temperatures and high pressures (50 Bar) coupled with longer reaction times as well as diffusion limitations rule out the wider commercial applicability of these catalysts.

In 2005 Raja *et al.* reported on the successful hydrogenation of a range of **nitro-substituted aromatics** under mild conditions employing silica supported nanoparticles of cobalt (**Scheme 4.4**).<sup>10</sup> This catalyst was found to be inexpensive to synthesize, recyclable, highly selective and reactive. For comparative studies a bimetallic Ni/Pd analogue of this colloidal catalyst was prepared. Raja *et al.* used a mesoporous silica support which was found to be more thermally stable than the highly ordered (micelle-templated) mesoporous silica typically used in the MCM and SBA families. The support was synthesized by controlled hydrolysis and does not require the use of expensive structure directing-agents for growth and or template removal before use. Employing 1 weight % of this catalyst and at hydrogen pressures of 25 bar, 82% conversion was achieved after a reaction time of 4 hours.

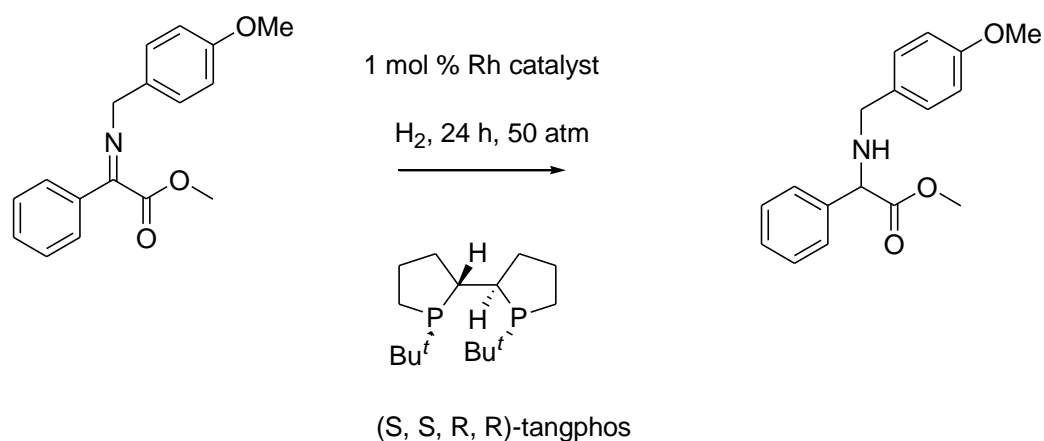


**Scheme 4.4** Hydrogenation of nitrobenzene by silica supported Co nanoparticles

This catalyst was also employed successfully in the hydrogenation of 3-nitro-*o*-cresols and was found to give repetitively high TOF ( $\sim 9670\text{ h}^{-1}$ ). These results were found to be comparable to the immobilized Ni/Pd nanoparticles (TOF  $\sim 9690\text{ h}^{-1}$ ). In addition, hot filtration studies and ICP measurements eliminate the possibility of leaching. TEM studies of the catalysts have shown these colloidal systems to have even distribution of the nanoparticles over the support.

For many years  **$\alpha$ -imino esters** have been known in synthetic organic chemistry for they are precursors to amino acids.<sup>11</sup> The importance of  $\alpha$ -imino esters stems not only from the vast appeal of the product classes but more importantly from their remarkable reactivity as highly electrophilic imines. The reduction of C=N double bond using hydrogen is, as a result of its low cost and complete atom-efficiency, a very important process in industrial organic syntheses. Although the available literature in this area is relatively small, interest is growing yearly.<sup>12, 13</sup> However, this reaction is not readily achieved and remains a challenging task.

In 2006 Zhang *et al.* reported upon the successful enantioselective hydrogenation of a series of  $\alpha$ -aryl imino esters with a homogeneous Rh-tangphos catalyst (see **Scheme 4.5**).<sup>14</sup> Para-methoxyphenyl protected  $\alpha$ -aryl imino esters were prepared as substrates as they could be synthesized in high yield and in one step. In addition, the resulting products could be deprotected under mild conditions using cerium ammonium nitrate (CAN). High *e.e.* values and yields were obtained from these systems by use of 1 mol % catalyst, pressure of 50 atm and reaction time of 24 hours.



**Scheme 4.5** Hydrogenation of protected imines using asymmetric Rh catalysts with tangphos ligands

### Summary

From the literature search it is clearly evident that silica supported metal catalysts for hydrogenation reactions are relatively rare. Although a number of functionalities can be catalysed by such systems, the catalysts reported have one drawback or another. For example, Diosady *et al.* report that the silica supported Ru catalyst prepared shows good activity, however it suffers from extensive leaching. Raja *et al.* reported excellent activity in the hydrogenation of amino aromatics and substituted amino aromatics, however the reaction conditions required, reflux temperatures and 25 bar H<sub>2</sub> pressures, is undesirable. Mastorilli *et al.* report on Ru catalysts immobilised on organic polymer supports which show excellent activity in the hydrogenation of a number of functionalities, however the pre-swelling requirement of such systems can be troublesome. And finally, the good activity displayed by Rh catalysts with tangphos ligands in the hydrogenation of  $\alpha$ -imino esters is marred by the homogeneous nature of the reaction; separation of the active metal from the product is difficult, as reported by Zhang *et al.* It is evident that new silica supported metal catalysts which display high activity and are resistant to leaching would be welcomed in this field of chemistry.

### 4.2. Results and Discussion

In Chapter 3, the catalyst **silica-60-C<sub>3</sub>-Pd(OAc)<sub>2</sub>** was described to be highly active in the Suzuki-Miyaura reaction and successfully catalysed the coupling of a number of aryl bromides and phenyl boronic acid. In this chapter, the scope of this catalyst was further explored by testing its activity in the hydrogenation of a number of functionalities, including

nitriles, alkenes and imines. In addition, the effect of pore size of this catalyst is investigated in the kinetic study of the hydrogenation of nitrobenzene.

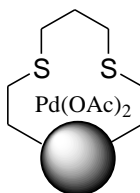
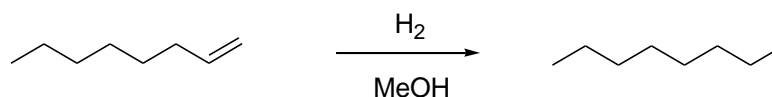


**Figure 4.2** Catalyst silica-60-C<sub>3</sub>-Pd(OAc)<sub>2</sub>

#### 4.2.1 Hydrogenations with catalyst silica-60-C<sub>3</sub>-Pd(OAc)<sub>2</sub>

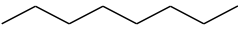
Typical hydrogenation experiments were carried out in methanol, with 10 mmol of substrate (e.g. alkene, nitro, nitrile or imine), and the required amount of **silica-60-C<sub>3</sub>-Pd(OAc)<sub>2</sub>**. This reaction mixture was placed in a pyrex conical flask and the flask placed in an autoclave bomb reactor. The reaction flask was covered with a watch glass to avoid any splashing of the mixture within the autoclave. The reaction mixture was purged with nitrogen thrice and then with hydrogen and set to the required reaction pressure. The reaction mixture was heated if necessary (to a maximum of 50 °C) by placing the autoclave in an oil bath.

The hydrogenation of 1-octene was first screened (**Scheme 4.6**). Employing 0.4 mol % Pd, which corresponded to 100 mg of **silica-60-C<sub>3</sub>-Pd(OAc)<sub>2</sub>**, hydrogenations were carried out at atmospheric pressure at temperatures from ambient to 50 °C. No conversion was achieved below 40 °C. After a reaction time of 1 hour at 50 °C, quantitative conversions were achieved to give octane equating to a TOF of 357.14 h<sup>-1</sup> (TOF 0.992 s<sup>-1</sup>) (**Table 4.1, entry 1**). This result was found to be comparable to the TOF as reported by Diosady *et al.* in the hydrogenation of 1-hexene (TOF 0.792 s<sup>-1</sup>) as catalysed by the phosphorus modified silica supported Ru catalysts. Re-use of the catalysts gave quantitative conversions up to run 6, after which activity dropped slightly to 95% in run 7. The hydrogenation of 1-octene was also carried out in the absence of catalyst under the same conditions to eliminate the possibility of any contaminant from the autoclave catalysing the reaction. Reactions without catalyst under the same reaction conditions with pressures of up to 10 bar revealed no conversion to the reduced product, even after a reaction time of 4 hours.



Scheme 4.6 Hydrogenation of 1-octene

Table 4.1 Hydrogenations with 0.4 mol % Pd, with catalyst **silica-60-C<sub>3</sub>-Pd(OAc)<sub>2</sub>**

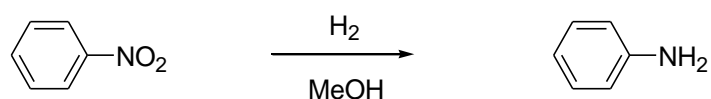
Entry <sup>a</sup>	H <sub>2</sub> Pressure	Temperature °C	Product	% conversion <sup>c</sup> (time/ hours)
1	Atm	< 40	-	0 (1)
2	Atm	50		99, 99, 99, 99, 99, 99, 99, 95 (1)
3 <sup>b</sup>	10	50	-	0 (4)

<sup>a</sup> Taken 10 mmol 1-octene, 30mL methanol and 100mg **silica-60-C<sub>3</sub>-Pd(OAc)<sub>2</sub>**. Reaction mixture heated to 50 °C. <sup>b</sup> No catalyst employed. <sup>c</sup> % conversion determined by GC.

Leaching studies were also carried out for these reactions. After a reaction time of 30 minutes, the catalyst was filtered from the hot reaction mixture immediately and then the filtrate transferred back to the autoclave and the reaction continued. A further reaction time of 1 hour revealed no increase in conversion.

Next, the hydrogenation of nitro aromatics was explored. The hydrogenation of nitrobenzene was carried out initially at room temperature and at atmospheric pressures, employing 0.4 mol % **silica-60-C<sub>3</sub>-Pd(OAc)<sub>2</sub>** which corresponded to 100mg of catalyst. Unfortunately, no hydrogenated product was formed after one hour. Subsequent increase to 5 bar hydrogen pressure also resulted in no product being formed after one hour reaction time. However with reaction temperatures of 50 °C and hydrogen pressure of 10 bar, quantitative conversions to give phenylamine were achieved. The amount of Pd used was then reduced to 0.1 mol % which corresponded to 25 mg **silica-60-C<sub>3</sub>-Pd(OAc)<sub>2</sub>**, and with reaction temperatures of 50

°C and hydrogen pressure of 10 bar, quantitative conversions to give phenylamine were achieved. Re-use of the catalyst up to run 5 gave quantitative conversion in one hour, in run 6 however, the activity dropped a little to 87%. The TOF was calculated as  $1000 \text{ h}^{-1}$  after run 6. By comparison Raja *et al.* report TOFs of  $9670 \text{ h}^{-1}$  for the Co/Pd silica catalyst system. Clearly there is a need to run this reaction for a considerably longer time to make fair performance comparisons and to see if the drop off in activity observed after 5 runs was irreversible. The silica material was slightly darker in colour post hydrogenation but no overt sign of deactivated Pd black formation was observed. Hydrogenation of nitrobenzene was also carried out without catalyst under the same reaction conditions and found to give no hydrogenated product.



**Scheme 4.7** Hydrogenation of nitrobenzene

**Table 4.2** Hydrogenations of nitrobenzene with 0.1 mol % Pd, with catalyst **silica-60-C<sub>3</sub>-Pd(OAc)<sub>2</sub>**

Entry <sup>a</sup>	H <sub>2</sub> Pressure	Product	% conversion <sup>c</sup> (time/ hours)
1	10		99, 99, 99, 99, 99, 87 (1)
2 <sup>b</sup>	10	-	0 (2)

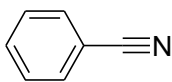
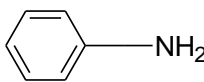
<sup>a</sup>. Taken 10 mmol nitrobenzene, 30mL methanol and 25mg **silica-60-C<sub>3</sub>-Pd(OAc)<sub>2</sub>**. Reaction mixture heated to 50 °C. <sup>b</sup>. No catalyst employed. <sup>c</sup>. % conversion determined by GC.

Leaching tests revealed no Pd to be found in solution. For comparative work, the hydrogenation of nitrobenzene catalysed by Pd/C (10 %) was also carried out. Complete conversion to the amine was achieved at H<sub>2</sub> pressures of 5 bar and at ambient temperatures. Interestingly however, ICP-OES analysis of the filtrate solution revealed a significant amount of Pd had leached; 24% in fact.

Many hydrogenations reported have been catalysed by rhodium.<sup>15</sup> Wilkinson's catalyst is a highly active homogeneous hydrogenation catalyst and was discovered in 1964 by Geoffrey Wilkinson. This hydrogenation catalyst is reported to be highly compatible with a number of functionalities, including, ketones, nitriles, esters, nitro groups and acids. Given the high activity of this metal in such reactions, catalyst **silica-60-C<sub>3</sub>-RhClPPh<sub>3</sub>** was prepared and tested in the hydrogenation of nitrobenzene. Under the reaction conditions, H<sub>2</sub> pressures of 10 bar and reaction temperature of 50 °C, employing 0.1 mol% Rh, catalyst **silica-60-C<sub>3</sub>-RhClPPh<sub>3</sub>** gave 56 % hydrogenated product.

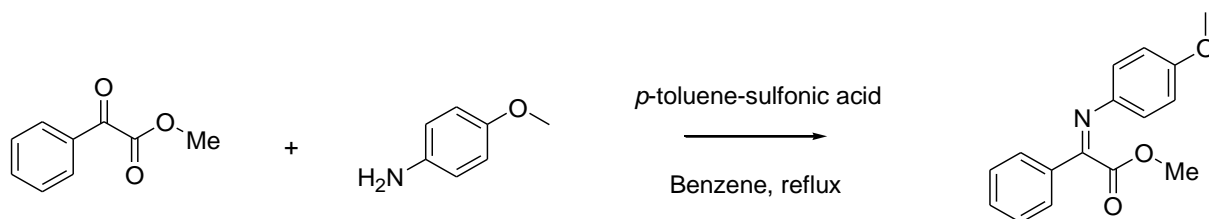
The activity of catalyst **silica-60-C<sub>3</sub>-Pd(OAc)<sub>2</sub>** was also tested in the more difficult hydrogenation of aromatic nitriles exemplified by benzonitrile. Initial conditions of 0.5 mol % catalyst **silica-60-C<sub>3</sub>-Pd(OAc)<sub>2</sub>**, ambient temperature to 50 °C and atmospheric H<sub>2</sub> pressure to 10 bar gave no conversion. Quantitative conversions were achieved with pressures of 15 bar and reaction temperatures of 50 °C to give the reduced product in a total reaction time of 6 hours (**Table 4.3**, entry 1). Re-use of the catalyst gave quantitative conversion in the same reaction up to run 3, after which activity dropped only slightly to 90 % in run 4. The TOF was calculated as 83 h<sup>-1</sup>. The hydrogenation of nitriles was clearly more difficult for the catalyst and so required longer reaction times and higher pressures and thus a low TOF was obtained.

**Table 4.3** Hydrogenations of benzonitrile with 0.5 mol % Pd, with catalyst **silica-60-C<sub>3</sub>-Pd(OAc)<sub>2</sub>**

Entry	Substrate	H <sub>2</sub> Pressure	Product	% conversion (time/ hours)
1		15		99, 98, 97, (6)

The importance of hydrogenating  $\alpha$ -imino esters has been discussed in the literature. As a result of catalyst **silica-60-C<sub>3</sub>-Pd(OAc)<sub>2</sub>** successfully catalysing aromatic nitriles, it was then assessed in the hydrogenation of  $\alpha$ -imino-esters. These prochiral substrates are not commercially available and had to be synthesised in the lab. (4-methoxy-phenylimino)-phenyl-acetic acid methyl ester was synthesized from *para*-anisidine and methyl benzoylformate using a method previously reported by Lane and Shimizu *et al.*<sup>16, 17</sup> The

reaction is driven to completion by removal of water. This is achieved by azeotropic distillation either with benzene/ toluene under Dean Stark conditions.



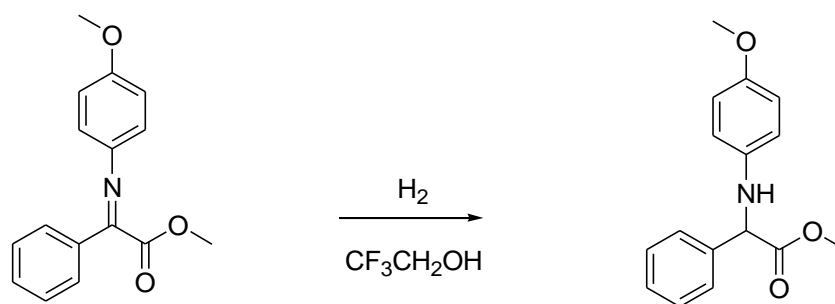
**Scheme 4.8** Synthesis of highly substituted  $\alpha$ -imino ester, (4-methoxy-phenylimino)-phenyl-acetic acid methyl ester

There are two distinct features of imine (4-methoxy-phenylimino)-phenyl-acetic acid methyl ester (a) the presence of an adjacent ester group, which acts as a protecting group making this imine more reactive and (b) the presence of the substituted phenyl groups adds steric hindrance to the imine site. Hydrogenation of this imine has been reported by de Vries *et al.* using 5 mol % Ir catalysts with secondary phosphine oxide ligands, at 25 bar  $\text{H}_2$ , to give 65% conversion (64 % *e.e.*) in a total reaction time of 24 hours.<sup>18</sup>

In this work, the hydrogenation of (4-methoxy-phenylimino)-phenyl-acetic acid methyl ester with **silica-60-C<sub>3</sub>-Pd(OAc)<sub>2</sub>** was firstly carried out at  $\text{H}_2$  pressures from atmospheric to 10 bar with reaction temperatures of ambient to 50 °C. The solvent used was trifluoroethanol as the solubility of the imine was better in this solvent. The amount of palladium used with respect to the  $\alpha$ -imino ester was 0.1 mol %; this corresponded to 20 mg **silica-60-C<sub>3</sub>-Pd(OAc)<sub>2</sub>**. Unfortunately under these reaction conditions, no conversion to the amine was formed. An increase of pressure to 20 bar gave quantitative conversion to the reduced product after 24 hours.

The hydrogenation of (4-methoxy-phenylimino)-phenyl-acetic acid methyl ester was also carried out using reducing agent  $\text{NaBH}_4$  under the same reaction conditions. In a total reaction time of 24 hours, quantitative conversion of the imine to the amine was achieved; however this was also coupled with reduction of the ester group to the alcohol. Further, hydrogenation of (4-methoxy-phenylimino)-phenyl-acetic acid methyl ester with 0.1 mol %  $\text{Pd}(\text{OAc})_2$  also gave quantitative conversion, however this was more chemoselective than  $\text{NaBH}_4$ , as only reduction of the imine functionality was observed.



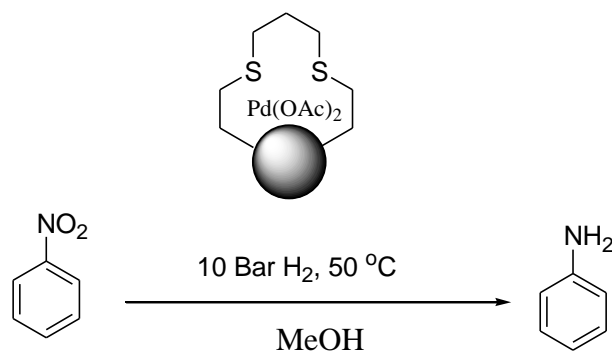
**Scheme 4.9** Hydrogenation of (4-methoxy-phenylimino)-phenyl-acetic acid methyl ester**Table 4.4** Hydrogenation of (4-methoxy-phenylimino)-phenyl-acetic acid methyl ester

Entry	Catalyst/ reducing agent	H <sub>2</sub> Pressure	Product	% conversion (time/ hours)
1		20		99 (24)
2	NaBH <sub>4</sub>	-		99 (24)
3	Pd(OAc) <sub>2</sub>	20		99 (24)

**Conditions:** Taken 10.0 mmol  $\alpha$ -imino ester, 10 mL trifluoroethanol, 0.1 mol % Pd (20 mg silica-60-C<sub>3</sub>-Pd(OAc)<sub>2</sub>/ 22mg Pd(OAc)<sub>2</sub>) or 10.0 mmol (stoichiometric quantity) NaBH<sub>4</sub> and the reaction heated to 50 °C with H<sub>2</sub> pressures of 20 bar.

## 4.2.2 Pore size effects on the hydrogenation of nitrobenzene

So far, all the catalytic work described has been achieved with heterogeneous palladium materials prepared from silica-60. Herein, the effect of the silica pore size is investigated in the hydrogenation of amino aromatics. Catalysts **silica-90-C<sub>3</sub>-Pd(OAc)<sub>2</sub>** and **silica-150-C<sub>3</sub>-Pd(OAc)<sub>2</sub>** were prepared from silica-90 and silica-150 respectively. The synthesis and characterisation of these catalysts has previously been described in Chapter 2. The catalytic activity of catalysts **silica-90-C<sub>3</sub>-Pd(OAc)<sub>2</sub>** and **silica-150-C<sub>3</sub>-Pd(OAc)<sub>2</sub>** in the hydrogenation of nitrobenzene as well as catalyst **silica-60-C<sub>3</sub>-Pd(OAc)<sub>2</sub>** is shown below in **Table 4.5**. As mentioned earlier, catalyst **silica-60-C<sub>3</sub>-Pd(OAc)<sub>2</sub>** was shown to give excellent activity in the hydrogenation of nitrobenzene at pressures of 10 bar and reaction temperatures of 50 °C. At a reaction time of 1 hour, quantitative conversions were achieved. Under the same reaction conditions, catalyst **silica-90-C<sub>3</sub>-Pd(OAc)<sub>2</sub>** gave 87% conversion in 1 hour and quantitative conversion was achieved at a total reaction time of 1.5 hours. The activity of catalyst **silica-150-C<sub>3</sub>-Pd(OAc)<sub>2</sub>** was found to be a little more sluggish with 79% conversion of nitrobenzene to benzamine at a reaction time of 1 hour. Complete conversion was achieved at 2 hours.



**Scheme 4.10** Hydrogenation of nitrobenzene

**Table 4.5** Hydrogenation of nitrobenzene with catalyst **silica-C<sub>3</sub>-Pd(OAc)<sub>2</sub>** of different pore sizes

Entry <sup>a</sup>	Catalyst	mol % <sup>b</sup>	% conversion <sup>c</sup>
1	Silica-60-C <sub>3</sub> -Pd(OAc) <sub>2</sub>	0.10	99
2	Silica-90-C <sub>3</sub> -Pd(OAc) <sub>2</sub>	0.12	87
3	Silica-150-C <sub>3</sub> -Pd(OAc) <sub>2</sub>	0.12	79

<sup>a</sup> **Conditions.** Reaction time of 1 hour <sup>b</sup> mol % reference to nitrobenzene <sup>c</sup> % conversion as determined by GC.

A closer look at the kinetics of this reaction reveals an important distinction between the hydrogenation of nitrobenzene with catalyst **silica-60-C<sub>3</sub>-Pd(OAc)<sub>2</sub>** and catalysts **silica-90-C<sub>3</sub>-Pd(OAc)<sub>2</sub>** and **silica-150-C<sub>3</sub>-Pd(OAc)<sub>2</sub>** (Figure 4.3). An induction period at the start of the reaction is clearly evident for catalysts **silica-90-C<sub>3</sub>-Pd(OAc)<sub>2</sub>** and **silica-150-C<sub>3</sub>-Pd(OAc)<sub>2</sub>**. An induction period usually indicates metal leaching from a heterogeneous catalyst.<sup>19</sup> It is important to note that no leaching was observed from standard tests on the C<sub>3</sub> catalyst systems. However it cannot be ruled out that some release and recapture of metal occurs. Given that roughly 40% of the ligand sites are unoccupied effective recapture would be facilitated. It would seem that an induction period in the hydrogenation of nitrobenzene in the presence of **silica-60-C<sub>3</sub>-Pd(OAc)<sub>2</sub>** was either absent or considerably shorter under the same reaction conditions. The initial induction period could be related to the time taken for the reaction mixture to heat to the set reaction temperature, 50 °C, however, as the induction period is different for all three catalysts, this would seem unlikely to be the case. These catalysts are clearly distinguished by their different porosimetry. The observed trends could indicate lower selectivity between substrate and product in pore and solvent medium environments in the larger pore materials.

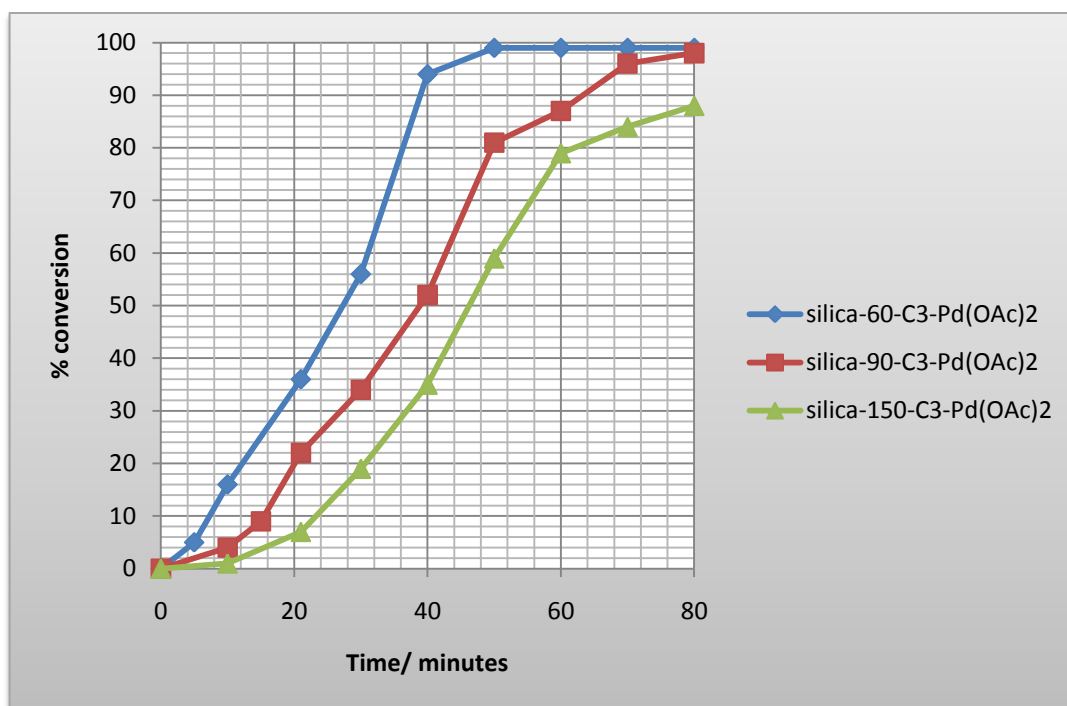


**Figure 4.3** Kinetic profile for the hydrogenation of nitrobenzene with catalysts **silica-60-C<sub>3</sub>-Pd(OAc)<sub>2</sub>**, **silica-90-C<sub>3</sub>-Pd(OAc)<sub>2</sub>** and **silica-150-C<sub>3</sub>-Pd(OAc)<sub>2</sub>**

In a reaction time of 40 minutes, catalyst **silica-60-C<sub>3</sub>-Pd(OAc)<sub>2</sub>** achieved 94% conversion, however to achieve quantitative conversion required a further reaction time of 10 minutes. This pattern was also seen for catalysts **silica-90-C<sub>3</sub>-Pd(OAc)<sub>2</sub>** and **silica-150-C<sub>3</sub>-Pd(OAc)<sub>2</sub>**, for example catalyst **silica-90-C<sub>3</sub>-Pd(OAc)<sub>2</sub>** achieved 96% conversion in 70 minutes and to achieve quantitative conversion required a total reaction time of 80 minutes. The longer reaction time needed to achieve quantitative conversion could be a result of pore blockage from products formed, making access to active sites more difficult.

As mentioned above the kinetic studies can be related to the pore size studies carried out with these systems. The calculated surface areas, average pore sizes and average pore diameters are shown in the table below. Catalyst **silica-60-C<sub>3</sub>-Pd(OAc)<sub>2</sub>** is shown to have the largest surface area of 320 m<sup>2</sup>/g, this evidently drops as the pore size of the silica is increased, with **silica-150-C<sub>3</sub>-Pd(OAc)<sub>2</sub>** having a surface area 238 m<sup>2</sup>/g. As expected the average pore volume is shown to increase with increasing silica pore size, the catalyst **silica-60-C<sub>3</sub>-Pd(OAc)<sub>2</sub>** has average pore volume of 0.39 cc/g and **silica-150-C<sub>3</sub>-Pd(OAc)<sub>2</sub>** has an average pore volume of 0.71 cc/g, which is almost twice as large.

**Table 4.6** The calculated pore size measurements from the BJH method for catalysts silica-**60-C<sub>3</sub>-Pd(OAc)<sub>2</sub>**, silica-**90-C<sub>3</sub>-Pd(OAc)<sub>2</sub>** and silica-**150-C<sub>3</sub>-Pd(OAc)<sub>2</sub>**

	silica- <b>60-C<sub>3</sub>-Pd(OAc)<sub>2</sub></b>	silica- <b>90-C<sub>3</sub>-Pd(OAc)<sub>2</sub></b>	silica- <b>150-C<sub>3</sub>-Pd(OAc)<sub>2</sub></b>
Surface area m <sup>2</sup> /g	319.9	278.1	238.2
Average pore volume cc/g	0.39	0.47	0.71
Average pore diameter Å	51.3	72.4	137.0

The measured isotherms for catalysts **silica-60-C<sub>3</sub>-Pd(OAc)<sub>2</sub>**, **silica-90-C<sub>3</sub>-Pd(OAc)<sub>2</sub>** and **silica-150-C<sub>3</sub>-Pd(OAc)<sub>2</sub>** are shown in the **Figure 4.4**. As expected, the total volume of the pores increases from catalyst **silica-60-C<sub>3</sub>-Pd(OAc)<sub>2</sub>** which has the smallest pore volume to catalyst **silica-150-C<sub>3</sub>-Pd(OAc)<sub>2</sub>** with the largest. The shape of the hysteresis loops are the same for catalysts **silica-60-C<sub>3</sub>-Pd(OAc)<sub>2</sub>** and **silica-90-C<sub>3</sub>-Pd(OAc)<sub>2</sub>**, however catalyst **silica-150-C<sub>3</sub>-Pd(OAc)<sub>2</sub>** showed a different hysteresis loop shape. This difference in hysteresis shapes can be further correlated with the pore size distributions where it is evident that there is larger range of pore sizes within catalyst **silica-150-C<sub>3</sub>-Pd(OAc)<sub>2</sub>** and these contribute to the hysteresis shape seen which covers a wide relative pressure region. The shape of isotherms reveal that the mesoporous nature of the catalysts are retained after modification with Pd(OAc)<sub>2</sub>. The adsorption desorption branches of the isotherms are aligned increasingly more parallel from the 60 to 150 Å material indicative of a change from ink bottle shape to more cylindrical shaped pores.

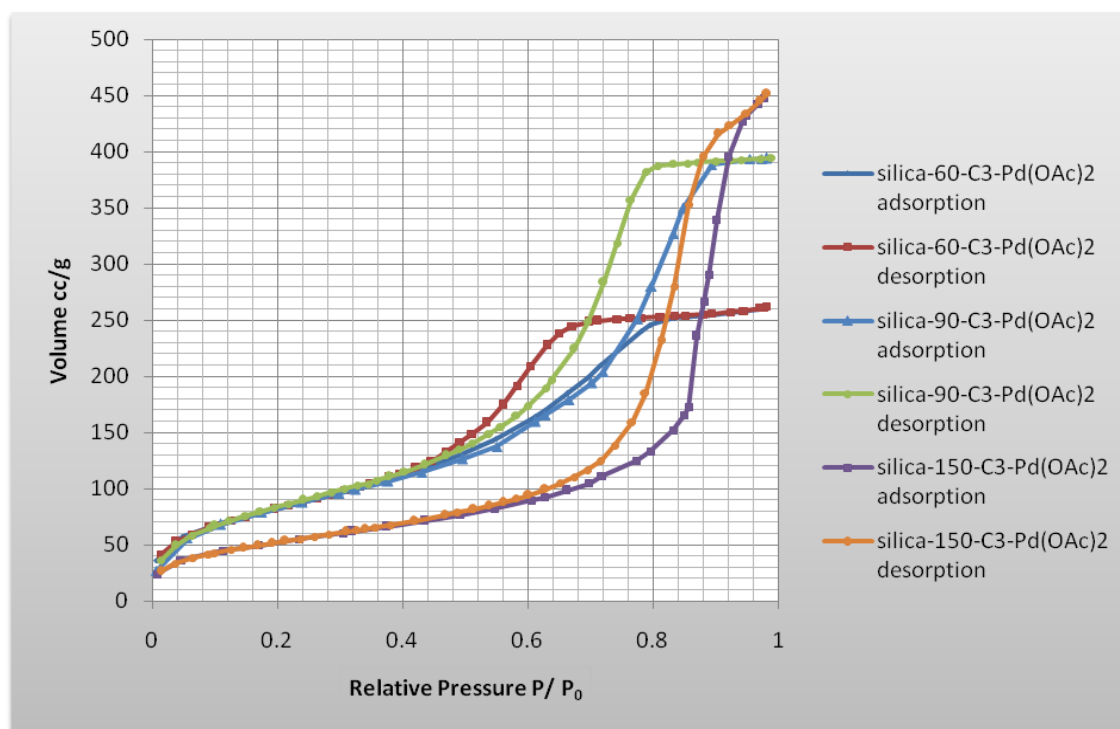


**Figure 4.4** Sorption isotherm graph for **silica-60-C<sub>3</sub>-Pd(OAc)<sub>2</sub>**, **silica-90-C<sub>3</sub>-Pd(OAc)<sub>2</sub>** and **silica-150-C<sub>3</sub>-Pd(OAc)<sub>2</sub>**

The pore size distribution chart for catalysts **silica-60-C<sub>3</sub>-Pd(OAc)<sub>2</sub>**, **silica-90-C<sub>3</sub>-Pd(OAc)<sub>2</sub>** and **silica-150-C<sub>3</sub>-Pd(OAc)<sub>2</sub>** is shown in the figure below. The pore size distribution mainly falls over a much narrower range for catalyst **silica-60-C<sub>3</sub>-Pd(OAc)<sub>2</sub>** (40-60 Å) in comparison to **silica-90-C<sub>3</sub>-Pd(OAc)<sub>2</sub>** where the pore size distribution is much wider (60-100 Å). The range of pore size distribution is wider still for catalyst **silica-150-C<sub>3</sub>-Pd(OAc)<sub>2</sub>** (90-180 Å).

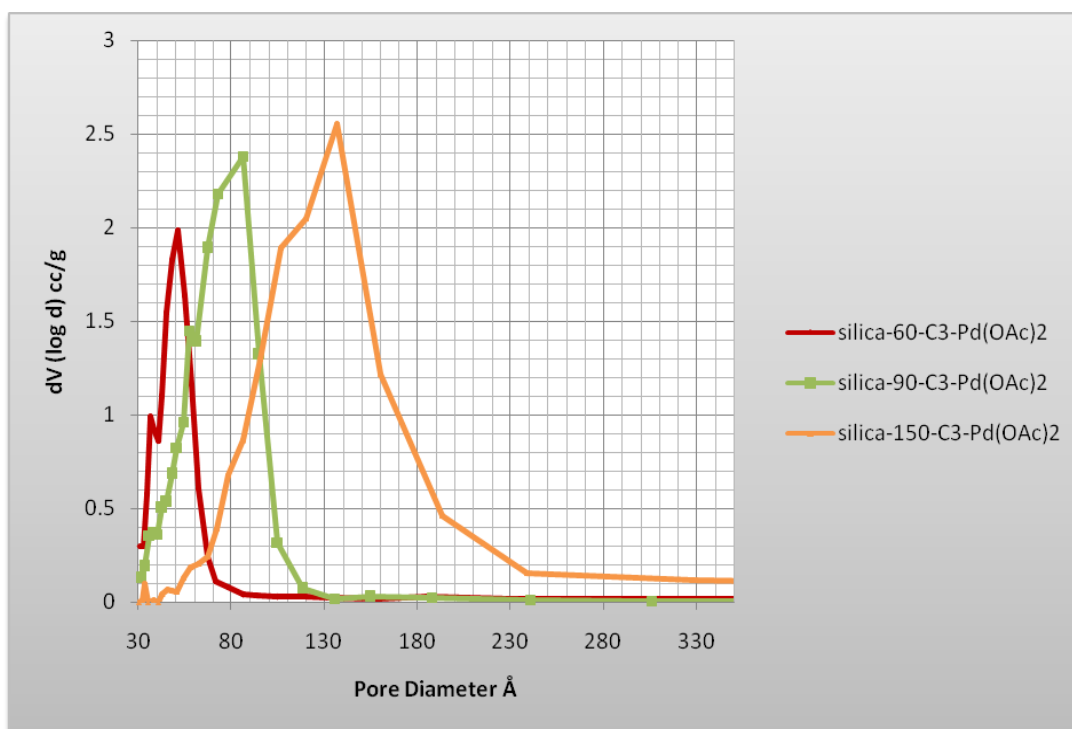


**Figure 4.5** Pore size distribution chart as calculated from desorption point by the BJH method for catalysts **silica-60-C<sub>3</sub>-Pd(OAc)<sub>2</sub>**, **silica-90-C<sub>3</sub>-Pd(OAc)<sub>2</sub>** and **silica-150-C<sub>3</sub>-Pd(OAc)<sub>2</sub>**.

The metal loading of all the catalysts are found to be roughly similar as shown in **Table 4.7**. Interestingly, while the metal loading (shown in table below) of catalyst **silica-60-C<sub>3</sub>-Pd(OAc)<sub>2</sub>** is slightly lower, this is also shown to give the highest activity of these three catalysts screened in hydrogenation of nitrobenzene. The percentage of ligand sites occupied by metal in catalyst **silica-60-C<sub>3</sub>-Pd(OAc)<sub>2</sub>** is approximately 60% (from difference between sulfur and Pd analysis). In the case of catalysts **silica-90-C<sub>3</sub>-Pd(OAc)<sub>2</sub>** and **silica-150-C<sub>3</sub>-Pd(OAc)<sub>2</sub>** it is found to be 90 and 95 % respectively.

Higher rates of conversion was initially expected from catalysts prepared with silica of larger pore size however this was not found to be the case. Certainly more palladium is captured by these systems, and a slightly higher palladium mol% is employed in the reaction but even so, catalyst **silica-60-C<sub>3</sub>-Pd(OAc)<sub>2</sub>** displays the highest activity and fastest kinetics. The higher activity as displayed by catalyst **silica-60-C<sub>3</sub>-Pd(OAc)<sub>2</sub>** may be rationalised as discussed in the text above, by this system having a narrower distribution of pore sizes and therefore mass transport of substrate and product to and from catalytic sites might be expected to be more efficient.

**Table 4.7** Pd and ligand loading for catalysts silica-**60**-C<sub>3</sub>-Pd(OAc)<sub>2</sub>, silica-**90**-C<sub>3</sub>-Pd(OAc)<sub>2</sub> and silica-**150**-C<sub>3</sub>-Pd(OAc)<sub>2</sub>

silica-C <sub>3</sub> - Pd(OAc) <sub>2</sub> pore size	-60-	-90-	-150-
Metal loading mmol/ g	0.49	0.59	0.54
Ligand loading mmol/g	0.78	0.66	0.58

### 4.2.3 Summary

The scope of catalyst **silica-60-C<sub>3</sub>-Pd(OAc)<sub>2</sub>** in hydrogenation reactions was found to be quite successful. The catalyst effectively reduced a number of functionalities, including the more difficult aromatic nitriles as well as a highly substituted imine. The hydrogenation of a range of other imines is discussed later in this chapter. Calculated TOFs have shown to be comparable to those reported in literature by other heterogeneous systems. In addition, **silica-60-C<sub>3</sub>-Pd(OAc)<sub>2</sub>** was found to be resistant to leaching under the reaction conditions employed and separation of the catalyst from the reaction media is achieved simply by filtration. Recycling of the catalyst **silica-60-C<sub>3</sub>-Pd(OAc)<sub>2</sub>** further demonstrates high activity.

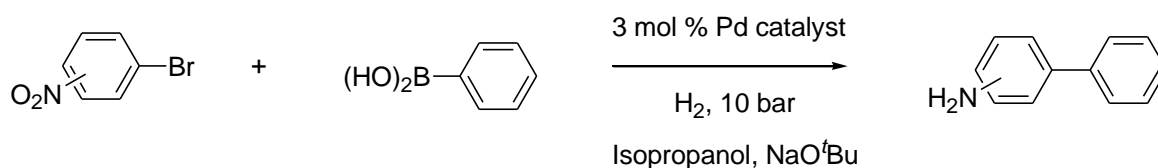
The work carried out here with catalysts **silica-C<sub>3</sub>-Pd(OAc)<sub>2</sub>** of varying pore sizes clearly demonstrate that the most efficient catalyst was the one with the narrowest pore size distribution. The more confined environments and the ink bottle shaped pores of **silica-60-C<sub>3</sub>-Pd(OAc)<sub>2</sub>** provide a more effective environment for hydrogenations to occur than the broad pore size cylindrical pores of catalysts **silica-90-C<sub>3</sub>-Pd(OAc)<sub>2</sub>** and **silica-150-C<sub>3</sub>-Pd(OAc)<sub>2</sub>**.



### 4.2.3 Room temperature Suzuki-Miyaura and hydrogenation catalysed by silica-C<sub>3</sub>-Pd(OAc)<sub>2</sub>

Tandem one pot synthesis allows for molecular diversity and complexity to be achieved in the formation of several new covalent bonds in a one pot transformation.<sup>20</sup> Such multi component reactions involving a tandem process with at least three different simple substrates has emerged as a powerful synthetic technique.<sup>21</sup> Tandem one pot synthesis readily improves the efficiency of a reaction and demonstrates the scope of the catalyst used. With the excellent activity demonstrated by **silica-60-C<sub>3</sub>-Pd(OAc)<sub>2</sub>** in both the Suzuki-Miyaura and hydrogenation reactions, this catalyst was explored for a tandem one pot Suzuki-Miyaura hydrogenation reaction. A literature search revealed no research group to have reported the use of silica supported metal catalysed tandem one pot Suzuki-Miyaura-hydrogenation reactions. However, Park *et al.* report that Pd nanoparticles encapsulated in a silica matrix have shown to give excellent activity in the hydrogenation reactions of alkenes and alkynes and in cross coupling reactions such as Suzuki-Miyaura and Mizoroki-Heck.<sup>22</sup>

A simultaneous coupling and nitro reduction, with **silica-60-C<sub>3</sub>-Pd(OAc)<sub>2</sub>** as catalyst was explored with 4-nitro-bromophenyl and phenyl boronic acid as reagents. Isopropanol was taken as a solvent and sodium *tert*-butoxide as a base for the coupling step. The amount of palladium used was 3 mol %, with respect to the aryl bromide, which corresponded to 70 mg **silica-60-C<sub>3</sub>-Pd(OAc)<sub>2</sub>**. A total reaction time of seven hours gave quantitative conversion to the coupled amine product, 4-amino-biphenyl. The reaction was carried out at room temperature with atmospheric H<sub>2</sub> pressures. In the hydrogenation of nitrobenzene, quantitative conversions were achieved with H<sub>2</sub> pressures of 10 bar. The conversion of the nitro group here occurs at atmospheric pressure, this could be because of the higher metal loading used in these reactions or perhaps the choice of solvent. It may be that the use of isopropanol may have played a role of H-transfer in reducing the nitro group to the amine. The high activity of this system was further demonstrated by the re-use of catalyst **silica-60-C<sub>3</sub>-Pd(OAc)<sub>2</sub>**; quantitative conversion was achieved under the same reaction conditions and reaction times (run 2, 99%; run 3, 97%).



**Scheme 4.11** Room temperature Suzuki-Miyaura hydrogenation reaction catalysed by **silica-60-C<sub>3</sub>-Pd(OAc)<sub>2</sub>**

**Table 4.8** Room temperature Suzuki-Miyaura Hydrogenation reactions with catalyst **silica-60-C<sub>3</sub>-Pd(OAc)<sub>2</sub>**

Entry	Aryl Halide	Product	% conversion
1			99, 99, 95
2			94
3			84

**Conditions:** Taken 1.5 mmol Phenyl boronic acid, 1.0 mmol aryl halide, 1.2 mmol NaO<sup>t</sup>Bu, 70mg catalyst and 5mL Isopropanol. % conversion determined by <sup>1</sup>H NMR and GC.

Following this, the one pot Suzuki-Miyaura hydrogenation reaction was applied to phenyl boronic acid and 2,4-nitro-bromobenzene. Under the same reaction conditions, 94% conversion to the 2,4-amino-bi-phenyl product was achieved (**Table 4.8**, entry 2). More difficult one pot coupling and hydrogenation of substituted 3-nitro-phenyl boronic acid and 2,4-dinitro-bromobenzene was also explored. Using the same conditions, 84% conversion to the coupled, amine product was achieved.

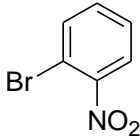
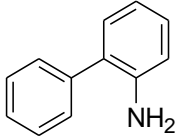
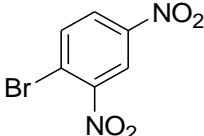
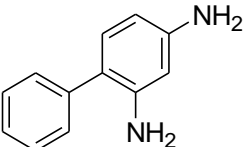
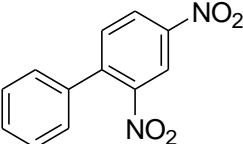
It is proposed that this coupling/hydrogenation sequence could be applied more generally to Suzuki coupling partners with functional groups like nitriles, alkenyls, imines and esters.

### 4.2.5 Microwave-assisted Suzuki-Miyaura and hydrogenation catalysed by silica-60-C<sub>3</sub>-Pd(OAc)<sub>2</sub>

The application of microwave chemistry in Suzuki reactions was introduced in Chapter 3. The tandem one pot Suzuki-Miyaura hydrogenation microwave assisted reactions were also explored under these conditions. A typical reaction consisted 1.5 mmol phenyl boronic acid, 1.0 mmol nitro substituted aryl bromide, 4 mL isopropanol and 1.5 mmol NaO<sup>t</sup>Bu. 3 mol % Pd was also taken which corresponded to 70 mg **silica-60-C<sub>3</sub>-Pd(OAc)<sub>2</sub>**.

The cross coupling and reduction of 2-nitro-bromobenzene and phenyl boronic acid proceeded smoothly, giving quantitative conversion to 2-amino-biphenyl (**Table 4.9**). The more difficult cross coupling of 2,4-dinitrobromobenzene and phenyl boronic acid resulted in 99% of the coupled product, however, only 54% of the nitro functionality was reduced to the amine. It would seem that in such reactions, the Pd catalyst first acts as a coupling catalyst and then subsequently reduces the nitro functionality of the coupled product.

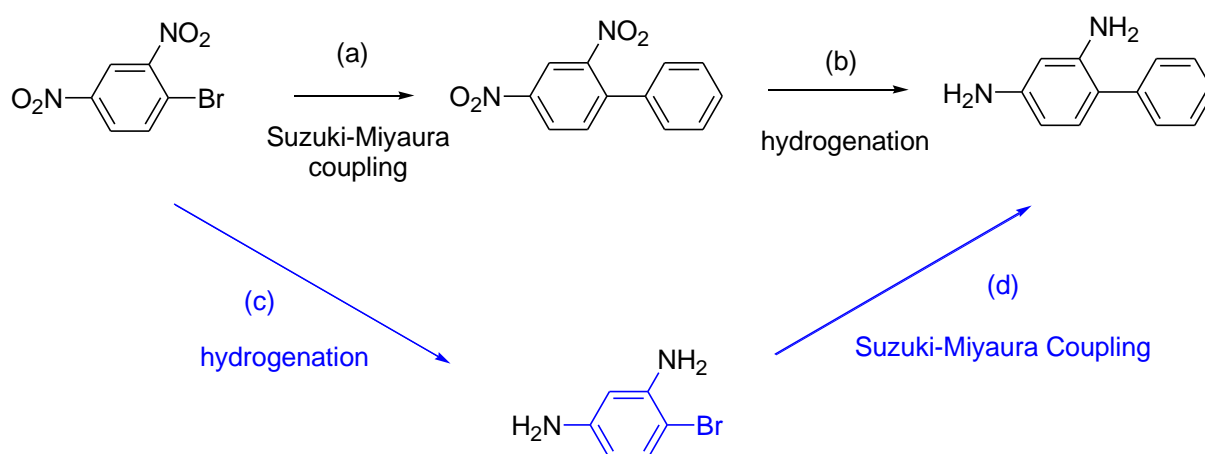
**Table 4.9** Microwave-assisted Suzuki-Miyaura and hydrogenation with catalyst silica-60-C<sub>3</sub>-Pd(OAc)<sub>2</sub>

Entry	Aryl Halide	Product(s)	% conversion
1			99
2			54
			46

**Conditions:** Taken 1.5 mmol Phenyl boronic acid, 1.0 mmol aryl halide, 1.2 mmol NaO<sup>t</sup>Bu, 70mg catalyst and 5mL Isopropanol. A balloon of hydrogen was attached to the reaction vessel. Microwave, 6 minutes at 140 °C. % conversion determined by <sup>1</sup>H NMR and GC-MS.

The question arises as to whether hydrogenation of the nitro substituted aryl bromides occurs before or after cross coupling and a closer look at the reaction intermediates would suggest that the latter is the case. On the one hand the electron withdrawing effects of the nitro substituents may make the Suzuki-Miyaura cross coupling of nitro substituted aryl bromides

more difficult, however the hydrogenation of nitro substituted bromo aryls is even more challenging. Further the hydrogenation of biaryl disubstituted nitro molecule is favoured over the hydrogenation of the di-nitro substituted aryl bromide precursor as the additional phenyl ring can assist in binding to the metal centre and provide faster kinetics as well as a more electron rich environment than in the parent bromide compound. Thus it may be rationalised that the reaction pathway follows steps (a) and (b) as shown in the scheme below.



**Scheme 4.12** Possible one-pot Suzuki- Miyaura hydrogenation pathways (a) and (b) Suzuki-Miyaura cross coupling occurs first and then hydrogenation; pathways (c) and (d) hydrogenation occurs first then cross coupling.

Further the one-pot process apparently showed no evidence of regioselectivity since all the nitro substituents were reduced. Finally the conditions used for these reactions apparently avoid homocoupling.

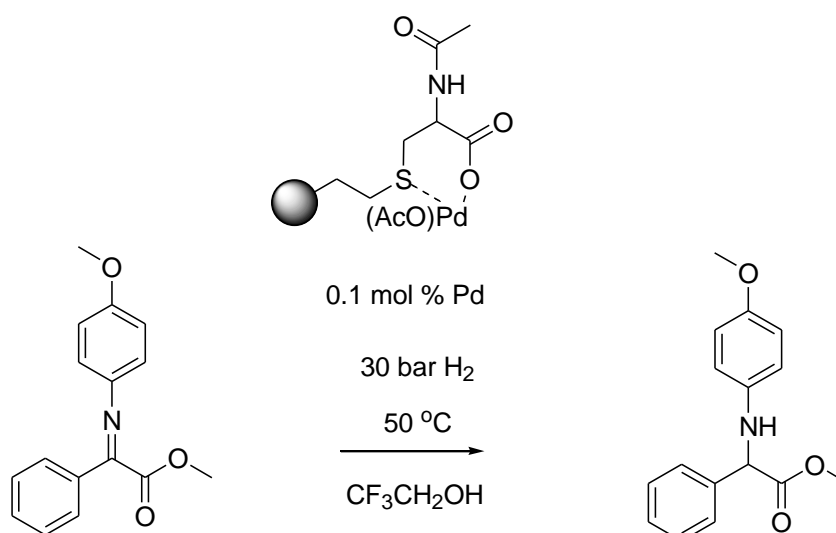
#### 4.2.6 Summary

The one pot novel Suzuki-Miyaura and hydrogenation reaction is a simple and efficient procedure for the preparation of amine substituted biaryls and is potentially very attractive. These reactions as catalysed by **silica-60-C<sub>3</sub>-Pd(OAc)<sub>2</sub>** have demonstrated to be efficient and involve a simple procedure for product separation/ isolation.

### 4.3 Asymmetric hydrogenation

#### 4.3.1 Asymmetric hydrogenation of imines with silica-60-N-derivatised-L-cysteine-Pd(OAc)

The scope of catalyst **silica-60-C<sub>3</sub>-Pd(OAc)<sub>2</sub>** was shown to be quite versatile. The catalyst reduced a number of organic functionalities under relatively mild conditions, including difficult substrates such as aromatic nitriles. Re-use of the catalyst also proved successful, with quantitative conversion being achieved up to run 6 in the hydrogenation of 1-octene. The hydrogenation of imine 4-methoxy-phenylimino)-phenyl-acetic acid methyl ester proved interesting and this then lead to design and synthesis of chiral Pd catalysts immobilized on silica and to explore enantioselective reduction of selected imines. The synthesis of catalysts **silica-60-N-acetyl-L-cysteine-Pd(OAc)** has already been described in chapter 2. This catalyst was utilised in the hydrogenation of imines under the same conditions as described before. The reactions were carried out at temperatures of 50 °C and hydrogen pressures of 20 bar were used. A total reaction time of 24 hours gave quantitative conversion. However enantioselectivity proved to be low with only 4 % *e.e.* Interestingly, reduction of the imine under the same reaction conditions with NaBH<sub>4</sub> gave quantitative conversion with reduction of the imine to the amine as well a reduction of the ester to the acid. Therefore chemoselectivity of the catalyst **silica-60-N-acetyl-L-cysteine-Pd(OAc)** was by comparison excellent, with only reduction of the imine to the amine occurring. Unfortunately the enantioselectivity of the catalyst was poor.



**Scheme 4.13** Hydrogenation of (4-methoxy-phenylimino)-phenyl-acetic acid methyl ester with **silica-60-N-acetyl-L-cysteine-Pd(OAc)**

In an attempt to improve the enantioselectivity the synthesis of catalyst **silica-60-N-4-methoxybenzyl-L-cysteine-Pd(OAc)** was undertaken. It was reasoned that greater steric bulk on the nitrogen would aid in discriminating the two faces of the prochiral substrate, hence giving greater enantioselectivity. Under the same reaction conditions as before, quantitative conversion to the amine was achieved, with the no reduction of the ester protecting group. Enantioselectivity of the catalyst proved to be marginally more successful with a low *e.e.* of 6% being achieved.

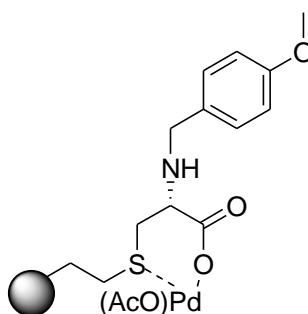
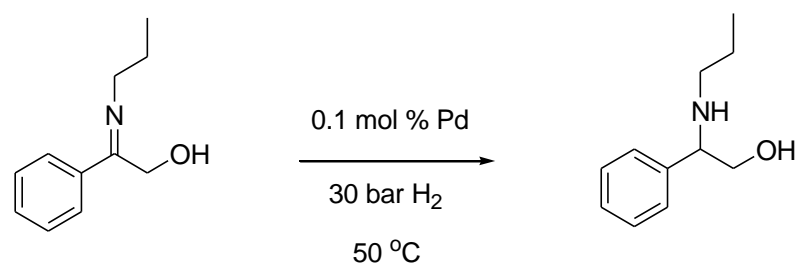


**Figure 4.6** silica-60-N-4-methoxybenzyl-L-cysteine-Pd(OAc)

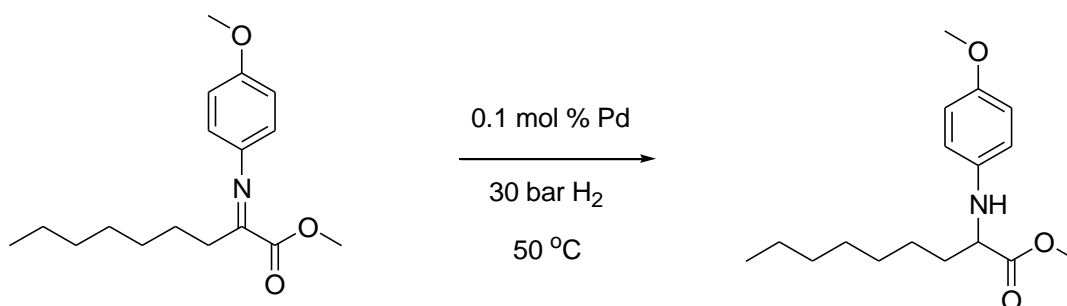
The formation of the sodium acetate before introduction of palladium is important for these catalysts as this complexation prevents leaching of the palladium during a reaction. Initial studies were carried out with catalyst **silica-60-N-acetyl-L-cysteine-Pd(OAc)** where the sodium salt had not been prepared and in these reactions the catalyst suffered from excessive metal leaching. It would seem that formation of the sodium salt provides a catalyst that is resistant to metal leaching after a reaction has stopped.

The activity and enantioselectivity of catalyst **silica-60-N-4-methoxybenzyl-L-cysteine-Pd(OAc)** was further tested in the hydrogenation of less sterically hindered imines 2-phenyl-2-propylimino ethanol and 2-(4-methoxy-phenylimino)-nonanoic acid methyl ester under the same reaction conditions. These imines were prepared by a method as reported by J. G. De Vries *et al.* As is shown in the figure below, with 0.1 mol % of catalyst **silica-60-N-4-methoxybenzyl-L-cysteine-Pd(OAc)**, quantitative reduction of the imine functionality to the amine was achieved in a reaction time of 24 hours. Unfortunately, enantioselectivity for this reaction was not so great with only 5% *e.e.* found.



**Scheme 4.14** Hydrogenation of 2-phenyl-2-propylimino ethanol with **silica-60-N-4-methoxybenzyl-L-cysteine-Pd(OAc)**

In the hydrogenation of 2-(4-methoxy-phenylimino)-nonanoic acid methyl ester under the same reaction conditions, with hydrogen pressures of 30 bar and reaction temperatures of 50 °C, a total reaction time of 24 hours gave quantitative conversion to the reduced amine. The catalyst was found to be highly chemoselective with only reduction of the imine group. Unfortunately, the enantioselectivity of catalyst was shown to be quite poor for this reaction too with 6% *e.e.*



**Scheme 4.16** Hydrogenation of 2-(4-methoxy-phenylimino)-nonanoic acid methyl ester with catalyst **silica-60-N-4-methoxybenzyl-L-cysteine-Pd(OAc)**

Thus it would appear that immobilisation has the effect of nullifying any chiral induction possibly as a consequence of confinement effects on the supported ligand minimising any preferential discrimination of substrate binding direction.

In addition, **silica-60-N-isopropyl-L-cysteine-Pd(OAc)** was also prepared wherein the nitrogen atom was derivatised with isopropyl group (**Figure 4.7**). The immobilization of the derivatised cysteine ligand onto silica was achieved in the same way as for **silica-60-N-**



**Acetyl-*L*-cysteine-Pd(OAc)** (see **Appendix 4** for experimental details). Analysis of  $^{13}\text{C}$  CP NMR revealed a large proportion of residual vinyl groups even so the material was then complexed to  $\text{Pd}(\text{OAc})_2$  to give the catalyst as shown in the scheme below.

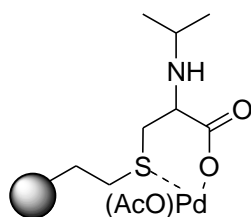


**Figure 4.7** Catalysts **silica-60-*N*-isopropyl-*L*-cysteine-Pd(OAc)**

In the hydrogenation of imine (4-methoxy-phenylimino)-phenyl-acetic acid methyl ester, this catalyst afforded complete conversion of the imine to the amine, 99%. However enantioselectivity was very poor with 0% selectivity. Interestingly leaching studies carried out for these reactions showed the Pd to be retained by the support, as no Pd was detectable by ICP-OES measurements of the filtrate solution separated from the catalyst during the imine hydrogenation.

#### 4.3.2 Pd co-ordination to *N*-derivatised cysteine ligands

In an attempt to deduce the nature of co-ordination of palladium to these silica supported *N*-derivatised-*L*-cysteine catalysts, the crystal structure of Pd complexed *S*-propyl-*L*-cysteine was explored. The preparation of *S*-propyl-*L*-cysteine followed a procedure from Tsuge *et al.*<sup>23</sup> Here, *L*-cysteine was dissolved in a solution of 2.0M sodium hydrochloride and ethanol and then reacted with *n*-bromopropane to give *S*-propyl-*L*-cysteine. The  $^1\text{H}$  NMR confirmed synthesis of this molecule. The Pd complex was then prepared by first synthesizing the sodium salt of the compound and then coupling it to  $\text{Pd}(\text{OAc})_2$ . Many attempts were made to obtain a crystal structure but this proved to be difficult.

L. P. Battaglia *et al.* report that co ordination within *S*-methyl-*L*-cysteine Pd chloride, it is shown that the amino acid acts as a bidentate ligand forming a five membered chelate ring with Pd metal coordinating to the S and N atom.<sup>24</sup> These findings have also been reported by Shehata *et al.*<sup>25</sup> Interestingly, Li and Maning and Lenz and Martell report have stated that

these ligands can play different roles in different cases as they have three different points of coordination to the metal.<sup>26</sup> In the case of silica-60-N-derivatised-L-cysteine-Pd(OAc) catalysts prepared, it would seem that coordination of the Pd metal occurs to the S and the carboxylate group. This assumption is supported by firstly the preparation of catalysts silica-60-N-derivatised-L-cysteine-Pd(OAc) without sodium salt formation resulting in severe Pd leaching occurring into solution. Catalysts prepared by sodium salt formation prior to complexation to Pd were found to be resistant to leaching. Secondly, the low enantioselective activity displayed by these systems would suggest that the substituted groups upon the N have very little influence on the coordination sphere of the Pd metal and so coordination of the Pd metal to the N is unlikely. Lastly, the formation of a six membered ring is known to be more stable than a five membered ring system.



**Figure 4.5** Possible co-ordination of Pd metal to the ligand sites of silica-60-N-derivatised-L-cysteine

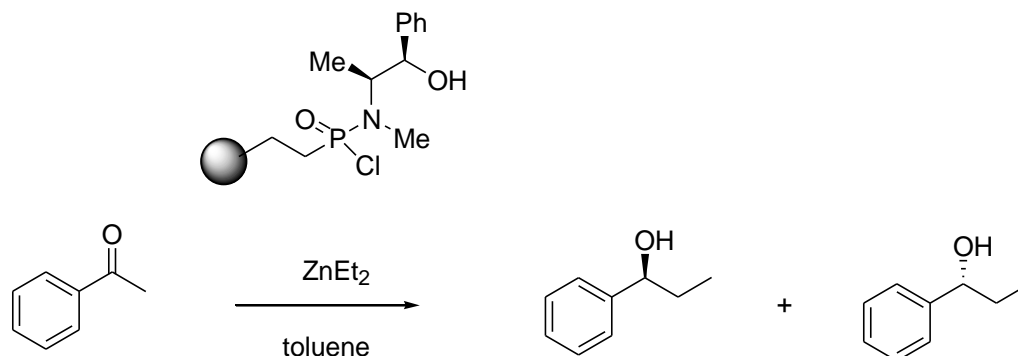
#### 4.3.4 Conclusions

Very good catalytic activity was observed for **silica-60-N-acetyl-L-cysteine-Pd(OAc)** and **silica-60-N-4-methoxybenzyl-cysteine-Pd(OAc)** in the hydrogenation of highly substituted imines and in addition the catalyst was resistant to leaching. These reactions were marred however, by the low enantioselectivity obtained. Such results demonstrate that the chiral centre has little influence on the surrounding environment of the palladium metal resulting in low enantioselectivities being obtained. Interestingly, these catalysts demonstrated excellent chemoselectivity with only reduction of the imine functionality and not the protecting ester group. Promisingly, reaction times and conditions employed were found to be comparable to those reported in literature.

#### 4.4 Enantioselective addition of Diethylzinc to benzaldehyde

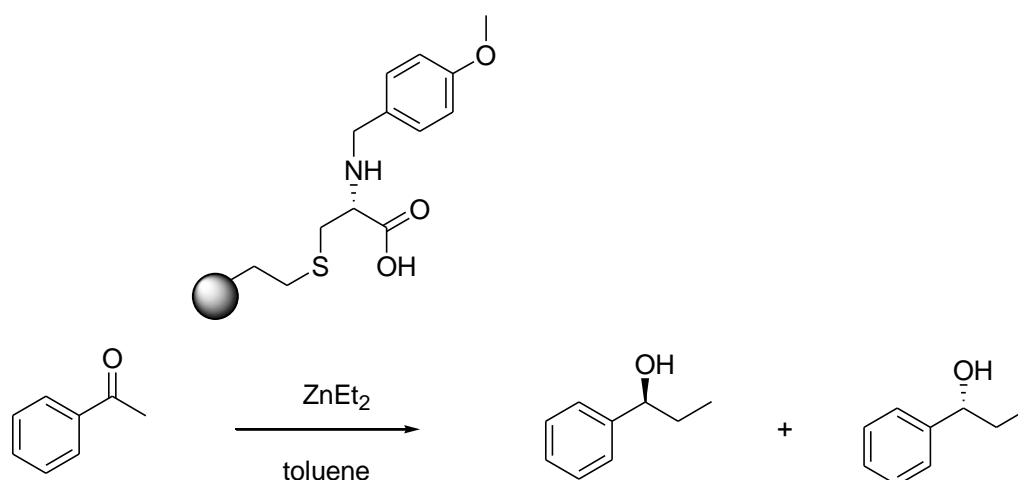
Previous enantioselective catalysis work carried out by the Sullivan research group involved enantioselective addition of diethyl zinc to benzaldehyde. For these reactions, catalyst silica-

ethyl-(1R, 2S)-ephidrine phosphiniamide chloride was used and in a given reaction time of 48 hours, 90% conversion was achieved with 72% enantioselectivity (**Scheme 4.16**).



**Scheme 4.16** Asymmetric addition of diethyl zinc to benzaldehyde using silica ethyl-(1R, 2S)-ephidrine phosphiniamide chloride as a chiral auxiliary

Catalyst **silica-60-N-4-methoxybenzyl-L-cysteine** was also tested in the enantioselective addition of diethyl zinc to benzaldehyde under the same reaction conditions. A shorter reaction time of 24 hours gave 99% conversion to the alcohol product with 12% *e.e.* for the (*R*)-enantiomer.



**Scheme 4.17** Asymmetric addition of diethyl zinc to benzaldehyde using **silica-60-N-4-methoxybenzyl-L-cysteine** as a chiral auxiliary catalyst

The chiral induction shown by **silica-60-N-4-methoxybenzyl-L-cysteine** is rather poor in comparison to silica ethyl-(1R, 2S)-ephidrine phosphiniamide chloride. This could be a result of the additional steric centre on silica ethyl-(1R, 2S)-ephidrine phosphiniamide chloride increasing the chiral induction in the reaction.

## 4.5 References

- <sup>1</sup> C. A. McNamara, M. J. Dixon and M. Bradley, *Chem Rev.*, 2002, **102**, 3275-330; P. McMova and G. J. Hutchings, *Chem. Soc. Rev.*, 2004, **33**, 108-122; P. Mastrorilli and C. F. Nobile, *Co-ord. Chem. Rev.*, 2004, **248**, 377-395; M. Heitbaum, F. Glorius and I. Escher, *Angew Chem. Int. Ed.*, 2006, **45**, 4732-4762; H. Yang, X. Han, Z. Ma, R. Wang, J. Lui and X. Ji, *Green Chem.*, 2010, **12**, 441-451;
- <sup>2</sup> C. Cateriela and M. P. Diaz-de-Villegas, *Tetrahedron, Asymmetry*, 1998, **9**, 3517; C. Catriela and M. D. Diaz-de-Villages, *Tetrahedron : Asymmetry*, 2000, **11**, 645; K. Maruoka and T. Ooi, *Chem. Rev.*, 2003, **103**, 3013; A. Viso, R. F. De la Pradilla, A. Garcia and A. flores. *Chem Rev.*, 2005, **105**, 3167;
- <sup>3</sup> A. J. Wright, S. Reinyer, S. Skonieczny and D. S. Dosady, *Int. J. Appl. Sci. Eng.*, 2003, **1**, 2, 89-100;
- <sup>4</sup> M. M. Dell Anna, V. Gallo, P. Mastrorilli and G. Romanazzi, *Molecules*, 2010, **15**, 3311-3318;
- <sup>5</sup> F. Figueras and B. Coq, *J. Mol. Catal. A: Chemical*, 2001, **173**, 117; G. Booth, *Ullmanns Encyclopedia of Industrial Chemistry*, Wiley-VCH, Verlag, Germany, 2002;
- <sup>6</sup> S. Xu, X. Xi, J. Shi and S. Cao, *J. Mol. Catal. A: Chem.*, 2000, **160**, 287;
- <sup>7</sup> V. R. Choudhary and M. G. Sane, *J. Chem. Technol. Biotechnol.*, 1998, **73**, 4, 336;
- <sup>8</sup> N. T. S. Phan, M. van der Sluys and C. W. Jones, *Adv. Synth. Catal.*, 2006, **348**, 609-679;
- <sup>9</sup> F. Ciardelli, E. Tsucida and D. Wohrle, *Macromolecules and Catalysis*, Springer, Berlin, 1996; N. Toshima, Y. Shiraishi and T. Teranishi, *J. Mol. Catal. A: Chemical*, 2001, **177**, 139; D. Huber, G. Andermann and G. Leclerc, *Tet. Lett*, 1988, **29**, 635; E. A. Gelder, S. D. Jackson and C. M. Lok, *Catal. Lett.*, 2002, **84**, 205;
- <sup>10</sup> R. Raja, V. B. Golovko, J. M. Thomas, A. Berenguer-Murcia, W. Zhou, S. Xie and B. F. G. Johnson, *Chem Comm.*, 2005, 2026-2028;
- <sup>11</sup> A. E. Taggi, A. M. Hafez and T. Lectka, *Acc. Chem. Res.*, 2003, **36**, 10-19;
- <sup>12</sup> Q. Kang, Z. A. Zhou and S-L You, *Communications, Adv. Synth. Catal.*, 2007, **349**, 1657-1660;
- <sup>13</sup> C. Moessner and C. Bolm, *Angew. Chem Int. Ed.*, 2005, **44**, 7564-7567; Q. Yang, G. Shnag, W. Gao, J. Deng and X. Zhang, *Angew. Chem. Int. Ed.*, 2006, **45**, 3832-3835; S. F.

Zhu, J. B. Xie, Y. Z. Zhang and S. Li, Q-L Zhou, *J. Am. Chem. Soc.*, 2006, **128**, 12886-12891;

<sup>14</sup> G. Shang, Q. Yang and X. Zhang, *Angew. Chem.* 2006, **118**, 6508-6510;

<sup>15</sup> E. Egbegi, V. Schwartz, S. H. Overbury and J. S. Spivey, *Catal Today*, 2010, **149**, 91-97; B. H. G. Swennenhuis, R. Chen, P. W. N. M. Van Leeuwen, J. G. De Vries and P. C. J. Kamer, *Eur. J. Org. Chem.*, 2009, 5796-5803; T. Miyake, T. Makino, S. Taniguchi, H. Watanuki, T. Niki, S. Shimuzu, Y. Kojina and M. Sano, *Appl. Catal. A. Gen.*, 2009, **364**, 108-112;

<sup>16</sup> C. F. Lane, *Synthesis*, 1975, 135

<sup>17</sup> Y. Niwa and M. Shimuzu, *J. Am. Chem. Soc.*, 2003, **125**, 3720-3721, See supporting information;

<sup>18</sup> X. B. Jiang, A. J. Minnaard, B. Hessen, B. L. Feringa, A. L. L. Duchateau, J. G. O. Andrien, J. A. F. Boogers and J. G. De Vries, *Org. Lett.*, 2003, **5**, 1503;

<sup>19</sup> K. K. Kurokhtina and A. F. Schmidt, *Arkivoc*, 2009, **XI**, 185-203;

<sup>20</sup> D. J. Raon and Y. Miguel, *Angew. Chem. Int. Ed.*, 2005, **44**, 1602; G. Balme, E. Bossharth and N. Montiero, *Eur. J. Org. Chem.*, 2003, 4101; L. Webber, K. Illgen and M. Almsletter, *Synlett*, 1999, 366;

<sup>21</sup> Q. F. Wang and C. G. Yan, *Cent. Eur. J. Chem.*, 2009, **6** (3) 404-409;

<sup>22</sup> N. Kim, M. S. Kwon, C. M. Park and J. Park, *Tet. Lett.*, 2004, **45**, 7057-7059;

<sup>23</sup> K. Tsuge, M. Kataoka and Y. Seto, *J. Agric. Food Chem.*, 2002, **50**, 16;

<sup>24</sup> L. P. Battaglia, A. Bonamartini Conradi, C. Grasselli Palmiere, M. Nardelli and M. E. Vidoni Tani, *Acta. Cryst.*, 1973, **B29**, 762

<sup>25</sup> M. R. Shehata, M. M. Shoukry, F. M. H. Nasr and R. Van Eldik, *Dalton Trans.*, 2008, 779-786;

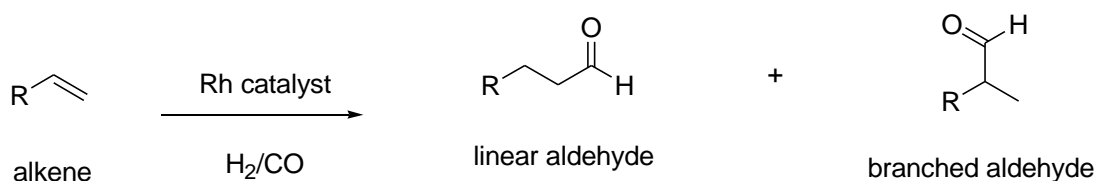
<sup>26</sup> D. T. Cromer and G. B. Mann, *Acta. Cryst.*, 1968, **424**, 321-324; M. G. Drew and A. Kay, *J. Chem. Soc. (A)*, 1971, 1846-1850.

## Chapter 5

### Hydroformylations with Precious Metal Silica-Phosphadamantane Catalysts

#### 5.1 Background literature

Hydroformylation reactions are organic transformations in which aldehydes are produced from the reaction of alkenes with a mixture of  $H_2/CO$ . The reaction entails the addition of a formyl group (CHO) and a hydrogen atom to a carbon-carbon double bond. Hydroformylation reactions are an excellent example of a clean reaction, with potentially 100% atom efficiency.<sup>1</sup> The aldehydes produced are important intermediates in a number of reactions, for example hydroformylation products are widely employed as solvent, plasticizer or as raw materials for detergent fabrication.<sup>2</sup> Often, rhodium is present in hydroformylation catalysts as the reaction proceeds under much milder conditions and presents high alkene conversion as well as high selectivity of the aldehydes with these systems (**Scheme 5.1**).<sup>3</sup>

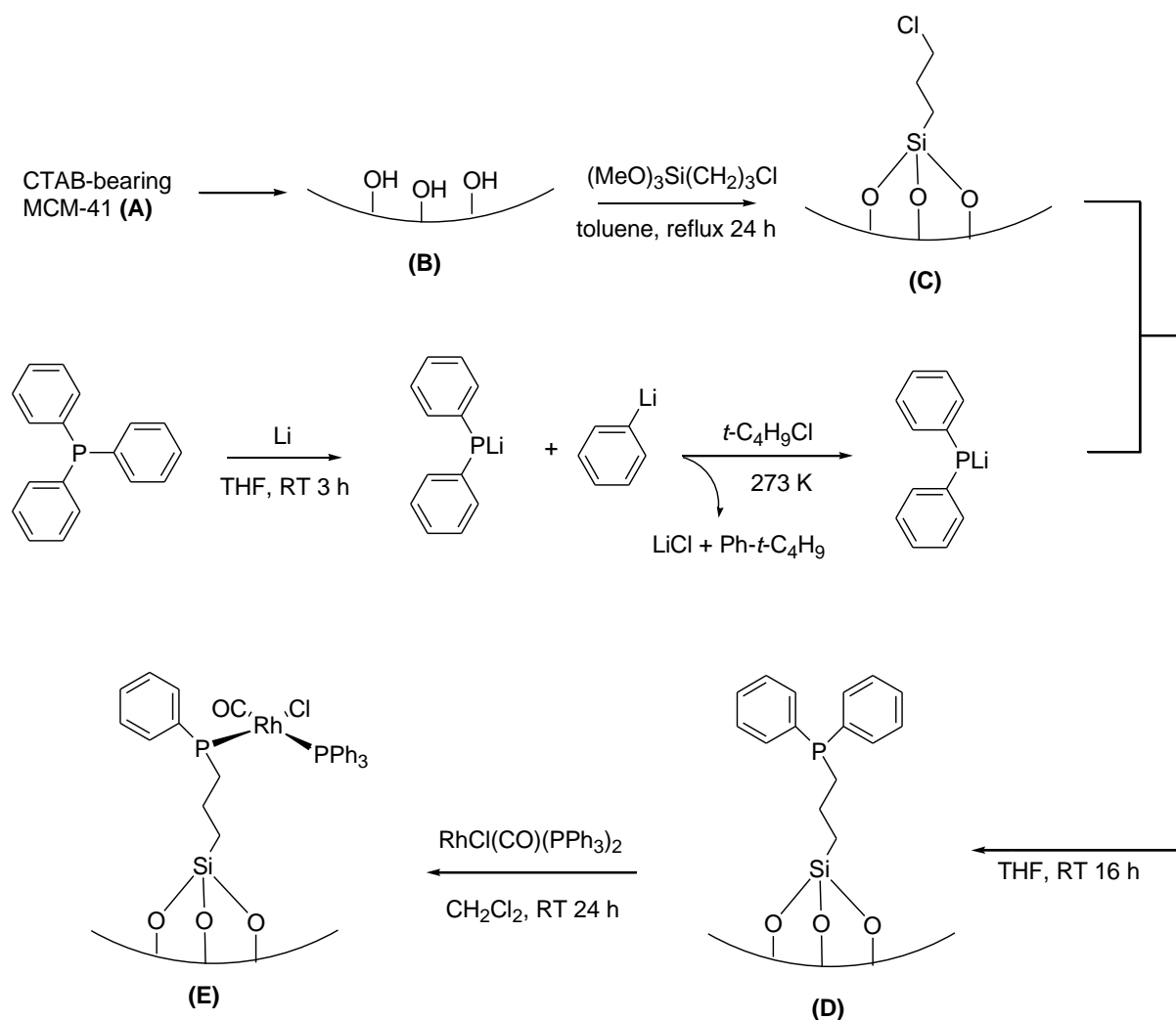


**Scheme 5.1** Hydroformylation reaction

In the hydroformylation of an alkene, there are two possible regiochemical outcomes; a linear aldehyde or branched aldehyde (quaternary in the case of quaternary feedstock), with a greater production of the linear aldehyde expected based on Keueleman's rule. Keueleman's rule states that "in hydroformylation reactions, formyl groups are not produced at quaternary carbon centres".<sup>4</sup> Although many reports in literature find the linear aldehyde to be favoured, there are however some isolated examples wherein the branched aldehyde is the preferentially formed aldehyde. Although, linear aldehydes are found to generate more interest from the industrial sector as these are important bulk chemicals, there is now an increasing interest for the branched aldehydes as these have potential applications in organic synthesis and fine chemicals production.<sup>5,6</sup>

Like many homogeneous processes, large scale hydroformylation, suffers from the difficulty of separating the homogeneous catalyst. Thus there is great importance in immobilising rhodium complexes onto suitable supports. Many approaches have been explored to form heterogeneous catalysts of homogeneous systems including, covalent immobilisation, encapsulation or adsorption of homogeneous catalysts. The background literature review provided below will focus on silica supported rhodium complexes in hydroformylation reactions. It should be noted that little work has been reported on such transformations with heterogeneous systems and this review will cover phosphines and amines immobilised onto silica.

In organometallic chemistry, organophosphines are among the most common auxiliary ligands used. This is mainly due to their excellent ability to stabilise low metal oxidation states as well as having the capacity to influence both steric and electronic properties of the catalytic species. Phosphine ligands can easily be modified by changing one of the substituents and so allowing the fine tuning of the electronic and steric properties of the metal complexes. The use of sterically demanding, electron rich tertiary phosphine ligands has been widely reported in the transformations of many different chemistries. Catalytic systems incorporating these bulky phosphine ligands has allowed for the successful coupling of even the least reactive partners in the Suzuki-Miyaura, Stille, Sonogashira and Mizoroki-Heck couplings.<sup>7</sup> Recently, Zhou *et al.* reported on modifying MCM-41 with diphenyl phosphine ligands (-PPh<sub>2</sub>) and then coordinating a rhodium complex, RhCl(CO)(PPh<sub>3</sub>)<sub>2</sub>.<sup>8</sup> Preparation of the catalyst is described in **Scheme 5.2**. After preparation of chloropropyl-functionalised –MCM-41, this was then connected to diphenyl phosphine ligands by mixing in excess LiPPh<sub>2</sub> and stirring the resulting mixture for sixteen hours at room temperature. The solid formed was then mixed with RhCl(CO)(PPh<sub>3</sub>)<sub>2</sub> in dichloromethane at room temperature for 24 hours to give MCM-PrPPh<sub>2</sub>Rh.<sup>9</sup>



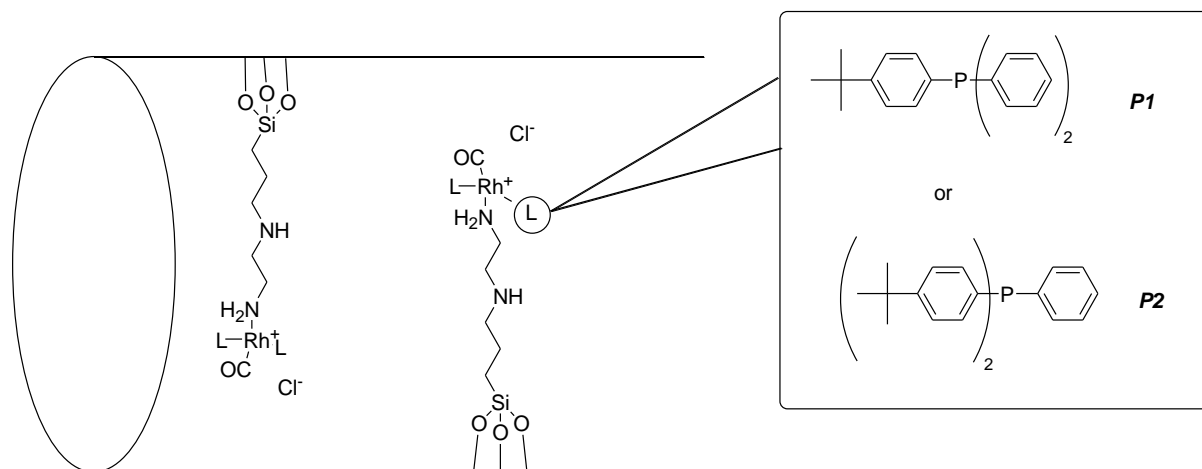
**Scheme 5.2** Preparation of  $\text{MCM-PrPPhRhCl}(\text{CO})(\text{PPh}_3)$  catalyst.<sup>8</sup>

In the hydroformylation of 1-octene at 50 bar, with toluene as a solvent and 1.5 wt % Rh, at 120 °C, high conversion were reported (85%). Catalyst  $\text{MCM-PrPPhRhCl}(\text{CO})(\text{PPh}_3)$  was also found to be very selective, giving 95% aldehydes with a linear: branched ratio of 1.5:1. Re-use of the catalyst gave the same high conversions and selectivity up to run six. Zhou *et al.* reported significant leaching of the Rh into solution in run 1 (0.15%) however, this was dramatically reduced in subsequent runs, <0.05%.

In 2004, Peng *et al* also reported on the immobilisation of rhodium complexes ligated with **P1** and **P2** onto amino functionalised MCM-41 and MCM-48 for 1-hexene hydroformylation.<sup>10</sup> Preparation of the catalysts started with the synthesis of MCM-41 and MCM-48 by procedures typically described in literature.<sup>11</sup> Further modification followed with amino alkylsilanes, such as 3-aminopropyltrimethoxysilane (1N-functional reagent) and [3-(2-



aminoethyl)-aminopropyl]-trimethoxysilane (2N-functional reagent). This was followed by immobilization of Rh-P complexes onto the functionalised support.



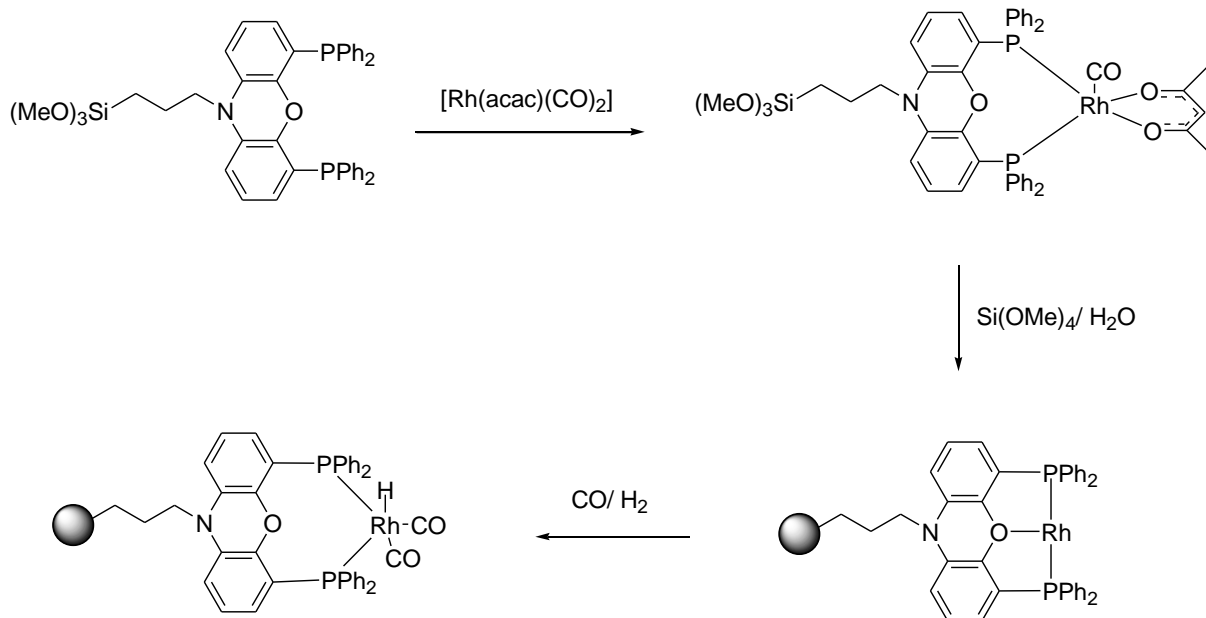
**Scheme 5.3** Possible structure for Rh-P1/2N-MCM-41 or Rh-P2/2N-MCM-41 as proposed by Peng *et al.*<sup>10</sup>

In the hydroformylation of 1-hexene, reactions were carried out in toluene at 100 °C with CO:H<sub>2</sub> pressures of 20 bar and reaction times of 1 hour. Direct immobilisation of Rh-P1 or Rh-P2 onto non functionalised MCM-41 or MCM-48, gave low catalytic activity, for example Rh-P1/ MCM-41 produced 14% conversion and a linear: branched ratio of 1.7:1. In sharp contrast, when Rh-P1 and Rh-P2 were immobilised onto the amino functionalised MCM-41 and MCM-48, high conversions were reported and increased selectivity of the linear aldehyde. For example, catalyst **Rh-P1/ 2N-MCM-48** gave 83% conversion with a linear: branched ratio of 1.8:1 whilst catalyst **Rh-P2/ 2N-MCM-48** gave 80% conversion with a linear: branched ratio of 2.5:1.

Peng *et al.* attributed these results to a strong interaction between the Rh-P complexes and the surface amino groups as well as the resulting high dispersion of the active rhodium species at the catalyst surfaces as shown by XRD and HRTEM studies. Recycling of the catalysts revealed that direct immobilisation of Rh-P2 on the non-functionalised MCM-41, deactivated quickly as a result of severe leaching of the rhodium species during the reaction, as was observed by the strong yellow colour of the organic product. In comparison, **Rh-P2/2N-MCM-41** and **Rh-P2/2N-MCM-48** displayed rather good catalytic stability. A drop in *ca* 20% activity was reported in the second run in both cases; however the catalytic performance remained unchanged in the next several runs. These heterogenised catalysts showed greater catalytic activity and selectivity than their homogeneous counterparts. The higher activity

displayed by anchoring Rh-P2 complex to the amino functionalised mesoporous silica is attributed to the high dispersion of Rh-P complexes through a chemical interaction with the surface amino groups at MCM-41 and MCM-48. In addition, the increased selectivity towards linear aldehyde has been principally ascribed to the contribution of the large cone angle of phosphorus ligands **P1** and **P2** over Rh-(PPh<sub>3</sub>)<sub>2</sub> as well as the confinement of the pore sizes after amino grafting of the mesoporous silica.

One of the first reports on silica supported Rh complexes with phosphorus type ligands was reported by Sandee *et al.*<sup>12</sup> The authors reported on the synthesis and utilisation of such a system in the hydroformylation of octene. The immobilization of xanthene-based ligands, which exhibit large P-M-P angles (110°) was achieved by the addition of [Rh(acac)(CO)<sub>2</sub>] to siloxant phos, as shown in **Scheme 5.4**, and the cationic complex [Rh(siloxantphos)(CO)]<sup>+</sup> was formed. [Rh(siloxantphos)(CO)]<sup>+</sup> was then anchored to a silicate matrix by the sol gel technique. NMR studies revealed that exposure of [Rh(siloxantphos)] to an atmosphere of CO/H<sub>2</sub> (1: 1), resulted in the transformation to [HRh(siloxantphos)(CO)<sub>2</sub>], which is a key intermediate for a selective hydroformylation catalyst. This was coupled with the observation that the colour of the catalyst changed from an orange to yellow.



**Scheme 5.4** Schematic illustration of the preparation of sol gel immobilized [HRh(siloxantphos)(CO)<sub>2</sub>].<sup>12</sup>

Sandee *et al.* reported that TEM experiments revealed no clustered rhodium particles were present in the material. The authors further commented that the coordination of the xanthene

ligand in the tridentate manner, could very likely be an important stabilizing factor for the complex during the sol gel process. In the hydroformylation of 1-octene, with toluene/ n-propanol (13: 1) as a solvent and CO/H<sub>2</sub> pressures of 50 bar at 80 °C, catalyst **[HRh(siloxantphos)(CO)<sub>2</sub>]** was found to be fairly active, with 93% conversion towards the linear aldehyde (32: 1, linear: branched ratio) and an overall conversion of 69%. The reaction was run for 24 hours and metal leaching was reported to be <1%. In the absence of the xanthene ligand, the selectivity was reported to be very low, with a linear: branched ratio of 16: 1. The authors also reported on the preparation of a second catalyst, **[Rh(siloxPNP)CO]<sup>+</sup>**, with a much smaller bite angle (93°) immobilized onto silica via the sol gel process as shown in **Figure 5.1** **[Rh(siloxPNP)CO]<sup>+</sup>** was utilised in the hydroformylation of 1-octene in the same conditions as described above and although good activity was reported (72 % conversion), the linear: branched product ratio was found to be very low (2.4: 1).

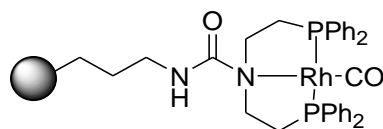


**Figure 5.1** Sandee *et al.* Hydroformylation catalyst **[Rh(siloxPNP)CO]<sup>+</sup>**

Recycling catalyst **[HRh(siloxantphos)(CO)<sub>2</sub>]** showed no deterioration in catalytic activity in eight consecutive cycles and the high linear: branched ratio was maintained. In addition, leaching of Rh was still reported to be <1% in all runs.

Catalysts for hydroformylation reactions based on chirally modified noble metal and inorganic supports have been rarely reported, and the enantioselectivity reported has been rather low, 9%.<sup>13</sup> Li *et al.* reported on the preparation of chirally modified Rh/SiO<sub>2</sub> catalysts and their activity in asymmetric hydroformylation. Chiral phosphorus ligands, such as (*R*)-**BINAP**, (*S,S*)-**DIOP** and (*S*)-**MeO-BIPHEP** were used as chiral modifiers (**Figure 5.2**).

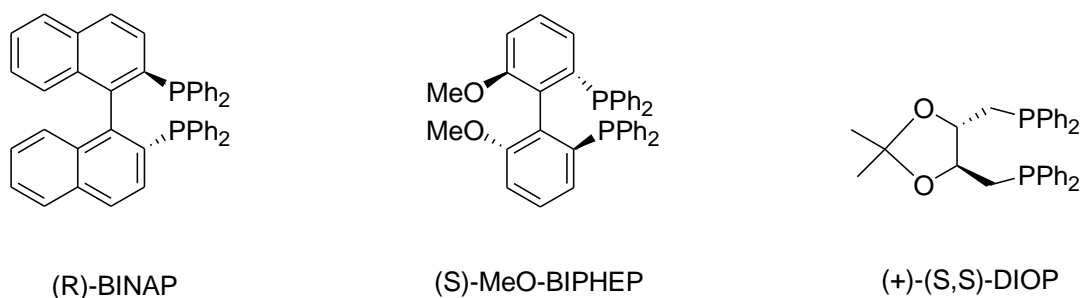
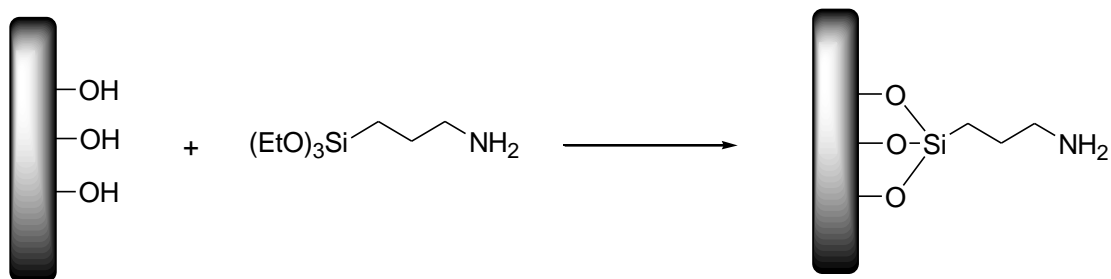


**Figure 5.2** Some of the phosphorus modifiers used in the study by Li *et al.*

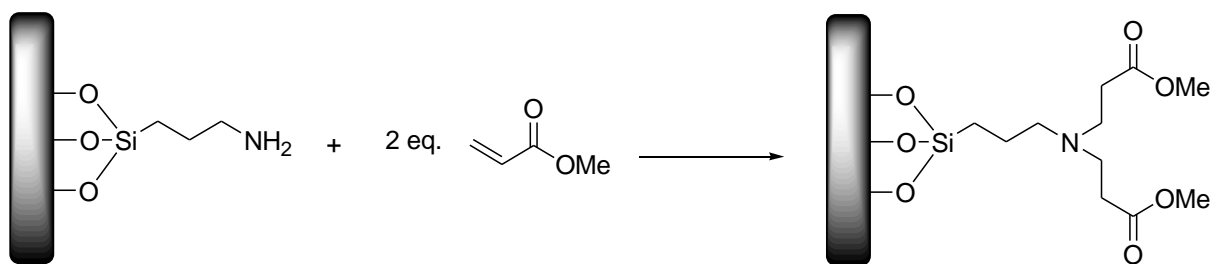
Li *et al.* report that in the hydroformylation of vinyl acetate, (*S,S*)-DIOP ligand adsorbed on the Rh/SiO<sub>2</sub> surface showed good activity, 60%, and good enantioselectivity (32%). These reactions were carried out in toluene at 60 °C with 50 bar pressure for 4 hours. In the same reaction conditions, Rh/SiO<sub>2</sub> catalysts modified with (*S*)-MeO-BIPHEP displayed higher enantioselectivity, 46%, of the opposite isomer (*R*), but again activity reported was very low with 13% conversion to the branched aldehyde. Recycling tests revealed no loss in activity or enantioselectivity from the first run to subsequent reaction cycles. Leaching tests were also carried out and no increased activity was reported on the filtered solution. These hydroformylation results were found to be comparable to homogeneous Rh(COD)(L)Cl catalyst performed under the same general conditions, although longer reaction periods of 10 hours was required.

More recently, Kawi *et al.* reported on SBA-15 modified with PAMAM dendrimers in order to immobilize Wilkinson's catalyst for hydroformylation reactions.<sup>14</sup> These catalysts were prepared by passivating the silanol groups outside the SBA-15 mesopore channels so that functionalization with the dendrimers occurred only within the pores. The catalyst was prepared by first synthesizing SBA-15 following procedures as described in the literature.<sup>15</sup> Before functionalization of the support with dendrimers, SBA-15 was dried under vacuum at 220 °C for 12 hours. The silanol groups outside the mesopores of SBA-15 were then passivated by reaction with dichlorodiphenylsilane. Next step in the synthesis involved reaction of the silanol groups inside the pores with aminopropyltriethoxysilane to give aminated SBA-15 (**Scheme 5.5**).

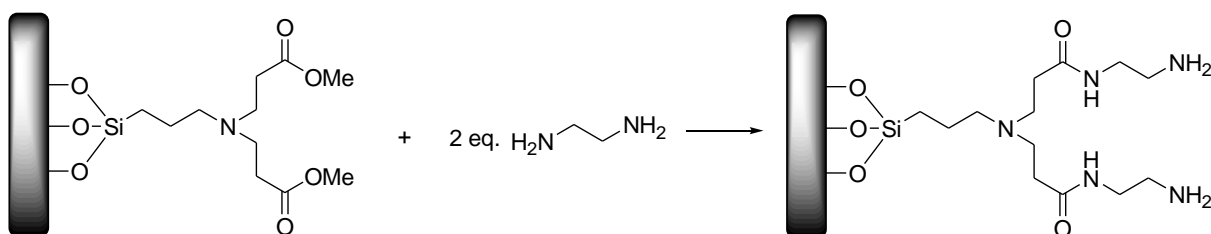


**Scheme 5.5** Functionalisation of SBA-15 by aminotriethoxysilane.<sup>14</sup>

These amine groups are so called ‘initiator sites’, otherwise known as zeroth generation sites and higher generation sites are grown on these (**Scheme 5.6**). Introduction of ester functionality is achieved by the Michael addition of methyl acrylate to the supported amine. This is further reacted with ethyl diamine to give 1<sup>st</sup> generation PAMAM- functionalised SBA-15 (**Scheme 5.7**).



**Scheme 5.6** Michael addition of Methyl acrylate to the amino groups of the surface of SBA-15.<sup>14</sup>

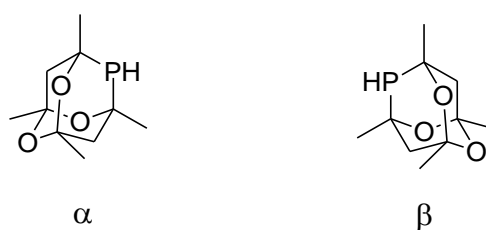


**Scheme 5.7** Amidation of terminal groups on the surface of SBA-15 with ethyldiamine to give 1<sup>st</sup> generation PAMAM modified SBA-15.<sup>14</sup>

This was followed by reacting dendritic SBA-15 supports with RhCl(PPh<sub>3</sub>)<sub>3</sub> through co-ordination of the surface ligand donors to the rhodium precursor to give SBA-15 tethered

rhodium catalysts. Hydroformylation results of styrene showed that catalysts that were non-passivated displayed lower activity and selectivity than the catalyst that were passivated.<sup>16</sup> Regioselectivity of these catalysts shows a climax to be reached with the second generation of dendrimers which then decreases at higher generation. The authors report that in this case, the synergistic effect from the combination of positive dendrimer effects and the pore size of SBA-15 balances the negative effect of the decrease in surface area, making **WPS2** (Wilkinson's catalyst immobilised on passivated SBA-15 with second generation dendrimers) the most selective catalyst formed by the group (branched: linear ratio of 1.8: 1). Leaching studies carried out showed the % weight loss of rhodium to be quite significant in the non passivated catalysts, with as much as 0.6% reported, with decreasing loss of metal with increased growth of dendrimers.

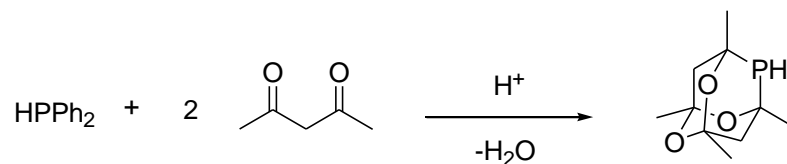
From this literature it is clearly evident that triphenylphosphine is an excellent ligand for hydroformylation catalysis.<sup>17</sup> Even better however, are the bulky triaryl phosphites which display greater selectivity and reactivity.<sup>18</sup> However, a major drawback in using phosphites is that they are prone to hydrolysis as well as reaction to the aldehydes that are produced by hydroformylations. The combination of the high activity of the phosphite based catalysts and the robust properties of the triphenylphosphine derived catalysts is highly sought after by researchers. And so cage phosphines such as 1,3,5,7-tetramethyl-2,4,8-trioxa-6-phosphaadamantane, **PAD**, are hugely attractive candidates as ligands for hydroformylation catalysis. This is because firstly, they are inert to decomposition and secondly, the ligands are stereochemically similar to bulky phosphites.



**Scheme 5.8** Phosphine cages **PAD** are racemic mixtures (labelled  $\alpha$  and  $\beta$ ) and are associated with the  $C_1$  symmetry of the cages.

Recently a surge of interest has developed in the coordination chemistry and potential catalytic applications of these cage-phosphines.<sup>19</sup> In 2005, Clarke *et al.* reported on the synthesis of rhodium catalyst modified with 1,3,5,7-tetramethyl-2,4,8-trioxa-6-phosphaadamantane and the utilisation of this homogeneous catalyst in hydroformylation

reactions.<sup>20</sup> Preparation of the phosphadamantane cage was done by reaction of primary phosphines with acetylacetone.



**Scheme 5.9** Preparation of 1,3,5,7-tetramethyl-2,4,8-trioxa-6-phosphaadamantane

Complexation to rhodium metal was achieved by mixing  $[\text{Rh}(\text{acac})(\text{CO})_2]$  with an excess of ligand, 1,3,5,7-tetramethyl-2,4,8-trioxa-6-phosphaadamantane in the reaction mixture. In the hydroformylation of 1-hexene at 20 bar pressure and reaction temperatures of 60 °C, Clarke *et al.* report utilising 0.2 mol %  $[\text{Rh}(\text{acac})(\text{CO})_2]$  and 0.9 % phosphine ligand to give excellent activity. At 3 hours reaction time, 99% aldehyde was produced, although low regioselectivity was reported with linear: branched ratio of 61: 37. Van Leeuwen *et al.* report similar findings with bulky phosphite derived Rh catalysts and thus reasoned the high activity and low regioselectivity in terms of a mono-phosphite Rh complex,  $[\text{RhH}(\text{CO})_2(\text{L})]$  being the active species.<sup>21</sup> In the hydroformylation of methyl acrylate esters, such as methyl atropate, cage phosphorus ligand, **PAD**, with  $[\text{Rh}(\text{acac})(\text{CO})_2]$  proved to be the most selective catalyst, giving high regioselectivity (49:1 linear: branched ratio) and good yields (98%). This was coupled with reaction times of 70 hours and reaction conditions of 50 bar syngas pressure and temperatures of 45 °C. The selectivity of the catalyst also proved to be rather good as 15% hydrogenated product was only formed.

In a more recent report Clarke *et al.* report on trioxaphosphaadamantane ligand and Rh catalyst in the hydroformylation of methyl atropate, in reactions carried out at 100 °C, the amount of linear product reduced quite significantly from 5 bar  $\text{H}_2$  pressure to 50 bar, from a 1:100 branched: linear ratio to a 1.6: 1.<sup>22</sup> The amount of hydrogenated product was also found to decrease from 55 to 24% as well as an increase in activity from 45% (70 hours) to 76% (24 hours). In experiments in which the pressure was kept constant at 50 bar, the amount of linear product and amount of hydrogenation decreased with decreasing temperature. At temperatures of 75 °C, 87% conversion was observed with 13% hydrogenated product. The selectivity was found to be rather good as well with 16:1 branched: linear ratio. When the temperature was dropped to 15 °C, the hydroformylation of

methyl atropate gave 55% conversion with 1% hydrogenated product. This was coupled with longer reaction times of 70 hours and a branched: linear ratio of 100:1.

Clarke *et al.* further report that all other commonly used monodentate ligands, such as  $\text{PPh}_3$ , and bidentate ligands such as xantphos, BINAP, all performed badly in this reaction giving low conversions or favouring hydrogenation.<sup>20</sup> For example the use of  $\text{PPh}_3$  at 50 bar pressure, heated to 50 °C and a reaction time of 24 hours lead to 99% conversion with 35% hydrogenated product. The branched: linear ratio was found to be 100: 1. Clarke *et al.* report that the catalytic system as prepared by the research group clearly shows that Rh catalysts of the cage phosphane used in conjunction with 50 bar syngas pressure and lower temperature can reduce the amount of hydrogenation by-product and give excellent regioselectivity. This regioselectivity can be increased further by using a syngas rich in CO (5: 1 CO/H<sub>2</sub>).<sup>20</sup>

These findings from Clarke *et al.* are very promising. It is anticipated that immobilisation of this unusual caged phosphine would take advantage of both the easy separation from the reaction media as well as retaining the high activity and selectivity displayed by the homogeneous system. To date, no literature reports have been found to report on the use of immobilised of **PAD** in hydroformylation reactions.

### Summary

The literature review focuses on silica supported phosphorus and amine ligands complexed to rhodium for hydroformylation reactions of styrene and 1-octene. Although activity shown by most catalysts has been good, the catalytic systems seem to suffer from leaching as well as loss of activity in recycles. For example, SBA-15 modified with PAMAM dendrimers immobilized with Wilkinson's catalyst was reported to show excellent activity in the hydroformylation of styrene as reported by Kawi *et al.* However, these catalysts were marred by leaching of the Rh metal into solution, as well as the loss in activity in recycles. Catalysts that are resistant to leaching, such as  $[\text{HRh}(\text{siloxantphos})(\text{CO})_2]$  as prepared by Sandee *et al.*, are shown to demonstrate excellent activity in hydroformylation reactions, however, these reactions are carried out at high syngas pressures (50 bar) and high reaction temperatures (80 °C). Zhou *et al.* also report on the use of high syngas pressure (50 bar) and high reaction temperatures (120 °C) to achieve good conversions in the hydroformylation of 1-octene with catalyst **MCM-PrPPhRhCl(CO)(PPh<sub>3</sub>)**. From here it is clearly evident that there is huge demand for a highly active hydroformylation catalyst which will be not only resistant to



leaching in these reactions but also display high chemoselectivity for the formation of aldehydes as well as high regioselectivity under mild reaction conditions.

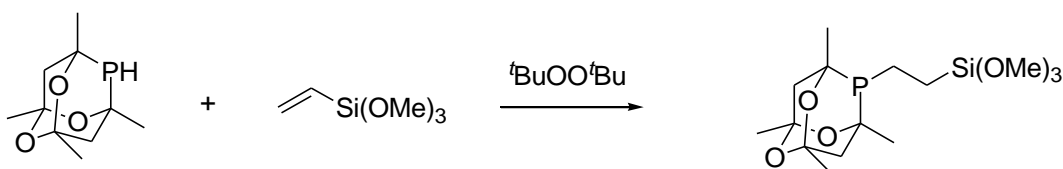
The high activity shown by rhodium coupled to PAD as recently reported by Clarke *et al.* is very promising; however separation of this homogenous catalyst from the product is very troublesome. An alternative option is to employ a silica supported PAD system and studies in this context are described below.

## 5.2 Results and discussion

As reported by Zhou *et al.* literature reports show that most heterogeneous catalysts reported for hydroformylation suffer from leaching. It is well known in organometallic chemistry, that triphenylphosphine ligands are very effective in forming stable transition metal complexes.<sup>23</sup> Further to this, encouraging results from the work of Clarke *et al.* have shown 1,3,5,7-tetramethyl-2,4,8-trioxa-6-phosphaadamantane, **PAD** to be an excellent ancillary ligand in the hydroformylation of styrene. Herein, the immobilisation of this highly active phosphine ligand to silica via method of grafting is reported. Initial studies were carried out in the hydroformylation reaction of vinyl compounds such as styrene and 1-octene in order to assess activity and regioselectivity in comparison to the homogeneous catalyst analogues.

### 5.2.1 Synthesis of silica-110-PAD

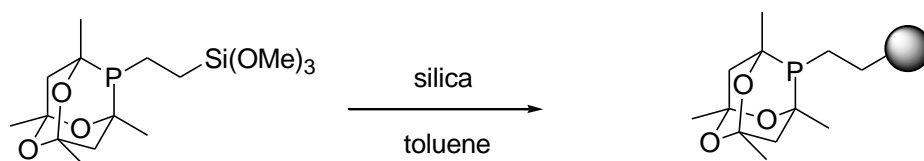
The preparation of silica-110-PAD involved radical addition of phosphatrioxaadamantane to vinyltrimethoxysilane. The reaction was monitored by <sup>1</sup>H NMR through the consumption of the vinyltrimethoxysilane by the disappearance of the peaks at 5.8-6.0 ppm. The reaction was considered complete when the vinyl peaks were no longer present, this gives trimethoxy silyl-2,4,8-trioxa-1,3,5,7-tetramethyl-6-phosphaadamantane.



**Scheme 5.10** Synthesis of trimethoxysilyl-PAD

The next step in the synthesis was grafting compound trimethoxy silyl-2,4,8-trioxa-1,3,5,7-tetramethyl-6-phosphaadamantane on to silica 110Å to give material silica-110-PAD.

Previous work carried out by group had shown that effective immobilisation of this rather large bulky ligand could be achieved on silica of pore size 110 Å.



**Scheme 5.11** Synthesis of silica-110-PAD

Silica-110-PAD was characterised by a combination of methods including solid state <sup>13</sup>C, <sup>29</sup>Si and <sup>31</sup>P NMR, elemental analysis and nitrogen sorption porosimetry.

### 5.2.2 Solid state NMR

#### <sup>13</sup>C CP MAS NMR

State <sup>13</sup>C CP MAS NMR proved to be very useful for the confirmation of the immobilisation of the trioxaphosphaadamantane ligand **Figure 5.3**. These observed resonances can be assigned as 13.3 (SiCH<sub>2</sub>CH<sub>2</sub>P), 28.4 (CH<sub>2</sub>CCH<sub>3</sub>), 37.1 (PCCH<sub>2</sub>), 45.2 (PCCH<sub>2</sub>), 71.6 (PCCH<sub>3</sub>) and 97.2 ppm (PCCH<sub>2</sub>CO).

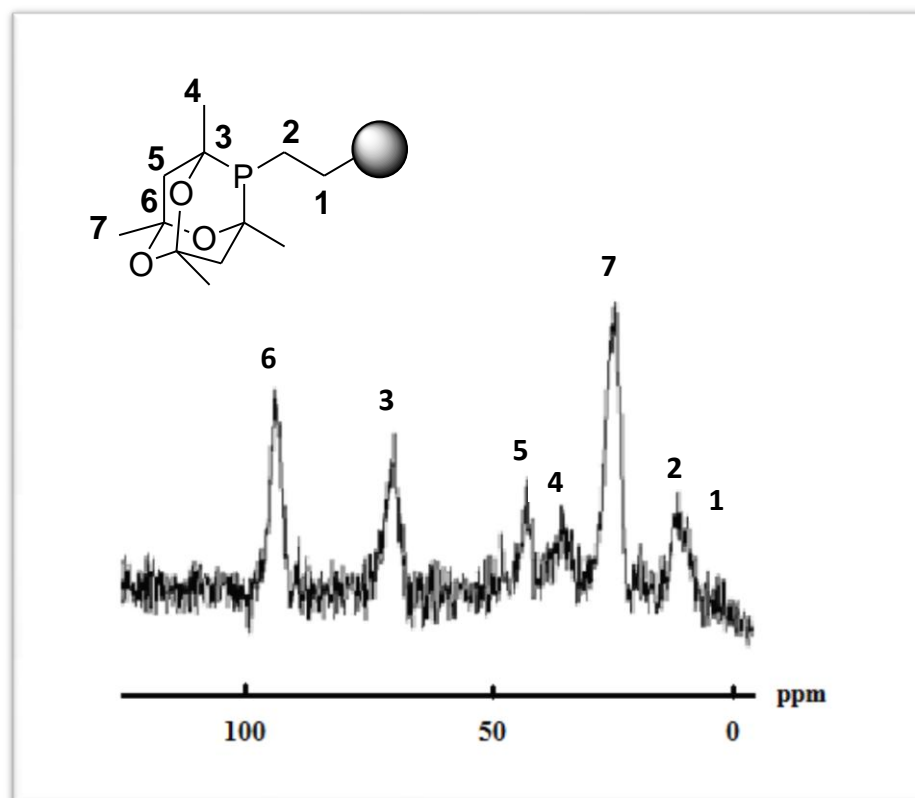


**Figure 5.3**  $^{13}\text{C}$  CP MAS NMR of silica-110-PAD

#### *$^{29}\text{Si}$ MAS NMR and Elemental analysis*

The  $^{29}\text{Si}$  MAS NMR also confirms immobilisation of PAD. Two distinct environments are observed, one corresponding to the  $T^n$  functionalities, -65ppm, and the other corresponding to the  $Q^n$  environments within the material, -108 and -115ppm. It can be seen from the  $^{29}\text{Si}$  MAS NMR that the organosilica environments of silica-110-PAD are mostly of  $T^2$  character. As measured from phosphorus analysis, silica-110-PAD was found to have a ligand loading of 0.5 mmol/g. Further, the  $T:Q$  ratio (that is the ratio of functional group silicon to the framework silicon) was obtained from the fitted  $^{29}\text{Si}$  MAS NMR and results were found to be comparable to those with elemental analysis.

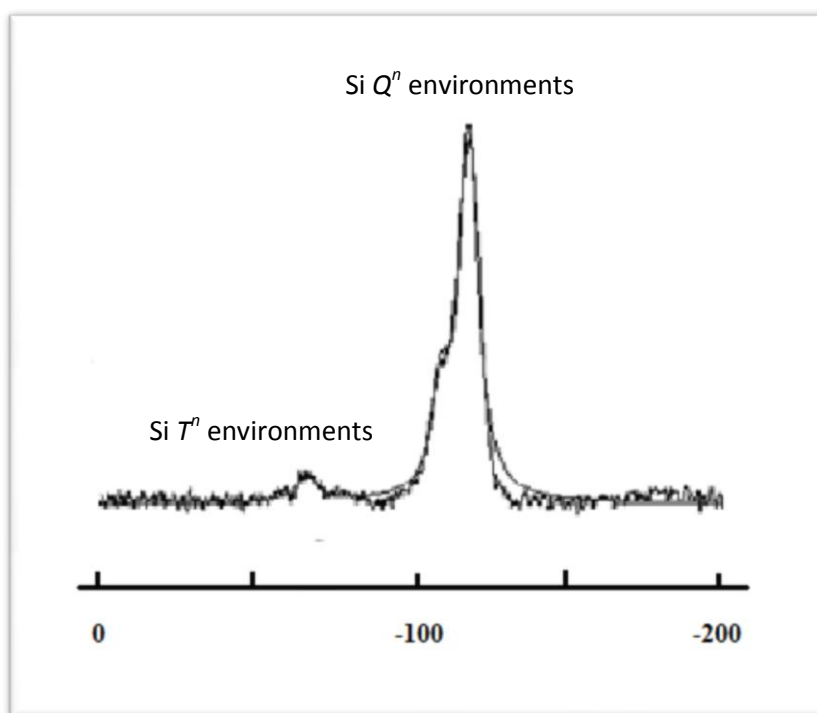


**Figure 5.4**  $^{29}\text{Si}$  MAS NMR of silica-110-PAD with Gaussian fitting

### $^{31}\text{P}$ CP MAS NMR

The  $^{31}\text{P}$  CP MAS NMR of silica-110-PAD was also recorded. A single broad peak found at -22 ppm corresponds to the phosphorus of the phosphadamantane cage. This is in agreement with those reports found in literature.

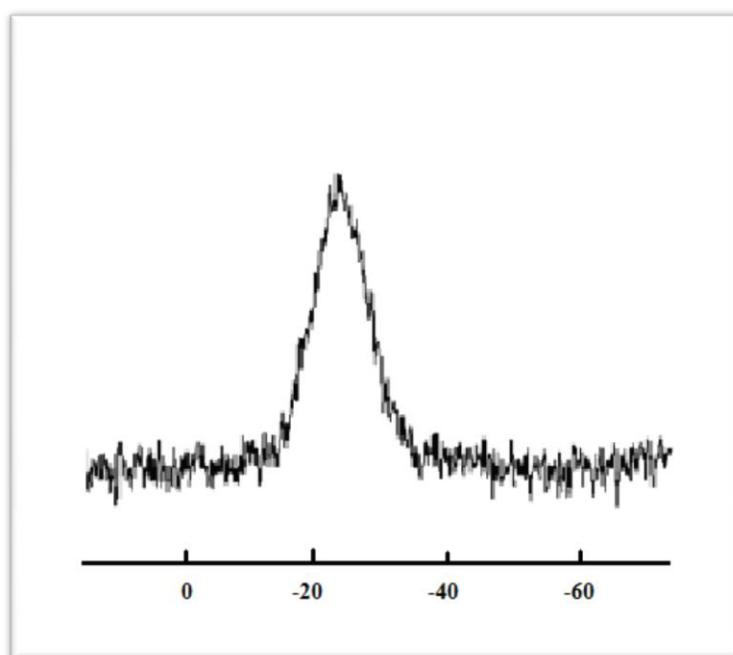


**Figure 5.5**  $^{31}\text{P}$  CP MAS NMR of silica-110-PAD

## 5.2.3 Porosimetry

Porosimetry data was also collected for silica-110-PAD and is tabulated below.

**Table 5.1** Porosimetry data for silica-110-PAD as calculated by the BJH method

	Surface area m <sup>2</sup> /g	Average Pore Diameter Å	Average Pore Volume cc/g
Silica-110-PAD	303.5	96.1	0.574

From the sorption isotherm graph obtained, silica-110-PAD was found to have retained a mesoporous texture and type IV isotherm shape according to the IUPAC classification. Further to this, the shape of the hysteresis loop is indicative of near cylindrical type pores.

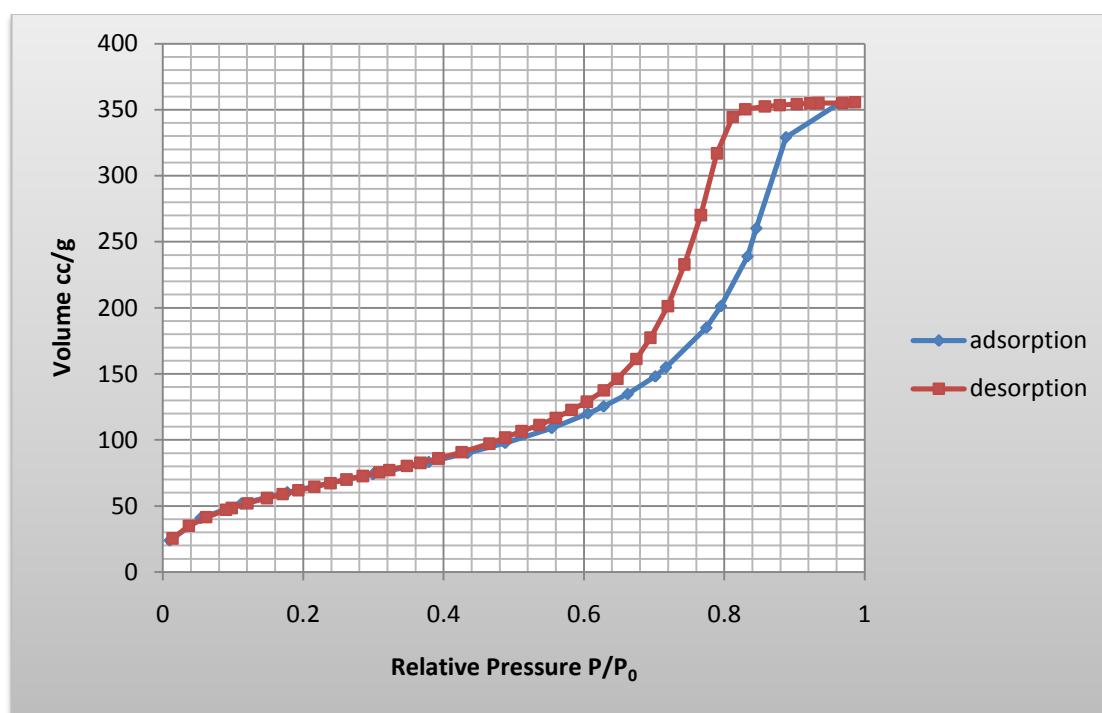


**Figure 5.6** Sorption isotherm for silica-110-PAD

The pore size distribution chart for silica-110-PAD was broad and is shown below. Here it can be seen that the pore sizes fall mainly in the range of 60-120 Å.

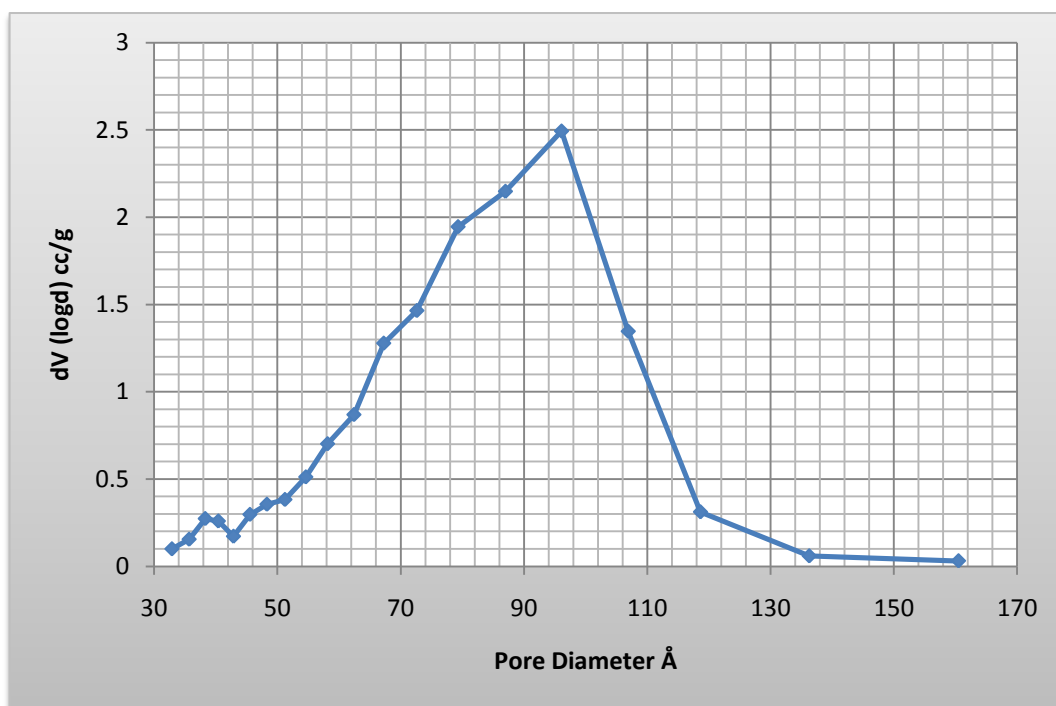
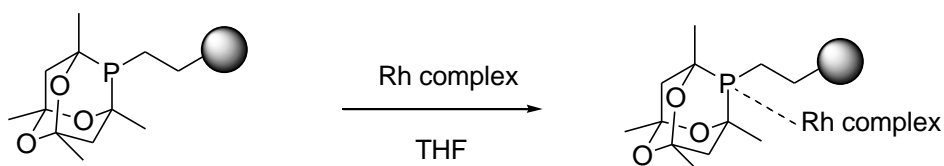


**Figure 5.7** Pore Size distribution chart for silica-110-PAD

#### 5.2.4 Synthesis of silica-110-PAD-Rh

Complexation of silica-110-PAD with commonly used rhodium compounds such as Wilkinson's catalyst  $\text{Rh}(\text{PPh}_3)_3\text{Cl}$  and  $\text{Rh}(\text{CO})_2(\text{acac})$  was carried out at room temperature in THF using a 1:1 PAD: metal ratio (**Scheme 5.12**). An indication of metal complexation to silica-110-PAD came from the change in colour of the solid.



**Scheme 5.12** Synthesis of silica-110-PAD-Rh complex

Catalysts **silica-110-PAD-RhCl(PPh<sub>3</sub>)<sub>2</sub>** and **silica-110-PAD-Rh(CO)(acac)** were characterised by ICP-OES analysis for metal content and by porosimetry. The metal content of **silica-110-PAD-RhCl(PPh<sub>3</sub>)<sub>2</sub>** and **silica-110-PAD-Rh(CO)(acac)** was determined by

stirring 25 mg of the catalysts in 7.5 mL of aqua regia (3:1 conc AnalR HCl: conc AnalR HNO<sub>3</sub>) and the resulting mixture refluxed for 6 hours. The solid was then filtered, washed with deionised water and the metal content in the filtrate measured by ICP-OES. The conditions required to displace rhodium from the supported ligand were rather harsh suggesting a tight binding of the metal to the phosphadamantane ligand. The measured metal loadings for **silica-110-PAD-RhCl(PPh<sub>3</sub>)<sub>2</sub>** and **silica-110-PAD-Rh(CO)(acac)** were 0.16 mmol/g and 0.13 mmol/g respectively. This suggests approximately 30 and 25% occupation of the ligand sites by metal, with a large proportion of the ligand sites metal-free.

### 5.2.5 Porosimetry for silica-110-PAD-Rh

Porosimetry data for **silica-110-PAD-RhCl(PPh<sub>3</sub>)<sub>2</sub>** and **silica-110-PAD-Rh(CO)(acac)** are shown **Figures 5.8** and **5.9**. In the former case ink-bottle type pores are seen while in the latter case the hysteresis appears to indicate a slit shaped pore structure. In the parent **silica-110-PAD** material the pore structure appeared to be cylindrical and therefore significant textural changes coincided with metal uptake.

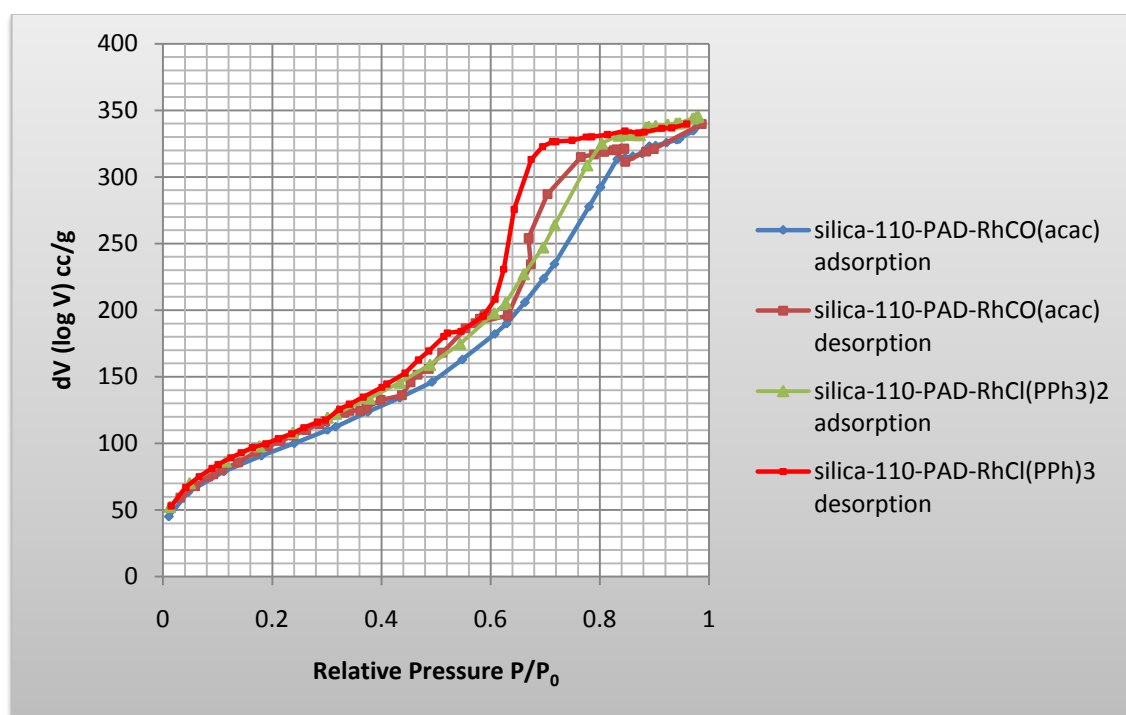


**Figure 5.8** Isotherm for silica-110-PAD-Rh complexes

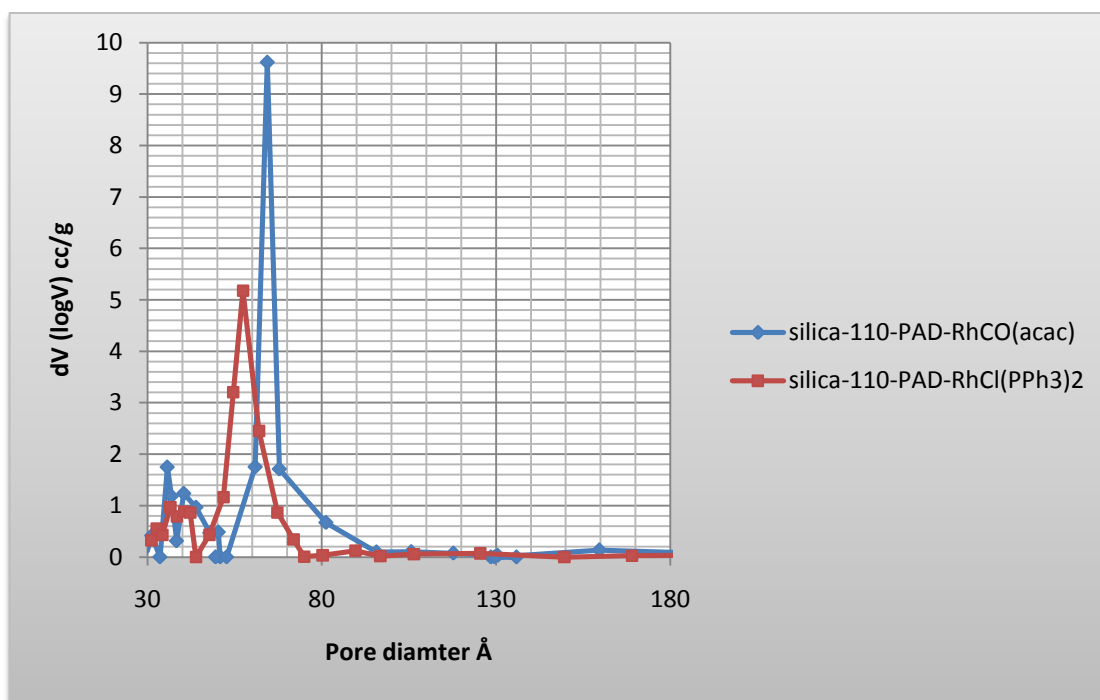


**Figure 5.9** Pore size distribution chart for **silica-110-Rh** complexes

**Table 5.2** Porosimetry data for **silica-110-PAD-Rh** complexes as calculated by BJH method

	Surface area $\text{m}^2/\text{g}$	Average Pore volume $\text{cc/g}$	Average Pore diameter $\text{Å}$
<b>silica-110-PAD-RhCl(PPh<sub>3</sub>)<sub>2</sub></b>	376.6	0.505	57.4
<b>silica-110-PAD-Rh(CO)(acac)</b>	350.7	0.498	64.4

The calculated surface area, average pore diameter and average pore volume are shown to be similar for both materials.

### Summary

The immobilisation of the phosphorus cage like system, PAD onto silica-110 was confirmed by  $^{13}\text{C}$ ,  $^{29}\text{Si}$  and  $^{31}\text{P}$  MAS NMR.  $^{29}\text{Si}$  NMR also revealed that the organosilane environments of silica-110-PAD are mainly of  $\text{T}^2$  character. Further porosimetry studies confirm the



mesoporous nature of silica-110-PAD. These materials have high surface area making them potentially excellent catalysts for organic transformations.

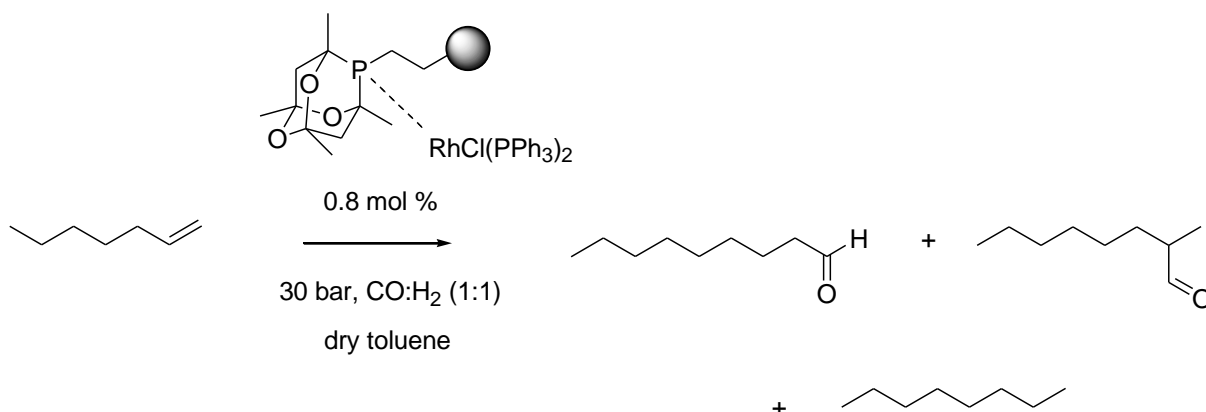
Metal analysis revealed approximately a quarter of the ligand sites to be occupied. The porosimetry measurements revealed a reduction of surface area, average pore volume and average pore diameter as expected after metal introduction.

### 5.2.6 Catalytic activity in Hydroformylation reactions

A typical olefin hydroformylation reaction was carried out in a stainless steel autoclave. The required amount of catalyst was added to a small conical flask along with olefin (2.0 mmol), and dry toluene (4 mL). This was covered with a watch glass and then placed in the autoclave. The reactor was purged three times with nitrogen and then purged with CO: H<sub>2</sub> (1:1) and then pressurised and heated to the reaction temperature. After the required reaction time, a sample was removed, solvent evaporated and the residue analysed by <sup>1</sup>H NMR. Toluene was used as a solvent for these reactions as this has been reported in the literature as a choice solvent for hydroformylations. In addition, Clarke *et al.* report the use of toluene as a solvent gives the best selectivity.<sup>22</sup>

Initial studies were carried out with 1-octene at room temperature at 30 bar syngas pressure employing 0.8 mol % **silica-110-PAD-RhCl(PPh<sub>3</sub>)<sub>2</sub>** corresponded to 100 mg of catalyst. At a reaction time of 5.5 hours, the catalyst showed high activity with 99% conversion and high selectivity with only 9% hydrogenated product. Regioselectivity of the catalyst was also good with 73:27 branched: linear ratio (**Table 5.3, entry 1**). When the reaction was carried out at higher temperatures of 60 °C, the rate of the reaction was much faster, with quantitative conversion achieved in 2 hours. The selectivity of the catalyst decreased with 20% hydrogenated product formed. There was no real change in regioselectivity at higher temperatures (branched: linear ratio 76: 24). In hydroformylation reactions, regioselectivity of a catalyst has been known to be greatly influenced by the temperature, pressure and the ligand used. Clarke *et al.* reported that catalytic systems employing common phosphine ligands such as PPh<sub>3</sub> and BINAP were ineffective at lower temperatures and that higher temperature afford hydrogenated product. The results found here show catalyst **silica-110-PAD-RhCl(PPh<sub>3</sub>)<sub>2</sub>** to be active at room temperature and the selectivity of the catalyst to be

unchanged when the temperature is increased from room temperature to 60 °C, although an increase in hydrogenated product, from 9% to 20%, is observed.



**Scheme 5.13** Hydroformylation of 1-octene with **silica-110-PAD-RhCl(PPh<sub>3</sub>)<sub>2</sub>**

**Table 5.3** Hydroformylation of 1-octene with **silica-110-PAD-RhCl(PPh<sub>3</sub>)<sub>2</sub>**

Entry	Temperature °C	Time h	% conversion (% hydrogenated)	Branched: Linear
1	Room temperature	5.5	99 (9)	73:27
2	60 °C	2	99 (20)	76:24

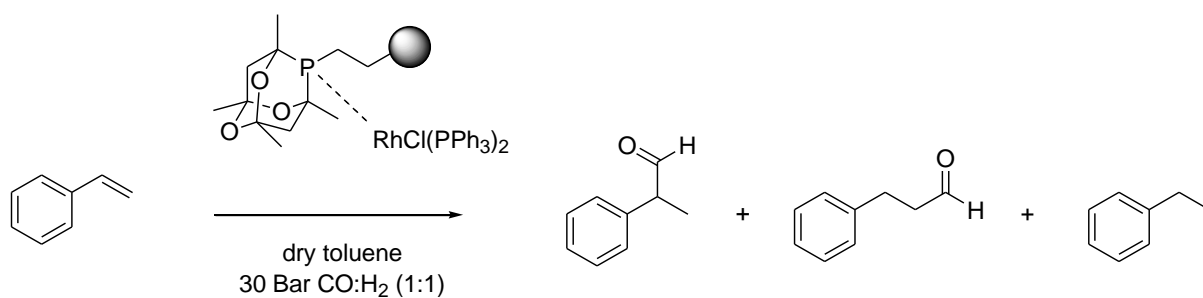
**Conditions:** Taken 2 mmol 1-octene, 5 mL dry toluene, 100 mg **silica-110-PAD-RhCl(PPh<sub>3</sub>)<sub>2</sub>**; 30 bar H<sub>2</sub>: CO (1: 1), heated if necessary; % conversion determined by <sup>1</sup>H NMR.

Interestingly, the catalytic system **silica-110-PAD-RhCl(PPh<sub>3</sub>)<sub>2</sub>** favours the formation of the branched aldehyde. The co-ordination of **PAD** with rhodium is anticipated to afford strong immobilization during the hydroformylation reaction. Leaching tests were carried out with the **silica-110-PAD-RhCl(PPh<sub>3</sub>)<sub>2</sub>** catalyst at 60 °C. At 1 hour, the reaction was stopped, the catalyst filtered, and the % conversion determined to be 56%. The filtrate was transferred to a

new conical flask and the reaction continued for a further hour. No increase in % conversion was measured. In addition, the metal content of the filtrate was measured and no rhodium was detected by ICP-OES analysis.

Next attention was turned to the hydroformylation of styrene catalysed with **silica-110-PAD-RhCl(PPh<sub>3</sub>)<sub>2</sub>**. The hydroformylation of vinyl aromatics has been applied to the synthesis of optically active non-steroidal anti inflammatory agents that are functional 2-aryl propionic acids, such as (S)-Naproxen.<sup>13</sup> Hydroformylations using styrene were carried out at room temperature with 30 bar syngas pressure and toluene as a solvent. Using 3 mmol styrene and reaction time of 6 hours, quantitative conversions of the styrene was observed with only 13% hydrogenated product (table 2, entry 1). The regioselectivity of the catalysts was also shown to be good with 80:20 branched: linear ratio. Hydroformylation reactions carried out at 60 °C gave quantitative conversion in 7 hours, with a slight increase in selectivity, branched: linear ratio of 83:17. This was coupled with 22% hydrogenated product. An increase in temperature to 80 °C, gave quantitative conversion of styrene in 3 hours. However, a drop in selectivity was found with branched: linear ratio of 74: 26. In addition, the amount of hydrogenated product formed was 53%.

These findings of hydroformylation of styrene with **silica-110-PAD-RhCl(PPh<sub>3</sub>)<sub>2</sub>** clearly show that at high temperatures regioselectivity of the catalyst is decreased with a preference for linear product increasing. In addition, an increase in temperature also leads to increased rates of the reaction; however these results are coupled with a decrease in chemoselectivity resulting in the formation of more hydrogenated product.



**Scheme 5.14** Hydroformylation of styrene with **silica-110-PAD-RhCl(PPh<sub>3</sub>)<sub>2</sub>**

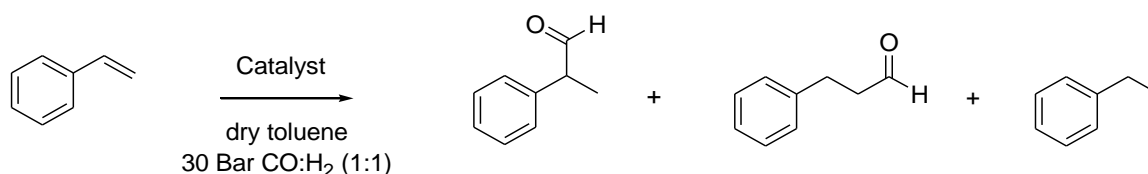
**Table 5.4** Hydroformylation of 1-octene with **silica-110-PAD-RhCl(PPh<sub>3</sub>)<sub>2</sub>**

Entry	Temperature °C	Time h	% conversion (% hydrogenated)	Branched: linear
1	Room temp	5.5	99 (13)	80: 20
2	60	7	99 (22)	83:17
3	80	3	99 (53)	74:26

**Conditions:** Taken 3 mmol styrene, 5 mL dry toluene, 100 mg **silica-110-PAD-RhCl(PPh<sub>3</sub>)<sub>2</sub>** (0.6 mol % Rh); 30 bar H<sub>2</sub>: CO (1: 1), heated if necessary; % conversion determined by <sup>1</sup>H NMR.

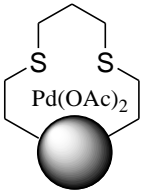
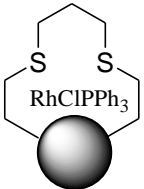
Catalyst **silica-60-C<sub>3</sub>-RhCl(PPh<sub>3</sub>)<sub>2</sub>** was also tried in the hydroformylation of styrene at 30 bar syngas pressure and 60 °C reaction temperatures. This catalyst has previously been reported in Chapter 4 for the hydrogenation of nitrobenzene. Employing 0.4 mol % **silica-60-C<sub>3</sub>-RhClPPh<sub>3</sub>** with 3 mmol styrene and 4 mL dry toluene, quantitative conversions were achieved after a total reaction time of 8 hours. The selectivity of the catalyst was found to be good with 66: 33 branched: linear ratio, this result was also coupled with 56% hydrogenated product.

Although rhodium is the choice metal for hydroformylation reactions, highly active hydrogenation catalyst **silica-60-C<sub>3</sub>-Pd(OAc)<sub>2</sub>** was also tried in the hydroformylation of styrene. This catalyst (1.4 mol %) was found to give 70% conversion of the olefin, 40% of which was hydrogenated product. The branched:linear ratio was found to be 67:33. The analogous rhodium system was more active but high levels of hydrogenated product were formed.



**Scheme 5.15** Hydroformylation of styrene with **silica-60-C<sub>3</sub>-Pd/Rh**

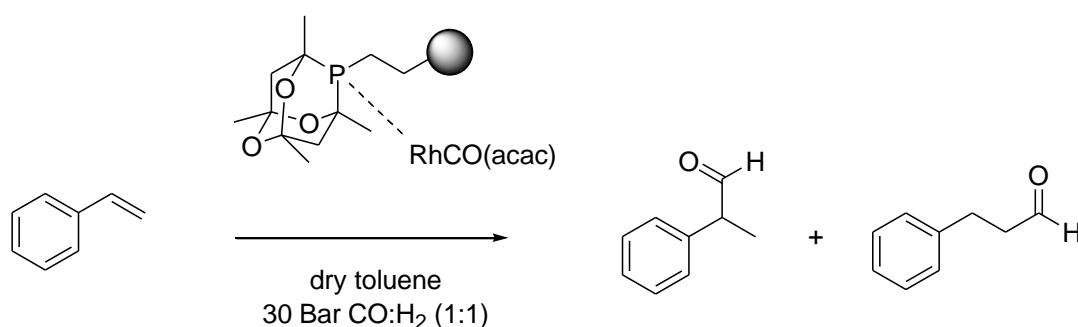
**Table 5.5** Hydroformylation of styrene at 60 °C with **silica-60-C<sub>3</sub>-Pd(OAc)<sub>2</sub>** and **silica-60-C<sub>3</sub>-RhClPPh<sub>3</sub>**

Entry	Catalyst	Time	% conversion (% Hydrogenated)	Branched: Linear
1		8	70 (40)	67:33
2		8	99 (56)	66:33

**Conditions:** Taken 3 mmol styrene, 5 mL dry toluene, 100 mg catalyst (**silica-60-C<sub>3</sub>-Pd(OAc)<sub>2</sub>** (1.4 mol %); **silica-60-C<sub>3</sub>-RhClPPh<sub>3</sub>** (0.4 mol %) 30 bar H<sub>2</sub>: CO (1: 1), heated at 60 °C; % conversion determined by <sup>1</sup>H NMR.

The results so far show that **PAD** is an excellent ligand for these reactions. Attention was thus turned to catalyst **silica-110-PAD-Rh(CO)(acac)** and its utilization in the hydroformylation of styrene. Initial reactions carried out at room temperature with 0.4 mol %

catalyst at 30 bar pressure gave no conversion to the aldehyde or hydrogenated product. An increase of the metal loading to 1.2 mol % also failed to give conversion at room temperature. Hydroformylation reactions were then carried out at 80 °C and after 2 hours, quantitative conversion of styrene was achieved with excellent selectivity for the aldehyde product as no hydrogenated product was formed. The metal loading was 0.4 mol % and this gave good regioselectivity with branched: linear ratio 63: 37 (**Table 5.6, entry 3**). The use of immobilised phosphadamantane ligands with  $\text{Rh}(\text{CO})_2(\text{acac})$  inhibits hydrogenation at high temperature.



**Scheme 5.16** Hydroformylation of styrene with **silica-110-PAD-RhCO(acac)**

**Table 5.6** Hydroformylation of styrene with **silica-110-PAD-RhCO(acac)**

Entry	Temperature °C	Time h	mol % Rh	% conversion (% hydrogenated)	Branched: linear
1	Room temp	8	0.04	0	0
2	Room temp	8	0.12	0	0
3	80	2	0.04	99 (0)	63:37

**Conditions:** Taken 3 mmol styrene, 5 mL dry toluene, 100 mg silica-110-PAD-RhCO(acac) (0.4 mol %) or 300 mg silica-110-PAD-RhCO(acac); 30 bar H<sub>2</sub>: CO (1: 1), heated at 60 °C; % conversion determined by <sup>1</sup>H NMR.

The factors influencing regioselectivity include Markovnikov addition which is dictated by the electronic properties of the Rh-H and spatial conformation of the styrene. Assuming hydridic character in Rh-H then linear addition products would be expected. On the other hand, the electronic properties of styrene, would anticipate branched products. It is difficult in this case to compare regioselectivity outcomes from the different rhodium species. Employing the more  $\pi$ -acid ligand, CO, does appear to increase overall selectivity with no hydrogenation product formed at 80 °C compared to 53% hydrogenation product when PPh<sub>3</sub> is present however the regioselectivity of aldehyde formation is similar in both cases. Some further observations merit comment, catalyst **silica-110-PAD-Rh(CO)(acac)** gave no conversion at room temperature in contrast to **silica-110-PAD-RhCl(PPh<sub>3</sub>)<sub>2</sub>**, although rhodium loading was similar in both cases. It seems unlikely that the rhodium sites are located in very different pore environments which could influence substrate diffusion. It may be that the presence of bidentate acac hinders hydrogen addition at room temperature but more work is needed to establish this.

#### 5.4 Conclusions

Aldehydes are immensely important building blocks for organic synthesis. Although linear aldehydes are of immense importance for many commodity chemical applications, this reaction is potentially important for the synthesis of more complex organic products where branched formyl product would be more desirable. Our results show this outcome to be preferred in the case of rhodium complexed phosphadamantane-modified silica catalysts. In these studies conditions where hydroformylation facilitates such regioselectivity were identified. The outcome is very condition sensitive and for example, the results show that an increase in reaction temperature readily increases the rate of conversion but this is marred by decrease in selectivity in favour of hydrogenated product. Catalyst **silica-110-PAD-Rh(CO)(acac)** gave excellent results, with no hydrogenated product formed. These initial studies are very promising and certainly future work will deal with optimisation of the reaction conditions and explore a range of quaternary substrates.

## 5.5 References

- <sup>1</sup> B. M. Trost, *Science*, 1991, **254**, 1471-1477;
- <sup>2</sup> P. W. N. M. Van Leeuwen and C. Claver, "Rhodium catalysed Hydroformylation", 2000, Kluwer, Amsterdam;
- <sup>3</sup> (a) F. Abyssou, J. F. Carpentier and A. Montriex, *Chem. Rev.*, 1995, **95**, 2485; (b) M. Diguez, O. Panies and C. Claver, *Tett.: Asym.*, 2004, **15**, 2113; (c) C. J. Cobley, K. Gardner, J. Klosin, C. Praquin, C. Hill, G. T. Whiteker, A. Zanotti-Gerosa, J. L. Petersen and K. A. Abboud, *J. Org. Chem.*, 2004, **69**, 4031; (d) C. J. Cobley, K. Kloisin, C. Qin and G. T. Whiteker, *Org. Lett.*, 2004, **6**, 3277; (e) S. Breeden, D. J. Cole-Hamilton, D. F. Foster and G. J. Shwarz, M. Wills, *Angew. Chem.*, 2000, **112**, 4272;
- <sup>4</sup> A. I. M. Keuleman, A. Kwantes and T. van Bavel, *Recl. Trav. Chim. Pays-Bas.*, 1948, **67**, 298;
- <sup>5</sup> M. L. Clarke, *Curr. Org. Chem.*, 2005, **9**, 701; B. Breit, W. Seiche, *Synthesis*, 2001, 1;
- <sup>6</sup> (a) I. J. Krauss, C. C-Y. Wang and J. L. Leighton, *J. Am. Chem. Soc.*, 2001, **123**, 11514; (b) C. Botteghi, M. Marchetti, S. Paganelli and B. Sechi, *J. Mol. Catal. A.*, 1997, **118**, 173;
- <sup>7</sup> (a) D. Gerristma, T. Brenstrum, J. McNulty and A. Capretta, *Tet. Lett.*, 2004, **45**, 15, 8319-8321; (b) G. Adjabeng, T. Brenstrum, J. Wilson, C. Frampton, A. Robertson, J. Hillhouse, J. McNulty and A. Capretta, *Org. Lett.*, 2003, **5**, 6, 953-955;
- <sup>8</sup> W. Zhou and D. He, *Catal. Lett.*, 2009, **127**, 437-443;
- <sup>9</sup> X-Y. Hao, Y-Q. Zhang, J-W. Wang, W. Zhou, C. Zhang and S. Liu, *Microporous Mesoporous Mater.*, 2006, **88**, 38;
- <sup>10</sup> Q. Peng, Y. Yang and Y. Yuan, *J. Mol. Catal. A.*, 2004, **219**, 175-181;
- <sup>11</sup> L. Y. Chen, T. Horiuchi, T. Mori and K. Maeda, *J. Phys. Chem. B*, 1999, **101**, 1216;
- <sup>12</sup> A. J. Sandee, L. A. Van der Veen, J. N. H. Reek, P. C. J. Kamer, M. Lutz, A. L. Spek and P. W. N. M. van Leeuwen, *Angew. Chem. Int. Ed.*, 1999, **38**, 21, 3231;
- <sup>13</sup> (a) J. M. Coronado, F. Coloma and J. A. Anderson, *J. Mol. Catal. A chem.*, 2000, **154**, 143; (b) A Fuerte, M. Iglesias, F. Sanchez, *J. Organomet. Chem.*, 1999, **588**, 186;
- <sup>14</sup> P Li and S. Kawi, *Catal. Today*, 2008, **131**, 61-69;
- <sup>15</sup> (a) D. Y. Zhao, Q. Huo, J. L. Feng, B. F. Chmelka and G. D. Stucky, *J. Am. Chem. Soc.*, 1998, **120**, 6024; (b) H. H. P. Yiu, P. A. Wright and N. P. Botting, *J. Mol. Catal. B: Enzyme*, 2001, **15**, 81;



- <sup>16</sup> M. C. Richard, B. I. Lemon III, L. Sun, L. K. Yeung and M. Zhao, *Top. Curr. Chem.*, 2001, **212**, 81;
- <sup>17</sup> C. Botteghi, M. Marchetti, S. Paganelli and B. Sechi, *J. Mol. Catal. A*, 1997, **118**, 173;
- <sup>18</sup> A. van Rooy, E. N. Orji, P. C. J. Kamer and P. W. N. M. van Leeuwen, *Organometallics*, 1995, **14**, 34;
- <sup>19</sup> (a) R. I. Pugh and E. Drent, *Adv. Synth. Catal.*, 2002, **344**, 837; (b) G. Adjabeng, T. Brenstrum, J. Wilson, C. Frampton, A. Robertson, J. Hillhouse, J. McNulty and A. Capretta, *Org. Lett.*, 2003, **5**, 6, 953-955 and references therein;
- <sup>20</sup> R. Angharad Baber, M. L. Clarke, K. M. Heslop, A. C. Marr, A. G. Orpen, P. G. Pringle, A. Ward and D. E. Zambrano-Williams, *Dalton Trans.*, 2005, 1079-1085;
- <sup>21</sup> (a) K. G. Moloy and J. L. Petersen, *J. Am. Chem. Soc.*, 1995, **117**, 7696; (b) K. A. Jensen, P. H. Nielsen and C. T. Penderson, *Acta. Chem. Scand.*, 1963, **17**, 115; (c) P. W. N. M. van Leeuwen and C. Claver "Rhodium catalysed Hydroformylation", Kluwer Academic Publications, Dordrecht, 2000;
- <sup>22</sup> M. L. Clarke and G. J. Roff, *Chem. Eur. J.*, 2006, **12**, 7978-7986;
- <sup>23</sup> M. T. Honaker, B. J. Sandefur, J. L. Hargett, A. L. McDaniel and R. N. Salvatore, *Tet. Lett.*, 2003, **44**, 8373.

## Chapter 6

### Experimental Section

#### 6.1 General Experimental Information

All glassware was dried for several hours in an oven and cooled prior to use. Reagents used were purchased from Aldrich, Avocado or Lancaster and were used without further purification, unless otherwise stated.

**Solvents** used were obtained from BDH and were of standard grade unless otherwise stated. Hexane and isopropanol were HPLC grade. Generally, solvents were purified prior to use. The solvents were dried by storing them over the appropriate drying agents, then heated to reflux for four hours under nitrogen and distilled as required. All solvents were stored in reservoirs with activated 4 Å molecular sieves under nitrogen. The most often used solvents are listed below:

<b>Solvents</b>	<b>Drying agents</b>
Toluene	distilled over sodium wire/benzophenone ketyl
Dichloromethane	distilled over calcium hydride
<i>o</i> -Xylene	distilled over sodium wire/benzophenone ketyl

**Melting points (m.p)** were determined using an Electrothermal melting point apparatus and are uncorrected.

**IR Spectroscopy** were recorded using a Bruker Tensor 27 running Hyper IR V. 1.0, either neat or by making KBr discs.

**<sup>1</sup>H NMR (solution) spectroscopy:** were determined using a JEOL 270 (270 MHz) spectrometer. The chemical shifts are reported in  $\delta$  (ppm) relative to chloroform (CDCl<sub>3</sub>, 7.26 ppm) and tetramethylsilane (TMS, 0 ppm). The coupling constants are given in Hertz (Hz). Characterisation of the signals: s = singlet, d = doublet, t = triplet, q = quartet,

m = multiplet, bs = broad singlet, bm = broad multiplet, dd = double doublet. Integration is determined by the relative number of atoms associated with a particular resonance.

**$^{13}\text{C}$  NMR (solution) spectroscopy:** were determined using a JEOL 270 (67.95 MHz) spectrometer. The chemical shifts are reported in  $\delta$  (ppm) relative to chloroform ( $\text{CDCl}_3$ , 77 ppm) and tetramethylsilane (TMS, 0 ppm).

**$^{29}\text{Si}$  NMR (solution) spectroscopy:** were determined using a Bruker 400 (79.51 MHz) spectrometer. The chemical shifts are reported in  $\delta$  (ppm) relative to tetramethylsilane (TMS, 0 ppm).

**$^{31}\text{P}$  NMR (solution) spectroscopy:** were determined using a JEOL 270 (109.30 MHz) spectrometer. The chemical shifts are reported in  $\delta$  (ppm) relative to phosphoric acid.

**Solid state NMR spectroscopy  $^{29}\text{Si}$ ,  $^{31}\text{P}$ ,  $^{13}\text{C}$ :** were determined using a Bruker AMX 600 and 400 MHz spectrometer.

600 MHz spectrometer:  $^{29}\text{Si}$  HPDec MAS- frequency 119.2 MHz, spinning speed 12 KHz; 1 minute recycle delay with  $2\ \mu\text{s}\sim 45^\circ$  pulse;  $^{13}\text{C}$  CP MAS- frequency 150.9 MHz, spinning speed 10 KHz, 1ms contact time, 5s delay,  $90^\circ$  pulse for  $3.5\ \mu\text{s}$ .  $^{31}\text{P}$  MAS-frequency 242.94 MHz, spinning 12 KHz, 1.5s delay,  $45^\circ$  pulse for  $2\ \mu\text{s}$ .

400 MHz spectrometer:  $^{29}\text{Si}$  SPE MAS- frequency 79.46 MHz, spinning speed 5 KHz; 1 minute recycle delay with  $2\ \mu\text{s}\sim 45^\circ$  pulse;  $^{13}\text{C}$  CP MAS- frequency 100.58 MHz, spinning speed 12 KHz, 1ms contact time, 5s delay,  $90^\circ$  pulse for  $3\ \mu\text{s}$ .  $^{31}\text{P}$  MAS-frequency 161.92 MHz, spinning 12 KHz, 5s delay,  $90^\circ$  pulse for  $3\ \mu\text{s}$ .

**Spin-Lattice relaxation time ( $T_1$ ) experiments:**  $^{13}\text{C}$  Spin-lattice relaxation times were measured using the inversion-recovery pulse sequence, two experiments were carried out; in the first experiment an inversion recovery pulse sequence of  $180^\circ\text{-}\tau\text{-}90^\circ$  was applied where  $\tau$  was  $6.0\ \mu\text{s}$ . In the second the same pulse sequence was applied followed by Fourier transformation of the free induction delay (FID), the dephasing time delay was  $4.0\ \mu\text{s}$ . Spectra were recorded at 150.903 MHz.

**Transmission electron microscopy (TEM):** For TEM analysis, samples were dispersed in ethanol and ultrasonically mixed. A drop of the suspension is placed onto a carbon film (from Agar Scientific Ltd.) supported by a copper grid. Specimens were allowed to dry before analysis using the JEOL JEM 2010 transmission electron microscope.

**Porosimetry:** Porosimetry measurements were obtained using a Quantachrome Nova instrument and data was analysed with Novawin<sup>TM</sup> software.

**Elemental analysis:** performed in the analytical laboratory of University of London (UCL) and Medac Ltd.

**Gas chromatography (GC):** was performed on Hewlett Packard 5890A. Chrompack capillary column CP-Chirasil-Dex CB 25m, 0.25mm, 0.25  $\mu$ m.

**High performance liquid chromatography (HPLC):** was performed on Shimadzu class VP, using normal phase chiral column; Chiralcel OD 0.46 x 25 cm. All traces were eluted in Hexane :*isopropanol* 80:20 % unless stated otherwise.

**Thin layer chromatography (TLC):** was performed on alumina plates coated with silica gel (Merck silica gel 60 F<sub>245</sub>, layer thickness 0.2 mm). Visualisation was accomplished by UV-light (wavelength  $\lambda = 254$  nm) and iodine or aqueous KMnO<sub>4</sub>.

**Column chromatography:** was performed on commercial silica gel purchased from BDH (60-200  $\mu$ m).

**Program used for fitting Solid State NMR data is Winfit dm2005:**

"Modelling one- and two-dimensional Solid State NMR spectra." *Magnetic Resonance in Chemistry*, 40 70-76 (2002). D. Massiot, F. Fayon, M. Capron, I. King, S. Le Calvé, B. Alonso, J-O. Durand, B. Bujoli, Z. Gan and G. Hoatson.

**ICP-OES:** measurements were taken using a Spectro Genesis ICP-OES (sensitivity ~10 ppb). The standards were used to measure metal content were as follows:

< 10 ppm Pd in samples: 10 mL standards of 1, 2, 5, 7.5, 10ppm

10-50 ppm Pd in samples: 100 mL standards of 5, 10, 20, 30, 40 and 60 ppm

**Microwave reactions:** were carried out using a Biotage Initiator<sup>TM</sup> microwave reactor (power level 400W).

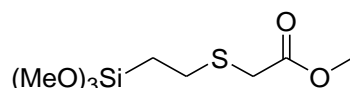
## 6.2 Chapter 2 Experimental

### Quantification of silanol groups on silica-60Å by adsorption of pyridine

This followed a procedure of Sierra *et al.*<sup>1</sup> Silica (1 g) was added to a small beaker. The beaker was placed in a pyrex bath containing pyridine (*ca* 30 mL). The bath was covered with a watch glass and the pyridine heated to 40 °C for 24 hours. After this the silica was dried under high vacuum at room temperature for 24 hours. A sample was then analysed by TGA in which a graph of weight loss as a function of temperature was obtained and the number of silanol groups thus calculated.

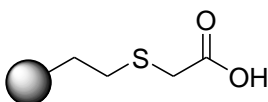
Notes: The silica needs to be as dry as possible as water in the pores will affect the TGA results, therefore it was dried at 200 °C overnight before the experiment. Further, to ensure good contact between the silica and the pyridine, the silica should be spread out in a thin layer. Calculations are based on the assumption of a 1:1 interaction between pyridine and silanol. The pyridine desorption was observed on a Perkin Elmer TGA7 machine while the sample was heated in air over the temperature range 30-400 °C.

### Synthesis of methyl (2-trimethoxysilylethyl) thio glycolate



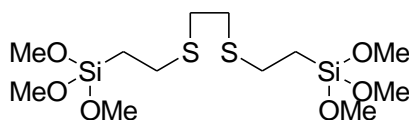
Into a two neck round bottom flask was added trimethoxyvinylsilane (156 mL, 1.02 mol) and methyl thioglycolate (87 mL, 0.97 mol) and the mixture stirred at room temperature. To this was then added di-*tert*-butyl peroxide (10 drops) and with continued stirring the mixture was warmed to 115 °C under an atmosphere of nitrogen. The mixture was maintained at this temperature for 1 h during which di-*tert*-butyl peroxide (10 drops) was added every 20 minutes. The solution was then cooled to room temperature to give methyl (2-trimethoxysilylethyl) thio glycolate. <sup>1</sup>H NMR (CDCl<sub>3</sub>, 270 MHz) δ<sub>H</sub>: 0.76–0.81 (2H, bm, SiCH<sub>2</sub>), 2.55 (2H, bm, CH<sub>2</sub>S), 3.18 (2H, s, CH<sub>2</sub>CO), 3.50 (9H, s, 3 x CH<sub>3</sub>), 3.66 (3H, s, OCH<sub>3</sub>); <sup>13</sup>C NMR (CDCl<sub>3</sub>, 270 MHz) δ<sub>C</sub>: 9.8 (SiCH<sub>2</sub>), 26.7 (CH<sub>2</sub>S), 32.9 (CH<sub>2</sub>CO), 50.3 (SiOCH<sub>3</sub>), 52.0 (C(O)OCH<sub>3</sub>), 170.7 (CO).

### Synthesis of silica-60-G<sub>1</sub>



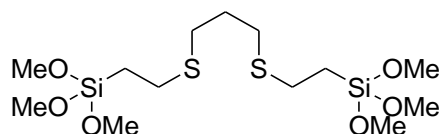
Into a three neck round bottom flask equipped with overhead stirrer, thermometer and reflux condenser was added methyl (2-trimethoxysilylethyl) thio glycolate (25.4 g, 0.1 mol), silica (80 g, 60 Å, 60-200 µm, Grace) and toluene (80 mL). The mixture was then heated at reflux temperature for 8 hours. After this, the solid was filtered, washed with methanol (2 x 20 mL) and dried under reduced pressure for 2 hours to give silica-60-thioglycolate ester as a white powder. Conversion of the immobilised thioglycolate ester to the corresponding acid was achieved by suspending silica-60-thioglycolate ester (10 g) in 1M hydrochloric acid (100 mL) and stirring this mixture at the reflux temperature for 2 hours. The white solid obtained was then filtered, washed with distilled water, methanol and finally ether. The white solid was then dried under reduced pressure overnight to give **silica-60-G<sub>1</sub>** (9.76 g, 99%). IR (KBr disc)  $\nu$ : 473, 811, 1101, 1276, 1732 and 3436  $\text{cm}^{-1}$ ;  $^1\text{H}$  NMR (NaOD/  $\text{D}_2\text{O}$ , 270 MHz)  $\delta_{\text{H}}$ : 0.51 (SiCH<sub>2</sub>), 2.47 (CH<sub>2</sub>S), 3.07 (SCH<sub>2</sub>C(O));  $^{13}\text{C}$  CP MAS NMR  $\delta_{\text{C}}$  16.9 (SiCH<sub>2</sub>), 30.26 (CH<sub>2</sub>S), 36.27 (CH<sub>2</sub>C(O)) and 177.02 (CO<sub>2</sub>H);  $^{29}\text{Si}$  MAS NMR  $\delta_{\text{Si}}$  -64, -87, -98, -107; Elemental analysis 4.06% S; Specific surface area 388.39  $\text{m}^2/\text{g}$ ; Average pore diameter 54.9 Å; Average pore volume 0.482 cc/g.

### Synthesis of 1,2-Bis(2-trimethoxysilylethylthio)ethane



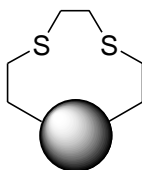
To trimethoxyvinylsilane (67 mL, 0.44 mol) was added 1,2-ethanedithiol (20 mL, 0.2 mol) and the mixture stirred at room temperature for 1 hour. The volatiles were then evaporated at 100 °C under reduced pressure to give a colourless oil, 1,2-bis(2-trimethoxysilylethyl)ethane.  $^1\text{H}$  NMR ( $\text{CDCl}_3$ , 270 MHz)  $\delta_{\text{H}}$ : 0.76 (4H, t,  $J = 8.1$ , SiCH<sub>2</sub>), 2.51 (8H, m, CH<sub>2</sub>SCH<sub>2</sub>), 3.37 (18H, s, OCH<sub>3</sub>);  $^{13}\text{C}$  NMR ( $\text{CDCl}_3$ , 270 MHz)  $\delta_{\text{C}}$ : 10.5 (SiCH<sub>2</sub>), 25.9 (CH<sub>2</sub>S), 31.6 (SCH<sub>2</sub>CH<sub>2</sub>S), 50.3 (OCH<sub>3</sub>);  $^{29}\text{Si}$  NMR ( $\text{CDCl}_3$ )  $\delta_{\text{Si}}$ : -49.06.

### Synthesis of 1,3-Bis(2-trimethoxysilylethylthio)propane



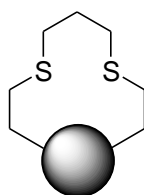
To trimethoxyvinylsilane (67 mL, 0.44 mol) was added 1,3-propanedithiol (20 mL, 0.2 mol) and the mixture stirred at room temperature for 1 hour. The volatiles were then evaporated at 100 °C under reduced pressure to give a colourless oil, 1,3-bis(2-trimethoxysilylethyl)propane.  $^1\text{H}$  NMR ( $\text{CDCl}_3$ , 270 MHz)  $\delta_{\text{H}}$ : 0.77 (4H, t,  $J = 8.1$ ,  $\text{SiCH}_2$ ), 1.63-1.69 (2H, m,  $\text{CH}_2\text{CH}_2\text{CH}_2$ ), 2.45 (8H, m,  $\text{CH}_2\text{SCH}_2$ ), 3.38 (18H, s,  $\text{OCH}_3$ );  $^{13}\text{C}$  NMR ( $\text{CDCl}_3$ , 270 MHz)  $\delta_{\text{C}}$ : 10.5 ( $\text{SiCH}_2$ ), 25.9 ( $\text{CH}_2\text{S}$ ), 29.1 ( $\text{SCH}_2\text{CH}_2\text{CH}_2\text{S}$ ), 30.6 ( $\text{SCH}_2\text{CH}_2\text{CH}_2\text{S}$ ), 50.4 ( $\text{OCH}_3$ );  $^{29}\text{Si}$  NMR ( $\text{CDCl}_3$ )  $\delta_{\text{Si}}$ : -45.04.

### Synthesis of silica-60-C<sub>2</sub>



To 1,2-bis(2-trimethoxysilylethylthio)ethane (12 g, 28 mmol) was added silica (40 g) and toluene (100 mL) and the mixture refluxed for 8 hours. After cooling, the mixture was filtered, washed with methanol and dried to give a white powder, **silica-60-C<sub>2</sub>**.  $^1\text{H}$  NMR ( $\text{NaOD}/\text{D}_2\text{O}$ , 270 MHz)  $\delta_{\text{H}}$ : 0.58 (4H, m,  $\text{SiCH}_2$ ), 2.56 (4H, m,  $\text{CH}_2\text{S}$ ) and 2.65 (4H, s,  $\text{SCH}_2$ );  $^{13}\text{C}$  NMR (CP MAS)  $\delta_{\text{C}}$  13.2 ( $\text{SiCH}_2$ ), 26.1 ( $\text{CH}_2\text{S}$ ), 33.6 ( $\text{SCH}_2\text{CH}_2\text{S}$ );  $^{29}\text{Si}$  NMR (MAS)  $\delta_{\text{Si}}$  -64.1, -68.3, -86.3, -97.8, -106.6; Elemental analysis, % S found 3.6%; Specific surface area 377.61  $\text{m}^2/\text{g}$ , average pore volume 0.469  $\text{cc}/\text{g}$ , average pore diameter 56.7 Å.

### GP-2.1 General Procedure for the synthesis of silica-C<sub>3</sub>



To 1,3-bis(2-trimethoxysilylethylthio)propane (6 g, 14.8 mmol) was added silica (20 g, 60-200  $\mu\text{m}$ ) and toluene (70 mL) and the resulting mixture stirred at reflux for 8 hours. After cooling, the mixture was filtered, washed with methanol and then dried to give a white powder, **silica-C<sub>3</sub>**.

#### Synthesis of silica-60-C<sub>3</sub>

Prepared following **GP-2.1** as described above with silica 60  $\text{\AA}$ , 60-200  $\mu\text{m}$ , Grace <sup>1</sup>H NMR (NaOD/ D<sub>2</sub>O, 270 MHz)  $\delta_{\text{H}}$ : 0.38 (4H, m, SiCH<sub>2</sub>), 1.54 (4H, m, CH<sub>2</sub>S) and 2.31-2.36 (6H, m, SCH<sub>2</sub>CH<sub>2</sub>CH<sub>2</sub>S); <sup>13</sup>C NMR (CP MAS)  $\delta_{\text{C}}$ : 13.3 (SiCH<sub>2</sub>), 26.1 (CH<sub>2</sub>S), 29.5 (SCH<sub>2</sub>CH<sub>2</sub>CH<sub>2</sub>S); <sup>29</sup>Si NMR (MAS)  $\delta_{\text{Si}}$  -70, -76, -98, -108 and -117; Elemental analysis % S found 3.29%; Specific surface area 371.3 m<sup>2</sup>/g; Average pore volume 0.479 cc/g; Average pore diameter 43.1  $\text{\AA}$ .

#### Synthesis of silica-90-C<sub>3</sub>

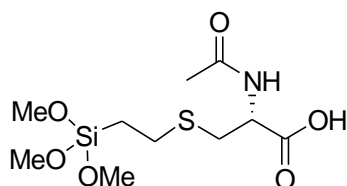
Prepared following **GP-2.1** as described above with silica 90  $\text{\AA}$ , 60-200  $\mu\text{m}$ , Grace. <sup>1</sup>H NMR (NaOD/ D<sub>2</sub>O, 270 MHz)  $\delta_{\text{H}}$ : 0.39 (4H, m, SiCH<sub>2</sub>), 1.52 ppm (4H, m, CH<sub>2</sub>S) and 2.30-2.34 (6H, m, SCH<sub>2</sub>CH<sub>2</sub>CH<sub>2</sub>S); <sup>13</sup>C NMR (CP MAS)  $\delta_{\text{C}}$ : 14.4 (SiCH<sub>2</sub>), 26.3 (CH<sub>2</sub>S) and 32.2 (SCH<sub>2</sub>); <sup>29</sup>Si NMR (MAS)  $\delta_{\text{Si}}$  -48.7, -56.5, -65.5, -107; Ligand loading from weight difference 0.66 mmol/g **silica-90-C<sub>3</sub>**. Specific surface area 378.8 m<sup>2</sup>/g; Average pore volume 0.629 cc/g; Average pore diameter 79.3  $\text{\AA}$ .

#### Synthesis of silica-150-C<sub>3</sub>

Prepared following **GP-2.1** as described above with silica 150  $\text{\AA}$ , 60-200  $\mu\text{m}$ , Grace. <sup>1</sup>H NMR (NaOD/ D<sub>2</sub>O, 270 MHz)  $\delta_{\text{H}}$  0.38 (4H, m, SiCH<sub>2</sub>), 1.53 ppm (4H, m, CH<sub>2</sub>S) and 2.28-2.33 (6H, m, SCH<sub>2</sub>CH<sub>2</sub>CH<sub>2</sub>S); Ligand loading 0.54 mmol/g from weight difference; Specific surface area 497.3 m<sup>2</sup>/g; Average pore volume 1.47 cc/g; Average pore diameter 120.3  $\text{\AA}$ .



### Synthesis of S-(2-trimethoxysilylethyl-N-acetyl-L-cysteine

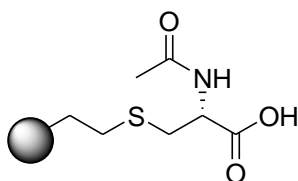


Into a two neck round-bottom flask fitted with reflux condenser and thermometer was added *N*-acetyl-L-cysteine (20.58 g, 0.126 mol) and vinyl trimethoxysilane (12.93 ml, 0.0845 mol). The mixture was heated to reflux with stirring (the material should become soluble above 60°C; initial reflux temp is around 100 °C). The mixture was heated for a further 8 hours at this temperature whilst adding di *tert*-butyl peroxide (0.25 ml) every hour (2 ml in total) and then cooled. <sup>1</sup>H NMR (CDCl<sub>3</sub>, 270 MHz) δ<sub>H</sub> 1.36 (2H, m, SiCH<sub>2</sub>), 2.21 (3H, s, C(O)CH<sub>3</sub>), 2.89 (2H, b m, CH<sub>2</sub>SCH<sub>2</sub>), 3.48 (9H, s, 3 x OCH<sub>3</sub>), 3.71 (2H, d, *J*= 5 Hz, CH<sub>2</sub>SCH<sub>2</sub>), 5.02 (1H, m, CHNH), 6.48 (1H, b s, NH); <sup>13</sup>C NMR (CDCl<sub>3</sub>, 270 MHz) δ<sub>C</sub>: 13.5 (SiCH<sub>2</sub>), 19.8 (SiCH<sub>2</sub>CH<sub>2</sub>), 26.8 (SCH<sub>2</sub>CH), 36.1 (C(O)CH<sub>3</sub>), 50.4 (Si(OCH<sub>3</sub>)<sub>3</sub>), 54.0 (CHNH), 170.7 (C(O)NH), 170.9 (C(O)OH).

**Note 1.** The product becomes orange when cooled and unless used immediately it is best to store as a solution in methanol.

**Note 2.** The progress of the addition reaction was monitored by the consumption of vinyl trimethoxysilane (vinyl peaks at 5.8-6.0 ppm in the <sup>1</sup>H-NMR run in CDCl<sub>3</sub>). The reaction was considered completed when the above peaks were no longer present.

### Synthesis of silica-60-N-acetyl-L-cysteine

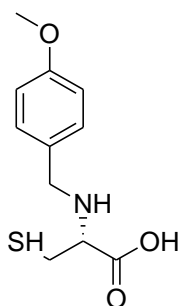


Into a three neck round bottom flask fitted with reflux condenser, thermometer and overhead stirrer was added silica (67.61 g, 70-200 μm, 60 Å, Grace) then methanol (65 ml) and toluene (70 ml). Agitation was applied and S-trimethoxysilylethyl-N-acetyl-L-cysteine (33.1 g, 0.0845 mol, in methanol 35ml) was added. The mixture was refluxed for 1 hour and the rate of temperature increase in the pot was recorded— every 10 minutes. A Dean –Stark apparatus

was fitted to the flask and methanol removed over the next two hours. During methanol recovery, toluene (150 ml) was added at a rate that was approximately proportional to the volume of solvent removed. A temperature rise from 65 to 110 °C was observed. At 4 hours total reflux time, water (4.5 ml, 0.25 mol) was added and the mixture refluxed for a further hour. Dean-Stark apparatus was also used to remove the water from the reaction. At 6 hours total reflux time (or when the solution reaches 110 °C) the mixture was cooled and filtered. The solid was then washed with toluene (170 ml), methanol (170 ml), conc. HCl (0.5 ml in 170 ml distilled water), distilled water (170 ml), methanol (2 × 170 ml) and dried to give a white solid.  $^{13}\text{C}$  CP NMR (MAS)  $\delta_{\text{C}}$ : 15.3 (SiCH<sub>2</sub>), 24.2 (CH<sub>2</sub>S), 29.9 (SCH<sub>2</sub>), 36.3 (C(O)CH<sub>3</sub>), 65.6 (CHNH), and 177.1 ppm (C(O)OH) (NHC(O));  $^{29}\text{Si}$  MAS NMR  $\delta_{\text{Si}}$ : -64.9, -98.4 and -107.8 ppm. Elemental analysis found % Sulfur found 1%.

### Synthesis of silica-*N*-4-methoxybenzyl-*L*-cysteine

This followed the same synthetic procedure as described above to synthesise silica-60-*N*-acetyl-*L*-cysteine, however as *N*-4-methoxybenzyl-*L*-cysteine was not commercially available, this was first synthesised from a procedure as reported by Park and Kim.<sup>2</sup>

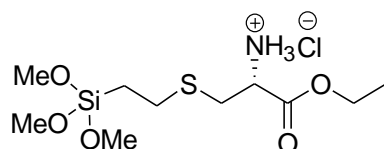


*L*-Cysteine (10.53 g, 0.087 mol) and methanol (100 mL) were placed into a round bottom flask. To this was added para-anisaldehyde (11.05 mL, 0.091 mol) and sodium cyanoborohydride (5.45g, 0.087 mol). The reaction was left to stir at room temperature for five days. The product was then filtered off, washed with methanol (2 x 20 mL), ether (20 mL) and then dried under vacuum to give *N*-4-methoxybenzyl-*L*-cysteine (10.98 g, 47 %). m.p 209-211 °C (lit. 212-213 °C). IR (neat)  $\nu$  (cm<sup>-1</sup>) 801, 1596 and 2568, 3430;  $^1\text{H}$  NMR (D<sub>2</sub>O, 270 MHz)  $\delta_{\text{H}}$ : 2.87 (2H, dd,  $J = 2.9, 8.4$ , HSCH<sub>2</sub>), 3.33 (1H, m, CH<sub>2</sub>CHNH), 4.00 (2H, m, NHCH<sub>2</sub>), 7.5-7.87 (4H, m, Ar *H*'s (AA'BB' system));  $^{13}\text{C}$  NMR (D<sub>2</sub>O, 270 MHz)  $\delta_{\text{C}}$ : 23.1 (HSCH<sub>2</sub>), 49.9 (CHNH), 55.6(OCH<sub>3</sub>), 59.9 (CH<sub>2</sub>NH), 114.8(Ar C x 2), 122.4 (Ar C x 2),

132.1 (Ar C), 160.1 (Ar C), 169.3 (C(O)OH). Assignments were in agreement with those reported in literature.

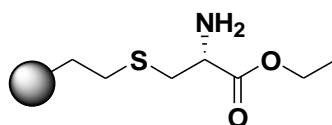
The next step involved the synthesis of S-(2-trimethoxysilylethyl)-N-4-methoxybenzyl-L-cysteine. This was carried out following the same procedure described above to prepare S-2-(trimethoxysilylethyl)-N-acetyl-L-cysteine. Due to the high viscosity of the reaction mixture it was difficult to monitor by  $^1\text{H}$  NMR. Unfortunately using this method solid state  $^{13}\text{C}$  CP NMR of **silica-60-N-4-methoxybenzyl-L-cysteine** revealed a large proportion of vinyl peaks to be present. Thus a new synthetic procedure was followed as described below.

### Synthesis of S-(2-trimethoxysilylethyl)-L-cysteine methyl ester hydrochloride



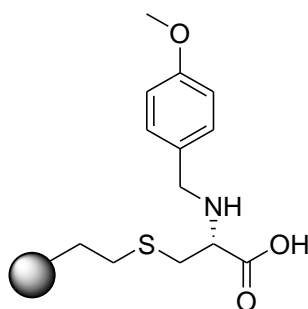
Into a 2 neck 50 mL round-bottomed flask equipped with reflux condenser was added L-cysteine hydrochloride (8.06 g, 0.043 mol) and *p*-xylene (8 ml). The mixture was heated to 118-120 °C. The addition funnel was charged with trimethoxyvinylsilane (4.59 g, 4.75 mL, 0.031 mol) and di-*tert*-butyl peroxide (2 ml) and the charge added dropwise over 15 minutes whilst maintaining reflux. The mixture was heated to 123-125 °C (at this point the cysteine is molten and solution looks homogeneous and clear) for a further 4 hours at this temperature whilst adding di *tert*-butyl peroxide every 90 minutes (4 ml in total) and then cooled. A cloudy orange solution is obtained. The reaction product was further dissolved in methanol (30 ml) obtaining a clear solution. The progress of the addition reaction was monitored by the consumption of vinyl trimethoxysilane (vinyl peaks at 5.8-6.0 ppm in the  $^1\text{H}$ -NMR run in  $\text{CDCl}_3$ ).  $^1\text{H}$  NMR ( $\text{CDCl}_3$ , 270 MHz)  $\delta_{\text{H}}$ : 1.06 (2H, m,  $\text{SiCH}_2$ ), 1.25 (3H, t,  $J = 7.3$ ,  $\text{CH}_2\text{CH}_3$ ), 2.63 (2H, m,  $\text{CH}_2\text{SCH}_2$ ), 3.13 (2H, m,  $\text{CH}_2\text{SCH}_2$ ), 3.42 (2H, m,  $\text{CH}_2\text{CH}_3$ ), 3.49 (9H, s, 3 x  $\text{OCH}_3$ ), 4.19 (1H, m,  $J = 5, 12$  Hz,  $\text{CHNH}_3$ ), 8.8 (3H, b s,  $\text{NH}_2$ ).

### Synthesis of silica-60-cysteine ethyl ester



Into a 150 mL 3 neck round-bottomed flask equipped with reflux condenser, overhead stirrer and thermometer was added S-trimethoxysilylethyl-*L*-cysteine methyl ester hydrochloride (as prepared above) and toluene (50 mL). To this stirring mixture was then added silica (15.41 g, 60 Å, 60-200 µm, Grace) and the mixture was refluxed for 2 hours at 68 °C. Methanol (45 mL) was then collected from the reaction *via* Dean-Stark apparatus during which a rise in the head temperature was observed from 68 °C to 110 °C. The total reflux time was 4 hours after which, the mixture was cooled to room temperature and then the solid washed with methanol (2 × 200 mL) and then water (2 × 200 mL). The material was then added to a solution 0.35 M NaOH and stirred for 20 minutes; final pH 9.8. The material was washed with water (2 × 200 mL) then methanol (2 × 200 mL) and dried, to give silica-60-*L*-cysteine ethyl ester with final weight 20.22 g (20.18 % mass increase). After titration with 0.2 M HCl, (14.5 mL) a loading of 1.16 mmol/g was found. <sup>1</sup>H NMR (NaOD/ D<sub>2</sub>O) δ<sub>H</sub>: 0.48 (2H, m, SiCH<sub>2</sub>), 0.87 (3H, m, CH<sub>2</sub>CH<sub>3</sub>), 2.32-2.50 (4H, m, CH<sub>2</sub>SCH<sub>2</sub>), 3.09 (1H, m, CHNH), 3.38 (2H, m, CH<sub>2</sub>CH<sub>3</sub>).

### Synthesis of silica-60-*N*-4-methoxybenzyl-*L*-cysteine



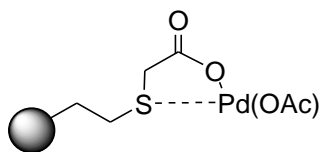
The synthesis of **silica-60-*N*-4-methoxybenzyl-*L*-cysteine** was carried out in two steps.

Step 1 Alkylation of silica-60-*L*-cysteine-ethyl ester: Into a 250 mL 3 neck round-bottomed flask equipped with reflux condenser, overhead stirrer and thermometer was added silica-60-*L*-cysteine ethyl ester (10.84 g, 0.011 mol), toluene (80 mL) and 4-methoxybenzyl chloride (6.26 g, 5.5 mL, 0.04 mol). To this stirred mixture was then added sodium iodide (0.0013 mol, 0.2 g.) and triethylamine (0.0287 mol, 4 mL). The mixture was heated at 70 °C for 18

hours. The solution was then cooled and filtered. The material was washed with methanol ( $2 \times 200$  mL) then water ( $2 \times 200$  mL).

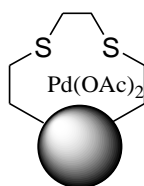
**Step 2 Hydrolysis:** Into 250 mL 3 neck round-bottomed flask equipped with reflux condenser, overhead stirrer and thermometer was added the material from Step 1 and 6M HCl (100 mL). The mixture was refluxed at 108 °C for 4 hours. The material was then washed with water ( $2 \times 200$  mL) and then methanol ( $2 \times 200$  mL) and dried to give **Silica-60-N-4-methoxybenzyl-L-cysteine** with final weight 10.97 g (mass increase 1.2 %). IR (KBr)  $\nu$  474, 810, 1434, 1585, 1656 and 3489  $\text{cm}^{-1}$ ;  $^1\text{H}$  NMR (NaOD/  $\text{D}_2\text{O}$ )  $\delta_{\text{H}}$ : 0.44 (2H, m,  $\text{SiCH}_2$ ), 2.29-2.60 (4H, m,  $\text{CH}_2\text{SCH}_2$ ), 2.87 (2H, m,  $\text{CH}_2\text{CH}$ ), 3.09 (1H, m,  $\text{NHCH}$ ), 3.32 (3H, s,  $\text{OCH}_3$ ), 6.92 (2H, d,  $J = 8.4$ , Ar  $H$ 's) and 7.08 (2H, d,  $J = 8.5$ , Ar  $H$ 's). Ligand loading as calculated from titration 0.8 mmol/g.

#### Synthesis of Silica-60-G<sub>1</sub>-Pd(OAc)



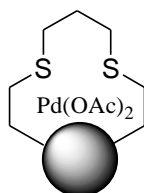
To a stirred solution of **silica-60-G<sub>1</sub>** (1 g) in distilled water (15 mL) was added 1M NaOH dropwise until pH 8.5 was attained. The sodium thioglycolate salt formed was then filtered and washed until the washings were neutral. The solid was further washed with ethanol and ether. The white solid was then dried under vacuum at 120 °C overnight to give a white powder. A portion of this powder (0.5 g) was added to a stirred solution of  $\text{Pd}(\text{OAc})_2$  (0.32 g, 1.4 mmol) in THF (20 mL). The mixture was stirred at room temperature for 24 hours and the orange solid that had formed was filtered from the supernatant. The solid was washed well with THF and  $\text{CH}_2\text{Cl}_2$  and then dried under reduced pressure to give **silica-60-G<sub>1</sub>-Pd(OAc)**. IR (KBr)  $\nu$  472, 810, 964, 1190, 1220, 1440, 1606 and 3400  $\text{cm}^{-1}$ ;  $^{13}\text{C}$  NMR (CP MAS)  $\delta_{\text{C}}$ : 11.2 ( $\text{SiCH}_2$ ), 20.7-23.5 (OAc/  $\text{CH}_2\text{CH}_2\text{S}$ ), 36.5 ( $\text{CH}_2\text{CO}$ ), 181.0 ( $\text{C}=\text{O}$ ); Specific surface area 287.89  $\text{m}^2/\text{g}$ ; Average pore volume 0.347  $\text{cc}/\text{g}$ ; Average pore diameter 47.9 Å; Pd analysis 0.8 mmol/g.

### Synthesis of silica-60-C<sub>2</sub>-Pd(OAc)<sub>2</sub>



To a solution of Pd(OAc)<sub>2</sub> (0.32 g, 0.14 mmol) in CH<sub>2</sub>Cl<sub>2</sub> (20 mL) was added silica-60-C<sub>2</sub> (2g). The mixture was stirred at room temperature for 24 hours and then filtered, washed with CH<sub>2</sub>Cl<sub>2</sub> until the washings were clear and then dried under reduced pressure to give an orange powder, **silica-60-C<sub>2</sub>-Pd(OAc)<sub>2</sub>**. IR (KBr)  $\nu$  472, 819, 1200, 1449, 1620 cm<sup>-1</sup>; <sup>13</sup>C CP NMR (MAS)  $\delta_C$ : 12.3 (SiCH<sub>2</sub>), 17.3 (CH<sub>3</sub>CO), 25.2 (CH<sub>2</sub>S), 38.3 (SCH<sub>2</sub>CH<sub>2</sub>S), 176.6 (C=O); Specific surface area 170.7 m<sup>2</sup>/g; Average pore volume 0.43 cc/g; Average pore diameter 78.6 Å; Pd loading 0.26 mmol/g.

### GP-2.2 General Procedure for Synthesis of Silica-C<sub>3</sub>-Pd(OAc)<sub>2</sub>



To a solution of Pd(OAc)<sub>2</sub> (0.32 g, 0.14 mmol) in CH<sub>2</sub>Cl<sub>2</sub> (20 mL) was added silica-C<sub>3</sub> (2 g). The mixture was stirred at room temperature for 24 hours and then filtered, washed with CH<sub>2</sub>Cl<sub>2</sub> until the washings were clear and then dried under reduced pressure to give an orange powder.

### Synthesis of silica-60-C<sub>3</sub>-Pd(OAc)<sub>2</sub>

Following general procedure **GP-2.2**, silica-60-C<sub>3</sub> was complexed to Pd. IR (KBr)  $\nu$  472, 819, 1200, 1429 cm<sup>-1</sup> and 1647 cm<sup>-1</sup>; <sup>13</sup>C NMR (CP MAS)  $\delta_C$ : 15.2 (SiCH<sub>2</sub>), 26.1 (CH<sub>2</sub>S), 35.5 (SCH<sub>2</sub>CH<sub>2</sub>CH<sub>2</sub>S), 93.7 (CH<sub>3</sub>CO<sub>2</sub>); Specific surface area 319.9 m<sup>2</sup>/g; Average pore volume 0.39 cc/g; Average pore diameter 51.3 Å; Pd loading 0.41 mmol/g

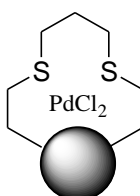
### Synthesis of silica-90-C<sub>3</sub>-Pd(OAc)<sub>2</sub>

Following general procedure **GP-2.2**, **silica-90-C<sub>3</sub>** was complexed to Pd. Specific surface area 278.1 m<sup>2</sup>/g; Average pore volume 0.47 cc/g; Average pore diameter 72.4 Å; Pd loading 0.59 mmol/g.

### Synthesis of silica-150-C<sub>3</sub>-Pd(OAc)<sub>2</sub>

Following general procedure **GP-2.2**, **silica-150-C<sub>3</sub>** was complexed to Pd. Specific surface area 238.2 m<sup>2</sup>/g; Average pore volume 0.71 cc/g; Average pore diameter 137.0 Å; Pd loading 0.54 mmol/g

### Synthesis of silica-60-C<sub>3</sub>-PdCl<sub>2</sub>

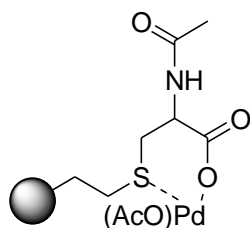


To a stirred solution of PdCl<sub>2</sub> (0.28 g, 1.4 mmol) in methanol (20 mL) was added silica-60-C<sub>3</sub> (2 g) and the mixture left to stir for 24 hours at room temperature. The solid was then separated from the supernatant, washed thoroughly with methanol until the washings were clear and dried under reduced pressure overnight to give a yellow solid, **silica-60-C<sub>3</sub>-PdCl<sub>2</sub>**. Specific surface area 325.8 m<sup>2</sup>/g; Average pore volume 0.43 cc/g; Average pore diameter 89.9 Å; Pd loading 0.48 mmol/g

### GP-2.3 General Procedure for synthesis of Silica-60-*N*-derivatised-*L*-cysteine-Pd(OAc)

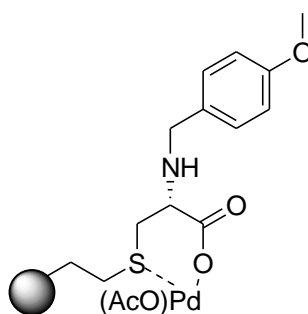
Silica-60-*N*-derivatised-cysteine (1 g) was added to a 1M solution of NaOH (30 mL) and stirred for 15 minutes. The solid was then filtered, washed with methanol and dried under reduced pressure. The material obtained as described above (2 g) was added to a solution of Pd(OAc)<sub>2</sub> (0.32 g, 1.4 mmol) in dichloromethane (20mL) for 24 hours at room temperature. The solid was then filtered and washed with dichloromethane until the washings were clear. The dark orange solid obtained was then dried under reduced pressure for 4 hours.

### Synthesis of silica-60-N-acetyl-L-cysteine-Pd(OAc)



Silica-60-N-acetyl-L-cysteine and Pd(OAc)<sub>2</sub> were reacted together following **GP-2.3**. IR (KBr)  $\nu$  799, 950, 1050, 1210, 1650, 2200, 3400 cm<sup>-1</sup>; <sup>13</sup>C (CP MAS)  $\delta_C$  16.8 (SiCH<sub>2</sub>), 22.4 (CH<sub>2</sub>S), 32.3 (CH<sub>2</sub>CH), 36.6 (C(O)CH<sub>3</sub>), 52.4 (CHNH), 170.6 (C(O)CH<sub>3</sub>), 172.9(CHC(O)); Specific surface area 452.5 m<sup>2</sup>/g, Average pore diameter 65.7 Å; Average pore volume 0.65 cc/g; Pd analysis 0.23 mmol/g.

### Synthesis of silica-60-N-4-methoxybenzyl-cysteine-Pd(OAc)



Silica-60-N-4-methoxybenzyl-L-cysteine and Pd(OAc)<sub>2</sub> were combined following **GP-2.3**. Specific surface area 354.2 m<sup>2</sup>/g, Average pore diameter 82.3 Å; Average pore volume 0.70 cc/g; Pd analysis 0.25 mmol/g.

### General Procedure for Pd Digestion

A solution of silica-ligand-Pd (25 mg) in conc AnalR HNO<sub>3</sub> (7.5 mL) was heated at reflux temperature for 6 hours. The solid was then filtered, washed with deionised water (5 mL) and the filtrates made up to 25 mL with deionised water. Pd content was measured by ICP-OES.



### Comparative Binding studies

- (1) Samples of supported ligand (200 mg, 0.2 mmol) and Pd(OAc)<sub>2</sub> various concentrations (0.06-0.20 mmol) in CH<sub>2</sub>Cl<sub>2</sub> (2 mL) were placed into small vials and stirred at room temperature for 24 hours. After this they were filtered and washed with 2 mL CH<sub>2</sub>Cl<sub>2</sub> or until the washings were clear. The solvent was removed by rotary evaporation and the residue made up to 10 mL with deionised water. The Pd content was thus measured using ICP-OES.
- (2) To a stirred solution of *L*-cysteine (0.32 g, 2.64 mmol) in methanol (5 mL) was added silica-60-C<sub>3</sub>-Pd(OAc)<sub>2</sub> (80 mg, 0.32 mmol) and the solution left to stir at reflux temperature for 24 hours. The solid was then filtered while hot and the Pd content in the filtrate measured by ICP-OES.

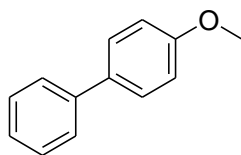
### 6.3 Chapter 3 Experimental

#### GP 3.1 General Procedure for Suzuki-Miyaura reaction at high temperatures

Into a small round bottom flask was added phenyl boronic acid (0.18 g, 1.5 mmol), aryl halide (1.0 mmol), K<sub>2</sub>CO<sub>3</sub> (0.21 g, 2.0 mmol) and *o*-xylene (4 mL). The flask was equipped with a reflux condenser and the mixture stirred. To this stirred solution was then added **silica-60-G<sub>1</sub>-Pd(OAc)** (60 mg, 0.8 mmol/g Pd, 5 mol % Pd) or **silica-60-C<sub>2</sub>-Pd(OAc)<sub>2</sub>** (50 mg, 0.3 mmol/g Pd, 1.3 mol % Pd) or **silica-60-C<sub>3</sub>-Pd(OAc)<sub>2</sub>** (50 mg, 0.4 mmol/g Pd, 2.1 mol % Pd) and the reaction heated to 90 °C and stirred for the required time. The reaction was monitored by <sup>1</sup>H NMR or GC-MS. For recycles, the catalyst was filtered, washed with solvent and then re-used.

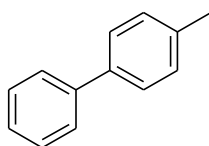
For leaching tests, catalyst was removed from the reaction mixture by filtering the hot solution after 3 hours reaction time. The filtered solution was then added to a new clean flask equipped with a new stirrer bar. To this was added fresh base and the reaction was heated to 90 °C and continued to stir at this temperature for a further 3 hours and monitored by <sup>1</sup>H NMR or GC-MS.

### Synthesis of 4-methoxybiphenyl



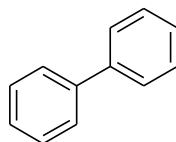
4-Bromoanisole (0.13 mL, 1.0 mmol) and phenyl boronic acid (0.18 g, 1.5 mmol) were combined following **GP 3.1**.  $^1\text{H NMR}$  ( $\text{CDCl}_3$ )  $\delta_{\text{H}}$ : 3.84 (3H, s,  $\text{OCH}_3$ ), 6.98 (2H, d,  $J = 9.4$ , Ar  $H$ 's), 7.25- 7.51 (7H, m, Ar  $H$ 's). % conversion was determined by  $^1\text{H NMR}$  (Cycle 1, 2 and 3; 99, 99 and 90 % conversion).

### Synthesis of 4-methylbiphenyl



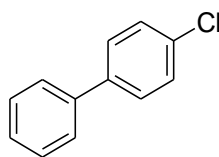
4-Bromotoluene (0.17 g, 1.0 mmol) and phenyl boronic acid (0.18 g, 1.5 mmol) were combined following **GP 3.1**.  $^1\text{H NMR}$  ( $\text{CDCl}_3$ )  $\delta_{\text{H}}$ : 2.41 (3H, s,  $\text{CH}_3$ ), 6.98 (2H, d,  $J = 10.8$ , Ar  $H$ 's), 7.44-7.59 (9H, m, Ar  $H$ 's). % conversion was determined by  $^1\text{H NMR}$  (Cycle 1, 2 and 3; 99, 90 and 90 % conversion).

### Synthesis of Biphenyl



4-Bromobenzene (0.16 g, 1.0 mmol) and phenyl boronic acid (0.18 g, 1.5 mmol) were combined following **GP 3.1**.  $^1\text{H NMR}$  ( $\text{CDCl}_3$ )  $\delta_{\text{H}}$ : 7.13-7.68 (10H, m, Ar  $H$ 's). % conversion was determined by GC (Cycle 1, 2 and 3; 99, 99 and 90 % conversion).

### Synthesis of 4-chlorobiphenyl



4-Bromochlorobenzene (0.19 g, 1.0 mmol) and phenyl boronic acid (0.18 g, 1.5 mmol) were combined following **GP 3.1**.  $^1\text{H}$  NMR ( $\text{CDCl}_3$ )  $\delta_{\text{H}}$ : 7.25-7.55 (9H, m, Ar  $H$ 's). % conversion was determined by GC (Cycle 1, 2 and 3; 97, 90 and 90 % conversion).

#### GP 3.2 General conditions for Suzuki-Miyaura reaction at room temperature

Into a small round bottom flask was added phenyl boronic acid (0.18 g, 1.5 mmol), aryl halide (1.0 mmol),  $\text{NaO}^t\text{Bu}$  (0.12 g, 1.5 mmol) and isopropanol (4 mL). To this stirred solution was next added either **silica-60-G<sub>1</sub>-Pd(OAc)** (60 mg, 0.8 mmol/g Pd, 5 mol % Pd), **silica-60-C<sub>2</sub>-Pd(OAc)<sub>2</sub>** (100 mg, 0.3 mmol/g Pd, 3 mol % Pd) or **silica-60-C<sub>3</sub>-Pd(OAc)<sub>2</sub>** (70 mg, 0.4 mmol/g, 3 mol % Pd) and the reaction stirred at room temperature for the required time. The reaction was monitored by  $^1\text{H}$  NMR. For recycles, the catalyst was filtered, washed with isopropanol and then added to the new reaction mixture. For leaching tests, the catalyst was removed after 3 hours by filtration and the filtrate added to a new reaction flask equipped with a new stirrer bar. To this was added fresh base and the reaction continued at room temperature for a further 3 hours. The  $^1\text{H}$  NMR for biphenyl, 4-chlorobiphenyl, 4-methoxybiphenyl and 4-methylbiphenyl is reported in experimental **GP 3.1** (above).

#### Synthesis of silica-60-C<sub>3</sub> with low Pd loading

To a stirred solution of  $\text{Pd}(\text{OAc})_2$  (0.16 g, 0.7 mmol) in  $\text{CH}_2\text{Cl}_2$  (20 mL) was added **silica-60-C<sub>3</sub>** (2 g). The mixture was left to stir at room temperature for 24 hours and then the solid was filtered, washed with  $\text{CH}_2\text{Cl}_2$  until the washings were clear. The solid formed was then dried under reduced pressure to give a yellow powder (2.06 g); Pd loading 0.23 mmol/g.

### Preparation of samples for TEM analysis

A sample (0.01 g) was immersed into ethanol (10 mL) and the resulting mixture placed in a sonicator bath for 10 minutes. The copper grids were then dipped into the dispersion and the grids left to dry. Prior to analysis on the TEM machine the sample loaded grids were coated with carbon to prevent drifting of material during analysis.

### Synthesis of silica-60-C<sub>3</sub>-Co(OAc)<sub>2</sub>

To a stirred solution of Co(OAc)<sub>2</sub> (0.35 g, 1.4 mmol) in THF (20 mL) was added **silica-60-C<sub>3</sub>** (2 g) and the reaction left to stir at room temperature for 24 hours. The solid was then filtered and washed thoroughly with methanol before being dried under reduced pressure to give an aqua marine coloured solid (2.06 g).

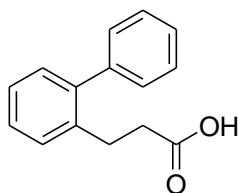
### Synthesis of silica-60-C<sub>3</sub>-Ni(OAc)<sub>2</sub>

To a stirred solution of Ni(OAc)<sub>2</sub> (0.35 g, 1.4 mmol) in CH<sub>2</sub>Cl<sub>2</sub> (20 mL) was added **silica-60-C<sub>3</sub>** (2 g) and the reaction left to stir at room temperature for 24 hours. The solid was then filtered and washed thoroughly with methanol before being dried under reduced pressure to give pink coloured solid (2.10 g).

### GP-3.3 General procedure for microwave-assisted reactions at room temperature

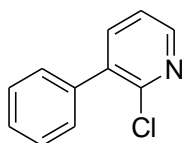
Into a microwave reaction vessel was added was added aryl bromide (1.0 mmol), phenyl boronic acid (0.18 g, 1.5 mmol), NaO<sup>t</sup>Bu (0.122 g, 1.2 mmol), **silica-60-C<sub>3</sub>-Pd(OAc)<sub>2</sub>** (30 mg, 0.4 mmol/g Pd, 1.2 mol % Pd) and isopropanol (4 mL). The flask was then sealed and placed in a microwave reactor and set up for 6 minutes microwave reaction time and heated to 140 °C. The samples were subsequently analysed by <sup>1</sup>H NMR. The <sup>1</sup>H NMR for cross coupled products biphenyl, 4-chlorobiphenyl, 4-methoxybiphenyl and 4-methylbiphenyl has been reported under Experimental section **GP 3.1**.

### Synthesis of 3-(biphen-2-yl) propionic acid



2-Propionic-phenyl boronic acid (0.30 g, 1.5 mmol) and bromobenzene (0.16 g, 1.0 mmol) were combined following **GP-3.3**.  $^1\text{H}$  NMR ( $\text{CDCl}_3$ , 270 MHz)  $\delta_{\text{H}}$ : 2.56 (2H, t,  $J = 7.3$ ,  $\text{CH}_2\text{C}(\text{O})$ ), 2.87 (2H, t,  $J = 7.3$ ,  $\text{CH}_2\text{CH}_2\text{C}(\text{O})$ ), 7.36 – 7.18 (3H, m, Ar  $H$ 's) and 7.22-7.35 (6H, m, Ar  $H$ 's). % conversion determined by GC-MS (cycle 1: 74 % conversion).

### Synthesis of 2-chloro-3-phenyl-pyridine



2-Chloro-3-boronic acid pyridine (0.30 g, 1.5 mmol) and bromobenzene (0.16 g, 1.0 mmol) were combined following **GP-3.3**.  $^1\text{H}$  NMR ( $\text{CDCl}_3$ , 270 MHz)  $\delta_{\text{H}}$ : 7.21-7.40 (5H, m, Ar  $H$ 's), 7.86 (1H, m, 5- $H$ ), 8.27 (1H, d,  $J = 7.2$ , 6- $H$ ), 8.52 (1H, d,  $J = 7.6$ , 4- $H$ ). % conversion determined by GC-MS (cycle 1: 64 % conversion).

### Suzuki-Miyaura reaction with silica-60- $\text{C}_3$ - $\text{Pd}(\eta^3\text{-allyl})\text{chloride}$

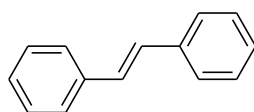
Into a round bottom flask was added phenyl boronic acid (0.18 g, 1.5 mmol), bromotoluene (0.17 g, 1.0 mmol),  $\text{NaO}^t\text{Bu}$  (0.12 g, 1.2 mmol), **silica-60- $\text{C}_3$ -  $\text{Pd}(\eta^3\text{-allyl})\text{chloride}$**  (70 mg, 0.4 mmol/g Pd, 4 mol % Pd) and isopropanol (4 mL). The reaction mixture was then stirred at room temperature for 6 hours and monitored by  $^1\text{H}$  NMR (cycle 1: 3 % conversion).

### GP-3.4 General Procedure for Mizoroki-Heck reaction

Into a round bottom flask was added styrene (0.19 mL, 1.5 mmol), aryl halide (1 mmol),  $K_2CO_3$  (0.22 g, 1.5 mmol), *N*-methylpyrrolidone (NMP) (5 mL) and catalyst (5 mol %, 100 mg silica-60-C<sub>3</sub>-PdCl<sub>2</sub>/ silica-60-C<sub>3</sub>-Pd(dba)/ silica-60-C<sub>3</sub>-PdCl<sub>2</sub> or 120 mg silica-60-C<sub>3</sub>-Pd(OAc)<sub>2</sub>). The flask was equipped with a reflux condenser and the reaction mixture heated to 110 °C and stirred for a further 24 hours at this temperature. The catalyst was then filtered and the filtrate diluted with water (5 mL) and extracted with petroleum ether (40-60 °C) (10 mL) and subsequently the organic layer was washed with water (3 x 5 mL). The combined organic layers were then dried over  $Na_2SO_4$  and the solvent removed under reduced pressure. The resulting residue was analysed by GC or <sup>1</sup>H NMR.

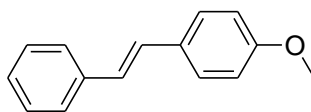
Recycles were performed by washing the filtered catalyst with NMP (5 mL) before its re-use. Leaching tests were carried out by filtering the catalyst after 10 hours, transferring the filtrate to a new clean round bottom flask equipped with a new clean magnetic stirrer bar. To this was then added fresh base (0.22 g) and the reaction continued with stirring at the reflux temperature (110 °C) for a further 10 hours. The reaction was taken through an aqueous work up as described above with petroleum ether (40-60 °C) to extract the organic layers. % conversion was determined by <sup>1</sup>H NMR or GC.

#### Synthesis of trans-stilbene



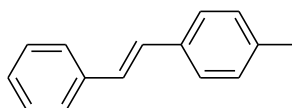
4-Bromobenzene (0.16 g, 1.0 mmol) and styrene (0.17 mL, 1.5 mmol), were combined according to GP-3.4. <sup>1</sup>H NMR ( $CDCl_3$ , 270 MHz)  $\delta_H$ : 7.15 (2H, s, *HC=CH*), 7.25-7.63 (10H, m, *Ar-H*). % conversion determined by GC (cycle 1, 2 and 3: 81, 81 and 79 % conversion).

### Synthesis of 4-methoxy stilbene



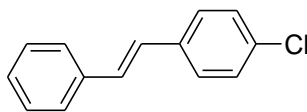
4-Bromoanisole (0.13 mL, 1.0 mmol) and styrene (0.17 mL, 1.5 mmol) were combined following **GP-3.4**.  $^1\text{H NMR}$  ( $\text{CDCl}_3$ , 270 MHz)  $\delta_{\text{H}}$ : 3.85 (3H, s,  $\text{OCH}_3$ ), 6.87 (2H, 'd', ' $J$ ' = 11.3, Ar H's), 6.98 (1H, d,  $J_{A-B}$  = 5,  $\text{HC}=\text{C}$ ), 7.04 (1H, d,  $J_{A-B}$  = 5,  $\text{HC}=\text{C}$ ), 7.30-7.55 (7H, m, Ar H's). % conversion determined by  $^1\text{H NMR}$  (cycle 1, 2 and 3: 79, 77 and 77 % conversion).

### Synthesis of 4-methyl stilbene



4-Bromotoluene (0.17 g, 1.0 mmol) and styrene (0.17 mL, 1.5 mmol), were combined according to **GP-3.4**.  $^1\text{H NMR}$  ( $\text{CDCl}_3$ )  $\delta_{\text{H}}$ : 2.36 (3H, s,  $\text{CH}_3$ ), 7.05 (2H, 'd', ' $J$ ' = 8.3, Ar H's), 7.13 (1H, d,  $J_{A-B}$  = 5,  $\text{HC}=\text{C}$ ), 7.18 (1H, d,  $J_{A-B}$  = 5,  $\text{HC}=\text{C}$ ), 7.23-7.55 (7H, m, Ar H). % conversion determined by  $^1\text{H NMR}$  (cycle 1, 2 and 3: 84, 85, 85%).

### Synthesis of 4-chloro stilbene

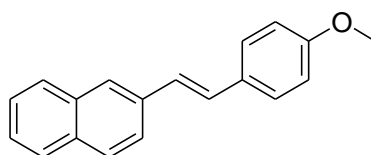


4-Bromochlorotoluene (0.19 g, 1.0 mmol) and styrene (0.17 mL, 1.5 mmol), were combined according to **GP-3.4**.  $^1\text{H NMR}$  ( $\text{CDCl}_3$ )  $\delta_{\text{H}}$ : 7.22 (1H, d,  $J_{A-B}$  = 5,  $\text{HC}=\text{C}$ ), 7.25 (1H, d,  $J_{A-B}$  = 5,  $\text{HC}=\text{C}$ ), 7.30-7.61 (9H, m, Ar H). % conversion determined by GC (cycle 1, 2 and 3: 67, 68, 65 % conversion).

### GP-3.5 General Procedure for Microwave assisted Mizoroki-Heck reactions with silica-60-C<sub>3</sub>-PdCl<sub>2</sub>

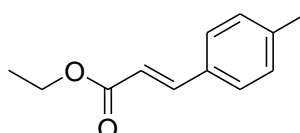
Into a small reactor flask was added styrene (0.19 mL, 1.5 mmol), aryl halide (1 mmol), K<sub>2</sub>CO<sub>3</sub> (0.22 g, 1.5 mmol), *N*-methylpyrrolidone (NMP) (5 mL) and catalyst (3 mol %, 70 mg). The flask was then sealed and placed in a microwave reactor and the heated to 200 °C for 20 minutes under microwave conditions (power level 400W). The catalyst was then filtered and the filtrate diluted with water (5 mL) and extracted with petroleum ether (40-60 °C) (10 mL) and subsequently the organic layer was washed with water (3 x 5 mL). The combined organic layers were then dried over Na<sub>2</sub>SO<sub>4</sub> and the solvent removed under reduced pressure. The resulting residue was monitored by GC or <sup>1</sup>H NMR. The <sup>1</sup>H NMR for 1-methoxy-4-styryl benzene has been reported in experimental **GP-3.4**.

#### Synthesis of 2-[2-(4-methoxy-phenyl)-vinyl]-naphthalene



2-Vinyl-naphthylene (0.23 g, 1.5 mmol) and 4-bromoanisole (0.13 mL, 1.0 mmol) were combined following **GP-3.5**. <sup>1</sup>H NMR (CDCl<sub>3</sub>, 270 MHz) δ<sub>H</sub>: 3.85 (3H, s, OCH<sub>3</sub>), 6.88 (2H, d, *J* = 10.9, Ar H's), 6.98 (1H, d, *J*<sub>A-B</sub> = 5.0, HC=), 7.03 (1H, d, *J*<sub>A-B</sub> = 5.0, HC=), 7.34-7.65 (9H, m, Ar H's). % conversion was determined by GC-MS (cycle 1: 98 % conversion).

#### Synthesis of 3-*p*-Tolyl-acrylic acid ethyl ester

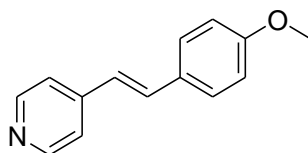


Acrylic acid ethyl ester (0.15 g, 1.5 mmol) and bromotoluene (0.17 g, 1.0 mmol) were combined according to **GP-3.5**. <sup>1</sup>H NMR (CDCl<sub>3</sub>, 270 MHz) δ<sub>H</sub>: 1.36 (3H, t, *J* = 7.5, CH<sub>2</sub>CH<sub>3</sub>), 2.38 (3H, s, CH<sub>3</sub>), 4.23 (2H, q, *J* = 7.4, CH<sub>2</sub>CH<sub>3</sub>), 6.32 (1H, d, *J* = 7.3, HC=CHAr),



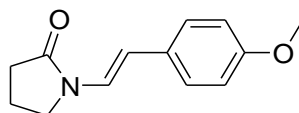
6.69 (1H, d,  $J = 9.4$ , HC=CHAr), 7.03 (2H, m, Ar H's), 7.14 (2H, m, Ar H's). % conversion was determined by GC-MS (cycle 1: 99 % conversion).

### Synthesis of 4-[2-(4-methoxy-phenyl)-vinyl]-pyridine



4-Bromoanisole (0.13 mL, 1.0 mmol) and 4-vinylpyridine (0.24 g, 1.5 mmol) were combined according to **GP-3.5**. <sup>1</sup>H NMR (CDCl<sub>3</sub>)  $\delta_{\text{H}}$ : 3.84 (3H, s, OCH<sub>3</sub>), 6.88 (2H, d,  $J = 10.6$ , Ar H's), 6.98 (1H, d,  $J_{A-B} = 5$ , HC=), 7.04 (1H, d,  $J_{A-B} = 5$ , HC=), 7.30-7.85 (8H, m, Ar H's). % conversion was determined by GC-MS (cycle 1: 76 % conversion).

### Synthesis of 1-[2-(4-methoxy-phenyl)-vinyl]-pyrrolidin-2-one



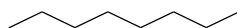
4-bromoanisole (0.13 mL, 1.0 mmol) and 1-vinylpyrrolidin-2-one (0.17 g, 1.5 mmol) were combined according to **GP-3.5**. <sup>1</sup>H NMR (CDCl<sub>3</sub>, 270 MHz)  $\delta_{\text{H}}$ : 2.13 (2H, m, CH<sub>2</sub>CH<sub>2</sub>C(O)), 2.26 (2H, t,  $J = 7.5$ , CH<sub>2</sub>C(O)), 3.49 (2H, t,  $J = 7.0$ , CH<sub>2</sub>N) 3.84 (3H, s, OCH<sub>3</sub>), 6.65 (1H, d,  $J = 8$ , NHC=CH), 7.05 (1H, d,  $J = 8$ , NCH=CH), 7.18 (2H, d, ' $J$ ' = 10.3, Ar H's), 7.23 (2H, d, ' $J$ ' = 7.2, Ar H's). % conversion was determined by GC-MS (cycle 1: 75 % conversion).

## 6.4 Chapter 4 Experimental

### GP-4.1 General Procedure for hydrogenations with catalyst silica-60-C<sub>3</sub>-Pd(OAc)<sub>2</sub>

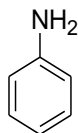
Into a small conical flask was added unsaturated substrate (10 mmol) and methanol (30 mL). To this stirred solution was then added **silica-60-C<sub>3</sub>-Pd(OAc)<sub>2</sub>** (20-100 mg, 0.4 mmol/g Pd, 0.1-0.5 mol % Pd) and the flask covered with a watch glass and transferred to a autoclave reactor. The vessel was then purged with nitrogen three times and then purged with hydrogen before being pressurized at the desired pressure. If heating the reaction mixture was required, the autoclave was positioned in to an oil bath set at the desired temperature. After the given reaction time, reaction was allowed to cool if need be, and the solid filtered. Solvent was removed by rotary evaporation and the residue analysed by <sup>1</sup>H NMR and GC.

### Synthesis of Octane



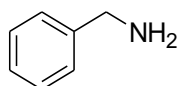
Hydrogenation of 1-octene (1 mL, 10.0 mmol) following **GP-4.1**; <sup>1</sup>H NMR (CDCl<sub>3</sub>, 270 MHz) δ<sub>H</sub>: 0.95 (6H, t, *J* = 8.5, 2 x CH<sub>3</sub>), 1.29 (8H, m, 4 x CH<sub>2</sub>), 1.33 (4H, m, 2 x CH<sub>2</sub>CH<sub>3</sub>). % conversion determined by GC (cycle 1, 2, 3, 4, 5, 6 and 7: 99, 99, 99, 99, 99, 99 and 95 % conversion).

### Synthesis of Aniline



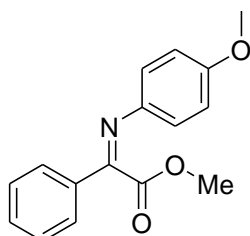
Hydrogenation of nitrobenzene (1 mL, 10.0 mmol) following **GP-4.1**; <sup>1</sup>H NMR (CDCl<sub>3</sub>) δ<sub>H</sub>: 3.90 (2H, broad s, NH<sub>2</sub>), 6.45-6.60 (3H, m, Ar H's), 7.01 (2H, m, Ar H's). % conversion determined by GC (cycle 1, 2, 3, 4, 5 and 6: 99, 99, 99, 99, 99 and 87 % conversion).

### Synthesis of Benzylamine

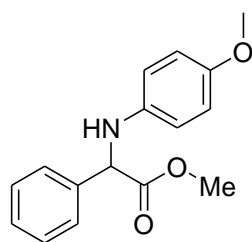


Hydrogenation of benzonitrile (1 mL, 10.0 mmol) following **GP-4.1**;  $^1\text{H}$  NMR ( $\text{CDCl}_3$ )  $\delta_{\text{H}}$ : 3.65 (2H, broad s,  $\text{NH}_2$ ), 3.90 (2H, s,  $\text{CH}_2$ ), 7.04-7.14 (5H, m, Ar H's). % conversion determined by GC (cycle 1, 2 and 3: 99.98 and 97 % conversion).

### Synthesis of 1-(4-methoxyphenylimino)-1-phenyl-acetic acid methyl ester



Into a round bottomed 100 mL flask was added *para*-anisidine (1.35 g, 11 mmol) and benzene (15 mL). To this solution was then added methyl benzoylformate (1.50 mL, 10.6 mmol) and *p*-toluenesulfonic acid (95 mg, 0.5 mmol). The reaction mixture was then heated at the reflux temperature (100 °C) for 20 hours with azeotropic removal of water. The solvent was then evaporated and the residue was purified by flash column chromatography (ethyl acetate/hexane = 1/10) to give a yellow oil which solidified on standing (2.65 g, 65 %). [Observations: crystallisation of product occurs during flash column chromatography therefore the polarity of the eluent had to be increased in order to elute more product. (ethyl acetate/ petrol (40-60) 1/5) and then increased to ethyl acetate/ petrol (40-60) 5/1.]  $^1\text{H}$  NMR ( $\text{CDCl}_3$ )  $\delta_{\text{H}}$ : 3.67 (3H, s,  $\text{C}(\text{O})\text{OCH}_3$ ), 3.84 (3H, s,  $\text{OCH}_3$ ), 6.81 (2H, d, ' $J$ ' = 10.5, Ar H's, AA'BB' system), 7.21-7.38 (7H, m, Ar H's);  $^{13}\text{C}$  NMR ( $\text{CDCl}_3$ )  $\delta_{\text{C}}$ : 54.11 ( $\text{CO}_2\text{CH}_3$ ), 56.3 ( $\text{OCH}_3$ ), 114.1 (Ar C's), 130.3 (Ar C's), 128.4 (Ar C's), 129.6 (Ar C's), 130.8 (Ar C), 137.1 (Ar C), 156.9 ( $\text{C}(\text{O})\text{CN}$ ), 164.4 ( $\text{C}(\text{O})\text{CN}$ ). Assignments were in agreement with literature reports.<sup>3</sup>

**Synthesis of 1-(4-methoxyphenylamino)-1-phenyl-acetic acid methyl ester**

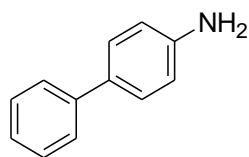
Hydrogenation of (4-methoxy-phenylimino)-phenyl-acetic acid methyl ester followed procedure **GP-4.1**;  $^1\text{H NMR}$  ( $\text{CDCl}_3$ )  $\delta_{\text{H}}$ : 3.57 (3H, s,  $\text{C(O)OCH}_3$ ), 3.63 (3H, s,  $\text{OCH}_3$ ), 4.74 (1H, s,  $\text{CHNH}$ ), 6.92 (2H, d, ' $J$ ' = 10.5, Ar H's, (AA'BB' system)), 7.18-7.32 (7H, m, Ar H's);  $^{13}\text{C NMR}$  ( $\text{CDCl}_3$ )  $\delta_{\text{C}}$ : 53.2 ( $\text{CO}_2\text{CH}_3$ ), 55.1 ( $\text{OCH}_3$ ), 67.6 ( $\text{C(O)CN}$ ), 112.2 (Ar C's), 126.3 (Ar C's), 134.7 (Ar C), 166.2 ( $\text{C(O)CN}$ ).

**G.P 4.2 General procedure for room temperature cross-coupling and hydrogenation catalysed by silica-60-C<sub>3</sub>-Pd(OAc)<sub>2</sub>**

To a small conical flask was added nitro-substituted aryl bromide (10 mmol), phenyl boronic acid (0.18 g, 1.5 mmol),  $\text{NaO}^t\text{Bu}$  (0.12 g, 1.2 mmol), **silica-60-C<sub>3</sub>-Pd(OAc)<sub>2</sub>** (70 mg, 0.4 mmol/g, 3 mol % Pd) and isopropanol (4 mL). This was then covered with a watch glass and placed in an autoclave and then purged with nitrogen thrice and then hydrogen twice and the reaction mixture left to stir at room temperature for 6 hours. The catalyst was then removed from the reaction mixture by filtration. Solvent was then removed from the filtrate by rotary evaporation and the residue analysed by  $^1\text{H NMR}$  ( $\text{CDCl}_3$ ) and GC.

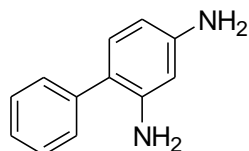
Recycles were carried out by removal of the **silica-60-C<sub>3</sub>-Pd(OAc)<sub>2</sub>** from the reaction mixture by filtration, the catalyst was then washed with isopropanol and placed in the new reaction mixture.

### Synthesis of Biphenyl-4-amine



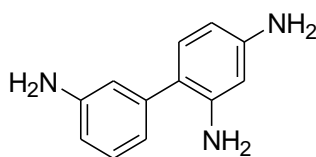
The reaction of phenyl boronic acid (0.18 g, 1.5 mmol) and 4-nitrobromobenzene (0.18 g, 1.0 mmol) followed **GP 4.2**.  $^1\text{H}$  NMR ( $\text{CDCl}_3$ , 270 MHz)  $\delta_{\text{H}}$ : 3.92 (2H, bs,  $\text{NH}_2$ ), 6.49 (4H, m, Ar  $H$ 's), 6.88 (5H, m, Ar  $H$ 's). % conversion determined by GC (% conversion cycle 1, 2 and 3: 99, 99 and 95%)

### Synthesis of Biphenyl-2,4-diamine



The reaction of phenyl boronic acid (0.18 g, 1.5 mmol) and 2,4-dinitrobromobenzene (0.25 g, 1.0 mmol) followed **GP 4.2**.  $^1\text{H}$  NMR ( $\text{CDCl}_3$ , 270 MHz)  $\delta_{\text{H}}$ : 3.93 (4H, broad s, 2 x  $\text{NH}_2$ ), 6.72-6.88 (2H, m, Ar  $H$ 's), 6.98 (1H, m, Aromatic  $H$ ), 7.22-7.48 (5H, m, Ar  $H$ 's). % conversion determined by GC (% conversion cycle 1: 94%).

### Synthesis of Biphenyl-2,4,3'-triamine

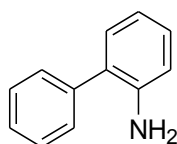


The reaction of 3-nitrophenyl boronic acid (0.25 g, 1.5 mmol) and 2,4-dinitrobromobenzene (0.25 g, 1.0 mmol) followed **GP 4.2**.  $^1\text{H}$  NMR ( $\text{CDCl}_3$ , 270 MHz)  $\delta_{\text{H}}$ : 3.97 (6H, broad s, 3 x  $\text{NH}_2$ ), 6.48 (1H, s, Ar  $H$ ), 6.86-6.88 (2H, m, Ar  $H$ 's), 6.97-7.08 (4H, m, Ar  $H$ 's). % conversion determined by GC (% conversion cycle 1: 84%).

### GP-4.3 Microwave-assisted cross-coupling and hydrogenation catalysed by silica-60-C<sub>3</sub>-Pd(OAc)<sub>2</sub>

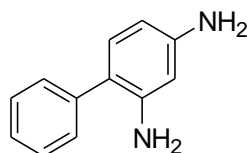
Into a reaction vessel was added was added aryl bromide (1.0 mmol), phenyl boronic acid (0.18 g, 1.5 mmol), NaO<sup>t</sup>Bu (0.122 g, 1.2 mmol), **silica-60-C<sub>3</sub>-Pd(OAc)<sub>2</sub>** (70 mg, 0.4 mmol/g Pd, 3 mol % Pd) and isopropanol (4 mL). Via the flask seal was also attached a balloon of hydrogen. The flask was then sealed and placed in a microwave reactor and set up for 6 minutes microwave reaction time and heated to 140 °C. The samples were subsequently analysed by <sup>1</sup>H NMR. The <sup>1</sup>H NMR for cross coupled products biphenyl, 4-chloro biphenyl, 4-methoxy biphenyl and 4-methyl biphenyl has been reported under Experimental section **GP-3.1**.

#### Synthesis of Biphenyl-2-ylamine



The reaction of phenyl boronic acid (0.18 g, 1.5 mmol) and 2-nitrobromobenzene (0.18 g, 1.0 mmol) followed **GP-4.3**. <sup>1</sup>H NMR (CDCl<sub>3</sub>, 270 MHz) δ<sub>H</sub>: 3.92 (2H, bs, NH<sub>2</sub>), 6.64 – 6.87 (3H, m, Ar H's), 7.27 (2H, m, Ar H's), 7.35-7.41 (4H, m, Ar H's). % conversion determined by GC-MS (% conversion cycle 1: 99%).

#### Synthesis of Biphenyl-2,4-diamine



The reaction of phenyl boronic acid (0.18 g, 1.5 mmol) and 2-nitrobromobenzene (0.18 g, 1.0 mmol) followed **GP-4.3**. <sup>1</sup>H NMR (CDCl<sub>3</sub>, 270 MHz) δ<sub>H</sub>: 3.97 (4H, broad s, 2 x NH<sub>2</sub>), 6.72-6.88 (2H, m, Ar H's), 6.98 (1H, m, Ar H), 7.22-7.48 (5H, m, Ar H's). % conversion determined by GC-MS (% conversion cycle 1: 54%).

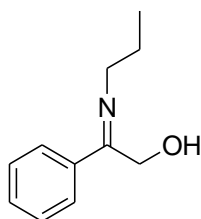
### GP-4.4 Asymmetric hydrogenation of imines with

#### silica-60-N-derivatised-L-cysteine Pd catalysts

The imines synthesised for hydrogenation reactions were prepared by a method described by Shimizu *et al.*<sup>4</sup> The hydrogenation of these imines was carried out following the general procedure described here. To a small conical flask was added imine (0.7 mmol) and 1,1,1-trifluoroethanol (10 mL) and the reaction mixture stirred at room temperature. To this stirred solution was then added **silica-60-N-derivatised-L-cysteine-Pd(OAc)** (30 mg, 0.1 mol % Pd) the flask covered with a watch glass and then transferred to an autoclave. The autoclave was then purged with nitrogen thrice and then hydrogen before being pressurised to 30 bar. The autoclave was placed in an oil bath at 50 °C and the contents allowed to stir for 24 hours. The solid catalyst was then filtered, and the filtrate analysed by <sup>1</sup>H NMR after removal of the solvent under reduced pressure. The product obtained was further characterised by HPLC on a chiral OD column using hexane/isopropanol 80/20 as a solvent.

Leaching tests were performed by removal of the catalyst by filtration from the reaction mixture after a total reaction time of 10 hours. A sample was removed from the filtrate for % conversion analysis. The remaining filtrate was then transferred to a new reaction flask equipped with a new stirrer bar and the reaction continued at 30 bar hydrogen pressure and heating to 50 °C for a further 14 hours.

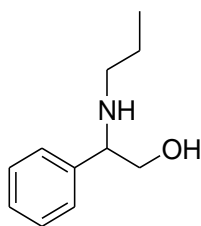
#### Synthesis of 2-phenyl-2-propylimino-ethanol



Into a round bottom flask was added propylamine (0.62 g, 10.0 mmol) and benzene (15 mL). To this solution was then added methyl benzoylformate (1.50 mL, 10.6 mmol) and *p*-toluenesulfonic acid (95 mg, 0.5 mmol). The reaction mixture was then heated at the reflux temperature (100 °C) for 20 hours with azeotropic removal of water. The solvent was then evaporated and the residue was purified by flash column chromatography (ethyl acetate/hexane = 1/10 and then ethyl acetate/ petroleum ether (40-60) 1/3) to give a yellow oil (1.02

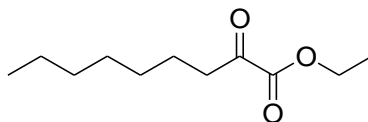
g, 58 %).  $^1\text{H}$  NMR ( $\text{CDCl}_3$ , 270 MHz)  $\delta_{\text{H}}$ : 0.87 (3H, t,  $J = 7.5$ ,  $\text{CH}_2\text{CH}_2\text{CH}_3$ ), 1.65 (2H, m,  $\text{CH}_2\text{CH}_2\text{CH}_3$ ), 3.55 (2H, t,  $J = 7.4$ ,  $\text{CH}_2\text{CH}_2\text{CH}_3$ ), 3.65 (2H, s,  $\text{CH}_2\text{OH}$ ), 7.23-7.29 (3H, m, Ar  $H$ 's), 7.66 (2H, m, Ar  $H$ 's);  $^{13}\text{C}$  NMR ( $\text{CDCl}_3$ , 270 MHz)  $\delta_{\text{C}}$ : 12.3 ( $\text{CH}_3\text{CH}_2\text{CH}_2$ ), 24.5 ( $\text{CH}_3\text{CH}_2\text{CH}_2$ ), 44.0 ( $\text{CH}_3\text{CH}_2\text{CH}_2$ ), 65.1 ( $\text{OHCH}_2$ ), 129.3 (Ar  $C$ 's), 131.4 (Ar  $C$ 's), 137.8 (Ar  $C$ 's), 167.3 ( $C=\text{N}$ ). Assignments were in agreement with literature reports.<sup>2,3,5</sup>

### Synthesis of 2-phenyl-2-propylamino-ethanol



The hydrogenation of 2-phenyl-2-propylimino-ethanol (0.90 g, 5 mmol) catalysed by **silica-60-N-4-methoxybenzyl-L-cysteine-Pd(OAc)** (15 mg, 0.06 mol % Pd) was carried out following **GP 4.3**.  $^1\text{H}$  NMR ( $\text{CDCl}_3$ , 270 MHz)  $\delta_{\text{H}}$ : 0.67 (3H, t,  $J = 7.5$ ,  $\text{CH}_2\text{CH}_2\text{CH}_3$ ), 1.43 (2H, m,  $\text{CH}_2\text{CH}_2\text{CH}_3$ ), 2.25 (2H, t,  $J = 7.3$ ,  $\text{CH}_2\text{CH}_2\text{CH}_3$ ), 3.88 (2H, dd,  $J = 7.2$ , 2.6,  $\text{CH}_2\text{OH}$ ), 4.11 (1H, m,  $\text{CHNH}$ ), 7.03-7.09 (3H, m, Ar  $H$ 's), 7.22 (2H, m, Ar  $H$ 's);  $^{13}\text{C}$  NMR ( $\text{CDCl}_3$ , 270 MHz)  $\delta_{\text{C}}$ : 11.3 ( $\text{CH}_3\text{CH}_2\text{CH}_2$ ), 24.5 ( $\text{CH}_2\text{CH}_3$ ), 46.3 ( $\text{CH}_3\text{CH}_2\text{CH}_2$ ), 60.6 ( $\text{CHNH}$ ), 60.2 ( $\text{CH}_2\text{OH}$ ), 125.3 (Ar  $C$ 's), 128.7 (Ar  $C$ 's), 137.8 (Ar  $C$ ). The product obtained was further characterised by HPLC on a chiral OD column. Retention time of the enantiomers was approximately 12.3 minutes and 13.9 minutes.

### Synthesis of 2-oxo-nonanoic acid ethyl ester

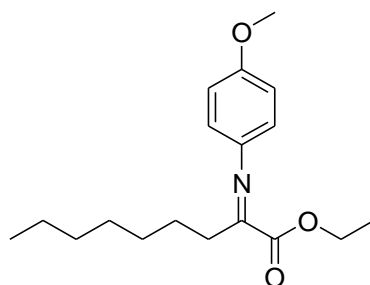


Into a round bottomed flask was added ethyl chloroacetate (3 g, 2.45 mL, 2.197 mmol) in dry diethyl ether. Into another flask is added hexyl magnesium bromide (4.22 mL, 2.197 mmol) in dry diethyl ether and the reagent kept under an atmosphere of nitrogen and placed in an ice bath. The solution of ethyl chloroacetate was then added dropwise. After the addition was complete, the mixture was stirred for a further 30 minutes at room temperature and then



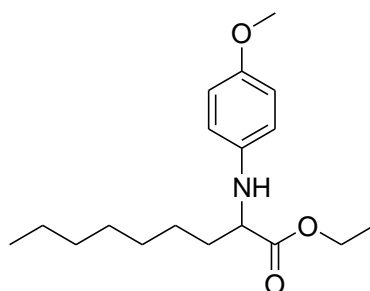
20 mL of ice water was added to the flask. Once the ice water had melted a further 10 mL of diethyl ether was added to the flask until the gummy solid dissolved. The mixture was then transferred to a separating funnel and the layers separated. The aqueous layer was extracted by diethyl ether and the organic layers collected, washed with 10 mL water and dried over  $\text{MgSO}_4$ . The drying agent was then filtered off and the solvent evaporated off to give dark brown oil (3.82 g, 87 %).  $^1\text{H}$  NMR ( $\text{CDCl}_3$ , 270 MHz)  $\delta_{\text{H}}$ : 0.86 (3H, t,  $J = 7.3$ ,  $\text{OCH}_2\text{CH}_3$ ), 1.25 (3H, t,  $J = 7.5$ ,  $\text{CH}_2\text{CH}_2\text{CH}_3$ ), 1.28 (2H, m,  $\text{CH}_2\text{CH}_2\text{CH}_3$ ), 1.34-1.45 (6H, m, 3 x  $\text{CH}_2$ ), 4.28 (2H, m,  $\text{CH}_2\text{CH}_2\text{C}(\text{O})$ ), 4.34 (2H, q,  $J = 7.0$ ,  $\text{CH}_2\text{C}(\text{O})$ ), 4.43 (2H, q,  $J = 7.1$ ,  $\text{OCH}_2\text{CH}_3$ ).

### Synthesis of 2-(4-Methoxy-phenylimino)-nonanoic acid ethyl ester



Into a round bottomed 100 mL flask was added *para*-anisidine (2.45 g, 20 mmol) and benzene (30 mL). To this solution was then added 2-oxo-nonanoic acid ethyl ester (3.85 g, 19 mmol) and *p*-toluenesulfonic acid (200 mg, 1.0 mmol). The reaction mixture was then heated at reflux temperature (100 °C) for 20 hours with azeotropic removal of water. The solvent was then evaporated and the residue was purified by flash column chromatography (ethyl acetate/petroleum ether (40-60) 1/10 and then ethyl acetate/petroleum ether (40-60) 1/5) to give a dark yellow oil (2.95 g, 76 %).  $^1\text{H}$  NMR ( $\text{CDCl}_3$ )  $\delta_{\text{H}}$ : 0.92 (3H, t,  $J = 7.4$ ,  $\text{CH}_3\text{CH}_2\text{CH}_2$ ), 1.30-1.42 (15H, m, 6 x  $\text{CH}_2$ /  $\text{OCH}_2\text{CH}_3$ ), 3.77 (3H, s,  $\text{OCH}_3$ ), 4.29 (2H, q,  $J = 7.1$ ,  $\text{OCH}_2\text{CH}_3$ ), 6.85 (2H, d, ' $J = 11.2$ , Ar  $H$ 's (AA'BB' system)), 7.15 (2H, d, ' $J = 11.2$ , Ar  $H$ 's (AA'BB' system));  $^{13}\text{C}$  NMR ( $\text{CDCl}_3$ , 270 MHz)  $\delta_{\text{C}}$ : 13.0 ( $\text{CH}_3\text{CH}_2\text{CH}_2$ ), 14.2 ( $\text{OCH}_2\text{CH}_3$ ), 23-30 (6 x  $\text{CH}_2$ ), 56.2 ( $\text{OCH}_3$ ), 60.4 ( $\text{OCH}_2\text{CH}_3$ ), 115.1 (Ar  $C$ 's), 123.6 (Ar  $C$ 's), 141.7 (Ar  $C$ 's), 160.8 (Ar  $C$ 's), 167.6 ( $\text{N}=\text{CC}(\text{O})$ ), 169.9 ( $\text{C}(\text{O})\text{O}$ ). Assignments were in agreement with literature reports.<sup>2,3,5</sup>

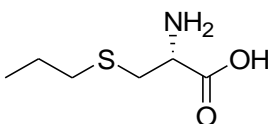
### Synthesis of 2-(4-methoxy-phenylamino)-nonanoic acid ethyl ester



The hydrogenation of 2-phenyl-2-propylimino-ethanol (0.90 g, 5 mmol) catalysed by **silica-60-N-4-methoxybenzyl-L-cysteine-Pd(OAc)** (15 mg, 0.25 mmol/g Pd, 0.1 mol % Pd) was carried out following **GP-4.3**.  $^1\text{H}$  NMR ( $\text{CDCl}_3$ , 270 MHz)  $\delta_{\text{H}}$ : 0.90 (3H, t,  $J = 6.5$ ,  $\text{CH}_3\text{CH}_2\text{CH}_2$ ), 1.30-1.42 (13H, m, 5 x  $\text{CH}_2$ /  $\text{OCH}_2\text{CH}_3$ ), 1.88 (2H, m,  $\text{CH}_2\text{CHNH}$ ), 3.44 (1H, m,  $\text{CHNH}$ ) 3.72 (3H, s,  $\text{OCH}_3$ ), 4.09 (2H, q,  $J = 7.3$ ,  $\text{OCH}_2\text{CH}_3$ ), 6.55 (2H, d,  $J = 11.3$ , Ar  $H$ 's (AA'BB' system)), 6.85 (2H, d,  $J = 11.3$ , Ar  $H$ 's (AA'BB' system));  $^{13}\text{C}$  NMR ( $\text{CDCl}_3$ , 270 MHz)  $\delta_{\text{C}}$ : 13.7 ( $\text{OCH}_2\text{CH}_3$ ), 14.4 ( $\text{CH}_3\text{CH}_2\text{CH}_2$ ), 23-30 (5 x  $\text{CH}_2$ ), 33.4 ( $\text{CH}_2\text{CHNH}$ ), 55.7 ( $\text{OCH}_3$ ), 59.4 ( $\text{OCH}_2\text{CH}_3$ ), 64.5 ( $\text{CHNH}$ ), 112.2 (Ar  $C$ 's), 114.9 (Ar  $C$ 's), 136.2 (Ar  $C$ ), 150.1 (Ar  $C$ ), 174.3 ( $\text{C}(\text{O})\text{O}$ ). The product obtained was further characterised by HPLC on a chiral OD column. Retention time of the enantiomers was approximately 11.2 minutes and 14.6 minutes.

### Pd co-ordination to N-derivatised cysteine ligands

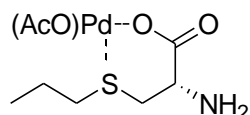
#### Synthesis of S-propyl-L-cysteine



This method was taken from Tsuge *et al.* and modified slightly.<sup>6</sup> L-cysteine (5.60 g, 0.046 mol) was dissolved in a mixture of 2M NaOH (10 mL) and ethanol (100 mL). 1-Bromopropane (5.64 g, 0.046 mmol) was then added and the resulting solution stirred at 25 °C for 1 hour. The solution was then adjusted to pH 5.25 by the addition of acetic acid and stirred for 1 hour in an ice bath. The precipitate (S-propyl-L-cysteine) was collected by centrifugation (1.65 g, 42%). Melting point 166-168 °C (lit.163-164 °C).  $^1\text{H}$  NMR ( $\text{D}_2\text{O}$ )  $\delta_{\text{H}}$ :

0.95 (3H, t,  $J = 7.3$ ,  $\text{CH}_3\text{CH}_2$ ), 1.60 (2H, m,  $\text{CH}_3\text{CH}_2$ ), 2.54 (2H, t,  $J = 6.8$ ,  $\text{CH}_3\text{CH}_2\text{CH}_2$ ), 2.90-2.95 (2H, m,  $\text{SCH}_2$ ), 3.78 (1H, m,  $\text{CHNH}_2$ ), 6.2 (2H, b s,  $\text{CHNH}_2$ ).

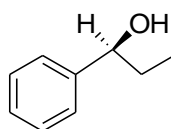
### Synthesis of S-propyl-L-cysteine-Pd(OAc)



To S-propyl-L-cysteine (1.07 g) stirred in distilled  $\text{H}_2\text{O}$  (20 mL) was added 1M NaOH dropwise until pH 8.5 was attained. The solid was then filtered, washed with  $\text{H}_2\text{O}$  until the washings were neutral and then washed with ethanol (20 mL). The sodium salt was introduced to a solution of  $\text{Pd}(\text{OAc})_2$  (0.323 g) in methanol (20 mL) and the mixture left to stir at room temperature for 24 hours. The solid was then filtered, washed well with methanol until the washings were clear and the sample dried under reduced pressure overnight to give a deep red coloured solid.

### Enantioselective addition of diethyl zinc to benzaldehyde

(*R*)-1-Phenyl-propan-1-ol

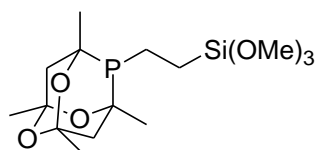


Benzaldehyde (200  $\mu\text{L}$ , 1.96 mmol) and **silica-60-N-4-methoxybenzyl-L-cysteine** (0.2 g, 0.2 mmol) was stirred in dry toluene (4 mL) at 0  $^\circ\text{C}$  for 15 minutes under an atmosphere of nitrogen. To this reaction mixture was then added diethyl zinc (4.4 mL, 1M solution in diethyl ether, 4.4 mmol) dropwise and the reaction mixture was then stirred at room temperature for 18 hours. The reaction was quenched with 1M HCl (14 mL). The catalyst was filtered and washed with 20 mL  $\text{CH}_2\text{Cl}_2$ . The filtrate was extracted with  $\text{CH}_2\text{Cl}_2$  and extracted with brine (2 x 10 mL). The combined organic layers were dried over anhydrous sodium sulfate and evaporated under reduced pressure to get a crude oil (0.23 g, 77 %). The product obtained was characterised by  $^1\text{H}$  NMR and HPLC on a chiral OD column. Retention time of the (*R*)-

enantiomer is approximately 12.8 minutes and for the (*S*)-enantiomer it is 14.9 minutes.  $^1\text{H}$  NMR ( $\text{CDCl}_3$ , 270 MHz)  $\delta_{\text{H}}$ : 0.91 (3H, t,  $J = 7.5$ ,  $\text{CH}_2\text{CH}_3$ ), 1.73 (2H, m,  $\text{CH}_2\text{CH}_3$ ), 4.57 (1H, t,  $J = 7.3$ ,  $\text{CHCH}_2$ ), 4.69 (1H, s, OH), 7.35-7.41 (5H, m, Ar  $H$ 's).

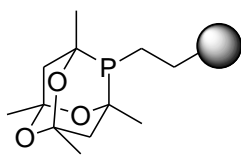
## 6.5 Chapter 5 Experimental

### Synthesis of trimethoxysilylethyl-PAD



A mixture of 2,4,8-trioxa-1,3,5,7-tetramethyl-6-phosphaadamantane (0.06 mol) and vinyl trimethoxysilane (0.05 mol) was heated at reflux temperatures with the aid of overhead stirring. Once the solid had dissolved, at *ca* 80°C, di-*tert*-butyl peroxide (20 drops) was added. The mixture was heated for an additional two hours at this temperature and then cooled. The reaction was monitored by  $^1\text{H}$  NMR through the consumption of the vinyltrimethoxysilane by the disappearance of the peaks at 5.8-6.0 ppm. The reaction was considered complete when the vinyl peaks were no longer present, this gives trimethoxy silyl-2,4,8-trioxa-1,3,5,7-tetramethyl-6-phosphaadamantane.  $^1\text{H}$  NMR ( $\text{CDCl}_3$ , 270 MHz)  $\delta_{\text{H}}$  0.65-0.77 (2H, m,  $\text{SiCH}_2$ ), 1.19-1.88 (18H, m,  $\text{PCH}_2$ ,  $\text{PCCH}_2$ ,  $\text{PCCH}_3$ ), 3.47 (9H, s,  $\text{SiOCH}_3$ );  $^{13}\text{C}$  NMR ( $\text{CDCl}_3$ )  $\delta_{\text{C}}$ : 7.7 (d,  $^2J_{\text{PC}} = 19$  Hz,  $\text{SiCH}_2$ ), 13.0 (d,  $J_{\text{PC}} = 24$  Hz,  $\text{PCH}_2$ ), 26.9 ( $\text{OCCH}_3$ ), 27.9 ( $\text{PCCH}_3$ ), 37.0 ( $\text{PCCH}_2$ ), 44.4 (d,  $^2J_{\text{PC}} = 15$  Hz,  $\text{PCCH}_2$ ), 50.5 ( $\text{SiOCH}_3$ ), 72.2 ( $\text{PCCH}_3$ ), 95.6 ( $\text{OCCH}_3$ ), 96.4 ( $\text{OCCH}_3$ );  $^{31}\text{P}$  NMR ( $\text{CDCl}_3$ )  $\delta_{\text{P}}$  -21.3. Assignments based on those reported for related methylphosphine cage.<sup>7</sup>

### Synthesis of silica-110-PAD

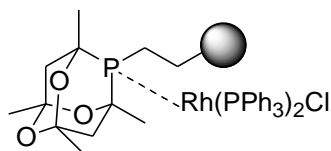


Without further purification trimethoxysilyl-2,4,8-trioxa-1,3,5,7-tetramethyl-6-phosphaadamantane (18.5 g, 0.05 mol) was dissolved in toluene (100 mL) and agitated while silica (40 g, 60-200  $\mu$  m, 110 Å) was added slowly. Distilled water was then added (3 mL) to the stirring mixture and it was then refluxed for 4 hours. The mixture was then cooled and the solid filtered and washed with toluene (75 mL) and methanol (2 x 75 mL) before being dried under reduced pressure to give a white solid, **silica-110-PAD**.  $^{13}\text{C}$  NMR (CP MAS)  $\delta_{\text{C}}$ : 13.3 (SiCH<sub>2</sub>CH<sub>2</sub>P), 28.4 (CH<sub>2</sub>CCH<sub>3</sub>), 37.1 (PCCH<sub>2</sub>), 45.2 (PCCH<sub>2</sub>), 71.6 (PCCH<sub>3</sub>), 97.2 ppm (PCCH<sub>2</sub>CO);  $^{29}\text{Si}$  NMR (MAS)  $\delta_{\text{Si}}$ : -65, -108, -115;  $^{31}\text{P}$  NMR (CP MAS)  $\delta_{\text{P}}$ : -22. Specific surface area 303.5 m<sup>2</sup>/g; Average pore volume 0.574 cc/g; Average pore diameter 96.1 Å

#### GP 5.1 Synthesis of silica-110-PAD-Rh complex

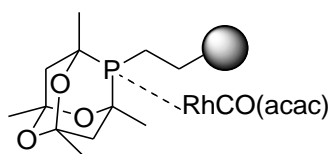
To a stirred solution of Rh complex (0.5 mmol) in THF (20 mL) was added **silica-110-PAD** (2 g) and the mixture left to stir overnight at room temperature. The solid was then filtered off and washed with THF until the washings were clear and the solid dried under reduced pressure.

#### Synthesis of silica-110-PAD-Rh(PPh<sub>3</sub>)<sub>2</sub>Cl



**Silica-110-PAD** (2 g) and RhCl(PPh<sub>3</sub>)<sub>3</sub> (0.45 g, 0.5 mmol) were combined following general procedure **GP-5.1**. Specific surface area 376.6 m<sup>2</sup>/g; Average pore volume 0.505 cc/g; Average pore diameter 57.4 Å; Rh loading 0.16 mmol/g.

### Synthesis of silica-110-PAD-Rh(CO)(acac)



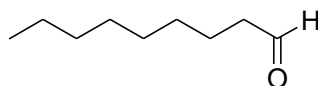
**Silica-110-PAD** (2 g) and  $\text{Rh}(\text{CO})_2(\text{acac})$  (0.85 g, 0.5 mmol) were combined following general procedure **GP-5.1**. Specific surface area 350.7  $\text{m}^2/\text{g}$ ; Average pore volume 0.498  $\text{cc}/\text{g}$ ; Average pore diameter 64.4  $\text{\AA}$ ; Rh loading 0.13  $\text{mmol}/\text{g}$ .

### Metal digestion of immobilised Rh complexes

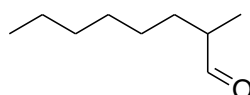
Silica-110-PAD-Rh-complex (25 mg) was stirred in conc AnalR  $\text{HNO}_3$  (7.5 mL) at reflux temperature for 6 hours. The solution was filtered; the solid washed with deionised water (5 mL) and then made up to 25 mL with deionised water. The Rh content was measured by ICP-OES.

### GP 5.2 General Procedure for 1-octene hydroformylation

The procedure for 1-octene hydroformylation was taken from Breit and Seiche.<sup>8</sup> To a small flask was added 1-octene (0.32 mL, 2 mmol) and dry toluene (5 mL). To this was then added silica-110-PAD-Rh catalyst (**silica-60-C<sub>3</sub>-RhCl(PPh<sub>3</sub>)<sub>2</sub>** (50 mg, 0.26  $\text{mmol}/\text{g}$  Rh, 0.6 mol %); **silica-110-PAD-RhCl(PPh<sub>3</sub>)<sub>2</sub>** (100 mg, 0.16  $\text{mmol}/\text{g}$  Rh, 0.8 mol % Rh)) and the flask covered with a watch glass. This was then placed in an autoclave and purged with nitrogen thrice and then pressurized with  $\text{CO}:\text{H}_2$  (1: 1) at 30 bar pressure. The vessel was placed in an oil bath, heated to the desired temperature and left to stir. After the required reaction time, the solid was then filtered and the filtrate collected and solvent removed by rotary evaporation. The residue was then analysed by  $^1\text{H}$  NMR.

**1-Nonanal**

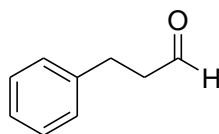
Hydroformylation of 1-octene (0.30 mL, 1.8 mmol) was carried out following **GP-5.2**.  $^1\text{H}$  NMR ( $\text{CDCl}_3$ , 270 MHz)  $\delta_{\text{H}}$ : 0.96 (3H, t,  $J = 7.3$ ,  $\text{CH}_3\text{CH}_2$ ), 1.29 (8H, m, 4 x  $\text{CH}_2$ ), 1.33 (2H, m,  $\text{CH}_3\text{CH}_2$ ), 1.62 (2H, m,  $\text{CH}_2\text{CH}_2\text{C}(\text{O})$ ), 2.40 (2H, t,  $J = 7.2$ ,  $\text{CH}_2\text{CH}_2\text{C}(\text{O})$ ), 9.77 (1H, t,  $J = 2.0$ ,  $\text{C}(\text{O})\text{H}$ ).

**2-Methyl-octanal**

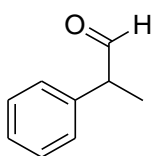
Hydroformylation of 1-octene (0.30 mL, 1.8 mmol) was carried out following GP 5.2.  $^1\text{H}$  NMR ( $\text{CDCl}_3$ , 270 MHz)  $\delta_{\text{H}}$  0.96 (3H, t,  $J = 7.3$ ,  $\text{CH}_3\text{CH}_2$ ), 1.18 (3H, d,  $J = 6.5$ ,  $\text{CH}_3\text{CH}$ ), 1.29 (6H, m, 3 x  $\text{CH}_2$ ), 1.33 (2H, m,  $\text{CH}_3\text{CH}_2$ ), 1.58 (2H, m,  $\text{CH}_2\text{CH}_2\text{C}(\text{O})$ ), 2.52 (1H, m,  $\text{CHNH}$ ), 9.72 (1H, d,  $J = 1.8$ ,  $\text{C}(\text{O})\text{H}$ ).

**GP-5.3 General Procedure for styrene hydroformylation**

Into a small round conical flask was added catalyst (**silica-60-C<sub>3</sub>-Pd(OAc)<sub>2</sub>** (100 mg, 0.41 mmol/g Pd, 1.4 mol % Pd) or **silica-60-C<sub>3</sub>-RhCl(PPh<sub>3</sub>)** (100 mg, 0.26 mmol/g Rh, 0.4 mol % Rh) or **silica-110-PAD-RhCl(PPh<sub>3</sub>)<sub>2</sub>** (100 mg, 0.16 mmol/g Rh, 0.6 mol % Rh) or **silica-110-PAD-RhCO(acac)** (100 mg, 0.12 mmol/g Rh, 0.4 mol % Rh), (dry toluene (7 mL) and styrene (0.30 mL, 2.6 mmol). The flask was then placed into an autoclave and purged with nitrogen thrice and then purged with CO: H<sub>2</sub> once before being pressurised to 30 bar. The vessel was placed in an oil bath and heated to the required temperature. After the required reaction time, the solid was then filtered, the filtrate collected and solvent removed by rotary evaporation. The residue was then analysed by  $^1\text{H}$  NMR.

**3-Phenyl-propionaldehyde**

Hydroformylation of styrene (0.30 mL, 1.8 mmol) was carried out following **GP-5.3**.  $^1\text{H}$  NMR ( $\text{CDCl}_3$ , 270 MHz)  $\delta_{\text{H}}$  2.73 (2H, t,  $J = 7.5$ ,  $\text{CH}_2\text{CH}_2\text{C}(\text{O})$ ), 2.88 (2H, t,  $J = 7.6$ ,  $\text{CH}_2\text{CH}_2\text{C}(\text{O})$ ), 7.12-7.18 (5H, m, Ar  $H$ 's), 9.77 (1H, t,  $J = 1.9$ ,  $\text{C}(\text{O})\text{H}$ ).

**2-Phenyl-propionaldehyde**

Hydroformylation of styrene (0.30 mL, 1.8 mmol) was carried out following **GP-5.3**.  $^1\text{H}$  NMR ( $\text{CDCl}_3$ , 270 MHz)  $\delta_{\text{H}}$  1.45 (3H, d,  $J = 5.5$ ,  $\text{CHCH}_3$ ), 3.81 (1H, m,  $\text{CHCH}_3$ ), 7.12-7.18 (5H, m, Ar  $H$ 's), 9.72 (1H, d,  $J = 2.0$ ,  $\text{C}(\text{O})\text{H}$ ).



## 6.6 References

- <sup>1</sup> A. Ramirez, B. L. Lopez, and L. Sierra, *J. Phys. Chem. B*, 2003, **107**, 9275-9280;
- <sup>2</sup> J. D. Park and D. H. Kim, *J. Med. Chem.*, 2002, **45**, 4, 917;
- <sup>3</sup> G. Shang, Q. Yang, X. Zhang, *Angew. Chem.* 2006, **118**, 6508-6510;
- <sup>4</sup> Y. Niwa, M. Shimuzu, *J. Am. Chem. Soc.*, 2003, **125**, 3720-3721;
- <sup>5</sup> X-B. Jiang, A. J. Minnaard, B. Hessen, B. L. Feringa, A. L. L. Duchateau, J. G. O. Adrien, J. A. F. Boogers, J. G. De Vries, *Org. Lett.*, 2003, **5**, 1503;
- <sup>6</sup> K. Tsuge, M. Kataoka, Y. Seto, *J. Agric. Food Chem.*, 2002, **50** (16), 4445-4451;
- <sup>7</sup> (a) R.A. Baber, M.L. Clarke, K.M. Heslop, A.C. Marr, A.G. Orpen, P.G. Pringle, A. Ward, E. Damaris, D.E. Zambrano-Williams, *Dalton Trans.* , 2005, 1079–1085; (b) M.L. Clarke, G.J. Roff, *Chem. Eur. J.*, 2006, **12**, 7078–7986.
- <sup>8</sup> B. Breit and W. Seiche, *Synthesis*, 2001, **1**, 1-36;

## Appendix 1

### B. J. H equation

#### Porosimetry

The nitrogen adsorption measurements were made using Quantachrome NovaWin 1200 Surface area analyser. The calculation points for adsorption were 30 and these were in the range of 0.1 and 0.95 P/P<sub>0</sub>. The calculation points for desorption were 40 and these were in the range 0.1 and 0.98 P/P<sub>0</sub>. The conditions for the run were 180 seconds thermal delay time and equilibration interval of 60 seconds.

The computational method used to derive pore size distribution from the nitrogen desorption data is the BJH procedure.

#### B. J. H. Equation

The Barrett Joyner Halenda equation (BJH) enables the pore volume and pore area distributions for mesoporous solids to be estimated. The basis for the BJH method is from Wheelers theory which combines aspects of capillary condensation and physical adsorption to evaluate the pore radii. Such a technique involves measuring the loss of liquid adsorbate from the pore as a function of decreasing relative pressure, i.e. the desorption branch of the isotherm. Calculation of the pore radius is done by the sum of the inner liquid core radius plus the depth of the adsorbed multilayer on the pore walls. The core radius is determined with the Kelvin equation which assumes the pore shape to be cylindrical.

Kelvin equation  $r_m = -2\gamma V / RT \ln (P/P_0)$

Whereby  $r_m$  = the mean radius of the curvature of the meniscus

$\gamma$  = surface tension of the adsorbate

V = the liquid molar volume of adsorbate

R = gas constant

T = temperature

P/P<sub>0</sub> = relative pressure

The Halsey equation is used to calculate the depth of the adsorbed layer in the pore. For reasons of simplicity, the thickness of this film is said to be equivalent to that on a given plane non-porous surface. And so the diameter (D) of the pore is given by

$$D=2(r_m+t)$$

Thus, the desorption pore volume distribution can be calculated by plotting the volume of adsorbate lost between successive pressure steps versus the pore diameter. A similar plot for the pore area is also possible.

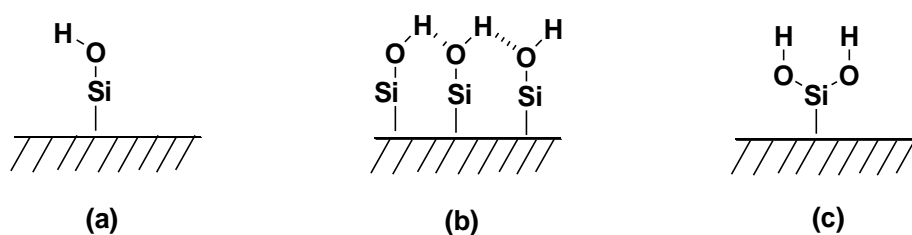
## Appendix 2

### Quantification of Silanol groups

As reported by the research groups of Kosslick, Zhou and Vinek, absorption properties of a given silica material is related to the density of the silanol groups (SiOH) which can be determined by  $^{29}\text{Si}$  MAS NMR, transmittance IR spectroscopy, and TGA/DTA in several studies.<sup>1</sup>

Ramirez *et al.* combined TGA (thermogravimetric analysis) and DRIFT (Diffused Reflectance Infrared Fourier Transform) measurements to characterise the silanol content in mesoporous silanol prepared in acidic medium, by using pyridine desorption. Ramirez *et al.* reported the highest silanol group concentration to be 6.5 groups/  $\text{nm}^2$  when the silica has been rehydroxylated during 24 hours.

For mesoporous silica MCM-41, as prepared in basic media, the silanol density varies between 2.5-3.0 silanol groups/ $\text{nm}^2$ . The value found here is much smaller than for amorphous silica, with average value of 4.9 groups/  $\text{nm}^2$  and has a contribution from three different silanol groups; single or isolated, hydrogen bonded and geminal. The single and geminal silanol groups have a weak acidic character. Aluminium containing MCM-41 samples have been found to have additional Bronsted and Lewis acid sites.



**A5.1** Schematic showing single (a), hydrogen bonded (b) and geminal (c) silanol groups present at the surface of the mesoporous silica.

The silanol group concentration depends on the mesoporous synthetic procedure undertaken to prepare the material. Hydrogen-bonded Si-OH groups are less reactive towards silylating reagents, due to their non acid character. As a result, only free silanol groups, single or geminal react during the modification process. Thus the presence of single and geminal silanol groups allow for the modification of the chemical nature of the silica by grafting different functionalities through covalent linkages. Hence, it is important to have not only a

high number of the silanol groups but also a high proportion of free silanol groups. Based on the acid properties of the different Si-OH groups, the number and type of silanol groups can be determined with a basic probe molecule whose characteristic depends on the chemical and physical nature of the solid under study. Pyridine is a base that is commonly used for determination of strong and weak acidic sites in materials with pore sizes larger than 5Å.

## Appendix 3

### $T_1$ measurement experiment

The inversion recovery method is a convenient way of measuring  $T_1$  values of  $^1\text{H}$  and  $^{13}\text{C}$  nuclei. In this multi pulse experiment, first net magnetization of the sample is inverted with a  $180^\circ$  pulse (“inversion”) and then allowed to relax along the z-axis with the characteristic time constant  $T_1$  (recovery). The  $180^\circ$  pulse interchanges all the spins between the upper and lower energy levels, resulting in the higher energy spin state having a slight excess in population and the lower energy spins state with a slightly depleted population. This causes the net magnetization vector to be turned upside down so  $M_z$  now equals  $-M_0$  ( $M_z$  is the magnetization at time  $t$  and  $M_0$  is the magnetization at equilibrium). According to the exponential law, recovery begins immediately, with  $R_1$ , characteristic rate =  $1/T_1$ . As the net magnetization is not directly observable quantity, this is converted to an observable x-y magnetization by applying a  $90^\circ$  pulse after the recovery period. The magnitude of the FID signal that results from this x-y magnetization (and the peak height in the spectrum) should be directly proportional to the samples z magnetization just before the  $90^\circ$  pulse. Repetition of the experiment at different time delays after the  $180^\circ$  pulse means that the return of the z magnetization to equilibrium can be monitored and the value of  $T_1$  can be determined by fitting the data obtained to an exponential function.

The phase correction parameters are set first using a  $90^\circ$  pulse acquisition (starting with equilibrium magnetization along the +z axis) and then applied to a series of inversion-recovery spectra acquired from an increasing value of the delay  $\tau$ . For  $\tau = 0$ , an upside down spectrum is observed with its peaks at maximum but inverted. As the delay is increased each peak will become less intense, pass through zero and essentially become positive. At very long  $\tau$  delays the spectrum looks like a normal spectrum. The spectrum for various  $\tau$  values are plotted on the same chart, thus giving the so called partially relaxed spectra for the system.  $T_1$  values for each chemical environment can be obtained by fitting the peak intensity of each peak to the equation

$$\ln(M_0 - M_z) = \ln(2M_0) - (\tau / T_1)$$

The point where a peak changes from negative to positive is a rough measure of  $T_1$  and is  $\tau = T_1 \ln 2$ . Relaxation times calculated depend heavily on the number of protons in the carbon and so comparisons of carbon atoms with the same number of protons is a good idea.

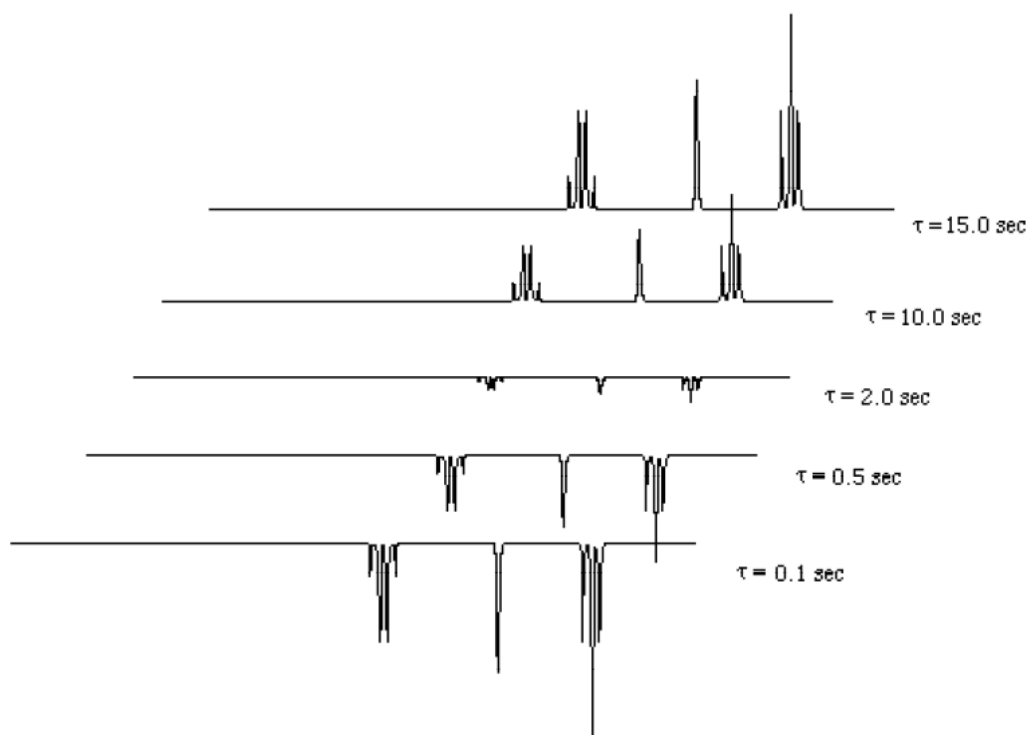
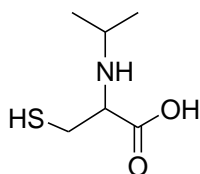


**Figure A3.1** Partially relaxed spectra for the different delay times where all the chemical environments have the same  $T_1$ .

## Appendix 4

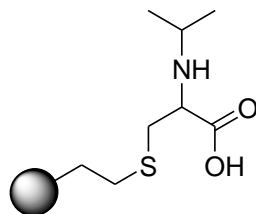
### Synthesis of silica-60-N-isopropyl-L-cysteine-Pd(OAc)

#### 4.1 Synthesis of N-isopropyl-L-cysteine



This was achieved by combining isopropanol and L-cysteine using the same synthetic procedure as described in Chapter 6, for the synthesis of **N-4-methoxybenzyl-L-cysteine**. <sup>1</sup>H NMR (D<sub>2</sub>O, 270 MHz) δ<sub>H</sub>: 0.69 (6H, d, *J* = 7.6, CH(CH<sub>3</sub>)<sub>2</sub>), 2.23 (1H, t, *J* = 7.4, CH<sub>2</sub>CH), 2.37 (2H, m, HSCH<sub>2</sub>), 2.79 (1H, m, CH(CH<sub>3</sub>)<sub>2</sub>); <sup>13</sup>C NMR (CDCl<sub>3</sub>, 270 MHz) δ<sub>C</sub>: 22.4 (CH<sub>3</sub>CH), 28.5 (HSCH<sub>2</sub>), 46.6 (CH<sub>3</sub>CH), 66.0 (CHNH), 182.7 (C(O)OH).

#### 4.2 Synthesis of silica-60-N-isopropyl-L-cysteine



This followed the same general procedure as described in Chapter 6 for the synthesis of **silica-60-N-acetyl-L-cysteine**. Thus S-trimethoxysilylethyl-N-isopropyl-L-cysteine was first synthesised and then grafted onto silica. Given the highly viscous nature of the alkoxyethyl intermediate, monitoring of the reaction by <sup>1</sup>H NMR was difficult and so a total reaction time of 8 hours was given after which it was then introduced to silica. The solid material obtained was characterised by <sup>13</sup>C and <sup>29</sup>Si NMR. This revealed a large proportion of vinyl had immobilised on the silica surface as is evident by the peaks appearing 130-140 ppm. From <sup>13</sup>C, it is clear that some N-isopropyl-L-cysteine ligand had also been immobilised on the surface.



#### 4.3 $^{13}\text{C}$ CP MAS NMR of silica-60-N-isopropyl-*L*-cysteine

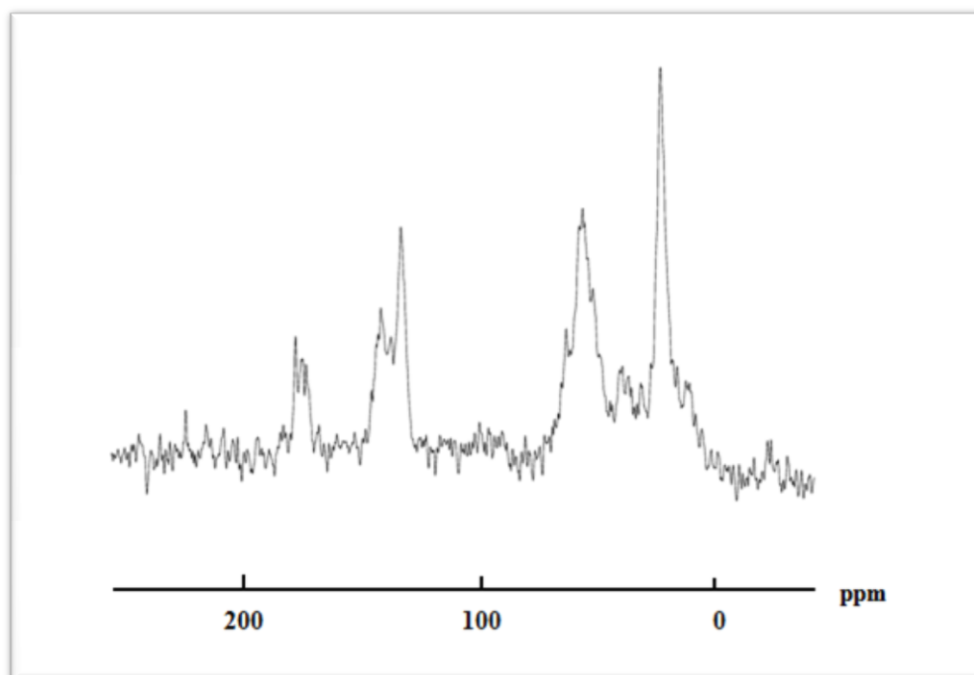


**Figure A4.1**  $^{13}\text{C}$  CP MAS NMR of silica-60-N-isopropyl-*L*-cysteine

#### 4.4 $^{29}\text{Si}$ MAS NMR of silica-60-N-isopropyl-*L*-cysteine

The  $^{29}\text{Si}$  MAS NMR of **silica-60-N-isopropyl-*L*-cysteine** revealed two Si environments. The peak found at -108.5 ppm corresponds to the presence of  $Q^n$  environments within the material, with percentage area of 96%. The peaks present at -67.4 ppm correspond to  $T^n$  environments within the material, and this is shown to have 4% area from the Gaussian fitting. From here, a  $T: Q$  ratio of 1:24 is calculated, which corresponds to a  $T$  loading of 0.48 mmol/g. It can further be noted that it is clearly evident that the  $T^n$  environments are mainly of  $T^2$  character.

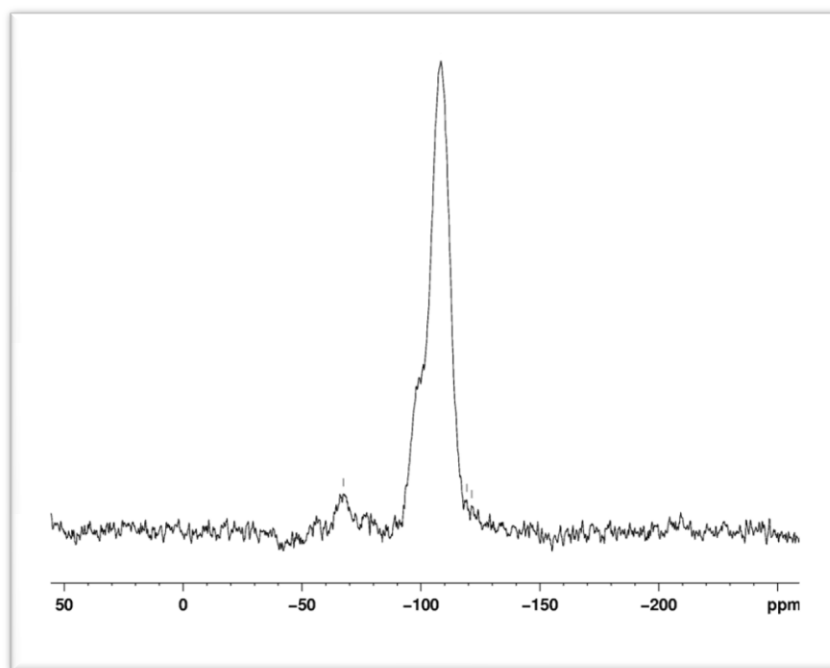
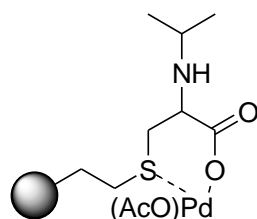


**Figure A4.2**  $^{29}\text{Si}$  MAS NMR of silica-60-N-isopropyl-*L*-cysteine

#### 4.5 Synthesis of silica-60-N-isopropyl-*L*-cysteine-Pd(OAc)

Silica-60-N-acetyl-*L*-cysteine and  $\text{Pd}(\text{OAc})_2$  were reacted together following **GP-2.3** as described in Chapter 6 to give silica-60-N-isopropyl-*L*-cysteine-Pd(OAc) as a orange solid. Metal analysis of silica-60-N-isopropyl-*L*-cysteine-Pd(OAc) revealed 0.23 mmol/g of Pd.



## Appendix 5

### Asymmetric Hydrogenation of Acetophenone with Silica Supported Phosphaadamantane Chiral Amine Ruthenium Catalysts

#### 5.1 Introduction

Phosphorus ligands can coordinate with a ruthenium atom through sigma-pi interaction to form an organometallic complex. The ligands can also be absorbed to the metal surface via the co-ordination interaction between the phosphorus atoms and the metal atoms.<sup>2</sup> Absorption of a chiral ligand produces a chiral environment on the metal surface, which may be somewhat analogous to that of the metal complex co-ordinated with chiral ligands. As a result, the chirally modified catalyst could have asymmetric induction ability.<sup>3</sup> The chiral environment formed by the ligand modification together with a heterogeneous surface can increase the enantioselectivity for hydrogenation reactions of prochiral substrates.

#### 5.2 Preparation and characterization of silica-110-PAD-Ru-DPEN

Previous work carried out by the Sullivan group has shown **silica-110-PAD** is an excellent ligand for hydroformylation reactions when loaded with Rh as described in Chapter 5 and in the Suzuki-Miyaura reaction when loaded with Pd. Herein, **silica-110-PAD** is modified with Ru and chiral amine ligands and its activity in the hydrogenation of acetophenone is explored. Catalyst **silica-110-PAD-Ru-DPEN** was prepared rather simply by stirring **silica-110-PAD** in a solution of  $[\text{RuC}_6\text{H}_6\text{Cl}_2]_2$  in DMF at reflux temperatures for 3 hours. The dark solution formed was then cooled before the addition of DPEN. The mixture was further stirred overnight at room temperature. It was then filtered, washed with cold methanol and dried under vacuo to give a lilac coloured solid, catalyst **silica-110-PAD-Ru-DPEN**, with proposed structure as shown in **Figure A5.1** below. The choice of DPEN as a chiral ligand was chosen to form a stable and rigid chiral environment around the metal. This would ensure good chelation ability of the ligand in comparison to a monodentate ligand.

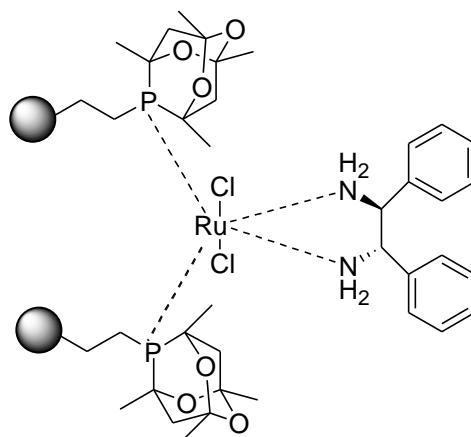


**Figure A5.1 silica-110-PAD-Ru-DPEN.**

The adsorbed chiral bidentate amine modifier with chelating configuration can promote the chiral induction of the catalysts. Further the PAD ligands contribute to a higher electronic density on the Rh metal and this can effectively benefit the adsorption and activation of prochiral substrates coordinating to the metal centre.

The catalyst was characterized by solid state  $^{13}\text{C}$  and  $^{29}\text{Si}$  NMR as well as dipolar dephasing experiments and  $T_1$  measurements. Metal loading was also determined by ICP-OES measurements.

### $^{13}\text{C}$ CP MAS NMR

Solid state NMR was used to confirm the immobilisation of the Ru complex on the immobilised phosphadmantane ligand (**Figure A5.2**). This was proved to be a very useful technique. Ten distinct environments are found in the  $^{13}\text{C}$  CP MAS NMR of silica-PAD-Ru-DPEN; 4.6 ( $\text{SiCH}_2\text{CH}_2\text{P}$ ), 12.8 ( $\text{SiCH}_2\text{CH}_2\text{P}$ ), 20.4 ( $\text{CH}_2\text{CCH}_3$ ), 25.6 ( $\text{PCCH}_2$ ), 39.3 ( $\text{NH}_2\text{CH}$ ), 44.9 ( $\text{PCCH}_2$ ), 72.7 ( $\text{PCCH}_3$ ), 95.5 ( $\text{PCCH}_2\text{CO}$ ), 127.3 ( $\text{NH}_2\text{CCCH}$ ), 164.9 (Ar C's). The carbon atoms adjacent to the phosphorus show line broadening in their resonant peaks; this would suggest complexation to the metal. In addition, the intensity of the resonant peaks from the chiral ligands is much smaller than the resonant peaks corresponding to the phosphadmantane ligand. This would suggest that the relative amount of chiral ligand complexed to the surface is much lower than the phosphadmantane ligands. Further suggesting, not all the silica supported phosphadmantane sites are complexed to metal.

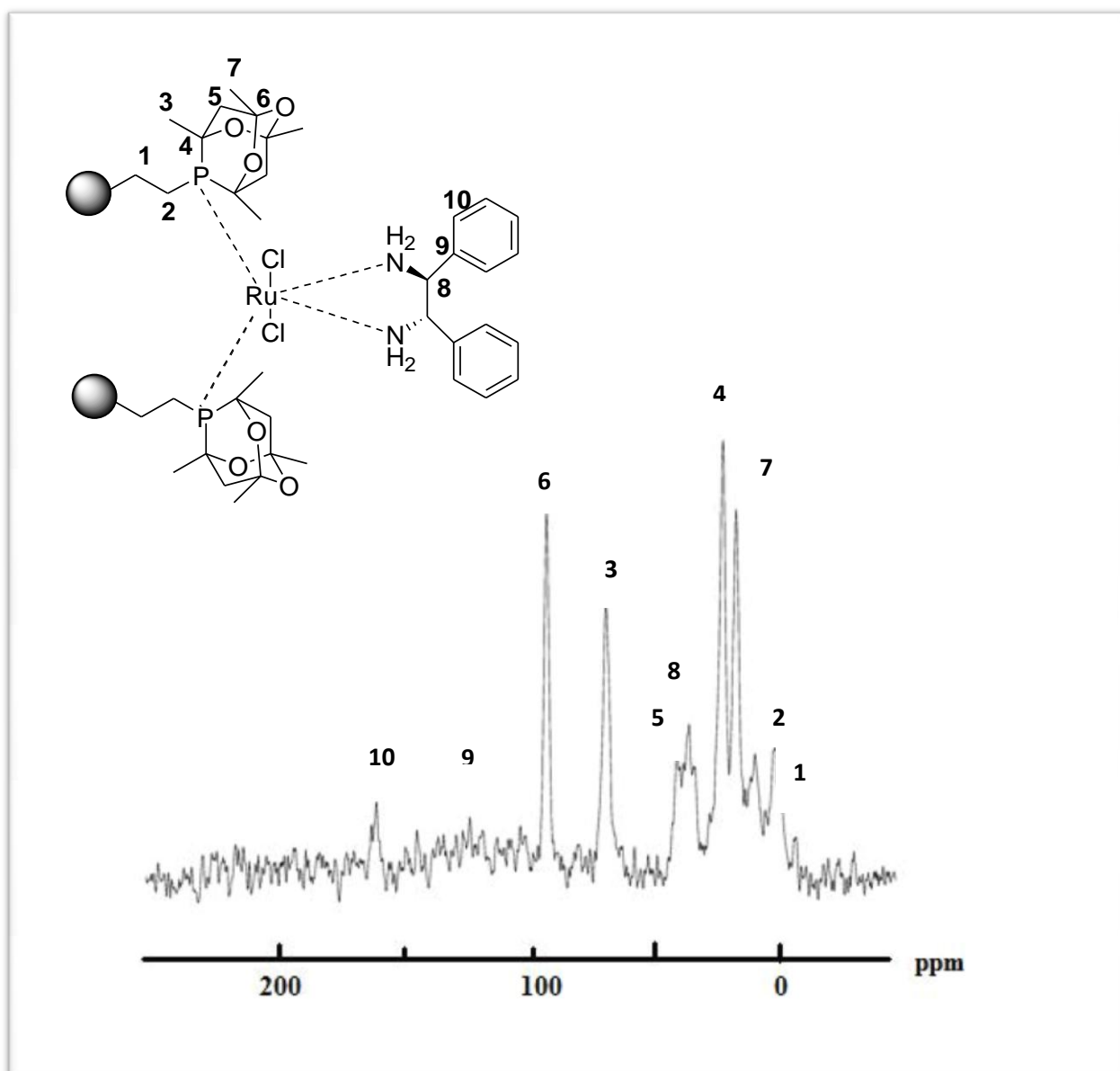


**Figure A5.2**  $^{13}\text{C}$  CP MAS NMR of silica-110-PAD-Ru-DPEN

### $^{29}\text{Si}$ MAS NMR

$^{29}\text{Si}$  MAS NMR also confirmed immobilisation of the metal complex (**Figure A5.3**). Two distinct environments are observed, one corresponding to the  $\text{T}^n$  functionalities, -56.7 ppm and the other corresponding to the  $\text{Q}^n$  environments within the material, these are found at -89, -98 and -107 ppm. The  $\text{T}^n$  environment found in silica-110-PAD is reported at -65ppm, suggesting a different chemical environment, i.e. some complexation to the metal with some of the ligand environments metal free. From  $^{13}\text{C}$  NMR, the presence of methoxy groups is not

evident, this suggests that the majority of organosilicon environments are of T<sup>3</sup> character, perhaps with some T<sup>2</sup> environments.

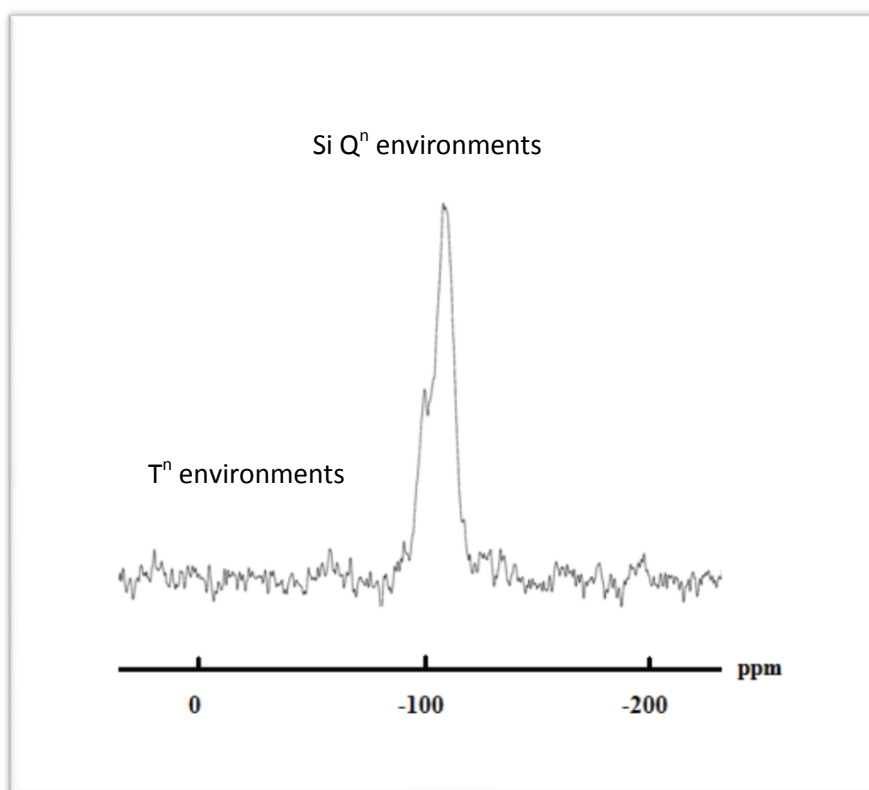


**Figure A5.3** <sup>29</sup>Si MAS NMR of **silica-110-PAD-Ru-DPEN**

#### Dipolar dephasing experiment

Dipolar dephasing experiments were also carried out on complex **silica-110-PAD-Ru-DPEN**. These studies showed suppression of all non-quaternary carbon environments, except for the four methyl groups of the phosphadamantane cage. These groups are very mobile in the given silica environment, in comparison the methylene groups of the phosphadamantane cage which are in very restricted environments with almost all of these environments being suppressed in the dipolar dephasing experiment. A huge suppression is also seen for the CH<sub>2</sub> groups adjacent to the silica framework as well as that the CH<sub>2</sub> adjacent to the phosphorus.

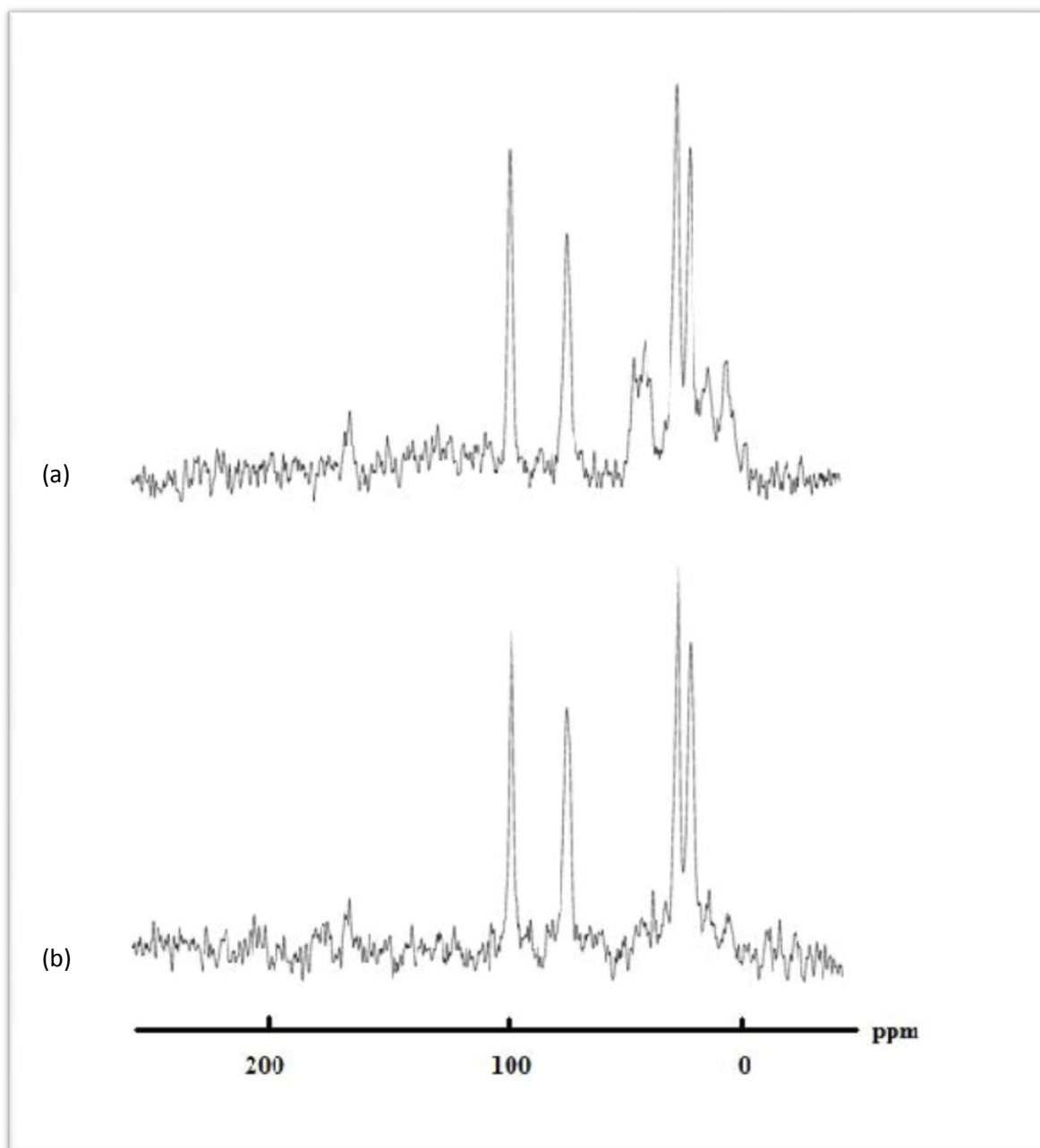


**Figure A.4** Dipolar dephasing experiment of silica-110-PAD-Ru complex (a) normal spectrum (b) with time delay of 180 seconds

#### Metal content determination

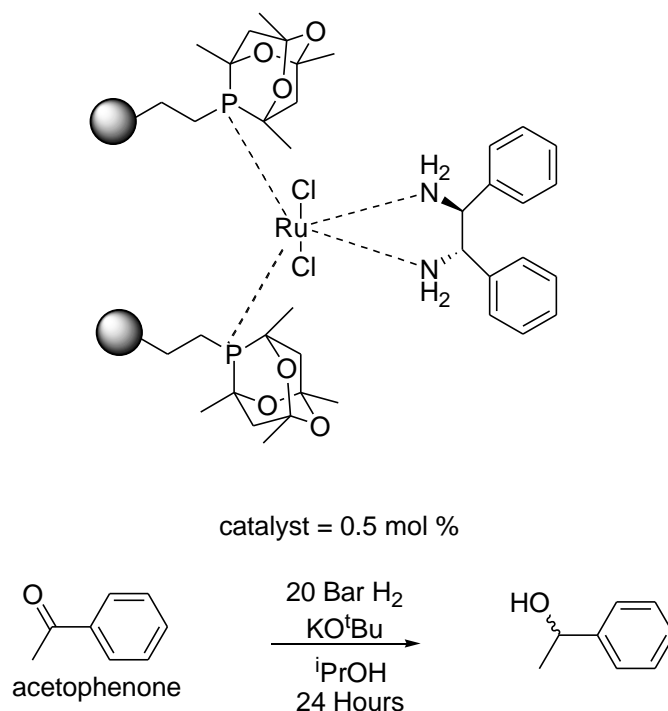
This was achieved by stirring 25 mg of **silica-110-PAD-Ru-DPEN** in an aqua regia (3:1 conc AnalR HCl: conc AnalR HNO<sub>3</sub>) solution (7.5 mL) and the resulting mixture refluxed for 6 hours. The solid was then filtered, and the metal content in the filtrate measured by ICP-OES. The metal loading was measured to be 0.17 mmol/g. Given that the ligand loading is 0.50

mmol/g and that in the proposed structure two phosphadamantane ligands are required to complex to one metal site, this would suggest approximately 70% of the ligand sites are bound to metal, with the remaining 30% being metal free. Just to note the solid filtered was a white solid, suggesting all the Ru metal had been cleaved. In addition, the harsh conditions required to remove the metal, such as the long reflux time and concentrated acid used suggests tight binding of the metal to the immobilised phosphadamantane ligand.

### 5.3 Hydrogenation of acetophenone with silica-110-PAD-Ru-DPEN

The catalytic activity of **silica-110-PAD-Ru-DPEN** was first tested in the hydrogenation of acetophenone. In these reactions dry isopropanol (5 mL) was taken as a solvent, potassium *tert*-butoxide as a base (2.0 mmol) and acetophenone (1.0 mmol) as the prochiral substrate. The amount of catalyst employed was 100 mg which corresponded to 5 mol % Ru. Initial reaction temperatures set at room temperature and hydrogen pressures of atmospheric to 5 bar gave no conversion to the reduced product. The hydrogen pressure was then increased to 10 bar and this resulted in good conversion to 1-phenyl ethanol (76 %) after a total reaction time of 24 hours. A further increase of hydrogen pressures to 20 bar resulted in quantitative conversions being achieved and the enantioselectivity demonstrated by **silica-110-PAD-Ru-DPEN** was found to be 18 % for the (*R*)-enantiomer. Noyori *et al.* report in the hydrogenation of acetophenone with homogeneous Ru (II) complex of the type trans-[RuCl<sub>2</sub>(BINAP)(diamine)] gives 90 % conversion and 95 % *e.e* when employing isopropanol as a solvent, Hydrogen pressures of 8 bar and a total reaction time of 24 hours.<sup>4</sup>





### Scheme A5. 1 Hydrogenation of acetophenone catalysed by silica-110-PAD-Ru-DPEN

Leaching tests were also performed. Removal of the catalyst by filtration after 6 hours revealed 35 % conversion. The filtrate was then transferred to a new reaction flask and to this was added fresh base (2.0 mmol) and the reaction continued to stir for a further 10 hours at room temperature with hydrogen pressures of 20 bar. Analysis of this solution by  $^1\text{H}$  NMR revealed no further conversion had occurred, i.e. conversion remained at 35 % and further analysis of the solution by ICP-OES revealed no detectable Ru was found. With these promising result, attention was the turned to synthesising the catalyst via a different route in order to increase the number of chiral environments and hence increase the chiral activity. This was carried out by combining  $[\text{RuC}_6\text{H}_6\text{Cl}_2]$  with DPEN in DMF for 2 hours at reflux temperature. To this was then added **silica-110-PAD** and the reaction mixture continued to stir for a further two hours. Interestingly, during the final two hours of the reaction time, a gel like substance had formed. And so a new route was pursued in which  $[\text{RuC}_6\text{H}_6\text{Cl}_2]$  and DPEN were stirred in DMF at room temperature overnight. To this was then added **silica-110-PAD** and the reaction mixture continued to stir overnight at room temperature. Once again a gel like substance had formed. This finding suggests that the assembly of catalyst silica-110-PAD needs to occur with the formation of Ru metal complexed to **silica-110-PAD** first before introduction of the chiral amine ligands.

Clearly access to the active metal sites by the substrates is not marred by the presence/coordination of the rather bulky chiral ligands as is shown by the high activity displayed (99% conversion). Thus modification of the chiral ligands perhaps could induce chiral activity. The easy synthesis of such complexes in high yield potentially allows the generation of a wide range of catalyst structures. Future work would entail the screening of a number of substrates and catalysts to find optimum conditions.

Often in such reactions the question always arises as to whether reduction is occurring via hydrogen or from hydrogen transfer from the solvent, isopropanol. It would be imagined that as no conversion is observed at low hydrogen pressures that the hydrogenation of acetophenone using **silica-110-PAD-Ru-DPEN** is most likely to be occurring via hydrogen gas.

## 5.4 Experimental

The synthesis of **silica-110-PAD** has been described in Chapter 6.

### Synthesis of silica-110-PAD-Ru-DPEN

To a small round bottomed flask was added silica supported phosphadamantane (2.0398 g, 1 mmol) and  $[\text{RuC}_6\text{H}_6\text{Cl}_2]_2$  (23.4224 mg, 0.5 mmol). To this was then added DMF (10 mL) and the resultant dark solution left to stir under reflux for 3 hours. The solution was then allowed to cool to room temperature and DPEN (18.1078 mg, 1 mmol) was then added. The mixture was left to stir overnight at room temperature. It was then filtered, washed with cold methanol and dried under pressure at 80 °C to give a pale maroon coloured powder.  $^{13}\text{C}$  CP NMR (MAS)  $\delta_{\text{C}}$ : 4.6 (SiCH<sub>2</sub>CH<sub>2</sub>P), 12.8 (SiCH<sub>2</sub>CH<sub>2</sub>P), 20.4 (CH<sub>2</sub>CCH<sub>3</sub>), 25.6 (PCCH<sub>2</sub>), 39.3 (NH<sub>2</sub>CH), 44.9 (PCCH<sub>2</sub>), 72.7 (PCCH<sub>3</sub>), 95.5 (PCCH<sub>2</sub>CO), 127.3 (NH<sub>2</sub>CCCH), 164.9 (Ar C<sup>2</sup>s);  $^{29}\text{Si}$  NMR (MAS)  $\delta_{\text{Si}}$  -56, -89, -98 and -107.

### Hydrogenation of Acetophenone

To a small conical flask was added potassium-*tert*-butoxide (0.25 g, 2.30 mmol), Catalyst (50 mg, 5 mol % Ru) and dry isopropanol (5 mL). To this solution was then added acetophenone (0.16 mL, 0.14g, 1.15 mmol) and the mixture covered with a watch glass. This was then

placed into an autoclave and purged with nitrogen three times and then with hydrogen and pressurized to 10 bar and left to stir at room temperature for 24 hours. % conversion was determined by  $^1\text{H}$  NMR and % *e.e* determined by HPLC using a chiral OD column.  $^1\text{H}$  NMR ( $\text{CDCl}_3$ , 270 MHz)  $\delta_{\text{H}}$ : 1.49 (3H, d,  $J = 7.5$ ,  $\text{CH}_3\text{CH}$ ), 2.2 (1H, s, OH), 4.69 (1H, q,  $J = 7.5$ ,  $\text{CH}_3\text{CH}$ ), 7.19 (5H, m, Ar H's). Retention times were found at 13.5 minutes for (*S*)-enantiomer and 14.7 minutes for (*R*)-enantiomer.

#### Preparation of Silica supported ethyl phosphadamantane Ruthenium complex

Taken  $[\text{RuC}_6\text{H}_6\text{Cl}_2]_2$  (23.4224 mg, 0.5 mmol) into a two necked flask. To this was added dry DMF (7 mL) and then a solution of DPEN in dry DMF (18.9 mg in 3mL dry DMF) was added dropwise and the reaction mixture heated to 120 °C for 2 hours. To this was then added **silica-110-PAD** (1.3g, 0.65 mmol) and the mixture left to stir for a further 2 hours. This reaction was stopped at this point as a gel like suspension had formed.

## References

- 
- <sup>1</sup> H. Landmesser, H. Kosslick, W. Storek and R. Fricke, *Solid State Ionics*, 1997, **271**, 101-103; X. S. Zhao, G. Q. Lu, A. K. Whitalaker, G. J. Millar and H. Y. Zhu, *J. Phys. Chem. B*, 1997, **101**, 6525; A. Jentys, A. K. Kleesturfer and H. Vinek, *Micropor. Mesopor. Mater.*, 1999, **27**, 321;
- <sup>2</sup> G. Wastermark and I. Perrson, *Colloids Surf. A*, 1998, **144**, 149;
- <sup>3</sup> M. O. Lorenzo, C. J. Baddeley, C. Muryn, and R. Raval, *Nature*, 2000, **202**, 376;
- <sup>4</sup> R. Noyori, M. Koizumi, D. Ishii and T. Ohkuma, *Pure Appl. Chem.* 2001, **73**, 227.